THE UNIVERSITY OF AUCKLAND
FACULTY OF ENGINEERING
Department of Civil and Environmental Engineering

FORCED AND AMBIENT VIBRATION TESTING OF FULL SCALE BRIDGES

By

Piotr Omenzetter[1]
Sherif Beskhyroun[2]
Faisal Shabbir[2]
Ge-Wei Chen[2]
Xinghua Chen[2]
Shengzhe Wang[2]
Alex Zha[2]

A report submitted to Earthquake Commission Research Foundation (Project No. UNI/578)

October 2013

1) The LRF Centre for Safety and Reliability Engineering
School of Engineering
University of Aberdeen
UK

2) Department of Civil and Environmental Engineering
The University of Auckland
New Zealand

NON-TECHNICAL ABSTRACT

Knowledge about the performance of structural systems, such as bridges, can be created using laboratory-scale experimentation, analytical and numerical simulations, and full-scale, in-situ experimentation on existing structures. The latter method has several advantages as it is free from many assumptions, omissions and simplifications inherently present in the former two. For example, soil-structure interaction, non-structural components, and nonlinearities in stiffness and energy dissipation are always present in their true form in full-scale, in-situ testing. Thus, full-scale experimentation results present the ground truth about structural performance. The performance evaluated this way is used for advanced assessment of the working condition of the structure, detection of the causes and effects of damage, aging and deterioration, evaluation of the quality of construction, checking of design assumptions, and also provides important lessons for future design and construction of similar structures.

In this research, four different bridges (a two-span cable-stayed pedestrian bridge, a two-span concrete motorway bridge, an 11-span post-tensioned concrete motorway off-ramp, and a major 12-span post-tensioned concrete motorway viaduct) were tested using environmental excitation (e.g. vehicular traffic) and/or forcing provided by shakers. Experimental data were analysed using techniques that were able to extract the resonant frequencies of the bridges, quantify vibration energy dissipation and visualise the shapes of bridge vibrations. The analyses of data collected in field experiments included observing how stiffness and energy dissipation change with the amplitude of forcing and response. Another way of gaining insights into the dynamics of the tested bridges was via detailed computer modelling of the structures. This enabled identification and understanding of the mechanisms responsible for their measured performance. Because the experimental results and numerical predictions always differ to a certain degree, novel methods for calibration, or updating, of structural models were investigated. These methods, based on mathematical metaphors describing of the behaviour of a swarm of bees or school of fish proved to be efficient tools for model calibration.

TECHNICAL ABSTRACT

A great deal of knowledge about the performance of structural systems, such as bridges, can be created using full-scale, in-situ experimentation on existing structures. Full-scale testing offers several advantages as it is free from many assumptions and simplifications inherently present in laboratory experiments and numerical simulations. For example, soil-structure interaction, non-structural components, and nonlinearities in stiffness and energy dissipation are always present in their true form in full-scale, in-situ testing. Thus, full-scale experimentation results present the ground truth about structural performance and indeed provide the ultimate test for both actual constructed systems and laboratory and numerical investigations. The performance evaluated this way can be used for advanced assessment of structural condition, detection of damage, aging and deterioration, evaluation of the construction quality, validation of design assumptions, and also as lessons for future design and construction of similar structures.

In this research, four different bridges (a two-span cable-stayed pedestrian bridge, a two-span concrete motorway bridge, an 11-span post-tensioned concrete motorway off-ramp, and a major 12-span post-tensioned concrete motorway viaduct) were tested using ambient excitation (e.g. vehicular traffic) and/or forcing provided by shakers. Experimental data were analysed using multiple system identification techniques to extract the resonant frequencies, damping ratios and mode shapes. For the 12-span viaduct, these techniques were compared and recommendations were made for their use in future testing exercises. The analyses of experimental data included quantification of resonant frequency and damping ratio changes with the amplitude of forcing and response for the 11-span motorway off-ramp. The frequencies were found to decrease and damping ratios to initially increase and then stabilise, respectively, with increasing response amplitude. Detailed computer modelling of the structures was also undertaken and enabled identification and understanding of the mechanisms responsible for their measured performance. A novel optimisation method for updating of structural models was proposed and investigated. The method, particle swarm optimisation with sequential niche technique, belongs to global optimisation algorithms, mimics the behaviour of a swarm of bees or school of fish in search for the most fertile feeding location, systematically searches the updating parameter domain for multiple minima to discover the global one, and proved effective when applied to the experimental data from the pedestrian bridge tested in this study.

ACKNOWLEDGEMENTS

This research was financially supported by Earthquake Commission Research Foundation (Project No. UNI/578 "Forced and ambient vibration testing of full scale bridges"). The authors are grateful for this support.

Ben Ryder of Aurecon and Graeme Cummings of HEB Construction assisted in obtaining access to the Clarks Lane bridge and information for modelling. NGA Newmarket facilitated the field testing of Newmarket Viaduct and Gillies Avenue bridge, and New Zealand Transport Agency allowed the use of Newmarket Viaduct, Nelson St off-ramp and Gillies Avenue bridge for research. Particular thanks go to David Leitner, Jonathan Lane and Jim Baker.

The authors would also like to acknowledge the efforts and help of the technical and laboratory staff at the Department of Civil and Environmental Engineering, the University of Auckland involved in this research, in particular Daniel Ripley. The assistance of research students at the University of Auckland: Lucas Hogan, Luke Williams, Graham Bougen, Shahab Ramhormozian, Peifen Chua, Jessica Barrell and Daphne Luez in conducting experimental field testing is much appreciated.

Piotr Omenzetter's work within The LRF Centre for Safety and Reliability Engineering at the University of Aberdeen is supported by Lloyd's Register Foundation (LRF). LRF, a UK registered charity and sole shareholder of Lloyd's Register Group Ltd, invests in science, engineering and technology for public benefit, worldwide.

TABLE OF CONTENTS

LIST OF ABBREVIATIONS

ASD	Auto Spectral Density
AC	Alternating Current
ASCE	American Society of Civil Engineers
AVT	Ambient Vibration Testing
CCF	Cross Correlation Function
CLM	Coupled Local Minimiser
CSD	Cross Spectral Density
DFT	Discrete Fourier Transform
DOF	Degree Of Freedom
EFDD	Enhanced Frequency Domain Decomposition
ERA	Eigenvalue Realisation Algorithm
FDD	Frequency Domain Decomposition
FFT	Fast Fourier Transform
FE	Finite Element
FRF	Frequency Response Function
FVT	Forced Vibration Testing
GA	Genetic Algorithm
GOA	Global Optimisation Algorithm
IDFT	Inverse Discrete Fourier Transform
IFR	Impulse Response Function
MAC	Modal Assurance Criterion
MEMS	Micro Electro Mechanical Systems
NExT	Natural Excitation Technique
OMA	Operational Modal Analysis
PP	Peak Picking
PSO	Particle Swarm Optimization
RC	Reinforced Concrete
SDOF	Single Degree Of Freedom
SA	Simulated Annealing
SM	Sensitivity Method
SNT	Sequential Niche Technique
SI	Spectrum Identification

SSI	Subspace System Identification
SVD	Singular Value Decomposing

NOTATION

The following notation is used throughout this report:

$\mathbf{0}$	null matrix
$\mathbf{A}$	state matrix
A	effective load area
$\mathbf{B}$	input matrix
$\mathbf{C}$	output matrix
c	cognition coefficient, social coefficient
$\mathbf{D}$	feedthrough matrix
d	constant, distance
E	expectation operator, elastic modulus, Young's modulus
f	frequency
$\mathbf{G}$	spectral density matrix
G	shear modulus, derating function
g	modal impulse response function
gbest	best swarm position
$\mathbf{H}$	Hankel matrix for outputs, frequency response function matrix
H	frequency response function
$\mathbf{I}$	identity matrix
Im	imaginary part
j	imaginary unit
K	stiffness
k	dimensionality
L	length, distance
m	modal mass, number of objects, derating parameter
N	total number
n	number of objects
Ob	oblique projection
$\mathbf{P}$	vector of updating parameters
p	number of minima
pbest	best particle position
$\mathbf{R}$	vector of updating responses

R	cross correlation function
r	niche radius
$rand$	random number
Re	real part
$\mathbf{S}$	sensitivity matrix
S	auto spectral density, cross spectral density, bearing shape factor
$\mathbf{s}$	minimum position
$\mathbf{T}$	matrix of left singular vectors
$\mathbf{t}$	left singular vector
t	time, thickness
$\mathbf{U}$	Hankel matrix for inputs
$\mathbf{u}$	state-space input vector
u	input
$\mathbf{V}$	matrix of right singular vectors
$\mathbf{v}$	state-space measurement noise vector, particle velocity
$\mathbf{W}$	combined matrix of inputs and outputs in SSI
$\mathbf{X}$	state sequence
X	Fourier transform of signal
$\mathbf{x}$	state vector, particle position
x	time history of signal
$\mathbf{Y}$	Hankel matrix for outputs
$\mathbf{y}$	state-space output vector
$\mathbf{\Gamma}$	extended observability matrix
Π	penalty function
α	weighting factor, numerical parameter
γ	inertia weight
γ^2	coherence
Δ	interval, increment
λ	eigenvalue
ξ	damping ratio
$\mathbf{\Sigma}$	matrix of singular values
σ	standard deviation

Φ	compression coefficient for elastomer
φ	mode shape
ψ	eigenvector of state matrix
ω	state-space process noise
ω	radial frequency
$\| \|$	absolute value

Subscripts:

a	analytical
$bearing$	bearing
c	continuous time system, compression
$cable$	cable
$comp$	complex
d	damped
e	experimental
i	location, index
j	index
f	frequency, future
k	time step, location
p	past, location
r	mode number, index
$real$	real part of complex quantity
rot	rotation
s	shear
t	torsional
u	input, updated
v	vertical
x	output
0	undamped, initial

Superscripts:

T	matrix transpose

$\sim$	time-shifted matrix
+	Moore-Penrose pseudoinverse
*	complex conjugate

LIST OF FIGURES

Chapter 3

Chapter 4

Chapter 5

Chapter 6

Chapter 7

LIST OF TABLES

CHAPTER 1

INTRODUCTION

1.1. Background and motivation for research

Constructed systems, such as bridges, have several characteristics that make the understanding of their behaviour and performance as well as modelling a challenge. These include uniqueness of individual structures, heterogeneity of materials used, complex boundary and continuity conditions, non-linearity and non-stationarity of responses, and changes in characteristics during their lifecycle due to damage, ageing and deterioration. Material properties, dimensions and detailing vary from member to member and within a member, and deterioration in these structures over their lifetime further complicates our understanding of their performance. Constructed systems often exhibit complicated soil-foundation interactions and are often non stationary in their behaviour. Continuity conditions of these structures, especially bridges, consist of movement systems (such as bearings, hinges and dilatations) which behave differently under different force levels. These systems are subjected to complex forces due to dead loads, live loads, pre-stress and post-tensioning, deteriorations, overloads, damage, staged constructions etc. Many different types of non-linearities such as yielding, connection slip, friction between interfaces, etc., that change at different response levels, further complicate the situation. Nearly every constructed system is unique and custom designed for its intended purpose.

There is thus constant need to improve our understanding of how constructed systems behave and perform. Knowledge about the performance of structural systems can be created using laboratory-scale experimentation, analytical and numerical simulations, and full-scale, in-situ experimentation on existing structures. The latter method has several advantages as it is free from many assumptions, omissions and simplifications inherently present in the former two. For example, soil-structure interaction, non-structural components, and nonlinearities in stiffness and energy dissipation are always present in their true form in full-scale, in-situ testing, as are actual loading and response mechanisms. Thus, full-scale experimentation results present the ground truth about structural performance. Indeed, is provides the ultimate test for the correctness of predictions obtained via laboratory experimentation and numerical simulations (Okada and Ha 1992). The performance evaluated this way can be used for advanced assessment of the working condition of structures, detection of the causes and effects of damage, aging and deterioration, evaluation of the quality of construction, checking of design assumptions, and also provides important lessons for future design and construction of similar structures.

In the project, full-scale testing was conducted under environmental, or ambient, as well as purposely imparted dynamic loads. Full-scale dynamic testing results represent structural responses with proper boundary conditions and eliminate any need for scaling. The results from full-scale testing can also provide a benchmark to calibrate structural models and help in developing new mathematical models capable of representing the true behaviour of structures. Dynamic identification of full-scale structures such as concrete and masonry buildings, towers and bridges have been performed by many researchers under different loading conditions; Ellis (1996), Li et al. (2004), De Sortis et al. (2005) and Chen and Zhou (2007) are but a few recent examples. However, there are still a number of poorly researched and understood aspects of structural performance and tolls used for its assessment, such as performance of different modal identification techniques and dependence of modal properties on the level of excitation and response. More research is also required in the challenging area of calibration of computer models so that they replicate well experimental data and there is strong need to improve the efficiency of model updating algorithms. Furthermore, there has been relatively little activity in these areas in New Zealand in the past decade and developing appropriate expertise was considered desirable.

1.2. Objective, contribution and scope of research

The overall objective of this research was to create enhanced understanding of the dynamic behaviour of bridges via full scale testing. The specific objectives were as follows:

- To build enhanced and world class expertise in full-scale structural dynamic testing in New Zealand by conducting a variety of testing exercises on a range of bridges and exploring various data analysis approaches and techniques,
- To perform ambient testing and operational modal analysis (OMA) of bridge structures and compare the performance of several commonly used modal identification techniques,
- To perform force vibration testing of full-scale structures using a variety of shakers, and, in particular, by varying the excitation amplitude quantify how stiffness and energy dissipation depend on response amplitude, and
- To develop and explore, using the experimental dynamic data acquired via full-scale testing, new and advanced methods for calibration of structural models (model updating) based on optimization techniques.

In this research, four different bridges (a two-span cable-stayed pedestrian bridge, a two-span concrete motorway bridge, an 11-span post-tensioned concrete motorway off-ramp, and a major 12-span post-tensioned concrete motorway viaduct) were tested using ambient environmental excitation (e.g. vehicular traffic, wind and possible microtremors) and/or forcing provided by shakers of different sizes. Experimental data were analysed using multiple system identification techniques to extract the resonant frequencies, damping ratios and mode shapes. For the 12-span viaduct, the performance of different modal identification methods in OMA was compared and conclusions drawn as to which methods are recommended for similar future testing exercises. The analyses of experimental data included quantification of resonant frequency and damping ratio changes with the amplitude of forcing and response for the 11-span motorway off-ramp. The frequencies were found to decrease and damping ratios to increase, respectively, with increasing response amplitude. Detailed computer modelling of the structures was also undertaken and enabled identification and understanding of the mechanisms responsible for their measured performance. A novel optimisation method for updating of structural models was proposed and investigated. The method, particle swarm optimisation (PSO) with sequential niche technique (SNT), belongs to global optimisation algorithms (GOAs), mimics the behaviour of a swarm of bees or school of fish in search for the most fertile feeding location, systematically searches the updating parameter domain for multiple minima to discover the global one, and proved effective when applied to the experimental data from the pedestrian bridge tested in this study.

1.3. Report layout

The layout of this report is as follows:

Chapter 2 – A review of past and current research trends in full-scale in-situ dynamic testing of structures and model updating including excitation, sensing, data acquisition and processing, uncertainties in the numerical modelling of structures, approaches to model updating including sensitivity method (SM) and GOAs, and past examples of testing and updating exercises.

Chapter 3 – An exposition of the theoretical concepts and methods related to system identification (spectral analysis and frequency response function (FRF), peak peaking (PP), enhanced frequency domain decomposition (EFDD), subspace system identification (SSI), and natural excitation technique – eigenvalue realisation algorithm (NExT-ERA)), and model updating (penalty function, sensitivity based updating, global optimisation algorithms (GOAs) including particle swarm optimisation (PSO) and sequential niche technique (SNT)).

Chapter 4 - Forced vibration testing using three small shakers (force capacity up to 3 × 0.4 kN), system identification and model updating of the cable-stayed footbridge. The updating uses the newly proposed method combining PSO with SNT.

Chapter 5 - Ambient vibration testing, operational modal analysis and computer modelling of the 12-span viaduct. Several OMA techniques are applied to the collected data and their performance evaluated and compared.

Chapter 6 - Ambient and forced vibration testing, system identification and computer modelling of the 11-span highway off-ramp bridge. Using various excitation levels provided by large shakers (force capacity up to 98 kN) trends in frequencies and damping ratios with increasing response amplitude are quantified.

Chapter 7 – Forced vibration testing using the large shakers, system identification and model updating of the two-span overbridge. This exercise, chronologically earlier than the 11-span of-ramp testing, provided important lessons for the subsequent off-ramp testing project.

Chapter 8 – Conclusions and recommendations for further research are provided.

1.4. References

Chen, X., & Zhou, N. (2007), Equivalent static wind loads on low-rise buildings based on full-scale pressure measurements, Engineering Structures, 29, 2563-2575.

De Sortis, A., Antonacci, E., & Vestroni, F. (2005), Dynamic identification of a masonry building using forced vibration tests, Engineering Structures, 27, 155-165.

Ellis, B.R. (1996), Full-scale measurements of the dynamic characteristics of buildings in the UK, Journal of Wind Engineering and Industrial Aerodynamics, 59, 365-382.

Li, Q.S., Wu, J.R., Liang, S.G., Xiao, Y.Q., & Wong, C.K. (2004), Full-scale measurements and numerical evaluation of wind-induced vibration of a 63-story reinforced concrete tall building, Engineering Structures, 26, 1779-1794.

Okada, H., & Ha, Y.-C. (1992), Comparison of wind tunnel and full-scale pressure measurement tests on the Texas Tech Building, Journal of Wind Engineering and Industrial Aerodynamics, 43, 1601-1612.

CHAPTER 2

LITERATURE REVIEW

2.1. Introduction

The following literature review focuses on modal testing and FE model updating, as these are the two major topics of this research project. The review starts with a discussion of modal dynamic testing, further subdivided into excitation sources, sensing equipment, and data acquisition and processing, and uncertainties associated with model tests. Methods for correlating experimental and analytical data are then discussed. Firstly, the sources and nature of uncertainties and errors in numerical modelling of structures are reviewed. Issues related to the selection of updating parameters and non-uniqueness of solution are covered. Common model updating approaches based on manual model updating, SM-based model updating, and GOA-based model updating are then explained. Lastly, selected literature related to applications of modal testing and model updating is discussed. This final section also emphasizes previous studies of the influence of response levels on the natural frequencies and damping ratios as this question is also tackled in the report.

2.2. Modal testing

To increase the knowledge and understanding of performance of actual constructed systems, their dynamic responses are often observed. Vibration testing to determine the experimental modal characteristics such as natural frequencies, mode shapes and damping is referred to as modal testing. This is accomplished by performing testing which includes exciting and capturing the responses of a structure by a set of sensors. The experimental setup generally consists of the following main components: excitation, sensing, data acquisition and data processing (Clarence and De Silva 2007).

2.2.1. Excitation

There are three different major types of dynamic tests (Salawu and Williams 1995) depending on the type of excitation used, i.e. forced vibration tests, ambient vibration tests and free vibration tests.

In forced vibration tests, the structure is excited by a known input force. The input excitation to the structure is provided by properly designed excitation systems, which entails application of a known force at particular frequencies or frequency bands of interest (Causevic 1987, De Sortis et al. 2005). This method is based on the fact that if the loading on the structure and resulting responses are known, then the structural characteristics can be more unambiguously determined. By the use of a known forcing function, several uncertainties related to data processing and collection can therefore be avoided. These types of tests also enable achieving higher signal-to-noise ratios in the response measurements (Salawu and Williams 1995). The structures are typically excited by shakers or instrumented impact hammers. Two different types of shakers can be used, a linear mass shaker and an eccentric mass shaker. Linear mass shakers can impart a combination of steady state sinusoidal as well as transient waves, whereas eccentric mass shakers can only impart sinusoidal forcing. Both shakers can be used for horizontal or vertical excitation of the structure. Impact hammers can only impart impulse type excitation to the structure. Impact hammers can be hand-held, machine-lifted or dropped. Different levels of forces can be generated by using different weights. The advantages associated with impact hammers are that they are fast in their application and tests can be quickly repeated a large number of times. Although heavy shakers and heavy drop weights are available, the size of the structure may limit the use of forced vibration testing to smaller structural systems. Also, the structure has often to be closed for operations for this type of forcing.

In ambient vibration tests, the excitation is not under control and is usually considered to be a stationary white noise random process, which means that the response data from the structure alone can be used to estimate the dynamic parameters. The increasing popularity of this method is because no forcing machinery is required. Ambient excitation can be from sources such as wind, pedestrian or vehicular traffic, earthquakes, waves or similar. For very large and massive structures, ambient excitation is often the only practical choice. Structural identification through ambient vibrations has been successful in numerous cases (Ivanovic et al. 2000, Ventura et al. 2003). However, ambient vibration testing has limitations, mostly associated with the lack of information on the actual forcing. Most of the ambient identification procedures assume a white noise excitation, which, if violated, may lead to imprecise system identification results. A considerable degree of non-linearity exhibited by real structures and a low signal to noise ratio can also complicate the analysis in these tests.

In free vibration tests, the vibration is introduced in the structure by initial inputs only. The structure is disturbed from its initial static equilibrium position and is allowed to move freely (Friswell and Mottershead 1995). No external force is applied to the structure during free vibration. The energy of the system decays due to material, structural and fluid damping. It is generally difficult to apply this type of excitation to large, full-scale structures.

2.2.2. Sensing

The sensing system is composed of transducers aimed to measure the structural responses. A detailed summary of different sensors used for measurement can be found in many text books, e.g. Ecke et al. (2008), Ohba (1992) and Wilson (2005). Different sensors are used for different measurement purposes such as velocity, displacement, acceleration, strain, temperature, pressure, wind speed etc. They are categorised on the basis of operating principle or measurand. For modal testing purposes, accelerations are a common choice for short and long term monitoring. Different types of accelerometers are available, such as capacitive accelerometers, piezoelectric accelerometers, strain gauge accelerometers, fibre grating accelerometers, micro-electro-mechanical systems (MEMS) accelerometers and servo accelerometers. The accelerometer measures accelerations at a specific point of the structure and typically generates electric signals in the form of voltage to be read by a data acquisition system. Conditioning amplifiers are used to amplify the signals if they are weak.

2.2.3. Data acquisition and processing

Data acquisition is a procedure in which the data from the sensing mechanism is converted into digital data and stored permanently on a computer. The data processing is a critical step aimed for error mitigation and parameter estimation. Data need to be checked for errors related to the quantization, aliasing, filtering and leakage in the first place. Parameter estimation involves identification of the magnitude and phase of different signals obtained from various parts of the structure and extraction of the modal information that includes modal frequencies, mode shapes and damping characteristics (Ewins 2000). Two different classes of analytical procedures are available, time domain methods and frequency domain methods. The first type determines the structural characteristics directly from the time domain data, whereas the second type converts the data into frequency domain first to extract modal information. More details of the time and frequency domain methods used in this study, including their mathematical formulations, are given in Chapter 3.

2.3. Model updating

In constructed systems, predictions of initial FE models and measured responses often differ in important ways exposing the inability to correctly model the systems based on the assumptions made in the modelling process. This, in turn, hampers the ability to understand and predict the behaviour of the systems. These discrepancies arise mainly from (Moon and Aktan 2006): i) incorrect assumptions related to physical properties such as modulus of elasticity of materials and mass densities, ii) discretization errors due to coarse or poor mesh or due to assumed FE shape functions, iii) inaccurate approximation of boundary and continuity conditions and joints, and iv) inaccuracies in estimation of spatial characteristics of actual members.

Model updating is an inverse problem in which uncertain parameters of the FE model are calibrated to minimize the errors between the predictions of the FE model and experimentally measured dynamic behaviour of the actual structure. Model updating can be posed as an optimization problem in which an optimal solution is sought by perturbing the uncertain parameters of the FE model so that the model prediction errors are minimized.

This chapter discusses several important aspects of model updating including uncertainties in numerical modelling of structures and selection of updating parameters, and presents qualitatively different approaches to model updating (manual, SM-based and GOA-based). Chapter 3 provides more details on the updating methods used in this study including their mathematical formalism.

2.3.1. Uncertainties in modelling of structures

Physics based models, such as these using FE methodology, are based on the laws of mechanics, continua models and discrete geometric models, and demand parameters that have clear physical meaning. Due to discretisation and idealizations, different errors in the continuum models are inevitable. If FE model is not able to conceptualize force distributions, loading mechanisms, and kinematic capabilities, the analytical predictions may be far from the actual behaviour. Preliminary FE models are usually generated from idealised drawings, material tests, site inspections as well as previous studies done on similar structures. Therefore, construction tolerances and exact materials properties may not be correctly modelled in the initial FE model. A satisfactory FE model should be capable of simulating geometry, stiffness and inertia, boundary and continuity conditions, load paths, and kinematics relationships.

Possible sources of modelling errors include discretization errors, conceptualization errors and parameter errors. Discretization errors are a result of mesh coarseness. Since constructed systems have infinite DOFs whereas FE realization is a discrete numerical model, the existence of these errors is inevitable. If the initial FE model has large discretization errors, the updating solution will try to compensate for those and may deviate from the true values of model parameters (Chen 2001). Different authors have attempted to address the problem of discretisation errors. A mesh density parameter was included in updating in an attempt to modify the mesh (Link and Conic 2000), and different mass distribution approach was also tried (Chen 2001).

Parameter errors basically highlight the as-built characteristics of the constructed systems such as geometry, material properties, degradation, construction tolerance, environmental actions and load effects cannot be assumed with absolute certainty. Most of the studies carried out in the context of model updating are aimed to correct this type of errors in the analytical model to make it a true realization of the structure. The parameters chosen for updating purposes should strongly influence the target responses; otherwise the updating results may deviate far from the true ones. Different parameter selection techniques have been investigated to reduce the number of parameters (Baker and Marsh 1996, Link 1991, Maia et al. 1994).

The constructed systems are highly complex with a large number of structural and non-structural members and loading mechanisms, boundary, continuity and joint conditions that are rarely understood in a precise manner. As a result, FE models usually employ physics laws, mathematical manipulations and other behaviour assumptions resulting in conceptualization errors. These types of errors have so far been largely neglected in the process of model updating although several researchers have mentioned their importance (Chen and Ewins 2004, Mottershead and Friswell 1993, Sanayei et al. 2001).

In a representative study, ambient vibration tests were conducted by Black and Ventura (1999) on the Crowchild Trail Bridge in Canada. Four different types of models, i.e. distributed beam, 2D uniform beam, 2D plane and 3D FE model were developed for the bridge and compared with experimental modal properties. Limitations and strengths of each of the models were reported. Ren et al. (2004a) investigated the Roebling bridge using ambient vibration testing. Two different models, i.e. 3D model with shell elements and a simplified model using an equivalent beam were investigated. It was found that both models were able to capture the vertical and longitudinal modes. However, the simplified model gave closer prediction of transverse modes compared to the detailed 3D model.

Sanayei et al. (2001) investigated the influence of modelling errors through numerical simulations with respect to measurement type and its location, error function and location of uncertain parameters. A vector projection method was proposed by Chen and Ewins (2004) to check the idealization errors, and applied on numerical examples and an aero engine. However, in case of constructed systems, large differences in measured and analytical DOFs can make it very difficult to localize conceptualization modelling errors accurately. Robert Nicoud et al. (2005) investigated a set of analytical models for system identification of a highway bridge to highlight the importance of modelling errors.

In many cases, a number of physically reasonable and different models are capable of correlating the experimental data with their analytical predictions. A systematic study has been carried out by Pan et al. (2010) for mitigation of epistemic uncertainty in modelling a long span steel arch bridge. A three dimensional FE model was updated using ambient vibration data. A series of incorrect modelling assumptions related to continuity conditions of vertical elements along the main arch and via duct spans have been identified. Sensitivity analysis along with engineering judgement was used to mitigate the a priori modelling uncertainty.

2.3.2. Approaches to model updating

Creating a good FE model which correctly represents the actual structure is not an easy task (Brownjohn et al. 2001). There is a degree of uncertainty in assessing the actual properties of the materials used as well as the most realistic representation of the element stiffness in the development of an analytical model (Yu et al. 2007). As discussed in the preceding section, the main reasons for the differences between the FE model and the original structure can be attributed to modelling and parametric errors. Modelling errors are associated with the simplification of a complex structure and its boundary and connectivity conditions, whereas parametric errors are associated with incorrect estimation of the material and geometric properties. Dynamic model updating calibrates the FE model by comparing the modal properties of the built structure with those of the FE predictions. The principle of modal updating process is that the system matrices such as stiffness, mass and damping are modified with respect to the experimental modal data, i.e. natural frequencies, mode shapes and damping coefficients.

There are two types of model updating procedures based on modification of system matrices, iterative and one-step procedures. Iterative procedures are based on updating the parameters (such as material and geometry properties of members), whereas the one-step procedures directly make the changes to the whole stiffness and mass matrices. The updated matrices using the latter method may exactly reproduce the experimental modal properties but generally do not provide an insight into the physical significance of the introduce changes (Brownjohn et al. 2001). In this research, iterative methods are therefore used.

For iterative procedures, the candidate parameters for updating describing the geometry, material properties and boundary conditions are grouped in an a vector of updating parameters. Similarly, the experimental and analytical modal responses, such as frequencies and mode shapes, also form the respective vectors. The difference between these two is referred to as the error or residual vector. An objective function is defined as a weighted norm of the residual vector. The objective function is iteratively minimised in the updating process by adjusting the values of the updating parameters and thus improving the correlation between the experimental and analytical model.

Due to many candidate parameters for updating of the FE model, several different combinations of the parameters can lead to acceptable results. It is difficult to determine all the natural frequencies and mode shapes experimentally, as the original structure has infinite degrees of freedom (DOFs). As the number of measurements available is usually much smaller than the number of uncertain parameters, and, consequently, not all uncertain parameters are selected for model updating, different solutions may exist in the solution space for a specific error function.

The search for the global minimum of the objective function is a challenging optimization problem. There are two main concerns for solving model updating problems, namely, the capability of the algorithms and complexity of the search domain (Horst et al. 2000). The capability of the algorithm is related to its ability in detecting the global solution and its computational efficiency in finding the global minimum. The complexity of the search domain is related to the number of parameters involved in the search process. An increase in the number of parameters leads to an increase in the dimensionality of the search domain, which may further complicate the problem. Thus structural updating is essentially a search process and suitable optimization techniques should be explored to deal with it. Common model updating techniques, to find a set of suitable parameters, in the context of model updating of civil structures are discussed in the following sections.

2.3.2.1. Manual model updating

This approach involves manual changes in the updating parameters by trial and error, but if the sensitivities of modal properties to parameter changes are available the process can be more systematic (Jaishi and Ren 2005). Most influential parameters to the experimental responses are selected, assisted by engineering judgment, and varied to calibrate the model. Manual model updating is often conducted as a preliminary step for the application of other methods to obtain reasonable starting values of the parameters (Zivanovic et al. 2007).

2.3.2.2. Sensitivity method for model updating

Contemporary methods of structural updating in buildings and bridges include the use of SM to improve the correlation between analytical and experimental modal properties (Brownjohn and Xia 2000, Yu et al. 2007). SM belongs in the category of local optimization techniques and the solution largely depends on the starting point or initial values (Deb et al. 2007).

These methods take advantage of the solution space characteristics by calculating gradients and converge quickly to (possible local) minimum values. A good guess of the initial point is necessary so as to converge to the global minimum. However, this has limited their efficient use to smooth and uni-modal objective functions.

SM computes the sensitivity coefficients defined as the rate of change of a particular response with respect to change in a structural parameter, and gathers them in the sensitivity matrix. Sensitivity parameters can be calculated by using perturbation techniques, finite differences or by direct derivation using modal parameters (Friswell and Mottershead 1995). In the formulation of SM, the experimental responses are expressed as a function of analytical responses and a sensitivity matrix (Zivanovic et al. 2007). This is done by a Taylor series expansion ignoring order terms higher than the first.

2.3.2.3. Global optimisation algorithms for model updating

GOAs are stochastic search methods for finding the global minimum in difficult optimization problems (Deb 2001). They are generally independent of the solution space (Tebaldi et al. 2006, Tu and Lu 2008) because they work on a population of points in parallel, whereas the traditional search techniques such as SM work only on a single point at one time utilizing information about the search space topology such as gradients. Thus, the tendency of traditional search techniques converging to a local minimum in the search space can be addressed by using GOAs. This makes the GOAs more robust in case of ill-behaved solution space.

These techniques are particularly efficient for finding the minimum of objective functions having constrained variables and a large number of dimensions. This makes them more suitable to use in model updating problems with different objective functions such as those based on frequencies and mode shapes. The global techniques attempt to find the global minimum out of local minima and often give better results where local optimization techniques perform less favourably (Deb 1998). Drawbacks of global optimization techniques are that they do not take advantage of the characteristics of the solution space such as the steepest gradients and slow rates of convergence. One of the GOAs used in this research, namely PSO, is discussed in detail in Chapter 3 together with the SNT technique that improves its performance.

2.4. Examples of past modal testing and model updating exercises

This chapter presents an overview of selected past modal testing and model updating research projects reported in the literature in order to illustrate how the frameworks outlined above find is practical implementation. A separate section is devoted to the studies that address the dependence of modal properties on the level of response as this topic is also studied later for the 11-span motorway off-ramp tested in this project. Model updating examples are divided into those using the more traditional SM based techniques and relatively new approaches based on GOAs.

2.4.1. Modal testing

Many researchers have successfully conducted forced vibration tests to obtain dynamic properties of bridge structures. Shepherd and Charleson (1971) conducted a series of steady-state vibration tests on a multi-span continuous deck bridge at several stages during construction by using an eccentric mass shaker. Kuribayashi and Iwasaki (1973) determined modal characteristics of 30 highway bridges when subjected to transverse harmonic excitation using an eccentric mass shaker. Ohlsson (1986) performed swept-sine tests on a cable-stayed bridge in Sweden using an eccentric mass shaker. Crouse et al. (1987) conducted a forced vibration test with a large eccentric mass shaker, which was bolted to the top of the bridge deck midway between two abutments. The testing consisted of harmonic forced vibration excitation of the bridge in the transverse and longitudinal directions.

Other studies reporting the use of shakers for bridge excitation include Salane and Baldwin (1990), Deger et al. (1995), Shelley et al. (1995), Haritos et al. (1995) and Link et al. (1996). Based on the previous testing experience, it was found that excitation by shakers generally produced the best results for short to medium span bridges (spans less than 100 m) (Green 1995).

Ambient vibration tests are a useful alternative, successfully applied to a large variety of civil engineering structures ranging from short- to long-span bridges, to high-rise buildings, to dams. This method only requires the measurement of the structural response under ambient excitation, usually due to wind, traffic or earthquake and avoids closing the bridge to traffic during the tests due to the installation of heavy shakers. For large structures, it is the only practical method as imparting excitation by other means is very difficult if not impossible. On the other hand some inherent drawbacks are the variable and uncertain nature of the excitation in terms of amplitude, direction, duration, as well the lack of any quantitative knowledge of its precise nature and characteristics. The usual ambient testing procedure consists of performing several measurements simultaneously at different points along the structure with one or more fixed reference points. Assuming that the excitation is close to white noise in the frequency band of interest, it is possible to estimate natural frequencies, damping ratios and mode shapes. Ambient vibration tests have been successfully applied to a variety of bridge structures such as the Vincent Thomas suspension bridge (Abdel-Ghaffar and Housner 1978), Golden Gate suspension bridge (Abdel-Ghaffar and Scanlan 1985), Roebling suspension bridge (Ren et al. 2004a), Safti Link curved cable-stayed bridge (Brownjohn et al. 1999), Vasco da Gama cable-stayed bridge (Cunha et al. 2001), twin curved cable-stayed bridges on the north and south sides of Malpensa airport in Milan (Gentile and Martinez y Cabrera 2004), Brent-Spence truss bridge (Harik 1997), and Tennessee River steel arch bridge (Ren et al. 2004b).

Free vibration testing is usually performed by giving the system an initial displacement and suddenly releasing the system from rest. This can be done by using a tensioned cable with a fusible connection anchored to the soil and increasing the corresponding tension to the limit. An alternative is a sudden release of a mass appropriately suspended from the deck (Delgado et al. 1998). Initial velocity or impulse loading can also be provided by dropping a weight which then strikes the deck. One difficulty with free vibration tests is that it is usually not easy to separate the effects of the individual modes of vibration in a complicated bridge structure. It is also usually difficult to accurately control the test conditions for repeated tests.

Generally speaking, forced vibration tests can provide more accurate modal identification results than ambient vibration tests, since well-defined and known input excitations are used in the modal identification procedure, and the excitations can be optimized to enhance the response of the vibration modes of interest. However, in the case of large and flexible bridges such as suspension and cable-stayed bridges or bridges with multiple spans it is challenging and costly to provide controlled excitation for a significant level of response. In such cases ambient testing is preferred.

2.4.1.1. Dependence of modal properties on response amplitude

Stiffness and damping both play critical roles in design and analysis of new and existing bridge structures because they greatly impact dynamic response level of bridge structures under dynamic loadings such as traffics, earthquake, and strong wind excitation. Various tests have shown that both the natural frequencies and damping ratios vary with the amplitude of vibration. Damping is a very uncertain parameter in the prediction of the dynamic response of structures and experimental determination is currently the only reliable way of quantifying it (Chopra 2007).

Ellis (1980) pointed out that the amplitude dependent characteristics of both natural frequencies and damping can be significant both for offshore structures and for buildings in a zone of high seismic risk. Currently a majority of dynamic analysis procedures of bridge structures design are developed around the assumption that the systems studied are time-invariant and linear. While it has been repeatedly demonstrated that these assumptions are quite adequate for many applications which involve small amplitude excitations, large excitations such as that encountered during the earthquake will bring out the non-linear features of the system, and erroneous results may appear if the above assumptions are still applied.

Ren et al. (2005) pointed out that the damping property of real large cable-stayed bridges is not fully understood yet due to the complicated damping mechanisms at play. Damping is responsible for the eventual decay of free vibrations and provides an explanation for the fact that the response of a vibratory system excited at resonance does not grow without limit. In general, there are several dissipation mechanisms within a structure, the individual contributions of which are extremely difficult to assess. They can be divided into two groups: ''dissipation'' mechanisms which dissipate energy within the boundaries of the structure, and ''dispersion'' or ''radiation'' mechanisms which propagate energy away from the structure. The overall damping in the structure which comprises both mechanisms is often called ''effective damping'' and it is this damping which is actually measured as modal damping in practice. However, it is very hard to model mathematically these damping mechanisms.

There are several damping models but the most often used one is the viscous damping. Although this model is only at best an approximation of the real behaviour of the structure, it is very convenient because of its simplicity and mathematical convenience. The usual way to express viscous damping is in its modal form, i.e. by using the damping ratios defined for each mode separately. In the case of bridges, this is very convenient both for the FE modelling and the experimental measurements. In real design process of bridge structures, damping values of structures are usually taken either as constants according to the construction material used or Rayleigh damping. However, doing so is not always justified because it is only based on material property without considering dynamic system factors. Rayleigh damping is only set up for decoupling in eigenproblem computations but without clear physical justification. Moreover, it has been showed in many research papers that under forced vibration damping values are greater than those obtained in free vibration tests and increase with the increase in stress or deformation.

Previous studies (Rebelo et al. 2008, Ülker-Kaustell and Karoumi 2011) have given indications that for certain bridges damping ratio and natural frequency have a dependency on the amplitude of vibration: damping increases and frequency decreases with the increase in deformations of the structure. The natures of these nonlinearities are not well known but candidates have been suggested in the non-linear material properties of soil, concrete and non-structural elements. Hisada and Nakagawa (1956) found a change in natural frequency with amplitude while conducting vibration tests on various types of building structures up to failure. Since then, many researchers have observed the dependence of the natural frequencies on the amplitude of vibration.

Trifunac (1972) found that the natural frequencies obtained by forced vibration test of buildings were 4% lower than those obtained using ambient vibration data. Hart et al. (1973) analysed response records obtained on several buildings during the February 9, 1971 San Fernando earthquake and drew the conclusion that modal damping increased linearly with the value of the Fourier modulus amplitude at the building natural frequency. Udwadia and Trifunac (1974) presented a summary of observations of dynamic behaviour of two typical modern buildings experiencing a series of earthquakes of different magnitude during a period of about ten years. They hypothesised that frequency reduction may be due to the effects of soil-structure interaction, non-linear response of soils and/or the non-linear response of structural elements. They also examined the quantitative aspects of amplitude variations of structural characteristics and found that reductions in the apparent fundamental frequency of vibration during moderate earthquake excitations may amount to as much as 50% without being accompanied by observable damage.

Minami (1987) conducted earthquake observations and micro-tremor measurements on a 12-storey steel RC building starting shortly after its completion. Fast Fourier transform (FFT) analyses of the recorded data showed a considerable decrease in the overall stiffness of the building that was due not only to ageing but to different amplitudes of vibration as well. It was observed that the large contribution made by non-structural elements to the apparent stiffness of the entire building was lost after experiencing several earthquakes. Foutch (1978) reported that the fundamental frequencies of a steel-framed building decreased from 7% to 5% based on a 15-fold increase in the excitation force. Ellis and Jeary (1980) conducted investigations into the dynamic behaviour of tall building under the research programme of the UK's Building Research Establishment. The results have shown that both natural frequencies and damping ratios of buildings vary with the amplitude of motion.

Luco et al. (1987) examined the apparent changes of the dynamic behaviour of a nine-story reinforced concrete (RC) building to determine their plausibility and possible sources. They believed that the permanent reduction in system frequency may have resulted from loss of stiffness in both the structure and the foundation. Satake and Yokota (1996) examined vibration properties of 31 steel-structure buildings on the micro-amplitude level and large-amplitude level by performing statistical analyses for vibration test data. The results showed that the natural period becomes longer and the damping factor becomes larger for the large-amplitude level in comparison with the micro-amplitude level. Trifunac et al. (2001) presented an analysis of the amplitude and time-dependent changes of the apparent frequency of a seven-story RC hotel building. Data of recorded response to 12 earthquakes were used, representing very small, intermediate and large excitations. The results showed the apparent frequency changed from one earthquake to another. The general trend was a reduction with increasing amplitudes of motion.

Li et al. (2003) conducted full-scale measurements of wind effects on a 70 storey tall building and obtained the amplitude-dependent characteristics of damping by using the random decrement technique from the field measurements of acceleration responses. Butterworth et al. (2004) investigated the damping properties of an 11-storey RC shear-core office building based on forced vibration tests. Frequency sweep and free vibration decay tests were conducted with varying excitation amplitudes, revealing a small, approximately linear, reduction in natural frequency with increasing amplitude.

Butt and Omenzetter (2012) presented analyses of the seismic responses of two RC buildings monitored for a period of more than two years. Trends of variation of seismic response were developed by correlating the peak response acceleration at the roof level with identified frequencies and damping ratios. A general trend of decreasing frequencies was observed with increased level of response, but damping did not show any clear dependence on the response level.

Farrar et al. (2000) report the results of vibration tests conducted on the Alamosa Canyon Bridge, in which several excitation sources were investigated including multiple impact, single impact, ambient traffic (from the traffic on an adjacent bridge), test vehicle, and electro-dynamic shakers. While the authors noted that the modal frequencies and mode shapes extracted from the data of each test were consistent (i.e. not statistically different), significant changes were observed in the damping ratios which were correlated with excitation amplitude.

Zhang (2002) conducted ambient tests on a cable-stayed bridge under a relatively steady wind and temperature environment and normal traffic conditions. In total 24 hours of acceleration response time histories were recorded and then the data were divided in two-hour long intervals. Thereby the modal parameter variability due to changing traffic loading was investigated in both amplitude and frequency domain. It was found that the damping ratios are sensitive to the vibration intensity, especially when deck vibration exceeds a certain level.

Fink and Mähr (2009) reported experimental findings from a laboratory scale model of a ballasted railway bridge which supports the hypothesis that the non-linear behaviour of ballast is one of the main sources to amplitude-dependent behaviour in such structures. Ülker-Kaustell and Karoumi (2011) studied the amplitude dependency of the natural frequency and the equivalent viscous modal damping ratio of the first vertical bending mode of a ballasted, single span, concrete–steel composite railway bridge by analysing the free vibration response after the passage of a freight train using continuous wavelet transform. It was shown that for the observed range of acceleration amplitudes, a linear relation exists between both the natural frequency and the equivalent viscous modal damping ratio and the amplitude of vibration.

Though much effort has been devoted to investigate amplitude-dependent structural stiffness and damping, it should be noted that most of the studies described above focus on either buildings under earthquake and wind excitation sources or vibration response of bridges within relative small force levels. A precise understanding or quantification of amplitude-dependent stiffness and damping effect for bridge structures within relative broad loading ranges via forced vibration testing by using mechanical eccentric mass shakes has not been achieved yet.

2.4.2. Updating using sensitivity method

Zivanovic et al. (2007) investigated a foot bridge with an aim of describing the complete model updating process for civil engineering structures. A detailed FE model of the bridge was formulated. The initial model underestimated the frequencies by up to 29%. A SM-based technique was used for model updating, however, an initial attempt to model updating based on SM produced some physically meaningless results. This confirmed the conclusions drawn in an earlier study by Brownjohn and Xia (2000) that, when large differences are present between the analytical modal properties and their experimental counterparts, it may not be possible to update a model using SM. This is mainly because, when large differences are present, the key assumption that a relationship between errors in responses and changes in the parameters could be expressed only by the linear first term of the Taylor series may be unreasonable. The authors decided to manually update the analytical model first. A trial and error approach was used for manual model updating and it was found that introduction of flexible supports at the girder ends in the longitudinal direction improved the correlation and successfully reduced the maximum frequency errors between the experimental and analytical results to only 4%. After manual model updating, an automatic model updating was performed using SM. Twenty four parameters were selected for updating related to stiffness of spring supports, modulus of elasticity of the deck, slab and column plate, mass density of deck and water pipe, and height of column plate and deck. These factors had been allowed to change in different ranges during automatic model updating and the maximum range was from -50% to +50%. Finally, a physical justification of the updated parameters was provided. A similar approach and observations were made in Brownjohn et al. (2001) where a laboratory-scale damaged steel portal frame was updated using SM. Manual updating was done prior to updating by SM.

Many other studies have been performed using the SM for different types of full scale civil engineering structures. Jaishi and Ren (2005) studied a concrete-filled steel tubular arch bridge tested by ambient vibration measurements. A sensitivity study was carried out to establish the most influential parameters of the FE model for updating. The updated FE model of the bridge was able to produce an agreement between the experimental and numerical results and preserved the physical meaning of the updated parameters. Wu and Li (2004) updated the FE model of a 310 m tall TV tower based on ambient vibration measurements. Good correlations of dynamic characteristics of the tower determined from the updated FE models and the full-scale measurements were found. A comparative study was conducted considering six updating cases with different groups of updating parameters. Several approaches for estimation the updating parameters based on the pseudo-inverse method, weighted least squares method and Bayesian estimation technique were tried, and the second method was deemed to be the most effective.

Zhang et al. (2001) considered a 430 m main span double-deck cable-stayed bridge. The developed FE model was updated based on the field measured dynamic properties. A comprehensive sensitivity study to demonstrate the effects of various structural parameters was first performed and structural parameters selected for adjustment. The updated finite element model was able to produce natural frequencies in good agreement with the measured ones for low frequency modes. However, significant discrepancies were seen between the predicted and the measured frequencies for higher modes.

Skolnik et al. (2006) updated the model of a building with a special steel moment resisting frame supported on concrete caissons that had been permanently instrumented with seismic sensors. The authors used a simple model comprising a stick column with lumped masses.

Floor model updating has also been tried using SM. A lively open plan office floor occupied by the office equipment has been dynamically tested using linear shakers and updated (Pavic et al. 2007). The model updating was proved to be successful.

Although SM is a fast method to obtain the updated results, it is essentially a local optimization technique and can converge to incorrect local minima. The model has to be manually updated in some cases and even after the manual model updating the performance vary.

2.4.3. Updating using global optimisation algorithms

A GA was used by Perera and Torres (2006) for assessment and damage detection of a simulated beam structure and an experimental beam structure. Multiple damage scenarios were studied along with the effect of different noise levels on a simulated beam structure. Later, the GA was applied to a laboratory beam structure to verify its effectiveness in the damage detection and its assessment. Raich and Liszkai (2007) presented an advanced GA and applied it on simulated beam and frame structures for improving the performance of damage detection via model updating. Tu and Lu (2006) used GA to tackle the problem of insufficient measured responses by adding artificial boundary condition frequencies to the FE model. Numerical examples demonstrated the effectiveness of the proposed approach for model updating.

A GA based multiobjective optimization scheme was developed by Perera and Ruiz (2008) to detect and assess the damage in simulated structures as well as a signature bridge structure. The initial two dimensional model of the bridge was used for damage detection and model updating. The bridge frequencies were successfully identified for the first three flexural modes. However, due to the simplifications of the FE model, the torsional modes were not matched. Perera et al. (2009) also compared different multicriteria GAs for damage detection and estimation in simulated structures and a simple laboratory beam structure.

Levin and Lieven (1998) investigated both SA and GA to update a numerical model of a cantilever beam and an experimental wing plate structure. A new blended SA algorithm was proposed to improve the model updating results. An adaptive hybrid of SA and GA (He and Hwang 2006) was also successfully implemented for detecting multiple damage occurrences in beam structures to improve the convergence speed and solution quality.

Saada et al. (2008) used PSO for model updating of a beam structure, whereas Begambre and Laier (2009) proposed a hybrid PSO-simplex method for model updating of a ten-bar truss and a free-free beam. The new method performed well for model updating of the numerically simulated structures. PSO and GA (Perera et al. 2010) were also applied in a multiobjective optimisation context to damage estimation problems with modelling errors. Marwala (2010) applied different GOAs to a simple beam and an unsymmetrical H-shaped structure and found that PSO gave best results as compared to other GOAs.

Coupled local minimiser method, applicable to global optimization of a function, was proposed by Teughels et al. (2003) for detection of multiple minima in a model updating problem. A population of local minimisers set up a cooperative search mechanism and were coupled using synchronization constraints. The method was successfully applied to a FE model updating problem in which damage was detected in a RC beam. Bakir et al. (2008) also proposed a similar but improved technique to correctly identify damage in a complex structure. The improved method was compared with the Levenberg–Marquardt algorithm, sequential quadratic programming and Gauss–Newton methods, and it was found that it gave better results.

In another study by Zarate and Caicedo (2008), multiple plausible solutions to model updating problem were identified for a full scale bridge. The authors selected the solution which had a better physical justification but higher objective function value instead of the global minimum.

A novel evolutionary algorithm which is able to identify the local and global optimal solutions was proposed by Caicedo and Yun (2011). This was accomplished by introducing two new operators in GA. The algorithm was used on the complex simulated numerical example of a three dimensional steel frame structure and several parameters were updated. Two minima were correctly detected by the proposed algorithm, where the local minimum had, due to noise, a lower objective function value than the global minimum. The proposed technique could detect multiple minima but did not guide the analyst to decide the correct solution.

It can be noticed form this literature survey that most research efforts have been made towards damage detection and assessment of simulated structures or simple laboratory scale structures. Only limited studies have reported algorithms for multiple alterative solutions. Moreover, updating of full scale structures still remains a challenging and poorly explored topic. GOAs have received less attention especially for complex updating problems. Many different sets of parameters in the initial FE model and different types of modal data available from the experiment may lead to potentially different solutions. Even if the modal values and their analytical counterparts match reasonably, the right solution is left to the judgment and experience of the analyst.

2.5. Summary

The literature review presented in this chapter comprised discussions of modal dynamic testing and methods for correlating experimental and analytical data. Also, a representative selection from previously published research related to applications of modal testing and model updating were discussed.

2.6. References

Abdel-Ghaffar, A.M., & Housner, G.W. (1978), Ambient vibration tests of suspension bridge, Journal of the Engineering Mechanics Division, ASCE, 104, 983-999.

Abdel-Ghaffar, A.M., & Scanlan, R.H. (1985), Ambient vibration studies of Golden Gate Bridge. I: Suspended structure, Journal of Engineering Mechanics, ASCE, 111, 463–482.

Baker, T., & Marsh, E. (1996), Error localization for machine tool structures, Proceedings of The International Society for Optical Engineering, 761-738.

Bakir, P.G., Reynders, E., & De Roeck, G.D. (2008), An improved finite element model updating method by the global optimization technique 'Coupled Local Minimizers', Computers and Structures, 86, 1339-1352.

Begambre, O., & Laier, J.E. (2009), A hybrid particle swarm optimization-simplex algorithm (PSOS) for structural damage identification, Advances in Engineering Software, 40, 883-891.

Black, C., & Ventura, C. (1999), Analytical and experimental study of a three span bridge in Alberta, Canada, Proceedings of IMAC XVII: 17th International Modal Analysis Conference, 1737-1743.

Brownjohn, J.M.W., Lee, J., & Cheong, B. (1999), Dynamic performance of a curved cable-stayed bridge, Engineering Structures, 21, 1015–1027.

Brownjohn, J.M.W., & Xia, P.Q. (2000), Dynamic assessment of curved cable-stayed bridge by model updating, Journal of Structural Engineering, ASCE, 126, 252-260.

Brownjohn, J.M.W., Xia, P.Q., Hao, H., & Xia, Y. (2001), Civil structure condition assessment by FE model updating: methodology and case studies, Finite Elements in Analysis and Design, 37, 761-775.

Butt, F., & Omenzetter, P. (2012), Seismic response trends evaluation via long term monitoring and finite element model updating of an RC building including soil-structure interaction, Proceedings of the SPIE Conference on Nondestructive

Characterization for Composite Materials, Aerospace Engineering, Civil Infrastructure, and Homeland Security 2012, 834704:1-12.

Butterworth, J., Lee, J.H., & Davidson, B. (2004), Experimental determination of modal damping from full scale testing, Proceedings of the 13th World Conference on Earthquake Engineering, 1-15.

Caicedo, J.M., & Yun, G. (2011), A novel evolutionary algorithm for identifying multiple alternative solutions in model updating, Structural Health Monitoring, 10, 491-501.

Causevic, M.S. (1987), Mathematical modelling and full-scale forced vibration testing of a reinforced concrete structure, Engineering Structures, 9, 2-8.

Chen, G. (2001), FE model validation for structural dynamics, University of London, London.

Chen, G., & Ewins, D. (2004), FE model verification for structural dynamics with vector projection, Mechanical Systems and Signal Processing, 18, 739-757.

Chopra, A.K. (2007), Dynamics of structures: theory and applications to earthquake engineering, Prentice Hall, Upper Saddle River, NJ.

Clarence, W.D.S., & De Silva, C.W. (2007), Vibration: fundamentals and practice, Taylor & Francis, Boca Raton, FL.

Crouse, C.B., Hushmand, B. & Martin, G. R. (1987), Dynamic soil-structure interaction of a single-span bridge, Earthquake Engineering and Structural Dynamics, 15, 711-729.

Cunha, A., Caetano, E., & Delgado, R. (2001), Dynamic tests on large cable-stayed bridge, Journal of Bridge Engineering, ASCE, 6, 54–62.

De Sortis, A., Antonacci, E., & Vestroni, F. (2005), Dynamic identification of a masonry building using forced vibration tests, Engineering Structures, 27, 155-165.

Deb, K. (1998), Optimization for engineering design: algorithms and examples, Prentice-Hall of India, New Delhi.

Deb, K. (2001), Multi-objective optimization using evolutionary algorithms, Wiley, Chichester.

Deb, K., Chakroborty, P., Iyengar, N.G.R., & Gupta, S.K. (2007), Advances in computational optimization and its applications, Universities Press, New Delhi.

Deger, Y., Cantieni, R., Pietrzko, S., Ruecker, W., & Rohrmann R. (1995). Modal analysis of a highway bridge: experiment, finite element analysis and link, Proceedings of IMAC XIII: 13th International Modal Analysis Conference, 1141-1149.

Delgado, R., Cunha, A., Caetano, E., & Calcada, R. (1998), Dynamic tests of Vasco da Gama Bridge, University of Porto, Porto.

Ecke, W., Peters, K.J., & Meyendorf, N.G. (2008), Smart sensor phenomena, technology, networks, and systems, SPIE, Bellingham, WA.

Ellis, B.R. (1980), An assessment of the accuracy of predicting the fundamental natural frequencies of buildings and the implications concerning the dynamic analysis of structures, Proceedings of the Institution of Civil Engineers, 69, 763-776.

Ellis, B.R., & Jeary, A.P. (1980), Recent work on the dynamic behaviour of tall buildings at various amplitudes, Proceedings of the 7th World Conference on Earthquake Engineering, 313-316.

Ewins, D.J. (2000), Modal testing: theory, practice and application, Research Studies Press, Baldock.

Farrar, C.R., Cornwell, P.J., Doebling, S.W., & Prime, M.B. (2000), Structural health monitoring studies of the Alamosa Canyon and I-40 bridges, Los Alamos National Laboratory, Los Alamos, NM.

Fink, J., & Mähr, T. (2009), Influence of ballast superstructure on the dynamics of slender railway bridge, Proceedings of Nordic Steel Construction Conference 2009, 81-88.

Foutch, D.S.A. (1987), The vibrational characteristics of a twelve-storey steel frame building, Earthquake Engineering and Structural Dynamics, 6, 265-294.

Friswell, M.I., & Mottershead, J.E. (1995), Finite element model updating in structural dynamics, Kluwer, Dordrecht.

Gentile, C., & Martinez y Cabrera, F. (2004), Dynamic performance of twin curved cable-stayed bridges, Earthquake Engineering and Structural Dynamics, 33, 15–34.

Green, M.F. (1995), Modal test methods for bridges: a review, Proceedings of IMAC XIII: 13th International Modal Analysis Conference, 552-558.

Harik, I.E. (1997), Free and ambient vibration of Brent-Spence Bridge, Journal Structural Engineering, ASCE, 123, 1262–1268.

Haritos, N., Khalaf, H., & Chalko, T. (1995), Modal testing of a skewed reinforced concrete bridge, Proceedings of IMAC XIII: 13th International Modal Analysis Conference, 703-709.

Hart, G.C., Lew, M., & Di Julio, R. (1973), High-rise building response: damping and period nonlinearities, Proceedings of the 5th World Conference on Earthquake Engineering, 1440-1444.

He, R.S., & Hwang, S.F. (2006), Damage detection by an adaptive real-parameter simulated annealing genetic algorithm, Computers and Structures, 84, 2231-2243.

Hisada, T., & Nakagawa, K. (1956), Vibration tests on various types of building structures up to failure, Proceedings of 1st World Conference of Earthquake Engineering.

Horst, R., Pardalos, P.M., & Thoai, N.V. (2000), Introduction to global optimization, Kluwer, Dordrecht.

Ivanovic, S.S., Trifunac, M.D., Novikova, E.I., Gladkov, A.A., & Todorovska, M.I. (2000), Ambient vibration tests of a seven-story reinforced concrete building in Van Nuys, California, damaged by the 1994 Northridge earthquake, Soil Dynamics and Earthquake Engineering, 19, 391-411.

Jaishi, B., & Ren, W.X. (2005), Structural finite element model updating using ambient vibration test results, Journal of Structural Engineering, ASCE, 131, 617-628.

Kuribayashi, E. & Iwasaki, T. (1973), Dynamic properties of highway bridges, Proceedings of 5th World Conference on Earthquake Engineering, 938-941.

Levin, R.I., & Lieven, N.A.J. (1998), Dynamic finite element model updating using simulated annealing and genetic algorithms, Mechanical Systems and Signal Processing, 12, 91-120.

Li, Q.S., Yang, K., Wong, C.K., & Jeary, A.P. (2003), The effect of amplitude-dependent damping on wind-induced vibrations of a super tall building, Journal of Wind Engineering and Industrial Aerodynamics, 91, 1175-1198.

Link, M. (1991), Comparison of procedures for localizing and correcting errors in computational models using test data, Proceedings of IMAC IX: 9th International Modal Analysis Conference, 479-485.

Link, M., & Conic, M. (2000), Combining adaptive FE mesh refinement and model parameter updating, Proceedings of the 18th International Modal Analysis Conference, 584-588.

Link, J., Rohrmann, R.G., & Pietrzko, S. (1996), Experience with automated procedures for adjusting the finite element model of a complex highway bridge to experimental modal data, Proceedings of IMAC XIV: 14th International Modal Analysis Conference, 218-225.

Luco, J.E., Trifunac, M.D., & Wong, H.L. (1987), On the apparent change in dynamic behavior of a nine-story reinforced concrete building, Bulletin of the Seismological Society of America, 77, 1961-1983.

Maia, N.M., Reynier, M., Ladeveze, P., & Cachan, E. (1994), Error localization for updating finite element models using frequency-response-functions, Proceedings of The International Society for Optical Engineering, 1299-1299.

Marwala, T. (2010), Finite element model updating using computational intelligence techniques, Springer, London.

Minami, T. (1987), Stiffness deterioration measured on a steel reinforced concrete building, Earthquake Engineering and Structural Dynamics, 15, 697-709.

Moon, F.L., & Aktan, A.E. (2006), Impacts of epistemic (bias) uncertainty on structural identification of constructed (civil) systems, Shock and Vibration Digest, 38, 399-420.

Mottershead, J., & Friswell, M. (1993), Model updating in structural dynamics: a survey, Journal of Sound and Vibration, 167, 347-375.

Ohba, R. (1992), Intelligent sensor technology, Wiley, Chichester.

Ohlsson, S. (1986), Modal testing of the Tjorn Bridge, Proceedings of IMAC IV: 4th International Modal Analysis Conference, 599-605.

Pan, Q., Grimmelsman, K., Moon, F., & Aktan, E. (2010), Mitigating epistemic uncertainty in structural identification: case study for a long-span steel arch bridge, Journal of Structural Engineering, ASCE, 137, 1-13.

Pavic, A., Miskovic, Z., & Reynolds, P. (2007), Modal testing and finite-element model updating of a lively open-plan composite building floor, Journal of Structural Engineering, ASCE, 133, 550-558.

Perera, R., Fang, S.E., & Ruiz, A. (2010), Application of particle swarm optimization and genetic algorithms to multiobjective damage identification inverse problems with modelling errors, Meccanica, 45, 723-734.

Perera, R., & Ruiz, A. (2008), A multistage FE updating procedure for damage identification in large-scale structures based on multiobjective evolutionary optimization, Mechanical Systems and Signal Processing, 22, 970-991.

Perera, R., Ruiz, A., & Manzano, C. (2009), Performance assessment of multicriteria damage identification genetic algorithms, Computers and Structures, 87, 120-127.

Perera, R., & Torres, R. (2006), Structural damage detection via modal data with genetic algorithms, Journal of Structural Engineering, ASCE, 132, 1491-1501.

Raich, A.M., & Liszkai, T.R. (2007), Improving the performance of structural damage detection methods using advanced genetic algorithms, Journal of Structural Engineering, ASCE, 133, 449-461.

Rebelo, C., Simões da Silva, L., Rigueiro, C., & Pircher, M. (2008), Dynamic behaviour of twin single-span ballasted railway viaducts - field measurements and modal identification, Engineering Structures, 30, 2460-2469.

Ren, W.X., Blandford, G.E., & Harik, I.E. (2004a), Roebling suspension bridge. I: Finite-element model and free vibration response, Journal of Bridge Engineering, ASCE, 9, 110-118.

Ren, W.X., Peng, X.L., & Lin, Y. Q. (2005), Baseline finite element modeling of a large span cable-stayed bridge through field ambient vibration tests, Computers and Structures, 83, 536-550.

Ren, W.X., Zhao, T., & Harik, I. E. (2004b), Experimental and analytical modal analysis of steel arch bridge, Journal of Structural Engineering, ASCE, 130, 1022–1031.

Robert Nicoud, Y., Raphael, B., Burdet, O., & Smith, I. (2005), Model identification of bridges using measurement data, Computer Aided Civil and Infrastructure Engineering, 20, 118-131.

Saada, M.M., Arafa, M.H., & Nassef, A.O. (2008), Finite element model updating approach to damage identification in beams using particle swarm optimization, Proceedings of the 34th Design Automation Conference, ASME, 522-531.

Salane, H. J., & Baldwin, J.W. (1990). Identification of modal properties of bridges, Journal of Structural Engineering, ASCE, 116, 2008-2021.

Salawu, O.S., & Williams, C. (1995), Review of full-scale dynamic testing of bridge structures, Engineering Structures, 17, 113-121.

Sanayei, M., Arya, B., Santini, E.M., & Wadia-Fascetti, S. (2001), Significance of modeling error in structural parameter estimation, Computer Aided Civil and Infrastructure Engineering, 16, 12-27.

Satake, N., & Yokota, H. (1996), Evaluation of vibration properties of high-rise steel buildings using data of vibration tests and earthquake observations, Journal of Wind Engineering and Industrial Aerodynamics, 59, 265-282.

Shelley, S.J., Lee, K.L., Aksel, T., & Aktan, A.E. (1995), Active-vibration studies on highway bridge, Journal of Structural Engineering, ASCE, 121, 1306-1312.

Shepherd, R., & Charleson, A.W. (1971), Experimental determination of the dynamic properties of a bridge substructure, Bulletin of the Seismological Society of America, 61, 1529-1548.

Skolnik, D., Lei, Y., Yu, E., & Wallace, J.W. (2006), Identification, model updating, and response prediction of an instrumented 15-story steel-frame building, Earthquake Spectra, 22, 781-802.

Tebaldi, A., Dos Santos Coelho, L., & Lopes Jr, V. (2006), Detection of damage in intelligent structures using optimization by a particle swarm: fundamentals and case studies, Controle y Automação, 17, 312-330.

Teughels, A., De Roeck, G., & Suykens, J.A.K. (2003), Global optimization by coupled local minimizers and its application to FE model updating, Computers and Structures, 81, 2337-2351.

Trifunac, M.D. (1972), Comparisons between ambient and forced vibration experiments, Earthquake Engineering and Structural Dynamics, 1, 133-150.

Trifunac, M.D., Ivanovic, S.S., & Todorovska, M.I. (2001), Apparent periods of a building. I: Fourier analysis, Journal of Structural Engineering, ASCE, 127, 517-526.

Tu, Z., & Lu, Y. (2008), FE model updating using artificial boundary conditions with genetic algorithms, Computers and Structures, 86, 714-727.

Udwadia, F.E., & Trifunac, M.D. (1974), Time and amplitude dependent response of structures, Earthquake Engineering and Structural Dynamics, 2, 359-378.

Ülker-Kaustell, M., & Karoumi, R. (2011), Application of the continuous wavelet transform on the free vibrations of a steel-concrete composite railway bridge, Engineering Structures, 33, 911-919.

Ventura, C.E., Liam Finn, W.D., Lord, J.F., & Fujita, N. (2003), Dynamic characteristics of a base isolated building from ambient vibration measurements and low level earthquake shaking, Soil Dynamics and Earthquake Engineering, 23, 313-322.

Wilson, J.S. (2005), Sensor technology handbook, Newnes, Burlington, MA.

Wu, J.R., & Li, Q.S. (2004), Finite element model updating for a high-rise structure based on ambient vibration measurements, Engineering Structures, 26, 979-990.

Yu, E., Taciroglu, E., & Wallace, J.W. (2007), Parameter identification of framed structures using an improved finite element model-updating method. Part I: Formulation and verification, Earthquake Engineering and Structural Dynamics, 36, 619-639.

Zarate, B.A., & Caicedo, J.M. (2008), Finite element model updating: multiple alternatives, Engineering Structures, 30, 3724-3730.

Zhang, Q.W. (2002), Variability in dynamic properties of cable-stayed bridge under routine traffic conditions, Journal of Tongji University, 30, 61-666.

Zhang, Q.W., Chang, T.Y.P., & Chang, C.C. (2001), Finite-element model updating for the Kap Shui Mun cable-stayed bridge, Journal of Bridge Engineering, ASCE, 6, 285-294.

Zivanovic, S., Pavic, A., & Reynolds, P. (2007), Finite element modelling and updating of a lively footbridge: the complete process, Journal of Sound and Vibration, 301, 126-145.

CHAPTER 3

THEORY

3.1. Introduction

This chapter present an overview of the theoretical concepts, approaches and methods used later in the research project. They can be grouped into two categories, namely these related to experimental modal analysis and system identification, and those related to model updating including SM and GOAs.

3.2. System identification concepts and methods

In this chapter, the following system identification concepts and methods are explained:

- Spectral analysis and frequency response function (FRF)
- Peak peaking (PP)
- Half-power
- Frequency domain decomposition (FDD) and enhanced frequency domain decomposition (EFDD)
- Subspace system identification (SSI)
- Natural excitation technique – eigenvalue realisation algorithm (NExT-ERA).

3.2.1. Spectral analysis and frequency response function

For system analysis and identification in the frequency domain, power spectra and FRFs are frequently used. To transform signals from the time domain to the frequency domain, a Fourier transform is performed (Friswell and Mottershead 1995). For a continuous time signal $x(t)$, its Fourier transform is determined as

$$X(f) = \int_{-\infty}^{\infty} x(t) e^{-j2\pi ft} dt \tag{3.1}$$

where f is frequency, $X(f)$ is the Fourier transform of $x(t)$, and j is the imaginary unit. The inverse Fourier transform is defined as

$$x(t) = \int_{-\infty}^{\infty} X(f) e^{j2\pi ft} df \tag{3.2}$$

For a more practical case of a discrete signal $x(k)$, its discrete Fourier transform (DFT) $X(n)$ is defined as

$$X(n) = \sum_{k=0}^{N-1} x(k) e^{-j2\pi kn/N} \tag{3.3}$$

where n is the discrete frequency, k is the discrete time and N is the total length of discrete signal. The inverse DFT (IDFT) is defined as

$$x(k) = \frac{1}{N} \sum_{n=0}^{N-1} X(n) e^{j2\pi kn/N} \tag{3.4}$$

The two-sided cross spectral density (CSD) S_{xy} between system response $x(k)$ and input $u(k)$ can be calculated using their discrete Fourier transforms $X(n)$ and $U(n)$ as

$$S_{xu}(f) = \frac{X(f) U^{*}(f)}{N^2} \tag{3.5}$$

where '*' denotes the complex conjugate. For a single signal, e.g. $x(t)$, its auto spectral density (ASD) S_{xx} can be obtained as

$$S_{xx}(f) = \frac{X(f) X^{*}(f)}{N^2} \tag{3.6}$$

FRF is the ratio of response to input at a given frequency and can be found using two alternative formulations:

$$H_1(f) = \frac{S_{ux}(f)}{S_{uu}(f)} \tag{3.7}$$

$$H_2(f) = \frac{S_{xx}(f)}{S_{xu}(f)} \tag{3.8}$$

While theoretically both of the above formulas should give the same result, in real world testing exercises the presence of noise and unmeasured input cause them to differ. Their ratio is referred to as coherence:

$$\gamma^2(f) = \frac{H_2(f)}{H_1(f)} \tag{3.9}$$

Coherence is a measure of correlation between input and output. It can take values between 0 and 1. In forced modal testing, high coherence values, typically above 0.9, help to distinguished true modes from spurious ones.

3.2.2. Peak picking

PP (Bendat and Piersol 1993) is probably the simplest, yet very useful, quick and practical, system identification method. In the case of measured input, it starts with the calculation of the FRF (as explained in Chapter 3.2.1). Modal frequencies are found from the peaks in the FRF magnitude plot. In case of operational modal analysis (OMA), only the ASD is available and is used instead of FRF. This is exact only in the case of input being uncorrelated white noise, but many ambient sources of excitation satisfy that assumption from a practical point of view.

3.2.3. Half-power

The half-power bandwidth method (Heylen et al. 1997) is a simple method for calculating damping ratios directly from the FRF. An estimate of the damping ratio can be obtained from examination of the acceleration response curve as shown in Figure 3.1. The frequencies f_1 and f_2 at which the FRF is $1/\sqrt{2}$ of the peak value can be used to calculate the damping ratio using

$$\xi = \frac{f_2 - f_1}{f_2 + f_1} \tag{3.10}$$

At these frequencies, the power is half the peak value, hence the name of the method. A good estimate of the damping ratio requires good resolution of the response curve around the half-power frequencies.

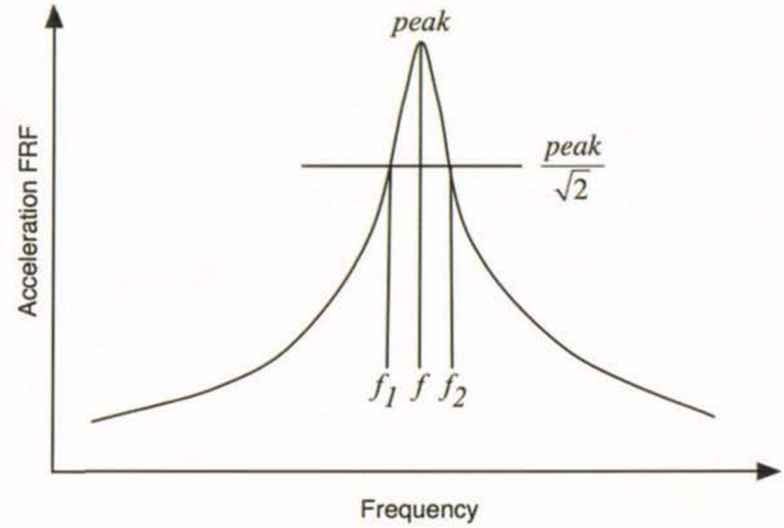

Figure 3.1. Half-power method.

3.2.4. Frequency domain decomposition and enhanced frequency domain decomposition

The EFDD technique (Jacobsen et al. 2007) is an extension to the Frequency Domain Decomposition (FDD) technique. FDD (Brincker et al. 2000) is a basic technique that is extremely easy to use. It can simply pick the modes by locating the peaks in the singular value decomposition (SVD) plots of the ASD/CSD of responses. As the FDD technique is based on using a single frequency line from the FFT analysis, the accuracy of the estimated natural frequency and mode shape depends on the FFT resolution and no modal damping is calculated. Compared to FDD, the EFDD gives an improved estimate of both the natural frequencies and mode shapes and also enables damping estimation.

If we denote by $\mathbf{G}_{uu}(\omega)$ the $r \times r$ ASD/CSD matrix of the inputs, by r the number of inputs, by $\mathbf{G}_{yy}(\omega)$ the $m \times m$ ASD/CSD matrix of the responses, by m the number of responses, by $\mathbf{H}(\omega)$ the $m \times r$ FRF matrix, and by superscripts '*' and '^{T}' denote complex conjugate and transpose, respectively, then the relationship between the unknown inputs and the measured responses can be expressed as:

$$\mathbf{G}_{yy}(\omega) = \mathbf{H}^*(\omega)\mathbf{G}_{uu}(\omega)\mathbf{H}^{*T}(\omega) \qquad (3.11)$$

For OMA, we also have to make use of the central assumption that the inputs are random both in time and space and have zero mean white noise distributions so that their spectral densities form a constant matrix. After some mathematical manipulations the output ASD/CSD matrix can be reduced to a pole/residue form as follows:

$$\mathbf{G}_{yy}(\omega)=\sum_{k=1}^{m}\left(\frac{\mathbf{A}_k}{j\omega-\lambda_k}+\frac{\mathbf{A}_k^*}{j\omega-\lambda_k^*}+\frac{\mathbf{B}_k}{-j\omega-\lambda_k}+\frac{\mathbf{B}_k^*}{-j\omega-\lambda_k^*}\right) \tag{3.12}$$

where $\mathbf{A}_k$ is the k-th residue matrix of the output ASD and λ_k is the k-th eigenvalue. Considering a lightly damped system and that the contribution of the modes at a particular frequency is limited to only one, the response ASD/CSD matrix can be written in the following final form:

$$\mathbf{G}_{yy}(\omega)=\sum_{k\in Sub(\omega)}\left(\frac{d_k\boldsymbol{\varphi}_k\boldsymbol{\varphi}_k^{*T}}{j\omega-\lambda_k}+\frac{d_k^*\boldsymbol{\varphi}_k^*\boldsymbol{\varphi}_k^T}{j\omega-\lambda_k^*}\right) \tag{3.13}$$

where d_k is a scalar constant and $\boldsymbol{\varphi}_k$ is the k-th mode shape vector, and $Sub(\omega)$ is the narrow frequency range where only the k-th mode contributes to the response. Performing SVD of the output ASD/CSD matrix at discrete frequencies $\omega = \omega_i$ one obtains:

$$\mathbf{G}_{yy}(j\omega_i)=\mathbf{T}_i\boldsymbol{\Sigma}_i\mathbf{T}_i^T \tag{3.14}$$

where matrix $\mathbf{T}_i$ is a unitary matrix holding the singular vectors $\mathbf{t}_{ij}$, and $\boldsymbol{\Sigma}_i$ is a diagonal matrix holding singular values σ_{ij}. Near a peak corresponding to the k-th mode in the spectrum, only the k-th mode is dominant, and the ASD/CSD matrix can be approximated by matrix of rank one as:

$$\mathbf{G}_{yy}(j\omega_k)\cong\sigma_{k1}\mathbf{t}_{k1}\mathbf{t}_{k1}^T \tag{3.15}$$

The first singular vector at the k-th resonance is an estimate of the k-th mode shape:

$$\boldsymbol{\varphi}_k\cong\mathbf{t}_{k1} \tag{3.16}$$

In FDD, modal frequencies can be identified from the peaks of the singular values vs. frequency plots, while the corresponding singular vectors give the mode shapes. In EFDD, the ASD/CSD identified around a resonance peak (Equation 3.13) is taken back to the time domain using IDFT (Equation 3.4). The natural frequency is obtained by determining the number of zero-crossing as a function of time, and the damping by the logarithmic decrement of the resulting time domain function (Chopra 2007). Alternatively, damping ratio can be found using the half-power method described in Chapter 3.2.3.

3.2.5. Subspace system identification

SSI is a time domain SI method. The core of many time domain identification algorithms is a state space model which gives a relationship between input and output of an unknown system to be identified. The state space model (Ljung 1987) is one of the most popular models of dynamical systems. SSI is a powerful technique for modal analysis in the time domain to estimate the unknown matrices of the state space model and is summarized here following Van Overschee and De Moor (1996).

At any arbitrary time step k, a discrete time state space model is given by

$$\mathbf{x}_{k+1} = \mathbf{A}\mathbf{x}_k + \mathbf{B}\mathbf{u}_k + \boldsymbol{\omega}_k \tag{3.17}$$

$$\mathbf{y}_k = \mathbf{C}\mathbf{x}_k + \mathbf{D}\mathbf{u}_k + \mathbf{v}_k \tag{3.18}$$

where $\mathbf{x}_k$, $\mathbf{u}_k$ and $\mathbf{y}_k$ are state, input and output vectors at time k, respectively, **A**, **B**, **C** and **D** are system, input, output and feedthrough matrices, respectively, to be estimated by the identification algorithm, and $\boldsymbol{\omega}_k$ and $\mathbf{v}_k$ are the process and measurement noises, respectively. SSI algorithms determine these matrices to estimate the unknown system characteristics such as natural frequencies, mode shapes and viscous damping ratios.

The SSI algorithm described below can be applied to output only or input–output identification problems. The algorithm starts with assembling block Hankel matrices from the input and output sequence. The block Hankel matrix for the input sequence is given by

$$\mathbf{U}_{0/2i-1} = \left[\begin{array}{cccc} \mathbf{u}_0 & \mathbf{u}_1 & \cdots & \mathbf{u}_{j-1} \\ \mathbf{u}_1 & \mathbf{u}_2 & \cdots & \mathbf{u}_j \\ \cdots & \cdots & \cdots & \cdots \\ \mathbf{u}_{i-1} & \mathbf{u}_i & \cdots & \mathbf{u}_{i+j-2} \\ \hline \mathbf{u}_i & \mathbf{u}_{i+1} & \cdots & \mathbf{u}_{i+j-1} \\ \cdots & \cdots & \cdots & \cdots \\ \mathbf{u}_{2i-1} & \mathbf{u}_{2i} & \cdots & \mathbf{u}_{2i+j-2} \end{array}\right] = \begin{bmatrix} \mathbf{U}_p \\ \mathbf{U}_f \end{bmatrix} \tag{3.19}$$

The Hankel matrix can be divided into the past $\mathbf{U}_p$ and future $\mathbf{U}_f$ parts. The value of index i separating the past from the future should be greater than the maximum order of the system to be identified. The value of j should be chosen such that $2i+j-2$ does not exceed the input and output sequence length. The block Hankel matrix for output **Y** can also be constructed in a similar way and partitioned into the past $\mathbf{Y}_p$ and future $\mathbf{Y}_f$ parts.

The combined matrix of past input and output sequence is defined as:

$$\mathbf{W}_p = \begin{bmatrix} \mathbf{U}_p & \mathbf{Y}_p \end{bmatrix} \tag{3.20}$$

The next step is to compute the oblique projection $\mathbf{Ob}_i$ of the row space of $\mathbf{Y}_f$ along row space of $\mathbf{U}_f$ on row space of $\mathbf{W}_p$:

$$\mathbf{Ob}_i = \mathbf{Y}_f /_{\mathbf{U}_f} \mathbf{W}_p = \mathbf{Y}_f \begin{bmatrix} \mathbf{W}_p^T & \mathbf{U}_f^T \end{bmatrix} \left[\begin{bmatrix} \mathbf{W}_p \mathbf{W}_p^T & \mathbf{W}_p \mathbf{U}_f^T \\ \mathbf{U}_f \mathbf{W}_p^T & \mathbf{U}_f \mathbf{U}_f^T \end{bmatrix}^+ \right]_{firt\ r\ columns} \mathbf{W}_p \tag{3.21}$$

where superscript '+' denotes the Moore-Penrose matrix inverse and r is the number of columns in $\mathbf{W}_p$.

It can be shown that the oblique projection is also the product of extended observability matrix $\mathbf{\Gamma}_i$ and state sequence $\mathbf{X}_i$:

$$\mathbf{Ob}_i = \mathbf{\Gamma}_i \mathbf{X}_i = \begin{bmatrix} \mathbf{C}^T & (\mathbf{CA})^T & \ldots & (\mathbf{CA}^{i-1})^T \end{bmatrix}^T \begin{bmatrix} \mathbf{x}_i & \mathbf{x}_{i+1} & \ldots & \mathbf{x}_{i+j-1} \end{bmatrix} \tag{3.22}$$

The extended observability matrix $\mathbf{\Gamma}_i$ and state sequence $\mathbf{X}_i$ can be calculated by singular value decomposition of $\mathbf{Ob}_i$:

$$\mathbf{Ob}_i = \mathbf{T\Sigma V}^T \tag{3.23}$$

where $\mathbf{T}$ and $\mathbf{V}$ are unitary matrices of singular vectors, and $\mathbf{\Sigma}$ is a diagonal matrix of singular values. The extended observability matrix $\mathbf{\Gamma}_i$ can be determined as

$$\mathbf{\Gamma}_i = \mathbf{T\Sigma}^{1/2} \tag{3.24}$$

The state sequence is the remaining half of the decomposition and is given by

$$\mathbf{X}_i = \mathbf{\Sigma}^{1/2}\mathbf{V}^T \tag{3.25}$$

System matrices $\mathbf{A}$ and $\mathbf{C}$, introduced in Equations 3.17 and 3.18, can be determined from the extended observability matrix $\mathbf{\Gamma}_i$. To obtain matrix $\mathbf{A}$, it is important to recognize the following shifting property of the extended observability matrix:

$$\mathbf{\Gamma}_i \mathbf{A} = \overline{\mathbf{\Gamma}}_i \tag{3.26}$$

where $\overline{\mathbf{\Gamma}}_i$ is obtained from the extended observability matrix by removing the first rows corresponding to the number of outputs. Matrix $\mathbf{A}$ can now be found using the pseudo-inverse of the extended observability matrix $\mathbf{\Gamma}_i^+$ as follows:

$$\mathbf{A} = \mathbf{\Gamma}_i^+ \overline{\mathbf{\Gamma}}_i \tag{3.27}$$

Matrix $\mathbf{C}$ can be determined by taking the first rows of the observability matrix corresponding to the number of system outputs (see Equation 3.22).

Matrices **A** and **C** can now be used to determine the natural frequencies, mode shapes and damping ratios. The natural frequencies and damping ratios can be extracted from the imaginary and real parts of the eigenvalues of $\mathbf{A}_c$, the continuous time equivalent of matrix **A**. Conversion to the continuous time matrix can be achieved using:

$$\mathbf{A}_c = \frac{\ln(\mathbf{A})}{\Delta t} \tag{3.28}$$

where Δt is the time step. The system eigenproperties are calculated from the complex eigenvalues λ_i and eigenvectors $\boldsymbol{\psi}_i$ of matrix $\mathbf{A}_c$. With the assumption of nearly classical and small damping, the modal properties can be calculated as (Alvin and Park 1994, Skolnik et al. 2006):

$$f_i = |\lambda_i| / 2\pi \tag{3.29}$$

$$\xi_i = -\frac{\mathrm{Re}(\lambda_i)}{2\pi f_i} \tag{3.30}$$

$$\boldsymbol{\varphi}_i = \mathbf{C}\boldsymbol{\psi}_i \tag{3.31}$$

where f_i is the i-th modal frequency in Hz, ξ_i is the i-th damping ratio, $\boldsymbol{\varphi}_i$ is the i-th mode shape, and Re denotes the real part of a complex variable. Often the obtained mode shapes are complex, but the following transformation (Friswell and Mottershead 1995) can be applied to convert to real mode shapes:

$$\boldsymbol{\Phi}_{real} = \mathrm{Re}\left(\boldsymbol{\Phi}_{comp}\right) + \mathrm{Im}\left(\boldsymbol{\Phi}_{comp}\right)\mathrm{Re}\left(\boldsymbol{\Phi}_{comp}\right)^{+}\mathrm{Im}\left(\boldsymbol{\Phi}_{comp}\right) \tag{3.32}$$

where subscripts *real* and *comp* denote the matrix of real and complex modes, and Im denotes the imaginary part.

The Numerical algorithm for Subspace State Space System Identification (N4SID) (Van Overschee and De Moor 1996), comprising a useful variety of subspace methods, has been used in this study for identification of modal properties.

3.2.6. Natural excitation technique – eigenvalue realisation algorithm

NExT was developed by James et al. (1993) as part of a study to determine the modal parameters of a wind turbine using ambient responses. It is a time domain technique. Its basic principle is that the cross correlation function (CCF) between two sets of response data measured on a structure that has been excited by ambient sources has the same analytical form as the impulse response function (or the free vibration response) of the structure. The following is a brief explanation of the main concepts.

The response $x_{ik}(t)$ at location i resulting from an input force $f_k(t)$ at location k can be calculated as:

$$x_{ik}(t) = \sum_{r=1}^{m} \varphi_{ri}\varphi_{rk} \int_{-\infty}^{t} f_k(\tau) g_r(t-\tau) d\tau \qquad (3.33)$$

where

$$g_r(t) = \frac{1}{m_r \omega_{d,r}} e^{-\xi_r \omega_{0,r} t} \sin\left(\omega_{d,r}\right) \qquad (3.34)$$

is the impulse response function associated with mode r. In Equation 3.33, φ_r is the r-th mode shape vector, $\omega_{d,r}$ is the r-th circular damped natural frequency, m_r is the r-th modal mass, and N denotes the total number of modes considered, respectively. When $f_k(t)$ is a Dirac delta function, e.g. a pure impulse, Equation 3.33 yields:

$$x_{ik}\left(t\right) = \sum_{r=1}^{N} \frac{\varphi_{ri}\varphi_{rk}}{m_r \omega_{d,r}} e^{-\xi_r \omega_{0,r} t} \sin\left(\omega_{dr} t\right) \qquad (3.35)$$

Assuming that $f_k(t)$ is a random white noise function, the following definition of CCF between the responses at point i and p, excited by a force at point k, is employed:

$$R_{ipk}(\tau) = E\left[x_{ik}\left(t+\tau\right) x_{pk}\left(t\right)\right] \qquad (3.36)$$

The CCF between two ambient responses can therefore be calculated as:

$$R_{ipk}\left(\tau\right) = \sum_{r=1}^{N}\sum_{s=1}^{N} \varphi_{ri}\varphi_{rk}\varphi_{sp}\varphi_{sk} \int_{-\infty}^{t}\int_{-\infty}^{t+T} g_r\left(t+\tau-\sigma\right) g_s(t-\sigma) E\left[f_k(\sigma) f_k(\lambda)\right] d\sigma d\lambda \qquad (3.37)$$

Then, by applying the following property of white noise:

$$E\left[f_k(\sigma) f_k(\tau)\right] = \alpha_k \delta\left(\tau - \sigma\right) \qquad (3.38)$$

where $\delta(t)$ is the Dirac delta function and α_k a numerical parameter, Equation 3.36 becomes:

$$R_{ipk}\left(\tau\right) = \sum_{r=1}^{N}\sum_{s=1}^{N} \alpha_k \varphi_{ri}\varphi_{rk}\varphi_{sj}\varphi_{sk} \int_{0}^{\infty} g_r(\lambda-\tau) g_s(\lambda) d\lambda \qquad (3.39)$$

where $\lambda = t - \tau$. Equation 3.39 represents the cross-correlation function between two responses resulting from an unknown white noise excitation, which has the form of decaying sinusoids scaled by a factor. These decaying sinusoids in turn have the same characteristics as the system's impulse response functions.

To compute the CCF between two responses, such as the accelerometer readings from two points on a structure during an ambient vibration test, CSD between the two responses is first derived as explained in Section 3.2.1. The CPS is then transformed into the CCF by applying the inverse Fourier transform.

ERA was developed by Juang and Pappa (1985) as an algorithm for identifying modal parameters. Combining NExT and ERA gives an effective modal identification methodology for structures under ambient excitation. Consider a system with a inputs and b outputs. The system response $y_j(k)$ at time step k due to the unit impulse u_j, or its impulse response function (IRF), can be written as:

$$\mathbf{y}(k) = [y_1(k)\ y_2(k) \ldots y_a(k)]^T \tag{3.40}$$

The first step of ERA is to form a Hankel matrix of the impulse response functions:

$$\mathbf{H}(k-1) = \begin{bmatrix} \mathbf{y}(k) & \mathbf{y}(k+1) & \cdots & \mathbf{y}(k+s) \\ \mathbf{y}(k+1) & \vdots & & \vdots \\ \vdots & & & \\ \mathbf{y}(k+r) & \cdots & & \mathbf{y}(k+s+r) \end{bmatrix} \tag{3.41}$$

where s and r are the numbers of time-shifted IRFs used in the Hankel matrix. The Hankel matrix is evaluated at k=1, i.e., $\mathbf{H}(0)$, and a singular value decomposition is performed:

$$\mathbf{H}(0) = \mathbf{T\Sigma V}^T = \mathbf{T\Sigma}^{1/2}\mathbf{\Sigma}^{1/2}\mathbf{V}^T \tag{3.42}$$

where $\mathbf{T}$ and $\mathbf{V}$ are matrices of singular vectors, and $\mathbf{\Sigma}$ is the diagonal matrix of singular values. Using the linear discrete time state space equation of motion, introduced in Equations 3.17 and 3.18, yields:

$$\mathbf{H}(k) = \left[\mathbf{C}^T \quad (\mathbf{CA})^T \quad \ldots \quad \left(\mathbf{CA}^{p-1}\right)^T\right]^T \mathbf{A}^{k-1}\left[\mathbf{Ax}(0) \quad \mathbf{A}^2\mathbf{x}(0) \quad \ldots \quad \mathbf{A}^r\mathbf{x}(0)\right] \tag{3.43}$$

where $\mathbf{A}$ and $\mathbf{C}$ are the system and output matrices of the discrete time state space system. By evaluating Equation 3.43 for $k=1$ and $k=2$, and combining them, the system and output matrices can be computed as follows:

$$\mathbf{A} = \mathbf{\Sigma}^{1/2}\mathbf{T}^T\mathbf{H}(1)\mathbf{V\Sigma}^{1/2} \tag{3.44}$$

$$\mathbf{C} = [\mathbf{I} \quad \mathbf{0} \quad \ldots \quad \mathbf{0}]\mathbf{T\Sigma}^{1/2} \tag{3.45}$$

With the set of eigenvalues and eigenvectors of $\mathbf{A}$ computed according to Equations 3.29-3.32, modal parameters of the continuous time system such as natural frequencies, damping ratios and modes shapes can be obtained.

3.3. Model updating concepts and methods

The following model updating related concepts and methods are explained:

- Penalty function
- Sensitivity based updating
- Global optimisation algorithms (GOAs) including particle swarm optimisation (PSO) and sequential niche technique (SNT).

3.3.1. Objective function for updating

An objective function, sometimes referred to as penalty function or error function, quantifies the deviation of the analytical predictions of modal parameters from those obtained experimentally. The following objective function is used in this study:

$$\Pi = \alpha_1 \sum_{i=1}^{n} \left(\frac{f_{a,i} - f_{e,i}}{f_{e,i}} \right)^2 + \alpha_2 \sum_{i=1}^{m} \frac{\left(1 - \sqrt{MAC_i}\right)^2}{MAC_i} + \alpha_3 \Pi_r \tag{3.46}$$

The first term is the total relative difference between the experimental and analytical frequencies, where f represents the frequency, subscripts a and e refer to analytical and experimental, respectively, and n is the total number of frequencies considered. The second term (Möller and Friberg 1998) measures the difference in mode shapes in terms of modal assurance criteria (MACs), where m is the total number of modes considered. MAC (Allemang and Brown 1982) between two mode shapes, $\boldsymbol{\varphi}_i$ and $\boldsymbol{\varphi}_j$, is defined as

$$MAC_{ij} = \frac{\left(\boldsymbol{\varphi}_i^T \boldsymbol{\varphi}_j\right)^2}{\left(\boldsymbol{\varphi}_i^T \boldsymbol{\varphi}_i\right)\left(\boldsymbol{\varphi}_j^T \boldsymbol{\varphi}_j\right)} \tag{3.47}$$

MAC takes a value of one for perfectly correlated mode shapes and zero for two orthogonal modes.

The third term in Equation 3.46 is related to regularization and for time being it is given in a general form to be specified later depending on particular applications. Regularization in model updating is often introduced for ill-posted problems that may not have a unique solution (Titurus and Friswell 2008). Regularization, following the original idea by Tikhonov

(1963), augments the objective function with new conditions, that dependent on updating parameters rather than the measured responses, in order to steer optimisation into the regions of search space where it is assumed their values belong. Finally, α_1 through α_3 in Equation 3.43 are weighting factors allowing for relative promotion and demotion of the error terms.

3.3.2. Sensitivity based updating

Contemporary methods of structural updating in buildings and bridges include the use of SM to improve the correlation between analytical and experimental modal properties (Brownjohn and Xia 2000, Yu et al. 2007). SM belongs in the category of local optimization techniques and the solution largely depends on the starting point or initial values (Deb et al. 2007). These methods take advantage of the solution space characteristics by calculating gradients and converge quickly to (possible local) maximum or minimum values. A good guess of initial point is necessary so as to converge to the global minimum. The SM computes the sensitivity coefficients defined as the rate of change of a particular response with respect to change in a structural parameter, mathematically expressed as

$$\mathbf{S}_{ij} = \frac{\partial \mathbf{R}_{a,i}}{\partial \mathbf{P}_j} \tag{3.48}$$

where $\mathbf{S}$ is the sensitivity matrix, $\mathbf{R}_a$ represents the vector of analytical structural responses, $\mathbf{P}$ represents the vector of parameters to be updated, and subscripts i and j refer to the respective entries of these vectors and matrix. The sensitivity matrix can be calculated using perturbation techniques, finite differences or by direct derivation using modal properties (Friswell and Mottershead 1995).

In the formulation of SM, the experimental responses $\mathbf{R}_e$ to be matched are expressed as a function of analytical responses and the sensitivity matrix (Zivanovic et al. 2007). This is done by a Taylor series ignoring all higher terms than the first order:

$$\mathbf{R}_e = \mathbf{R}_a + \mathbf{S}\left(\mathbf{P}_u - \mathbf{P}_0\right) \tag{3.49}$$

where $\mathbf{P}_u$ is a vector of updated parameter values and $\mathbf{P}_0$ is a vector of the current parameter values. From Equation 3.49, the updated parameter values can be calculated as

$$\mathbf{P}_u = \mathbf{P}_0 + \mathbf{S}^+\left(\mathbf{R}_e - \mathbf{R}_a\right) \tag{3.50}$$

where $\mathbf{S}^+$ is the Moore-Penrose pseudoinverse of the sensitivity matrix. Because the Taylor series of Equation 3.49 ignores higher order terms, several iterations are typically required to obtain satisfactory convergence and reduce the value of objective function. As the sensitivity matrix depends on the current values of the updating parameters it needs to be evaluated at each iterative step.

3.3.3. Global optimisation algorithms

GOAs are stochastic search-based methods and are efficient techniques for finding the global minimum in difficult optimization problems (Deb 2001). They are generally independent of the solution space (Tebaldi et al. 2006, Tu and Lu 2008) because they work on a population of points in parallel, whereas the traditional search techniques such as SM work only on a single point at one time. Thus, the tendency of traditional search techniques to converge to a local minimum in the search space can be addressed by using GOAs. This makes the GOAs much more robust in case of ill-behaved, complex solution spaces.

These techniques are particularly efficient for finding the minimum of objective functions having constrained variables and large number of dimensions. This makes them more suitable to use in model updating problems with different objective functions such as those based on frequencies, mode shapes or MACs. Global techniques find the global minimum out of local minima and often give better results where local optimization techniques perform less favourably (Deb 1998). Drawbacks of global optimization techniques are that they do not take advantage of characteristics of the solution space such as steepest gradients and they have a slow rate of convergence. The GOA used in this research, namely particle swarm optimisation (PSO), is discussed in detail in the following section. Also, a useful addition to GOA, sequential niche technique (SNT), which enables a systematic search for a number of local minima is introduced.

3.3.3.1. Particle swarm optimisation

PSO (Kennedy and Eberhart 1995) is a population-based stochastic optimization method that iteratively tries to improve the solution with respect to a given measure of quality. The concept of PSO was developed based on the swarm behaviour of fish, bees and other animals. In PSO, the members or particles making up the swarm and representing optimization parameters move in the search space in pursuit of the most fertile feeding location, or, in mathematical terms, the optimal location that minimizes an objective function. Each particle in the swarm is influenced by the rest of the swarm but is also able to independently explore its own vicinity to increase diversity. Likewise, if a swarm member sees a desirable path for the most fertile feeding location, the rest of the swarm will modify their search directions.

Thus, the movement of each particle is influenced by both group knowledge and individual knowledge. It is assumed and expected that this will eventually, over a number of generations, move the whole swarm to the global optimal solution. The implementation of PSO compared to the other optimization techniques is relatively fast and cheap as there are few parameters to adjust and it can be used for a wide range of applications (Knowles et al. 2008).

In the PSO algorithm, each particle is assigned a position and velocity vector in a multidimensional space, where each position coordinate represents a parameter value. The algorithm calculates the fitness of each particle according to the specified objective function. The particles have two reasoning capabilities: the memory of their own best positions in the past generations referred to as $\mathbf{pbest}_i(t)$, and knowledge of the overall swarm best position referred to as $\mathbf{gbest}(t)$. The position $\mathbf{x}_i(t)$ of each particle is updated in each generation by the simple recursive formula (see also Figure 3.2):

$$\mathbf{x}_i(t+1) = \mathbf{x}_i(t) + \mathbf{v}_i(t+1) \tag{3.51}$$

where i is the particle number and t is the generation number. The velocity of each particle $\mathbf{v}_i(t)$ towards its $\mathbf{pbest}_i(t)$ and $\mathbf{gbest}(t)$ locations is adjusted in each generation using the following formula:

$$\begin{aligned} \mathbf{v}_i(t+1) &= \gamma \times \mathbf{v}_i(t) + c_1 \times rand_1 \times (\mathbf{pbest}_i(t) - \mathbf{x}_i(t)) \\ &+ c_2 \times rand_2 \times (\mathbf{gbest}(t) - \mathbf{x}_i(t)) \end{aligned} \tag{3.52}$$

where $\mathbf{v}_i(t)$ is the initial velocity, $\mathbf{v}_i(t+1)$ is the updated velocity, γ is the inertial weight, c_1 and c_2 are the cognition and social coefficient, and $rand_1$ and $rand_2$ are random numbers between 0 and 1.

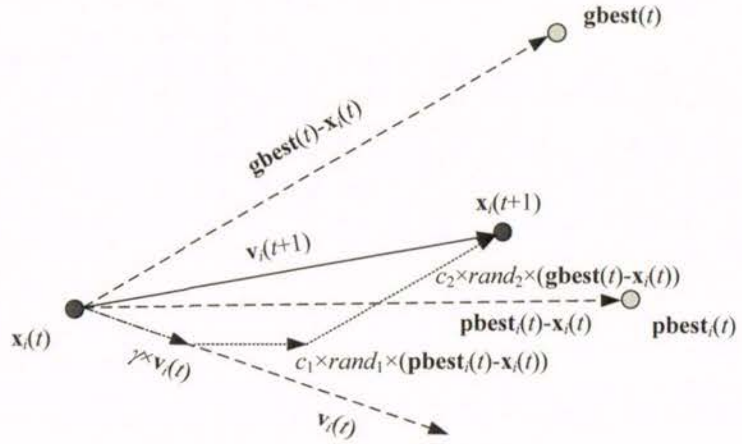

Figure 3.2. Pictorial view of particle behaviour showing position and velocity update.

In addition to the inertia term that holds the memory of all previous iterations, there are two terms in Equation 3.52: one related to the best global position which defines the swarm exploratory behaviour and other related to the particle's local best position which defines the exploitative behaviour (Konstantinos and Vrahatis 2010). Exploratory behaviour is related to the search of a broader region of the parameter domain, and exploitative behaviour is related to local search where a given particle tries to get closer and closer to the (possibly local) minimum. To avoid premature convergence, the cognition and social component coefficient, c_1 and c_2, respectively, should be carefully selected to ensure a good convergence rate to the global optimum. A constraint on the maximum velocity of the particle can also be imposed to ensure that particles remain in the search space and their values are kept within the maximum and minimum bounds. Both theoretical and empirical studies have been undertaken to help in selecting values of these parameters (Pedersen and Chipperfield 2010, Trelea 2003, Zheng et al. 2003).

3.3.3.2. Sequential niche technique

The principle of SNT is to carry over knowledge gained during subsequent iterations of an optimization algorithm (Beasley et al. 1993) so that different minima are discovered in turn. The basic approach is that when a minimum is found in the search domain, the surrounding area, referred to as niche, is 'filled in' and no longer attracts the particles in subsequent iterations. This forces the optimization algorithm to converge to another, yet unvisited, niche. The process continues until the criteria such as the maximum number of iterations, maximum number of discovered minima and the upper threshold value of the objective function at a minimum have been met.

Initial iterations in search of the first minimum are made with the basic search algorithm, PSO in this case, without SNT by using the raw objective function. Once the first minimum has been found, the objective function values of the particles in the vicinity of the minimum are modified, and the search for the next minimum commences. The modifications to the objective function are introduced by multiplying it by a derating function using the following recursive formula:

$$\Pi_{n+1}(\mathbf{x}) = \Pi_n(\mathbf{x}) \times G(\mathbf{x}, \mathbf{s}_n) \tag{3.53}$$

where $\Pi_{n+1}(\mathbf{x})$ is the modified objective function to be used for searching for the n+1-th minimum, $\Pi_n(\mathbf{x})$ is the previous objective function used for searching for the n-th minimum, $G(\mathbf{x},\mathbf{s}_n)$ is the derating function, and $\mathbf{s}_n$ is the n-th found minimum.

The following exponential derating function is used in this study (Beasley et al. 1993):

$$g(\mathbf{x},\mathbf{s}_n)=\begin{cases}\exp\left(\log m\times\dfrac{d(\mathbf{x},\mathbf{s}_n)}{r}\right) & \textit{if } d(\mathbf{x},\mathbf{s}_n)<r\\ 1 & \textit{otherwise}\end{cases} \tag{3.54}$$

where m is the derating parameter used to control concavity of the derating function, r is the niche radius, and $d(\mathbf{x},\mathbf{s}_n)$ defines the distance between the current point $\mathbf{x}$ and best individual $\mathbf{s}_n$.

The niche radius r is an important parameter as it is used to define the size of the part of the search domain in the neighbourhood of a minimum where the objective function is modified. Smaller values of niche radii produce more concavity possibly leading to the creation of artificial minima, while larger niche radii can affect the other true minima in the search space. The niche radius has been determined in this study by the method proposed by Deb (1989) who suggested using a value calculated as

$$r=\frac{\sqrt{k}}{2\times\sqrt[k]{p}} \tag{3.55}$$

where k represents the dimension of the problem (the number of parameters) and p is the expected number of minima. Each parameter has to be normalized between 0 and 1 for the use of SNT. This approach assumes that all minima are fairly equally distributed throughout the search domain.

3.4. Summary

This chapter lays the theoretical ground for the research reported in the subsequent chapters. The theoretical concepts and detailed analytical formulations have been provided for several system identification methods and approaches to model updating. The former include spectral analysis, PP, EFDD, SSI and NeXT-ERA, and the latter objective function, SM and GOAs, in particular PSO combined with SNT.

3.5. References

Allemang, R.J., & Brown, D.L. (1982), A correlation for modal vector analysis, Proceedings of IMAC I: 1st International Modal Analysis Conference, 110-116.

Alvin, K.F., & Park, K.C. (1994), Second-order structural identification procedure via state-space-based system identification, AIAA Journal, 32, 397-406.

Beasley, D., Bull, D.R., & Martin, R.R. (1993), A sequential niche technique for multimodal function optimization, Evolutionary Computation, 1, 101-125.

Bendat, J., & Piersol, A. (1993), Engineering applications of correlation and spectral analysis, (2nd Ed.), Wiley, New York, NY.

Brincker, R., Zhang, L., & Andersen, P. (2000) Modal identification from ambient responses using frequency domain decomposition, Proceedings of IMAC XVIII: 18th International Modal Analysis Conference, 625-630.

Brownjohn, J.M.W., & Xia, P.Q. (2000), Dynamic assessment of curved cable-stayed bridge by model updating, Journal of Structural Engineering, ASCE, 126, 252-260.

Chopra, A.K. (2007), Dynamics of structures, Pearson Prentice Hall, Upper Saddle River, NJ.

Deb, K. (1989), Genetic algorithms in multimodal function optimization, The University of Alabama, Tuscaloosa.

Deb, K. (1998), Optimization for engineering design: algorithms and examples, Prentice-Hall, India.

Deb, K. (2001), Multi-objective optimization using evolutionary algorithms, Wiley, Chichester.

Deb, K., Chakroborty, P., Iyengar, N.G.R., & Gupta, S.K. (2007), Advances in computational optimization and its applications, Universities Press, New Delhi.

Friswell, M.I., & Mottershead, J.E. (1995), Finite element model updating in structural dynamics, Kluwer, Dordrecht.

Heylen, W., Lammens, S., & Sas, P. (1997), Modal analysis theory and testing, Katholieke Universiteit Leuven, Leuven.

Jacobsen, N., Andersen, P., & Brincker, R. (2007), Using EFDD as a robust technique to deterministic excitation in operational modal analysis, Proceedings of the 2nd International Operational Modal Analysis Conference, 193-200.

James, G.H., Carne, T.G., & Lauffer, J.P. (1993), The natural excitation technique for modal parameters extraction from operating wind turbines, SAND92-1666, UC-261, Sandia National Laboratories, Sandia, NM.

Juang, J.N., & Pappa, R.S. (1985), An eigensystem realization algorithm for modal parameter identification and model reduction, Journal of Guidance, Control and Dynamics, 8, 620-627.

Kennedy, J., & Eberhart, R. (1995), Particle swarm optimization, Proceedings of the IEEE International Conference on Neural Networks, 1942-1948.

Knowles, J., Corne, D., & Deb, K. (2008), Multiobjective problem solving from nature: from concepts to applications, Springer, New York, NY.

Konstantinos, E.P., & Vrahatis, M.N. (2010), Particle swarm optimization and intelligence: advances and applications, Information Science Reference, Hershey, PA.

Ljung, L. (1987), System identification: theory for the user, Prentice-Hall, Upper Saddle River, NJ.

Möller, P.W., & Friberg, O. (1998), Updating large finite element models in structural dynamics, AIAA Journal, 36, 1861-1868.

Pedersen, M.E.H., & Chipperfield, A.J., (2010), Simplifying particle swarm optimization, Applied Soft Computing Journal, 10, 618-628.

Skolnik, D., Lei, Y., Yu, E., & Wallace, J.W. (2006), Identification, model updating, and response prediction of an instrumented 15-story steel-frame building, Earthquake Spectra, 22, 781-802.

Tebaldi, A., Dos Santos Coelho, L., & Lopes Jr, V. (2006), Detection of damage in intelligent structures using optimization by a particle swarm: fundamentals and case studies, Controle y Automação, 17, 312-330.

Tikhonov, A.N. (1963), Regularization of incorrectly posed problems, Soviet Mathematics, 4, 1624–1627.

Titurus, B., & Friswell, M.I. (2008), Regularization in model updating, International Journal for Numerical Methods in Engineering, 75, 440-478.

Trelea, I.C. (2003), The particle swarm optimization algorithm: convergence analysis and parameter selection, Information Processing Letters, 85, 317-325.

Tu, Z., & Lu, Y. (2008), FE model updating using artificial boundary conditions with genetic algorithms, Computers and Structures, 86, 714-727.

Van Overschee, P.V., & De Moor, B. (1996), Subspace identification for the linear systems: theory – implementation – applications, Kluwer, Dordrecht.

Yu, E., Taciroglu, E., & Wallace, J.W. (2007), Parameter identification of framed structures using an improved finite element model-updating method - Part I: formulation and verification, Earthquake Engineering and Structural Dynamics, 36, 619-639.

Zheng, Y.L., Ma, L.H., Zhang, L.Y., & Qian, J.X. (2003), On the convergence analysis and parameter selection in particle swarm optimization, Proceedings of the International Conference on Machine Learning and Cybernetics, 1802-1807.

Zivanovic, S., Pavic, A., & Reynolds, P. (2007), Finite element modelling and updating of a lively footbridge: the complete process, Journal of Sound and Vibration, 301, 126-145.

CHAPTER 4

FORCED VIBRATION TESTING, SYSTEM IDENTIFICATION AND MODEL UPDATING OF A CABLE-STAYED FOOTBRIDGE

4.1. Introduction

This chapter describes a study comprising full-scale, in-situ experiment, system identification and subsequent model updating conducted on a 59,500 mm long cable-stayed footbridge. The bridge was tested using three linear shakers providing a total input of 1.2 kN. Excitation was applied in both horizontal and vertical direction and an array of sensors was used to capture horizontal, vertical and torsional response of the deck. SI methods, such as PP and SSI (explained in Chapter 3), were used to extract natural frequencies, damping ratios and mode shapes.

The subsequent model updating exercise examined the performance of PSO combined with SNT. It is shown how using a SM-based approach leads to solutions that are only local minima, and that PSO can outdo SM and find the global minimum. Furthermore, combining PSO with SNT facilitates systematic search for multiple minima and provides an increased confidence in finding the global one.

The layout of the chapter is as follows. Firstly, the bridge geometry and structural system are described. This is followed by an explanation of the forced dynamic testing procedure and results of modal system identification. Numerical bridge modelling is then outlined. The main thrust of the chapter follows, i.e. updating of the FEM bridge model using SM, PSO alone and PSO in combination of SNT, respectively. A discussion and a set of conclusions summarizing the performance of each updating method round up the chapter.

4.2. Bridge description

The full-scale structure under study is a 59,500 mm long cable-stayed footbridge with two symmetrical spans supported on abutments, a central A-shaped pylon and six pairs of stays as shown in Figure 4.1. Figure 4.2 shows the deck cross-section, which comprises a trapezoidal steel girder with overhangs of a total width of 2,500 mm and depth of 470 mm, made of 16 mm thick plates, and a non-composite concrete slab of thickness 130 mm. Closed steel rectangular pipes having a cross-section of 250 × 150 × 9 mm also run on both sides of the bridge deck and enclose two 100 mm ducts for service pipes with surrounding void spaces filled with grout. Railing was provided on both sides of the bridge and it has a total height of 1,400 mm. The sections of railings were disconnected from each other at every 8,000 mm.

The girder is continuous over the entire bridge length. It is supported on two elastomeric pad-type bearings of dimensions 90 × 180 × 12 mm at the central pylon. At each abutment two 150 × 150 × 12 mm elastomeric pad-type bearings are also provided, but these allow for longitudinal sliding while constraining any lateral horizontal displacements. The sliding bearings were provided to accommodate creep, shrinkage and temperature deformations, and to allow the bridge to move longitudinally in the event of a strong seismic excitation. The distance between bearing axes is 450 mm. The abutments are supported by two concrete piles, and 10 concrete piles and a pile cap are used at the central pylon.

The six pairs of stay cables are fixed to the deck at distances of about 8,000 mm centre to centre as shown in Figure 4.3. All the cables have a diameter of 32 mm. Different post-tension forces, ranging from 55 kN to 95 kN in each cable, were specified in design. The cables were connected to the top of the 22,400 mm high centre pylon, which is composed of two steel I-sections joined with cross bracing that supports the deck. The size of the pylon I-sections is 400WC328 (Standards New Zealand 2010). The bridge has been considered as an appropriate candidate for mode updating as it has a number of potential uncertain parameters.

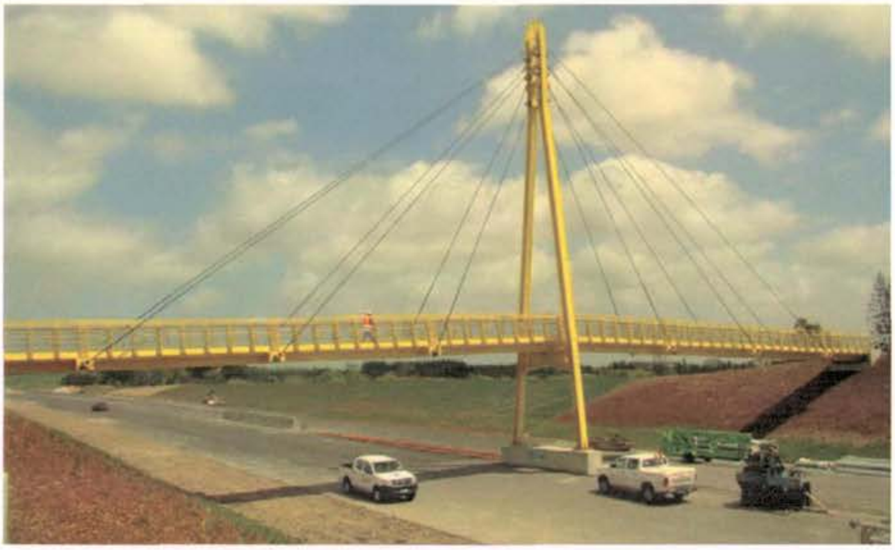

Figure 4.1. Full-scale cable-stayed footbridge.

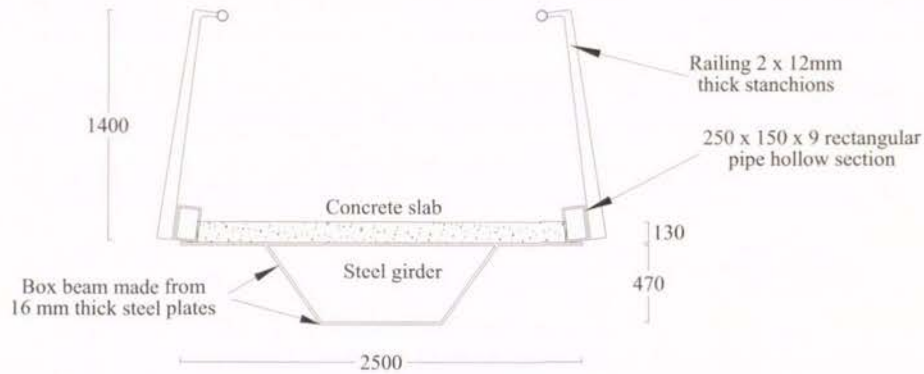

Figure 4.2. Cross-section of bridge deck (all dimensions in mm).

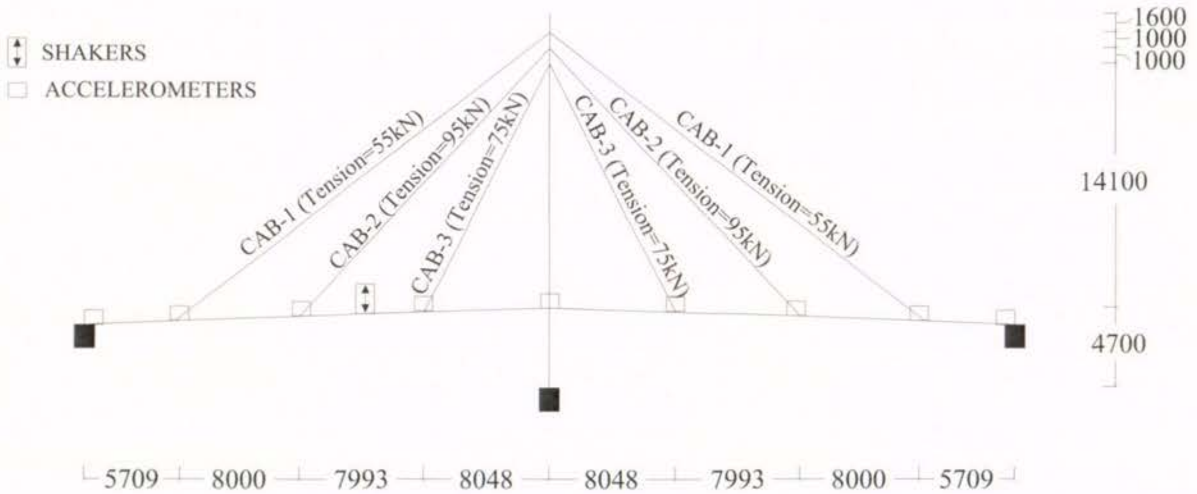

Figure 4.3. Basic bridge dimensions (in mm), cable post-tension forces and location of shakers and accelerometers in the experiment.

Figure 4.4. Accelerometers (in the centre) and shakers (at the back) on the bridge deck.

4.3. Forced vibration testing and system identification

Experimental work has been carried out using uni-axial Honeywell QA 750 accelerometers to measure structural response, uni-axial Crossbow CXL series MEMS accelerometers to measure shaker input force and a desktop computer fitted with an NI DAQ 9203 data acquisition card. Data was collected at a sampling rate of 200 Hz. Three APS ElectroSeis Model 400 long stroke linear shakers (APSDynamics 2012), capable of providing a combined dynamic force of up to 1.2 kN, were used in a synchronized mode to impart excitation to the structure.

Full scale tests can be conducted by output only (no measured force) or input-output (measured force) methods. The cable stayed bridge under study has been tested using both of these methods. The output only test was conducted using jumping as excitation to establish the initial estimation of the natural frequencies of the bridge. Two people jumped on the bridge in unison to excite the structure and thereafter the bridge was allowed to freely vibrate for two minutes. This was done to establish the range of excitation frequencies for subsequent forced vibration tests. References such as Brownjohn et al. (2003) and Pavic et al. (2007) demonstrate that frequency sweep tests are standard and successful approach to full scale testing. Different sweep rates have been used by various researchers to excite full scale structures. Pioneer bridge (Brownjohn et al. 2003) was excited using a frequency sweep ranging from 5 to 32 Hz for 20.48 s, whereas a full scale open plan floor (Pavic et al. 2007) was excited using a frequency sweep ranging from 3 to 19 Hz for approximately 15 s.

Following that, a sweep sine excitation ranging from 1 to 15 Hz with a total duration of 391 s was adopted to excite the structure. The shakers were located away from the centre line of the deck to excite both the vertical and torsional modes. To excite horizontal modes, the shakers were tilted by 90°. Figure 4.3 shows the locations of the shakers and accelerometers on the bridge during testing, whereas Figure 4.4 is a photo showing the physical setup. Accelerometers were placed on both sides of the deck to capture vertical and torsional responses. One of the accelerometers was also placed on the bridge abutment to measure its response. Figure 4.5 shows the time history of force delivered by a shaker, and Figure 4.6 shows the time history of bridge response recorded by one of the accelerometers during vertical testing. It can be seen in Figure 4.6 how subsequent modes are excited as the shakers sweep through their corresponding resonant frequencies. The vertical and horizontal tests were repeated thrice to ensure good quality data.

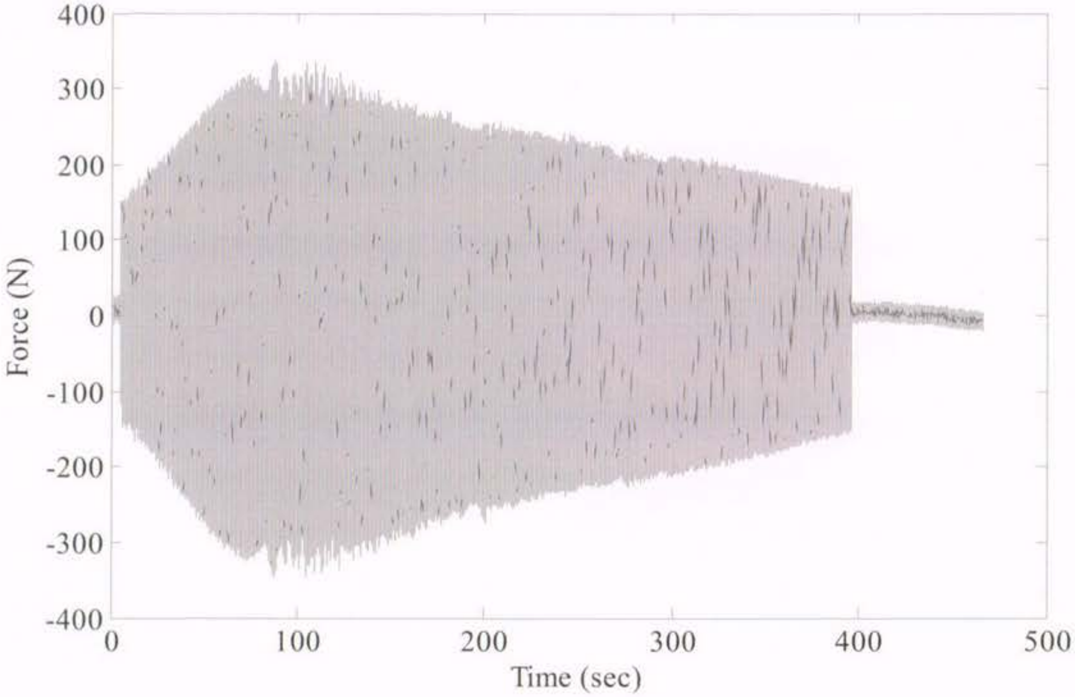

Figure 4.5. Time history of force applied by a shaker.

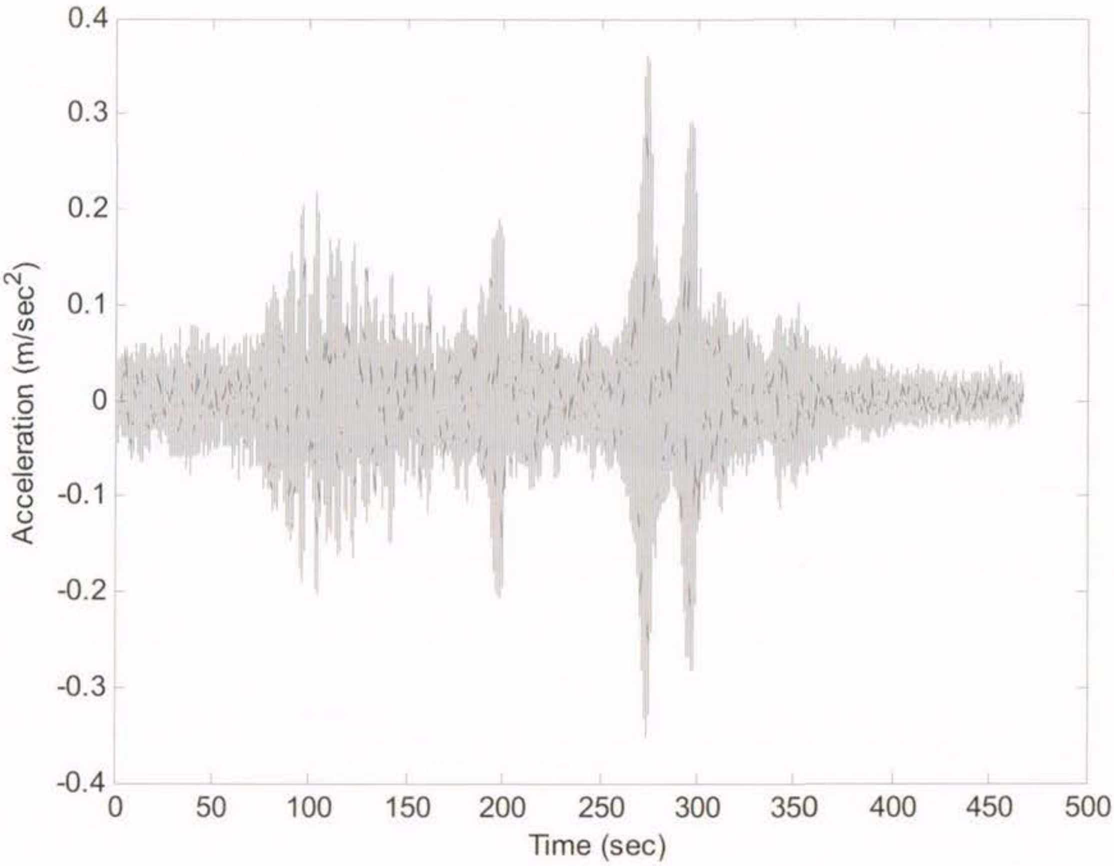

Figure 4.6. Time history of bridge response recorded during vertical shaker excitation.

For system identification in the frequency domain, PP method using FRF is a commonly used and simple method and was adopted in this study. FRF is a measure of system response to the input signal at each frequency and can be calculated from the auto-spectral density (ASD) of excitation and cross-spectral density (CSD) between response and excitation as explained in Friswell and Mottershead (1995) and also in Chapter 3.2.1. The PP method is explained in Ewins (2000) and also in Chapter 3.2.2. For calculating the spectra, the Welch averaging method was used (Proakis and Manolakis 1996) with each time history divided into five segments with 50% overlap and Hamming windowing. Finally, FRFs from all available experiments were averaged. To assess the quality of an FRF and distinguish between real and spurious peaks, coherence can be used (Ewins 2000). Coherence can be calculated using ASD and CSDs of the excitation and responses explained in Chapter 3.2.1. High coherence values, close to one, indicate that response at a given frequency is caused by the measured input rather than other sources of excitation or is a false result introduced by noise. An example of an FRF obtained during a vertical shaker test is shown in Figure 4.7a, where FRF magnitude, phase and coherence are shown. It can be noted that the magnitude has peaks at

1.64 Hz, 1.90 Hz, 3.66 Hz, 6.32 Hz, 7.42 Hz and 8.33 Hz. All but the last peak at 8.33 Hz, which is a torsional mode, correspond to vertical modes. Higher peaks are observed at modes corresponding to 6.32 Hz and 7.42 Hz, which shows that these modes are responding more strongly than the others. Also, the torsional mode peak at 8.33 Hz is less clearly visible possibly due to low levels of excitation torque delivered by the shakers. The phase of the FRF shows a change by 180° close to 1.64 Hz, 1.90 Hz, 3.66 Hz, 6.32 Hz, 7.42 Hz and 8.33 Hz further confirming that these are modal frequencies. The phase change is again much clearer at 6.32 Hz and 7.42 Hz as they are better excited than the other modes. The coherence between excitation and response have values of more than 0.8 at 1.64 Hz, 1.90Hz, 3.66 Hz, 6.32 Hz, 7.42 Hz and 8.33 Hz, indicating that a reasonably good correlation exists between the force and response signals. Much better coherence values, very close to one, were observed at 6.32 Hz and 7.42 Hz. Some other peaks, e.g. just above 10 Hz, can also be seen but the corresponding coherence values are low. Also, the auto power spectral density from jump test is shown in Figure 4.7b. Two peaks at 6.31 Hz and 7.39 Hz can be clearly seen along with a smaller peak at 1.66 Hz. These frequencies match well with the already identified frequencies from FRF. The well-known challenges of in-situ testing of full-scale large systems, like bridges, must be kept in mind while assessing the quality of the FRF obtained. These include, but are not limited to, poorer signal-to-noise ratios because of limited capacity of exciters, very limited control of several ambient sources of excitation and noise (wind, construction works, vehicles, occupants, machinery, etc. – some of which are always present), and limited data as, unlike in the lab, tests cannot typically be repeated tens or hundreds of times for averaging. Given those challenges, it can be concluded that data of sufficient quality has successfully been acquired. Similarly, two resonance frequencies were identified using horizontal shaker excitation at 4.85 Hz and 5.36 Hz, respectively.

For cross-checking the results of pick peaking and also to identify damping ratios and mode shapes the N4SID technique (Van Overschee and De Moor 1994), operating in time domain and utilizing a subspace identification algorithm, was used. The general subspace system identification algorithm (Van Overschee and De Moor 1996) can be applied to both input-only and input-output identification. In these approaches, state space system matrices are first obtained from the measurements, and then natural frequencies, damping ratios, and mode shapes can then be derived from these system matrices. Further details can be found in Chapter 3.3.5.

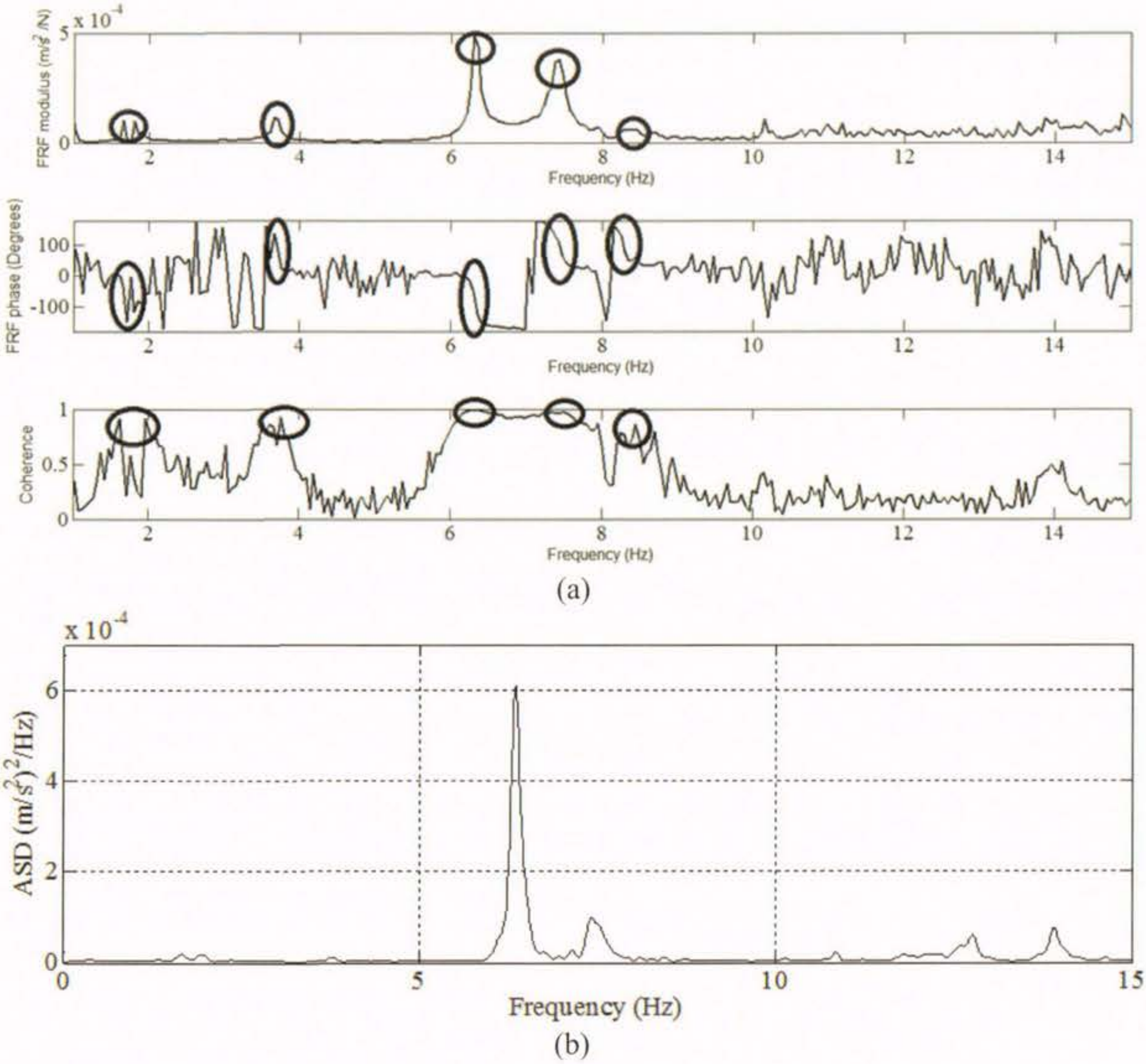

Figure 4.7. Frequency response of the bridge: a) FRF measured during vertical shaker test, b) ASD of response signal during jump test.

The adequate order of the state space model needs to be carefully determined. Theoretically, the system order should be twice the number of the DOFs, i.e. modes, of interest. However, due to measurement noise a higher model order is normally required to extract the modes of interest with higher confidence and discard spurious, artificial results. To that end, stability diagrams are employed. As the system order increases, the structural modes identified by the algorithm should remain consistent and stable (Bodeux and Golinval 2001). The model order selected for this study ranged from 10 to 80 for the vertical shaker configuration. Stability thresholds were selected based on previous experience and data quality. A threshold of 1% for frequency variation and a value above 0.8 for MAC (Equation 3.43.) between two subsequent model orders were used.

The stability diagram for a vertical shaking test is shown in Figure 4.8. It can be seen from the stability diagram that the six previously observed modes, five vertical and one torsional, are stable and can be identified from the vertical tests as shown by the black dots. Some spurious modes, that did not meet the stipulated stability criteria, were also detected as shown by the white dots. In a similar way, two modes previously seen in the FRFs were identified from the horizontal tests.

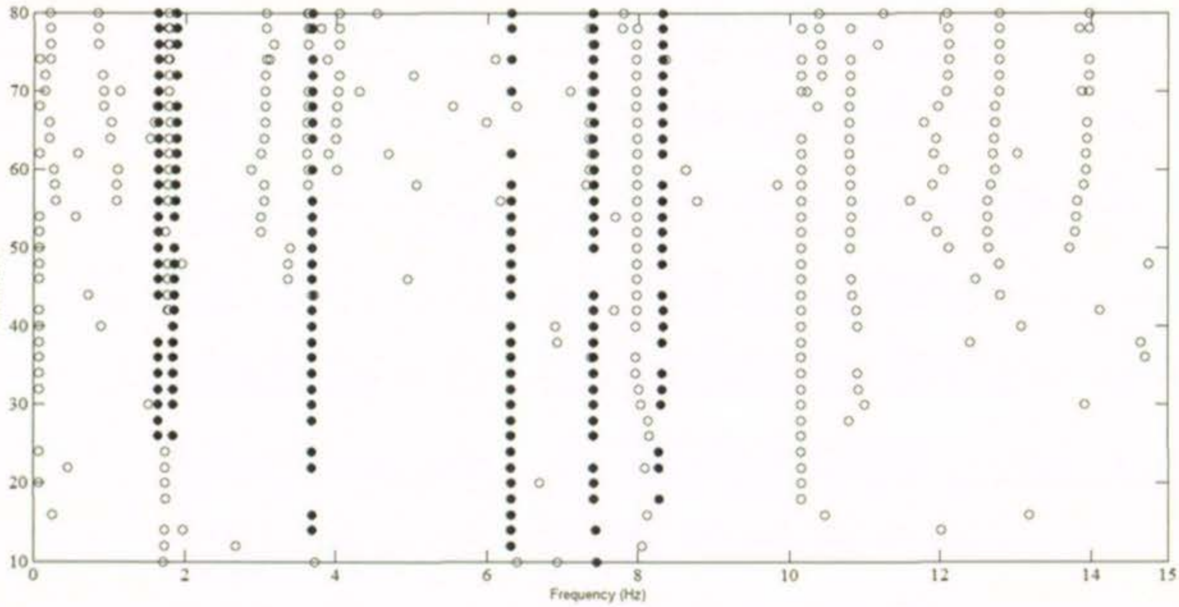

Figure 4.8. Stability diagram for a vertical shaker test (black dots indicate stable modes).

Table 4.1 summarizes the natural frequencies identified from the peak picking and N4SID method. It can be seen from the results that the frequencies identified by both methods match very well. The damping ratios identified by the N4SID method are also shown in Table 4.1. It is observed that damping in the bridge is small, ranging between 0.2% and 1.4%.

Five vertical, two horizontal and one torsional mode shape identified from modal tests using the N4SID method are shown in Figure 4.9. It has been observed from the system identification results that the first two vertical modes have nearly identical sinusoidal shapes over the deck. An additional accelerometer was attached to one of the cables closest to the abutments during the vertical shaker tests and it has been found that the cable vibrates laterally at the frequency of the second mode, i.e. at 1.90 Hz. FE simulations conducted later confirmed that the pattern of cable vibration sets the two modes apart.

Only one torsional mode of the system was identified by the forced vibration tests at 8.32 Hz. Typically, one would expect a torsional mode of a shape similar to a full sinusoid where the deck twists in the opposite directions in each span (Ren and Peng 2005). However, in the observed torsional mode the whole deck twists in the same direction. The reason behind this is that the main girder is a closed trapezoidal cross-section (Figure 4.2) thus having a large torsional stiffness, which makes it difficult to twist the bridge deck in a full-sine pattern. Also, the closed rectangular pipes with service ducts and railing that run near the edges throughout the length of the bridge further increase the torsional stiffness of the deck. It is thus easier to deform the pylon resulting in the torsional mode shape as indicated in Figure 4.9.

4.4. Finite element modelling

There are many ways to model cable-stayed bridges to obtain a realistic representation of their dynamic behaviour. The main elements to be modelled are the deck, pylon, cables, and connections of cables and deck. A good representation of bridge deck for box girder sections can be achieved by using beam elements with rigid links joining the cable elements with the deck elements (Chang et al. 2001, Ren and Peng 2005). In this research, the bridge was modelled in SAP2000 software (Computers and Structures 2009) and the FE model is shown in Figure 4.10a. The deck and pylon were modelled using beam type FEs. The deck was discretized into 48 elements, whereas the pylon was discretized into 40 elements. These numbers of elements were selected as further discretization did not appreciably affect the results of numerical modal analysis and only resulted in an increased computational cost. The cables were modelled using catenary elements provided in SAP2000 and were discretized into four elements for each cable.

Table 4.1. Experimentally identified natural frequencies and damping ratios.

Mode No.	Mode type	Experimental frequencies (Hz)		Damping ratios (%)
		Peak picking	N4SID	N4SID
1	1st vertical	1.64	1.64	0.2
2	2nd vertical	1.90	1.90	0.9
3	3rd vertical	3.66	3.69	0.5
4	1st horizontal	4.85	4.86	0.8
5	2nd horizontal	5.36	5.33	0.6
6	4th vertical	6.32	6.31	0.5
7	5th vertical	7.42	7.42	1.0
8	1st torsional	8.33	8.32	1.4

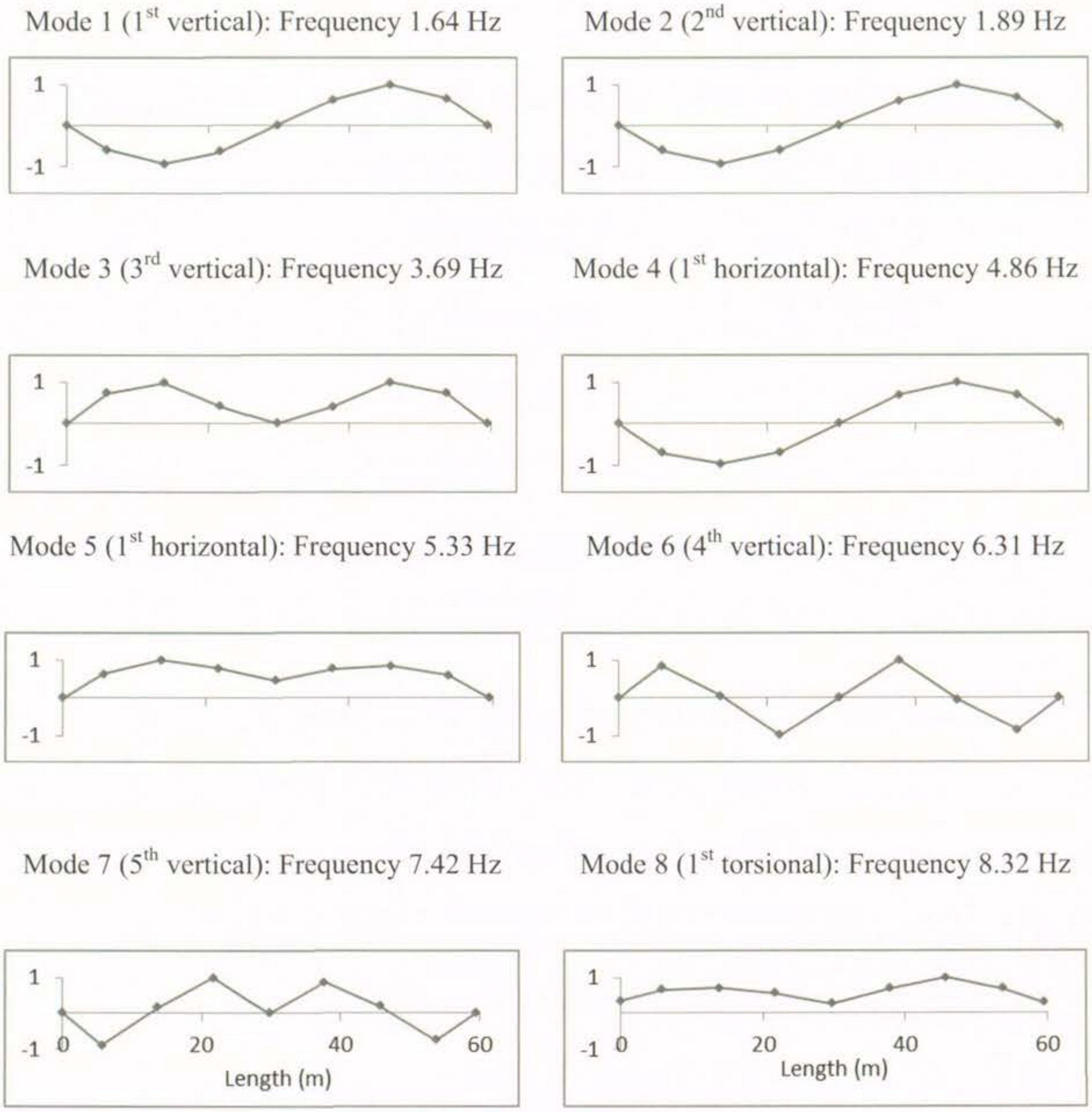

Figure 4.9. Vertical, horizontal and torsional modes identified using N4SID method.

As indicated earlier, the first two experimentally identified vertical modes (Figure 4.9) have very similar shapes of girder vibrations and an initial FE model with no discretization of the cables did not show the second of the two modes. After discretization of the cables into four elements all the experimentally observed modes were correctly replicated in the FE model. Figures 4.10b and c show the pattern of cable vibrations for the two vertical modes.

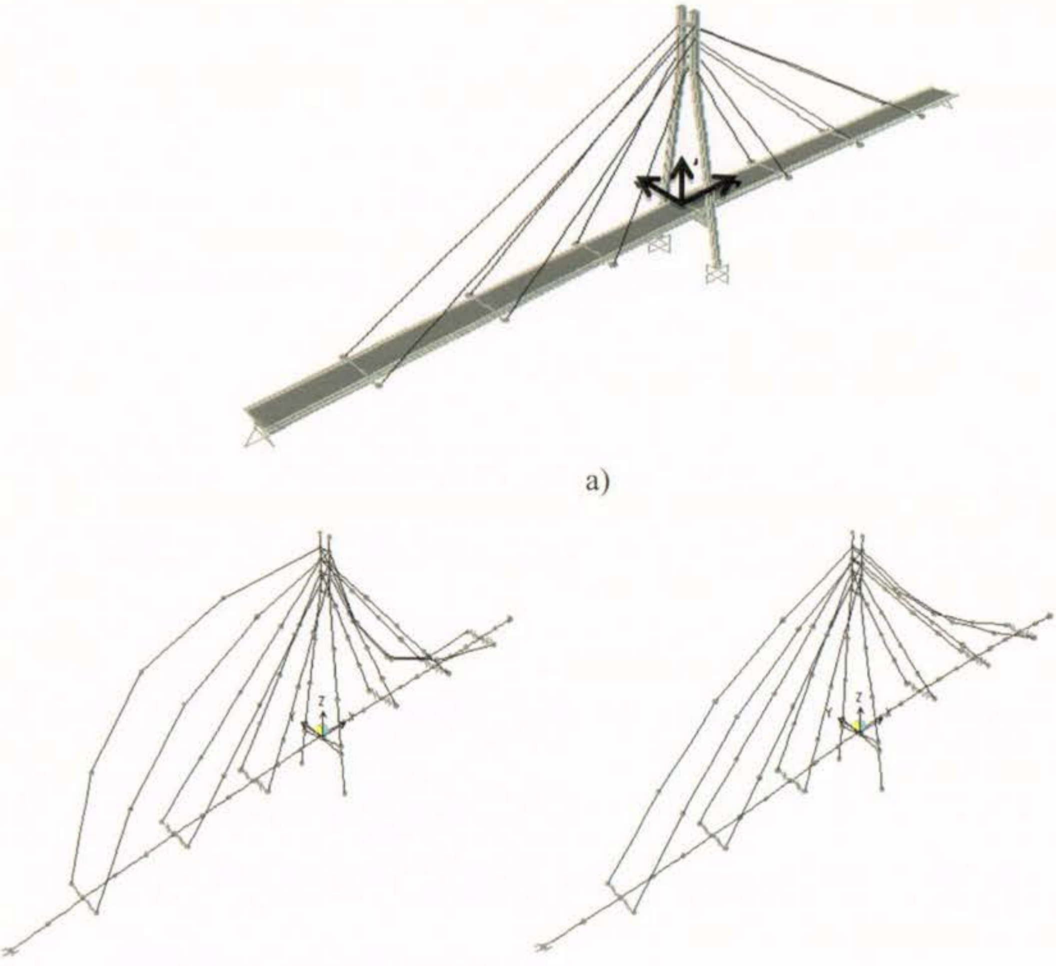

a)

b) c)

Figure 4.10. FE model of the bridge: a) general view, b) 3D view of Mode 1 showing cable vibrations, and c) 3D view of Mode 2 showing cable vibrations.

The modulus of elasticity for steel was taken as 200 GPa, for cables as 165 GPa and for concrete as 28 GPa. The cast is situ concrete slab was assumed to be fully composite with the steel girder resulting in a combined cross-sectional second moment of inertia of 0.06140 m^4 for horizontal bending, 0.00439 m^4 for vertical bending and torsional constant of 0.00810 m^4. (Note that this contradicts the assumption made in design that there is no composite action. However, it was anticipated that partial composite action did exist, as is often the case in real structures, and its actual extent would be quantified via model updating later.) An initial non-linear static analysis was performed to account for the geometric non-linearity caused by the cable sag and this was followed by a linear dynamic analysis to obtain natural frequencies and mode shapes. A linear analysis that uses stiffness from the end of non-linear static analysis for cable-stayed structures has been demonstrated to provide good results (Abdel-Ghaffar and Khalifa 1991).

The response of the bridge was also measured with sensors on the bridge abutment beneath the deck. The abutment did not show any appreciable response in the vertical or horizontal direction and so both abutments were ignored in the FE model. However, the stiffness of the bearings for shear and compression has been calculated in terms of their geometry and stiffness modulus. Shear stiffness K_s and vertical stiffness K_v of the bearings have been calculated using the formulas taken from Gent (2012):

$$K_S = \frac{AG}{t} \tag{4.1}$$

$$K_v = \frac{AE_c}{t} \tag{4.2}$$

where A is the effective loaded area, G is the shear modulus, E_c is the effective compression modulus and t is the thickness of bearing. Effective compression modulus has been calculated using the formula:

$$E_c = E\left(1 + 2\Phi S^2\right) \tag{4.3}$$

where E is Young's modulus, Φ is compression coefficient of the elastomer and S is the shape factor; for a rectangular block S can be determined as:

$$S = \frac{Load\ Area}{Bulge\ Area} = \frac{Lenght \times Width}{2\left(Lenght + Width\right)} \tag{4.4}$$

Furthermore, as explained before the distance between bearing axes is 450 mm and torsional restraint provided by bearings K_{rot} is calculated by the formula (Jaishi and Ren 2007):

$$K_{rot} = \frac{K_v L^2}{2} \tag{4.5}$$

The shear, vertical and torsion stiffness values for abutment bearings were found to be 2.58×10^6 N/m, 1.60×10^8 N/m and 8.86×10^8 Nm/rad, respectively. Likewise shear, vertical and torsion stiffness values for the pylon bearings were found to be 1.86×10^6 N/m, 7.70×10^7 N/m and 3.90×10^6 Nm/rad, respectively. The freedom of the abutment bearings to slide was ignored; this was not expected to have any strong effects on the model accuracy as neither was the bridge excited in the longitudinal direction during dynamic tests, nor were the corresponding modes experimentally identified or considered in the analysis.

Table 4.2 summarizes the errors between experimental frequencies and mode shapes and those identified by the initial FE model. To compare experimental and numerical mode shapes, MAC (Equation 3.43) was used. It has been found that the frequencies obtained from the initial FE model differ from the experimental frequencies by up to 8.6% and MAC values are between 0.980 and 0.999. The systematic attempts to improve the agreement between the experimental and numerical predictions via SM, and PSO and SNT-based model updating are discussed in the next section.

Table 4.2. Initial FE model and experimental frequencies and MACs.

	Frequency			
Mode No.	Experiment by N4SID (Hz)	Initial FE model (Hz)	Error (%)	MAC
1	1.64	1.66	1.2	0.999
2	1.90	1.88	-1.1	0.995
3	3.69	3.88	5.2	0.999
4	4.86	5.28	8.6	0.999
5	5.33	5.45	2.3	0.993
6	6.31	6.79	7.6	0.990
7	7.42	7.76	4.6	0.980
8	8.32	8.66	4.1	0.993

4.5. Model updating

In model updating, dynamic measurements such as natural frequencies and mode shapes are correlated with their FE model counterparts to calibrate the FE model. There is a degree of uncertainty in the assessment of the actual properties of the materials used in the full-scale structure as well as the most realistic representation of the element stiffness, supports and connections between structural parts in the initial FE model. The challenge of finding a set of suitable parameters having physical justification necessitates the need for use of physically significant updating parameters and suitable optimization tools.

4.5.1. Selection of updating parameters and objective function

The selection of parameters in model updating is critical for the success of any such exercise. An excessive number of parameters compared to the number of available responses, or overparametrisation, will lead to a non-unique solution, whereas insufficient number of parameters will prevent reaching a good agreement between the experiment and numerical model (Titurus and Friswell 2008). Updating parameters are selected with the aim of correcting the uncertainties in the FE model. It is necessary, therefore, to select those parameters to which the numerical responses are sensitive and whose values are uncertain in the initial model. Otherwise, the parameters may deviate far from the initial FE model and take on meaningless values while still resulting in good correlations between numerical and experimental results.

The discrepancies between the different parameters of the initial FE model and the full-scale structure can be attributed to many inherent uncertainties and modelling assumptions, such as material density, stiffness and boundary and connectivity conditions. Parameter selection therefore requires a considerable insight into the structure and its model. In this study, only a relatively small number of parameters were selected based on a prior knowledge of their potential variability and a sensitivity analysis was carried out to confirm they influence the responses. The various inertia parameters of the structure were not included as these are typically less uncertain than stiffness parameters. The bridge was also supported at clearly defined points using specialized bearings that permitted making good judgment about the appropriate modelling of boundary conditions, except the numerical values of bearing spring stiffness. Thus, candidate parameters considered for calibration in this study were cable tensions, cable axial stiffness, bending and torsional stiffness of the deck and stiffness of the bearings.

The likely uncertainty of the parameters characterizing cable stiffness, i.e. cable axial stiffness and tension force, can be attributed to many factors such as application of different tensioning forces than those specified in design, relaxation of steel stresses with time, and slippage in anchorages and between cable strands. Stiffness of the deck depends on Young's modulus of both steel and concrete; especially the latter shows considerable variability. The connection between steel girder and concrete slab will typically be designed to allow for either composite action or lack thereof. However, real bridges will always exhibit a certain degree of composite action (less than full because of connector flexibility, and more than none because of, for example, steel-concrete friction) eluding the analyst. Furthermore, non-structural elements, such as pavement, railings, services, also make a contribution to stiffness that is difficult to quantify and model precisely. Also, stiffness of the bearings was assumed from literature as the exact specifications were not known, and is thus prone to uncertainty further exacerbated by the inherent variability of elastomer properties.

There are three pairs of stay cables on each side of the central pylon. The four identical cables closest to the abutments are referred to as Cab-1, the four cables in the middle as Cab-2, and the four cables nearest to the pylon as Cab-3 (Figure 4.3). The cables were post-tensioned, as per design documentation, with forces $T_{Cab\text{-}1}$=55 kN for the four cables closest to the abutments, $T_{Cab\text{-}2}$=95 kN for the middle cables, and $T_{Cab\text{-}3}$=75 kN for the cables nearest to the central pylon (Figure 4.3). The effective axial stiffness of a cable depends on its projected length, self-weight, axial stiffness EA (where E is Young's modulus and A is cross-sectional area) and tension force in the cable (Nazmy and Abdel-Ghaffar 1990). For taut cables with small sag, the influence of axial stiffness EA on the effective stiffness is more pronounced than that of the tension force. A simple hand calculation using the Ernst formula for cable stiffness (Nazmy and Abdel-Ghaffar 1990) showed that the effect of tension force on stiffness is much more important in cables Cab-1 compared to the remaining cables. This was later confirmed by the sensitivity analysis on the FE model, and therefore only tension $T_{Cab\text{-}1}$ was included in the updating parameters.

Sensitivity analysis using the FEM model was conducted to confirm the selected updating parameters can influence the analytical responses. Relative sensitivity is the ratio of the relative change in the response value caused by a relative change in the parameter value. In this study, sensitivities were calculated using a finite difference method by changing the parameters by 0.1% with respect to their initial values. The selected parameters based on sensitivity analysis and engineering insight into their uncertainty were deck flexural stiffness for vertical ($K_{y,deck}$) and horizontal ($K_{x,deck}$) bending, deck torsional stiffness ($K_{t,deck}$), axial stiffness of all cables (K_{cable}), cable tension for Cab-1 ($T_{Cab\text{-}1}$), and stiffness of bearings ($K_{bearing}$). The bearing stiffness $K_{bearing}$ is to be understood as a single parameter whose changes affect proportionally the stiffness of bearing springs in the horizontal, vertical and torsional direction; this was done to keep the number of bearing related updating parameters to a minimum.

The sensitivities of modal frequencies to the updating parameters are shown in Figure 4.11. It can be noticed from the figure that, as expected, parameters $K_{y,deck}$, K_{cable} and $T_{Cab\text{-}1}$ influence appreciably, albeit to a varying degrees, the frequencies of vertical Modes 1, 2, 3, 6 and 7.

Additionally, K_{cable} influences the torsional Mode 8. Parameter $K_{x,deck}$ influences the horizontal Modes 4 and 5. Two parameters that influence the torsional Mode 8, $K_{bearing}$ and $K_{t,deck}$ require careful attention. Ignoring a very small influence $K_{bearing}$ has on the other modes, the two parameters practically only influence Mode 8. It can thus be expected, and indeed it was confirmed in preliminary calculations, that without constraining the two parameters attempts to update Mode 8 create an ill-posed problem with no unique solution. To overcome the problem, a regularization constraint was applied to keep the ratio of $K_{t,deck}/K_{bearing}$ approximately constant during updating. The objective function, given in its general form in Equation 3.42, now becomes as follows:

$$\Pi = \alpha_1 \sum_{i=1}^{n} \left(\frac{f_{a,i} - f_{e,i}}{f_{e,i}} \right)^2 + \alpha_2 \sum_{i=1}^{m} \frac{\left(1 - \sqrt{MAC_i}\right)^2}{MAC_i} + 0.0002 \left| \frac{K_{t,deck,i}}{K_{bearing,i}} - \frac{K_{t,deck,0}}{K_{bearing,0}} \right| \quad (4.6)$$

where subscript i denotes current values of parameters and subscript 0 represents their initial values. The value of the regularization term weighting factor 0.0002 was adjusted by trial and error so that the ratio of the two parameters did not change more than ±10%. It is acknowledged here that the way the two parameters were restrained can be considered arbitrary, but it can also be argued to be physically plausible. Furthermore, the examination of the potential ill-posing of the problem by checking the sensitivity plot should in future be performed in a more systematic and rigorous way.

Finally, selecting appropriate bounds on the allowable parameter variations during model updating is challenging and is normally done using engineering judgment. Different bounds have been used in previous research (Jaishi and Ren 2005, Zivanovic et al. 2007). From the frequency errors in Table 4.2, it can be concluded that the initial FE model generally overestimates the stiffness, therefore the lower bound has been selected as -40% and the upper bound was selected as +30% for all the parameters.

4.5.2. Assessment of the performance of model updating methodology

This section applies the proposed combination of PSO with SNT to the pedestrian bridge FE model updating in order to explore the performance of the approach. In the first phase, uncertain parameters were updated using available experimental information measured from physical testing using the traditional SM-based model updating. Effect of different starting points on results of SM-based model updating was explored. In the second phase, uncertain parameters were updated using the proposed approach using PSO and SNT.

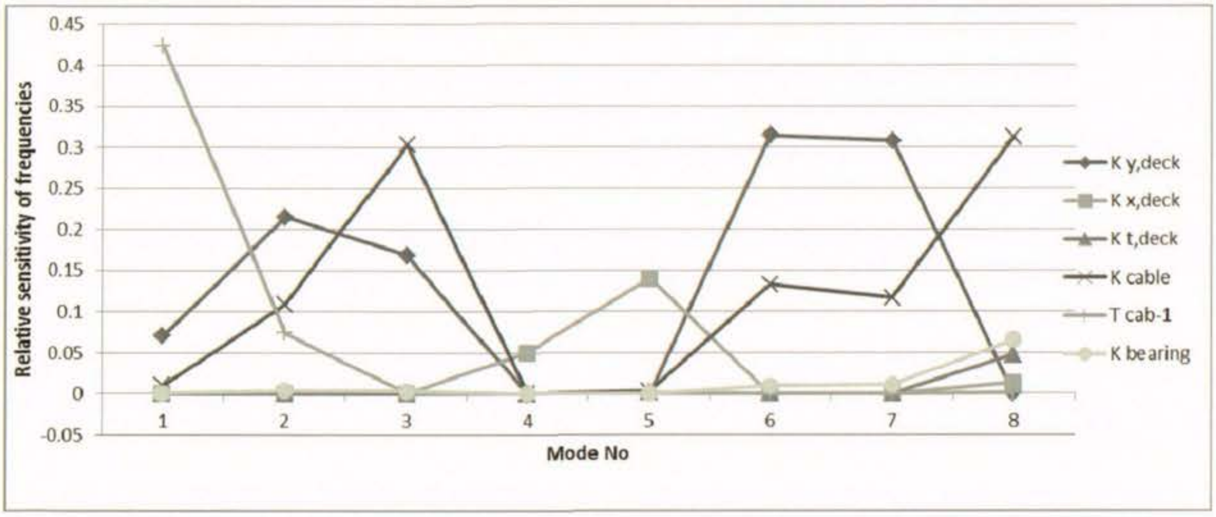

Figure 4.11. Sensitivity of modal frequencies to selected updating parameters.

4.5.2.1. Updating using a sensitivity-based technique

In this section, experimentally identified modal data from field tests were updated considering stiffness parameters as listed earlier in section 4.5.1. A sensitivity based iterative model updating method is applied to the full scale bridge to decrease the difference between modal properties of FE model and those identified from measurements. The vector of analytical eigenvalues and eigenvectors is a non-linear function of the uncertain parameters. It is the goal of optimization to determine the set of parameters which decrease the error residual. As explained in Chapter 3.3.2, one way to solve this problem is to expand the eigenproperties into a Taylor series, which is truncated to include only the linear term (Friswell and Mottershead 1995) including the sensitivity matrix (Equation 3.4.5). The initial FE model of the bridge was updated using a non-regularized version of Equation 4.6 to demonstrate limitation of SM and the need for regularisation. This simulation is referred to as Run 1. The updated solution obtained in the form of the ratios of updated to initial stiffness values is shown in Table 4.3.

The initial and updated frequencies, their errors compared to the experimental results, and initial and updated MACs are shown in Table 4.4. All frequency errors are less than 3% after updating. The largest error dropped from 8.6% to 2.8%, and in fact corresponds to a small error increase for the first vertical mode. This indicates that it is possible to improve the FE model considerably via adjusting the particular set of updating parameters considered, but some trade-off is inevitable. On the other hand, MAC values did not change appreciably, with some small positive and negative changes in different modes and the minimum value remaining at 0.987. This however, is not a problem because of high MAC values were achieved already in the initial model.

The updated parameters should be physically meaningful; otherwise it is difficult to justify the updating results. The vertical bending stiffness of the bridge deck has decreased by 15.5%, horizontal stiffness by 16.3% and torsional stiffness by 6.5%, respectively. This could be mainly attributed to the fact that the initial model takes the cast in-situ concrete slab as fully composite with the steel girder, whereas no concrete contribution to deck stiffness was assumed in design and, consequently, no special shear connectors were provided. (For comparison, when one ignores the concrete slab, the deck stiffness is 15.4%, 24.4% and 29.1% for vertical bending, horizontal bending and torsional stiffness, respectively, compared to the fully composite case.) The updated results reveal that there may be some, albeit at best only partial, composite action between the slab and the steel girder contributing to the stiffness of the whole deck. The consistent decrease in all the parameters related to the deck stiffness supports this conclusion. However, different than assumed stiffness of concrete and steel girder (e.g. due to stiffeners), and non-structural components can also be responsible. However, with only the limited number of measured modes available, further granularity in girder stiffness modelling cannot be further conclusively explored and has to be acknowledged as a limitation of this updating exercise.

The increase in cable tension $T_{Cab\text{-}1}$ by 12%, shows that these post-tension forces are more than the designed value of 55 kN, indicating possible overstressing of the cables. On the other hand, the cable axial stiffness shows a 7% decrease. The latter result can be attributed to many factors. The FEM model uses a rather coarse parameterization. As a result, potential localized stiffness changes may be lumped into those parameters. For example, the identified drop in the cable axial stiffness may be because of slippage in the cable anchorages, i.e. uncertainty in the modelling of structural connectivity.

As discussed in Chapter 2, there are a number of uncertainties associated with realization and subsequent FE modelling of any full scale structure. Therefore an attempt has been made to update the FE model using different initial values of updating parameters. The initial values of all the six parameters were multiplied by a factor of either 0.92 or 1.11. The corresponding simulations are referred to as Run 2 and Run 3, respectively. The corresponding model updating results are presented in Table 4.3. The corresponding frequency differences and MAC values for these runs are shown in Table 4.4. It can be seen that the SM-based algorithm has failed to converge to the same values of parameters as found in Run 1. This agrees with the experience of model updating attempts of full scale structure presented by other researchers that sensitivity based methods might lead to different solutions in the search space (Jaishi and Ren 2005, Zarate and Caicedo 2008). The authors in those papers have tried to update using different starting points within the search bounds and the final answer that satisfied the judgment of the analyst was taken as the final updated solution considering multiple alternatives. This illustrates a limitation of SM.

The analyst normally has little knowledge of the parameter interaction in a multi-dimensional solution space and a trial-and-error search is normally performed. Another important point is that the initial model has to be a very good realization of the actual structure (Friswell and Mottershead 1995), otherwise the updating results can move far away from the actual structure. This is also the reason why an initial stage of manual model updating has been required and/or recommended in several previous studies (Brownjohn and Xia 2000, Brownjohn et al. 2001) so that the initial FE model closely matches the as-built structure. Regularization techniques may also require that the initial FE model is a good representation as these mathematical techniques often try to decrease the change in the values of the parameters (Titurus and Friswell 2008).

GOAs can be applied with the aim of finding the best solution within the search bounds. In the next section, PSO was applied to the problem of updating of the footbridge. A combination of PSO and SNT is also presented in the next section, which searches for the minima sequentially thus giving more information about the search space and confidence in final results rather than running blind independent runs with different starting points.

4.5.2.2. Updating of uncertain parameters using particle swarm optimisation and sequential niche technique

In this section, experimentally identified modal data from the field tests were updated using PSO. A population of 20 points was used, the maximum number of generations was set to 200, and the upper threshold of the objective function to 0.001. The selection of parameters in

Table 4.3. Solutions obtained by SM-based model updating.

Run	Factors for starting values of parameters	Ratio of updated to initial stiffness $K_{y,deck}$	$K_{x,deck}$	$K_{t,deck}$	K_{cable}	$T_{Cab\text{-}1}$	$K_{bearing}$	Final value of objective function
1	1	0.845	0.837	0.935	0.930	1.120	0.981	0.0022
2	0.92	0.812	0.822	0.901	0.917	0.928	0.901	0.0072
3	1.11	0.967	0.803	1.056	0.661	1.279	1.065	0.0139

Table 4.4. Updated FE model and experimental frequencies and MACs using SM.

		Run 1			Run 2			Run 3		
Mode	Experimental frequencies by N4SID (Hz)	Updated FE model frequencies (Hz)	Error in frequencies (%)	MAC	Updated FE model frequencies (Hz)	Error in frequencies (%)	MAC	Updated FE model frequencies (Hz)	Error in freque ncies (%)	MAC
1	1.64	1.69	2.8	0.999	1.59	-3.3	0.999	1.72	4.9	0.999
2	1.9	1.86	-2.1	0.996	1.78	-6.5	0.996	1.94	2.2	0.995
3	3.69	3.70	0.2	0.999	3.66	-0.9	0.999	3.42	-7.2	1.000
4	4.86	4.97	2.2	0.990	4.92	1.2	0.990	4.86	0.1	0.990
5	5.33	5.28	-1.0	0.987	5.27	-1.2	0.987	5.25	-1.6	0.988
6	6.31	6.39	1.2	1.000	6.30	-0.2	1.000	6.40	1.4	0.999
7	7.42	7.30	-1.6	0.992	7.18	-3.3	0.992	7.38	-0.5	0.993
8	8.32	8.41	1.1	0.993	8.29	-0.4	0.993	7.70	-7.4	0.991

the PSO algorithm is critical to its success. On the basis of extensive studies conducted by Clerc and Kennedy (2002), the PSO parameters appearing in Equation 3.48 were set to γ=0.729, c_1=1.5 and c_2= 1.5 (known as the default contemporary PSO variant). The maximum velocity was constrained as half of the allowable parameter variation range (-40% - +30%). The niche radius for SNT was calculated according to Equation 3.51 for four minima as 0.97, but to account for possible closeness of some of these minima 50% of this value was adopted. The parameter m for derating function (Equation 3.50) was assumed as 1000.

Model updating by PSO alone (i.e. without SNT) was attempted initially. Ten independent runs were tested with different, randomly selected starting points to check the efficiency in detecting the best solution. The best solution in the form of the ratios of updated to initial stiffness values and their standard deviations from the 10 runs are shown in Table 4.5. It can be seen that the maximum standard deviation of the updated parameter ratios is 0.0058, giving confidence that all the solutions correspond to the same point in the search space. The results obtained are in close agreement with the ones obtained using SM-based method in Run 1.

PSO with SNT was then applied to confirm that there is no better solution than the solution found earlier by PSO alone. PSO with SNT was iterated five times and the results are shown in Table 4.6. It can be seen that the first solution found (shown in bold) is the same solution as the one found earlier by PSO alone (and by SM-based updating in Run 1). In further iterations, different solutions with increased objective function values were found. Also, the updated parameter values for those solutions were in many cases quite different than for the first minimum. This is because SNT forbids the search algorithm to converge again to the same niche. This systematic search through the updating parameter domain gives confidence that the basic PSO algorithm, i.e. without SNT, has converged to the global minimum in all 10 independent runs.

For checking the effect of the niche radius, the raw objective function values were compared with the modified function values obtained after the derating function was applied. It has been found that the niche radius used in this study has not affected the other solutions in the search space.

Table 4.5. Ratios of updated to initial stiffness and final objective function values for PSO-based updating.

Ratio of updated to initial stiffness (standard deviation)						Final value of objective function
$K_{y,deck}$	$K_{x,deck}$	$K_{t,deck}$	K_{cable}	$T_{Cab\text{-}1}$	$K_{bearing}$	
0.845 (0.0006)	0.837 (0.0003)	0.935 (0.0001)	0.925 (0.002)	1.160 (0.0011)	0.932 (0.0058)	0.0021

Table 4.6. Ratios of updated to initial stiffness and final objective function values for PSO with SNT.

Minimum No.	Ratio of updated to initial stiffness						Final value of objective function
	$K_{y,deck}$	$K_{x,deck}$	$K_{t,deck}$	K_{cable}	$T_{Cab\text{-}1}$	$K_{bearing}$	
1	**0.845**	**0.837**	**0.935**	**0.925**	**1.160**	**0.932**	**0.0021**
2	0.662	0.798	0.600	1.300	1.044	0.600	0.0060
3	0.880	0.801	0.600	0.600	1.300	0.600	0.0049
4	0.600	0.802	0.657	1.300	1.219	0.950	0.0079

By combining PSO with SNT an increased confidence in finding the global minimum is achieved as the solution space has been searched sequentially and the user can select the best solution from a list of different available solutions.

4.6. Conclusions

A combination of PSO and SNT has been proposed in this study to enhance the performance of model updating using GOAs. SNT works by 'filling in' the objective function niches, corresponding to the already known solutions, and forces PSO to expend its region of search, thereby increasing the chance of exploring the full search space. The performance of PSO augmented with SNT has been explored using experimental modal analysis results from a full-scale cable-stayed pedestrian bridge, and improved performance over PSO alone demonstrated. It has also been demonstrated that traditional, SM-based updating can easily be trapped in local minima, whereas PSO, especially when combined with SNT, gives much more confidence in finding the global minimum. The results show that the methodology proposed herein gives the analyst more confidence in the model updating results and that it can successfully be applied to full-scale structures.

4.7. References

Abdel-Ghaffar, A.M., & Khalifa, M.A. (1991), Importance of cable vibration in dynamics of cable-stayed bridges, Journal of Engineering Mechanics, ASCE, 117, 2571-2589.

APSDynamics (2012), Dynamic ElectroSeis shaker Model 400, http://www.apsdynamics.com/

Standards New Zealand (2010), AS/NZS3679.1:2010: Structural steel hot rolled bars and sections, Standards New Zealand, Wellington.

Bodeux, J.B., & Golinval, J.C. (2001), Application of ARMAV models to the identification and damage detection of mechanical and civil engineering structures, Smart Materials and Structures, 10, 479-489.

Brownjohn, J.M.W., & Xia, P.Q. (2000), Dynamic assessment of curved cable-stayed bridge by model updating, Journal of Structural Engineering, ASCE, 126, 252-260.

Brownjohn, J.M.W., Xia, P.Q., Hao, H., & Xia, Y. (2001), Civil structure condition assessment by FE model updating: methodology and case studies, Finite Elements in Analysis and Design, 37, 761-775.

Brownjohn, J.M.W., Moyo, P., Omenzetter, P., & Lu, Y. (2003), Assessment of highway bridge upgrading by dynamic testing and finite-element model updating, Journal of Bridge Engineering, , ASCE, 8, 162-172.

Computers and Structures (2009), SAP2000 structural analysis program, Computers and Structures, Berkeley, CA.

Chang, C.C., Chang, T.Y.P., & Zhang, Q.W. (2001), Ambient vibration of long-span cable-stayed bridge, Journal of Bridge Engineering, ASCE, 6, 46-53.

Clerc, M., & Kennedy, J. (2002), The particle swarm - explosion, stability, and convergence in a multidimensional complex space, IEEE Transactions on Evolutionary Computation, 6, 58-73.

Ewins, D.J. (2000), Modal testing: theory, practice and application, Research Studies Press, Baldock.

Friswell, M.I., & Mottershead, J.E. (1995), Finite element model updating in structural dynamics, Kluwer, Dordrecht.

Gent, A.N. (2012), Engineering with rubber - how to design rubber components, (3rd Ed.), Hanser, Munich.

Jaishi, B., & Ren, W.X. (2005), Structural finite element model updating using ambient vibration test results, Journal of Structural Engineering, ASCE, 131, 617-628.

Jaishi, B., & Ren, W.X. (2007), Finite element model updating based on eigenvalue and strain energy residuals using multiobjective optimisation technique, Mechanical Systems and Signal Processing, 21, 2295-2317.

Nazmy, A.S., & Abdel-Ghaffar, A.M. (1990), Three-dimensional nonlinear static analysis of cable-stayed bridges, Computers and Structures, 34, 257-271.

Pavic, A., Miskovic, Z., & Reynolds, P. (2007), Modal testing and finite-element model updating of a lively open-plan composite building floor, Journal of Structural Engineering, ASCE, 133, 550-558.

Proakis, J.G., & Manolakis, D.G. (1996), Digital signal processing: principles, algorithms, and applications, Prentice-Hall, Upper Saddle River, NJ.

Ren, W.X., & Peng, X.L. (2005), Baseline finite element modelling of a large span cable-stayed bridge through field ambient vibration tests, Computers and Structures, 83, 536-550.

Titurus, B., & Friswell, M. (2008), Regularization in model updating, International Journal for Numerical Methods in Engineering, 75, 440-478.

Van Overschee, P., & De Moor, B. (1994), N4SID: subspace algorithms for the identification of combined deterministic-stochastic systems, Automatica, 30, 75-93.

Van Overschee, P.V., & De Moor, B. (1996), Subspace identification for the linear systems: theory – implementation – applications, Kluwer, Dordrecht.

Zarate, B.A., & Caicedo, J.M. (2008), Finite element model updating: multiple alternatives, Engineering Structures, 30, 3724-3730.

Zivanovic, S., Pavic, A., & Reynolds, P. (2007), Finite element modelling and updating of a lively footbridge: the complete process, Journal of Sound and Vibration, 301, 126-145.

CHAPTER 5

AMBIENT VIBRATION TESTING, OPERATIONAL MODAL ANALYSIS AND COMPUTER MODELLING OF A TWELVE-SPAN VIADUCT

5.1. Introduction

For both newly constructed and for older existing bridges, it is essential to measure the actual dynamic characteristics to assists in understanding of their dynamic behaviour under traffic, seismic, wind and other live and environmental loads. Full scale dynamic testing of bridges can provide valuable information on the in-service behaviour and performance of the structures. From the measured dynamic responses, using system identification techniques dynamic parameters of bridge structures, such as natural frequencies, mode shapes and damping ratios, can be identified (Farrar and James III 1997).

For testing of large-scale bridges, ambient vibration tests are a simpler, faster, cheaper and often the only practical method for the determination of dynamic characteristics (Farrar et al. 1999). Such an approach where input excitation is not measured, and only responses are, is referred to as operational modal analysis (OMA). Ambient vibration tests have been successfully applied for assessing the dynamic behaviour of different types of full-scale bridges (Gentile 2006, Whelan et al. 2009, Liu et al. 2011, Altunisik et al. 2011, Magalhães et al. 2012). Nevertheless, there is still dearth of experimental and analytical studies for long, multi-span concrete bridges and data on the evaluation of existing and emerging identification techniques.

This chapter describes a study comprising full-scale, in-situ dynamic tests, OMA and FE model simulations conducted on Newmarket Viaduct, a post-tensioned, precast-concrete, segmental, hollow-box-girder structure that is located in Auckland, consists of 12 spans and is 690 m long. These tests are two extensive one-off ambient vibration tests using wireless sensors, conducted to evaluate the structural behaviour of the viaduct. The tests comprised the measurement of accelerations in the structure induced by typical everyday vehicular traffic crossing over the viaduct. Output-only modal identification methodologies were used to analyse the data obtained in those tests, in order to identify the modal properties of the viaduct in different stages of construction.

The layout of the chapter is as follows. A description of the bridge is first given, followed by an overview of the experimental testing methods. The following section addresses the modal identification techniques that were applied. System identification results are then presented, and numerical bridge modelling is outlined. Finally, a set of conclusions summarizes the study.

5.2. Bridge description

The Newmarket Viaduct, recently constructed in Auckland, New Zealand, is one of the major and most important bridges within the country's road network. It is a horizontally and vertically curved, post-tensioned concrete structure, comprising two parallel, twin bridges. The Southbound Bridge was constructed first and opened to traffic at the end of 2010; this was followed by the construction of the Northbound Bridge completed in January 2012. Now, both bridges are opened to traffic. The traffic on the Northbound deck is carried on three lanes, and on four lanes on the Southbound deck. Three different views of the Newmarket Viaduct appear in Figure 5.1.

The total length of the bridge is 690 m, with twelve different spans ranging in length from 38.67 m to 62.65 m and average length of approximately 60 m. Construction of the bridge consumed approximately 4,200 t of reinforced steel, 544 km length of stressing strands, and 30,000 m^3 of concrete. The superstructure of the bridge is a continuous single-cell box girder of a total width of 30 m (Figure 5.2). The deck of the bridge contains a total of 468 precast box-girder segments and was constructed with balanced cantilever and prestressed box-beam method. The Northbound and Southbound Bridges are supported on independent pylons and joined together via a cast in-situ concrete 'stitch'. Figure 5.3 shows images of the bridge soffit before and after casting of the 'stitch'.

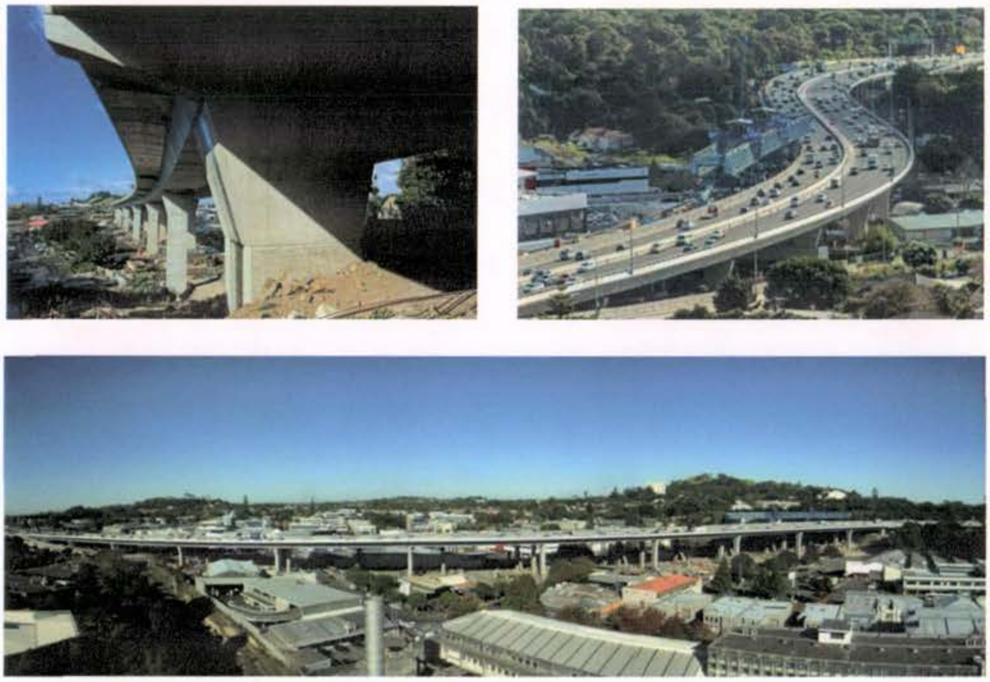

Figure 5.1. Views of Newmarket Viaduct.

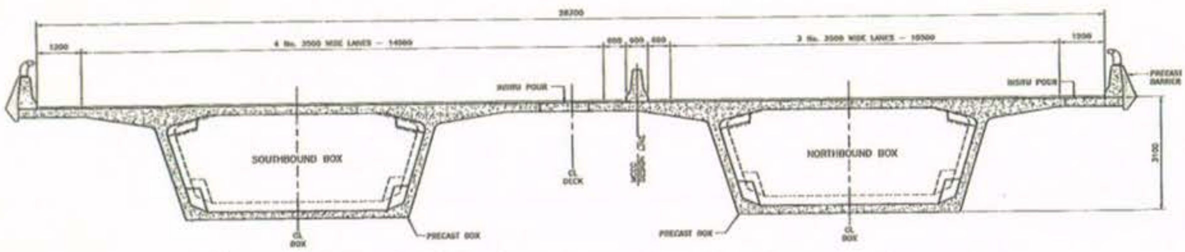

Figure 5.2. Typical deck cross section (all dimension in mm).

a) b)

Figure 5.3. Soffit of Northbound and Southbound Bridges a) before, b) and after casting of in-situ concrete 'stitch'.

5.3. Ambient vibration testing

5.3.1. Overview

A comprehensive ambient vibration testing program was conducted in two phases. The first one was carried out in November 2011 (Test 1), just before casting the in-situ concrete 'stitch' between the two bridges, and only included testing of the Southbound Bridge. The second one was carried out in November 2012 (Test 2), conducted just before completion and after casting of the 'stitch', covering both bridges (the Southbound Bridge and the Northbound Bridge). The two extensive one-off ambient vibration test campaigns were carried out in Newmarket viaduct to determine the actual bridge dynamic characteristics at a construction stage and for the final state.

5.3.2. Accelerometers

The accelerometers used for both tests were 56 USB wireless accelerometers (including two models: X6-1A and X6-2, show in Figure 5.4) developed by the Gulf Coast Design Concepts (2013). The X6-1A requires a single external battery and X6-2 contains an internal hardwired Lithium-Polymer battery rechargeable via a USB port. Both models have a number of attractive features such as low cost, 3-axis measurement, low noise, user selectable ±2/±6 g range and sampling rate of up to 320 Hz, 12-bit resolution, micro SD memory storage, accurate time stamp using real time clock with power back-up, easily readable comma separated output text data files, and USB connectivity. Note that these accelerometers do not have data transmission capability; they store the data to a micro SD card and after the test it needs to be downloaded to a computer. They are cost effective for conducting periodic experimental modal analysis but power limitations makes them only suited to short (several hours) to medium (several days) term vibration monitoring applications.

5.3.3. Instrumentation plan

For both tests, the one-off dynamic testing only used ambient effects, predominantly traffic, as excitation. No other forcing source was used to excite the bridge. When doing dynamic testing it was possible to enter bridge girders and place accelerometers inside. Therefore, the tests did not interfere with the normal flow of traffic over the bridge. For Test 1, a total of 96 locations inside the Southbound Bridge girder were chosen. A total of 292 locations inside the two bridge girders were chosen in Test 2. In both tests, the measurement points were on both sides of the girder (Figure 5.5), but the approximate span-wise distances were different (span/8 in Test 1 and span/6 in Test 2, respectively). The wireless USB type accelerometer/battery units were wrapped tightly onto a timber block. This block would be 'lightly' glued to the internal surface of the bridge deck using blue tack.

5.3.4. Test procedure

A similar testing procedure was adopted in the two tests, although with some slight differences. As the number of accelerometers available was limited (<60), several test setups were required to cover all the spans of the bridge. Four reference accelerometers were located in span 6 and span 7 of the Southbound Bridge during for the entire duration of the testing programme, while the remaining accelerometers were placed in different points in several test set-ups. Five test setups were used to cover the planned testing locations of the Southbound Bridge in Test 1, but only three setups to cover each bridge in Test 2. In both tests the sampling frequency was 160 Hz and the corresponding recording times were all approximately 1 hour for each setup. As an example, Figure 5.6 shows the time history of bridge response in all three directions recorded by one of the accelerometers near the middle of span 3 during Test 1.

a) 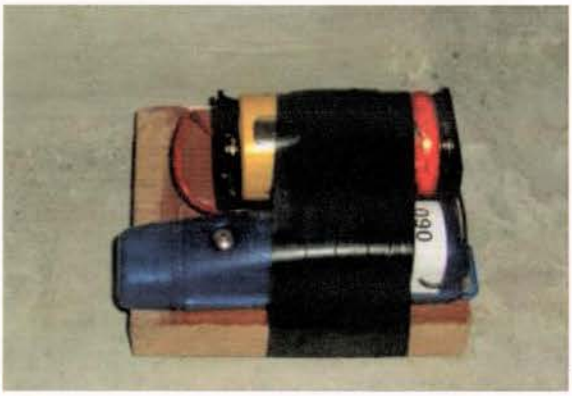 b) 

Figure 5.4. Wireless USB accelerometers used for the tests: a) model X6-1A, and b) model X6-2.

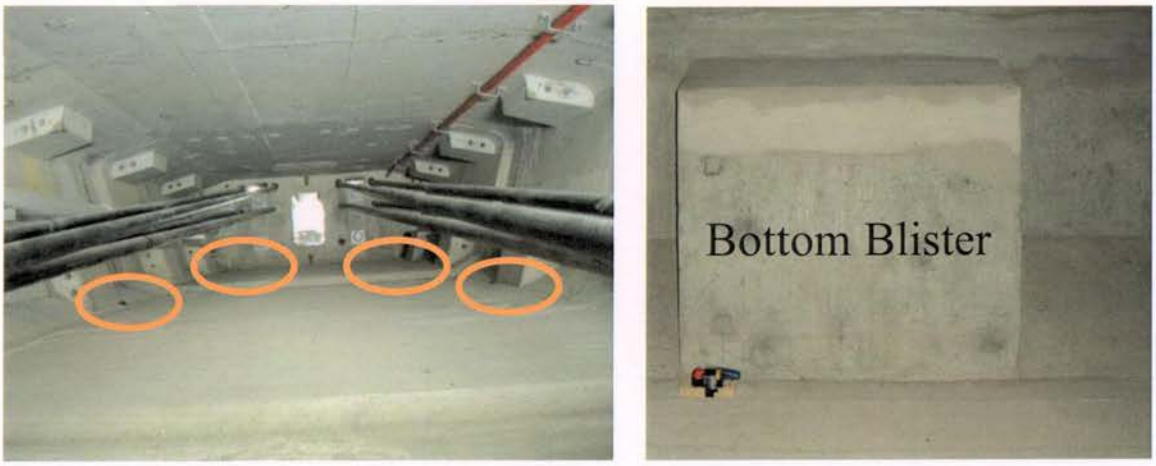

Figure 5.5 Location of accelerometers inside bridge girder.

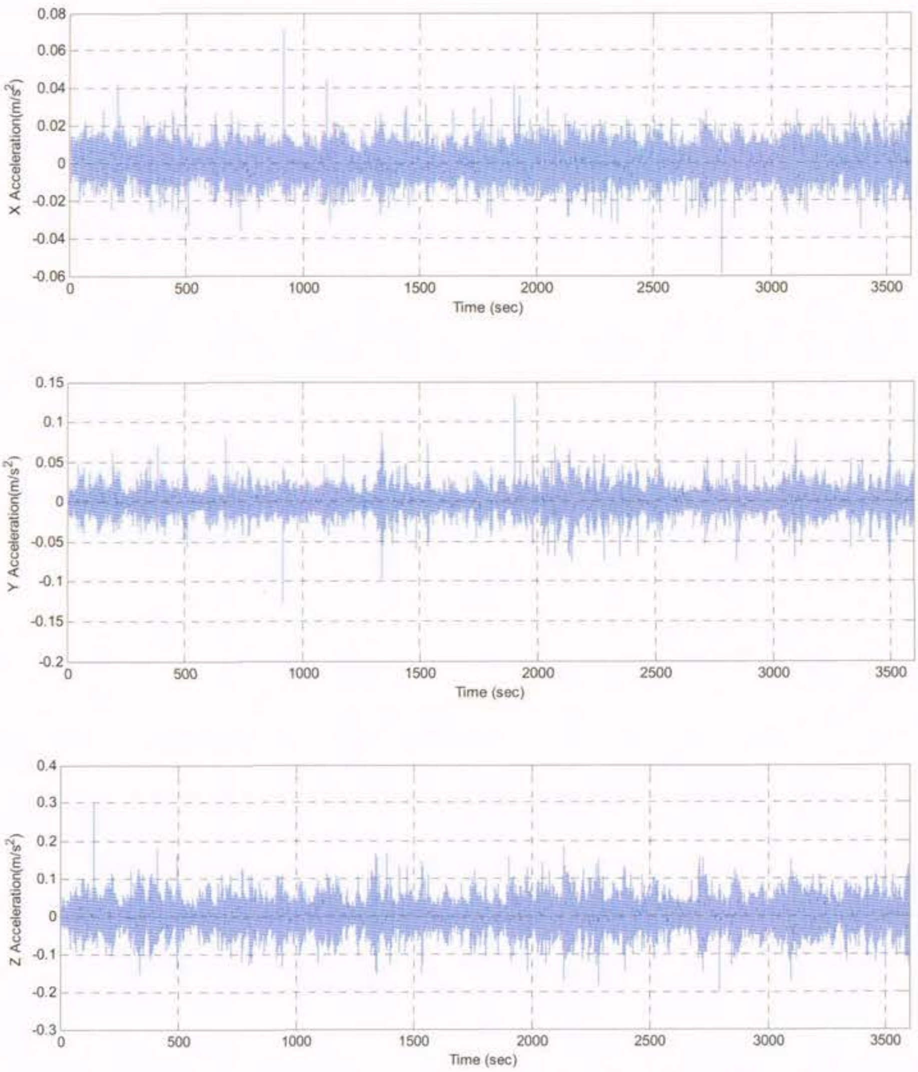

Figure 5.6. Example of tri-axial acceleration time histories.

5.4. Comparison of different system identification methods

Ambient vibration tests are not appropriate for FRF or impulse response function calculations because the input excitations are not measured. Different methods have been used to extract the modal parameters from ambient vibration data (Ren and Zong 2004). The mathematical background of output-only modal parameter identification, or OMA, methods is often very similar. Ambient excitation usually provides multiple inputs and wide-band frequency content, thus stimulating a significant number of vibration modes. For simplicity, output-only modal identification methods assume that the excitation input is a zero-mean Gaussian white noise. The difference between different OMA methods is often due to implementation aspects such as data reduction, type of equation solvers, sequence of matrix operations, etc. (Ren and Zong 2004). There are two main groups of output-only modal identification methods: nonparametric methods that essentially work in the frequency domain (such as PP and EFDD), and parametric methods, most of them in the time domain (such as NExT-ERA and SSI). The four methods referred to in the previous sentence are described in detail in Chapters 3.2.2-5.

Data processing and modal parameter identification were carried out using an in-house system identification toolbox written in MATLAB (Beskhyroun 2011). The four system identification techniques (PP, EFDD, NExT-ERA and SSI) were all programmed in this toolbox. Before processing of all the collected data, the performance of the four different system identification methods is compared using only a subset of measured data corresponding to the vertical vibrations of Test 2. The comparison will be based on the estimated natural frequencies and model shapes. Before applying an output-only modal identification method, the acceleration records were preprocessed with the following operations: i) mean removal and detrending, ii) filtering: high pass filtering at 1 Hz to remove low-frequency noise and low pass filtering at 20 Hz with a 5 pole Butterworth filter to keep only modes of interest, and iii) decimation and resampling from the frequency used in the tests to 50 Hz.

A comparison of modal identification results is presented in this section. Several vibration modes were identified using all four methods in the frequency range 0-10 Hz. Listed in Table 5.1 are the estimated natural frequencies and their standard deviations, σ_f. The standard deviations refer to the spread of results between the fours methods. As for the mode shapes, the accelerometers were placed in two rows along the girder edges of each bridge (see Figure 5.5), which means that each mode shape can be represented by four curves. However, in the comparison of mode shapes only the accelerometers located in Northbound Bridge were included. Figures 5.7-11 show comparison of the first five vertical modes. In Figure 5.12, MACs (Equation 3.43) between the four techniques are shown graphically in 3D bar plots.

Table 5.1. Natural frequencies for vertical modes identified by different methods.

Mode	PP (Hz)	EFDD (Hz)	NExT-ERA (Hz)	SSI (Hz)	σ_f (Hz)
Mode 1	2.03	2.03	2.07	2.03	0.020
Mode 2	2.34	2.34	2.37	2.35	0.014
Mode 3	2.54	2.54	None	2.54	0
Mode 4	2.81	2.81	2.83	2.81	0.010
Mode 5	3.12	3.12	3.13	3.13	0.005
Mode 6	3.32	3.32	3.33	3.32	0.006
Mode 7	3.67	3.67	3.68	3.68	0.005
Mode 8	3.83	3.83	3.87	3.84	0.019
Mode 9	4.30	4.30	4.29	4.29	0.006
Mode 10	7.46	7.46	7.48	7.47	0.010

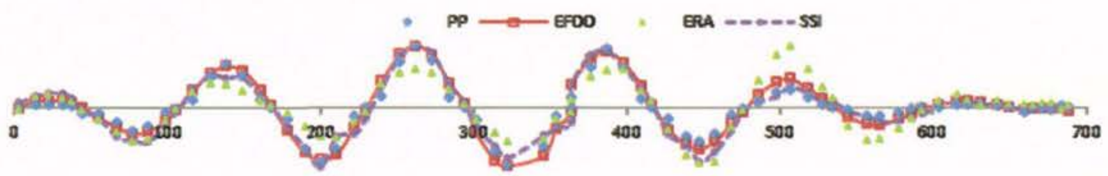

Figure 5.7. Comparison of the 1st vertical mode shape identified by different methods.

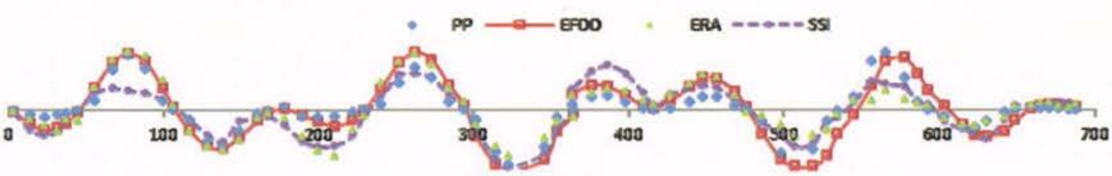

Figure 5.8. Comparison of the 2nd vertical mode shape identified by different methods.

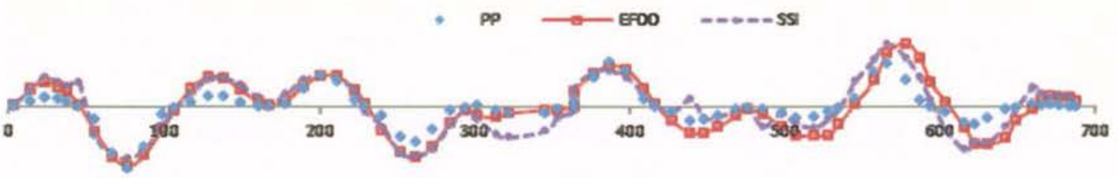

Figure 5.9. Comparison of the 3rd vertical mode shape identified by different methods.

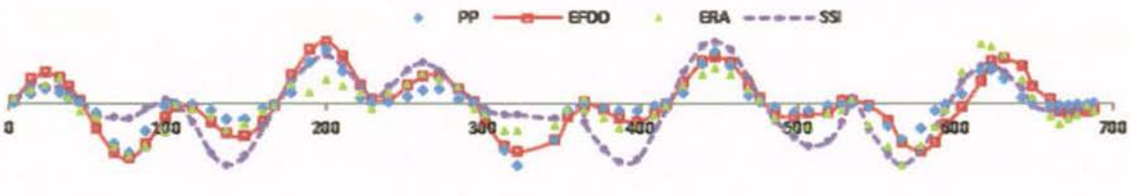

Figure 5.10. Comparison of the 4th vertical mode shape identified by different methods.

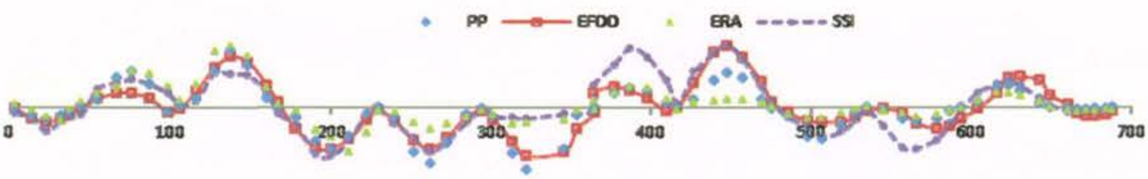

Figure 5.11. Comparison of the 5th vertical mode shape identified by different methods.

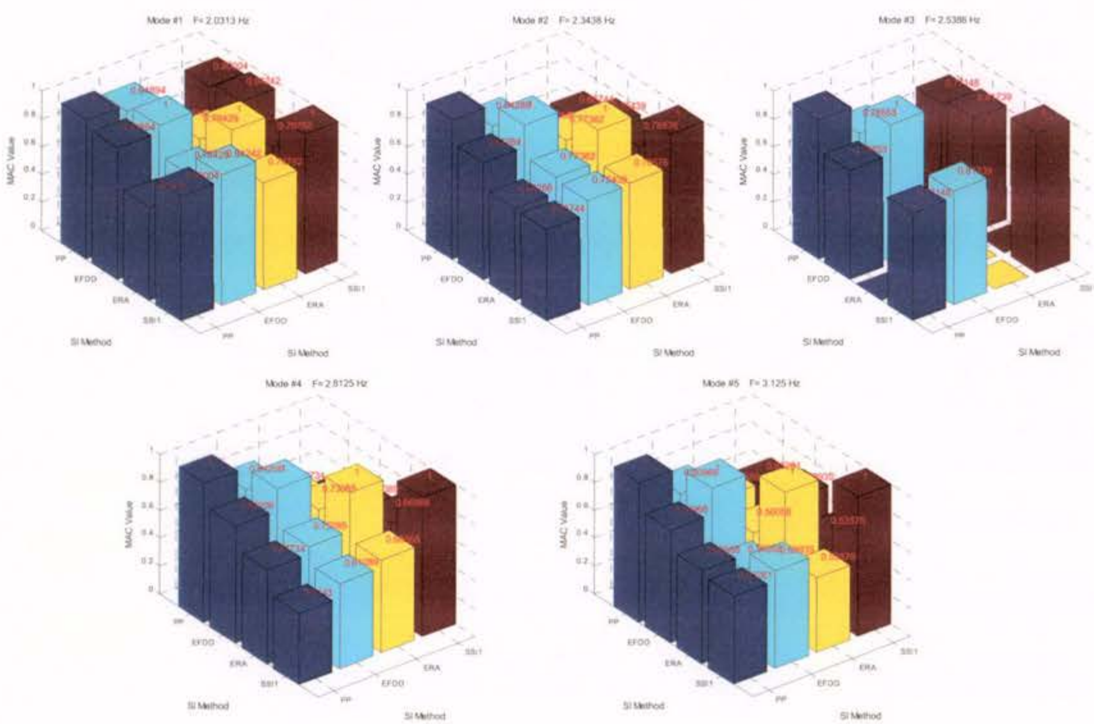

Figure 5.12. MACs for the first five vertical mode shapes identified by different methods.

All ten modal frequencies have been identified by three methods, except for the NExT-ERA method that has not identified the 3rd mode. In general, all the methods seem to agree well on the natural frequency estimates of the first ten modes. In the present case, it is found that the mode shape estimates of the EFDD method tend to return the best mode shape estimates judged based on their smoothness. The second best is the SSI method and the NExT-ERA is the worst one. Certainly, it is the first mode shape that the methods agree most on, as evidenced using the MAC values in Figure 5.12, which are at least 0.90 between for PP, SIS and EFDD. However, for NExT-ERA those values are as low as 0.67. For the higher modes MAC are lower dropping even to 0.53.

The advantage of the PP method is that it is easy to use and provides fast estimates (Bendat and Piersol 1993). The identified natural frequencies are simply obtained from the observation of the peaks on the graph of ASDs. An example of ASD for the vertical direction is shown in Figure 5.13. However, damping cannot be estimated using PP. The advantage of EFDD method is good estimate of natural frequencies and mode shapes that are comparable with the two other time-domain methods considered (Jacobsen et al. 2007). Since the mode shapes are estimated in frequency domain they are more comparable with the PP method than the two time domain methods. Note that the EFDD is also suitable for damping ratio identification (James et al. 1993), although damping ratio results from the EFDD method are not presented in this report.

The time domain methods have the advantages of operating directly on the measured time signals. However, they are typically more complicated, abstract, and computationally heavy. The results depend on the number of DOFs, or system order, assumed and different model orders have to be evaluated to determine the optimal one. However, the stabilization diagrams and other model validation techniques can be of aid to the user (Van Overschee and De Moor 1996). Figure 5.14 shows an example of the stabilization diagram using SSI. The SSI method solves the time and memory problem by reducing the amount of data used in the analysis. The ambient vibration tests have produced large volumes of data for analysis, but only small segments of them can be used in one calculation. The NExT-ERA method uses all available data. However, this did not seem to improve the modal parameter estimates significantly; indeed, NeXT-ERA missed one mode.

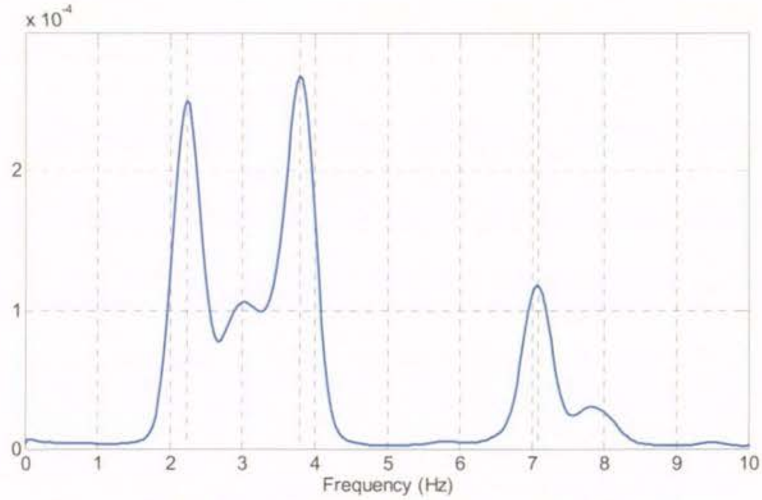

Figure 5.13. Example of ASD for vertical direction.

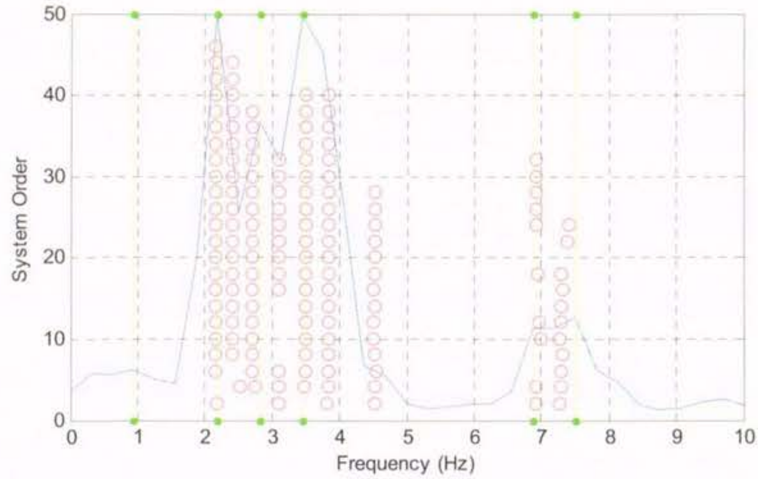

Figure 5.14. Example of SSI stabilization diagram for vertical data.

5.5. Comparison of bridge modal properties during construction and in-service stages

The EFDD method procedures were applied to the peaks identified in the singular value spectra in order to evaluate the frequencies and shapes of the natural modes of vibration of the viaduct. Several vibration modes were identified using the output-only measurements in the frequency range 0-10 Hz. For Test 1 data it was possible to identify 13 modes of vibration, while for Test 2 data 12 modes. The frequencies and general characteristics of the identified modes of vibration are presented in Table 5.2 for the tests performed before and after the in-situ casting of concrete 'stitch' between the two bridges. Vibration mode shapes of the bridge deck have also been extracted using EFDD. Figures 5.15-16 show selected identified transverse and vertical mode shapes for Test 2.

Table 5.2. Natural frequencies identified in Test 1 and Test 2.

Test 1			Test 2		
Mode no.	Type of mode	f (Hz)	Mode no.	Type of mode	f (Hz)
Mode 1	Transverse	1.64	Mode 1	Vertical	2.03
Mode 2	Transverse	2.11	Mode 2	Transverse	2.14
Mode 3	Vertical	2.15	Mode 3	Vertical	2.34
Mode 4	Vertical	2.42	Mode 4	Vertical	2.54
Mode 5	Vertical	2.62	Mode 5	Vertical	2.81
Mode 6	Transverse	2.73	Mode 6	Vertical	3.12
Mode 7	Vertical	2.89	Mode 7	Vertical	3.32
Mode 8	Vertical	3.20	Mode 8	Transverse	3.44
Mode 9	Vertical	3.52	Mode 9	Vertical	3.67
Mode 10	Transverse	3.63	Mode 10	Vertical	3.83
Mode 11	Vertical	3.75	Mode 11	Vertical	4.30
Mode 12	Vertical	4.20	Mode 12	Vertical	7.46
Mode 13	Vertical	6.88			

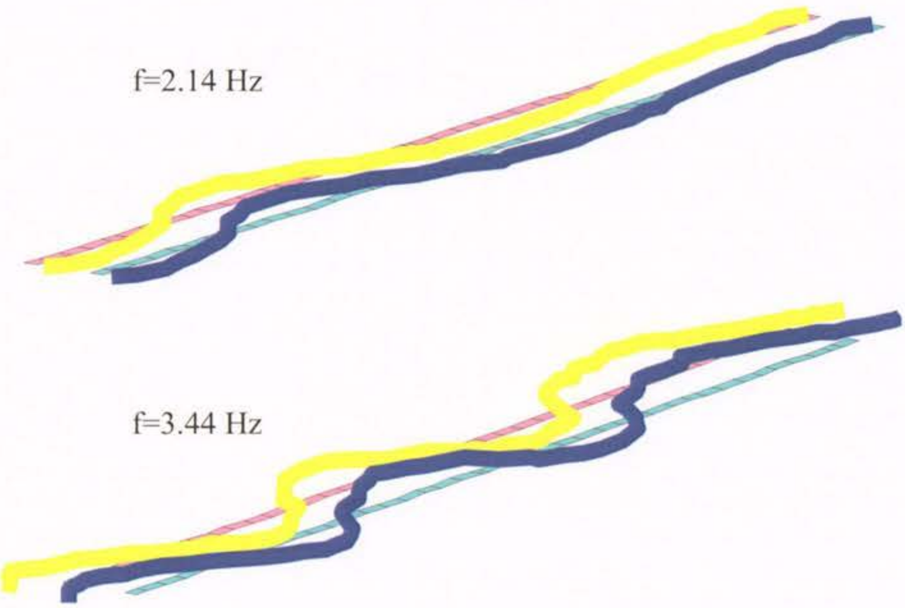

Figure 5.15. Views of the 1st and 2nd transverse bending modes for Test 2.

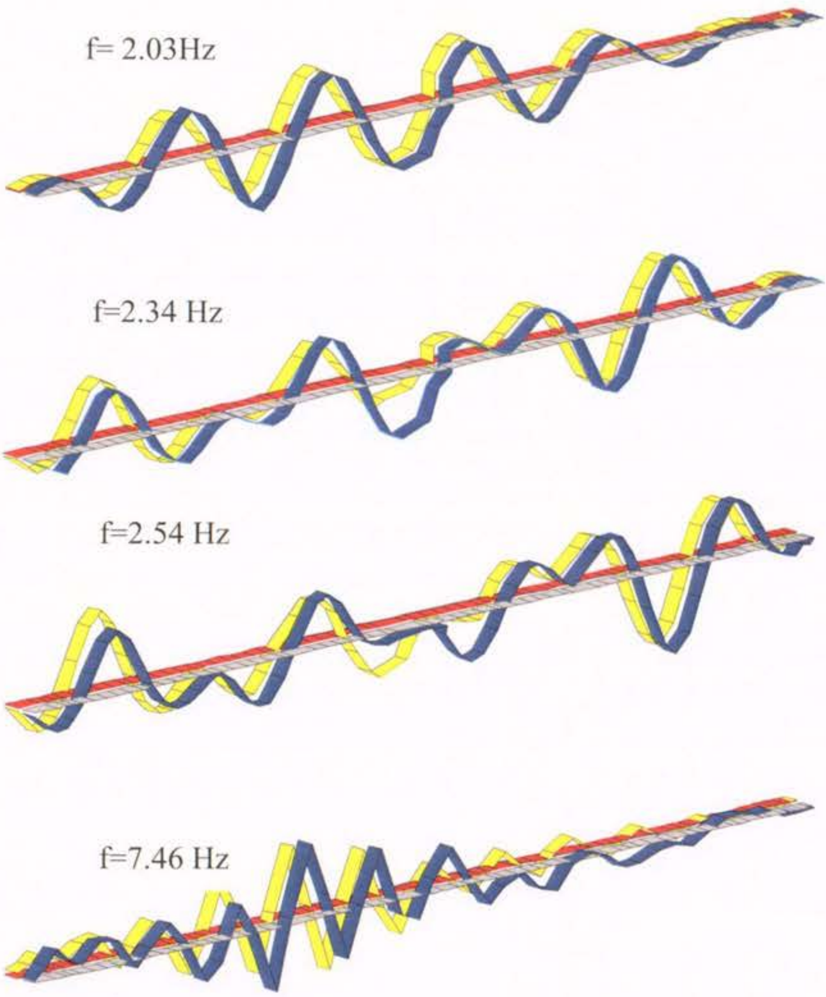

Figure 5.16. Views of the 1st, 2nd, 3rd and 10th vertical bending modes for Test 2.

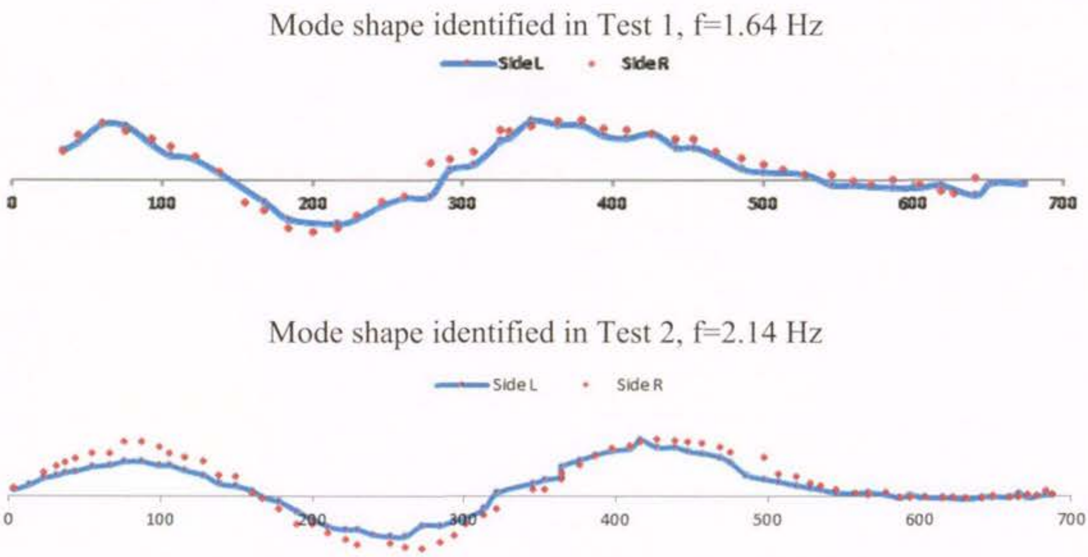

Figure 5.17. Comparison of mode shapes for the 1st transverse mode in Test 1 and Test 2.

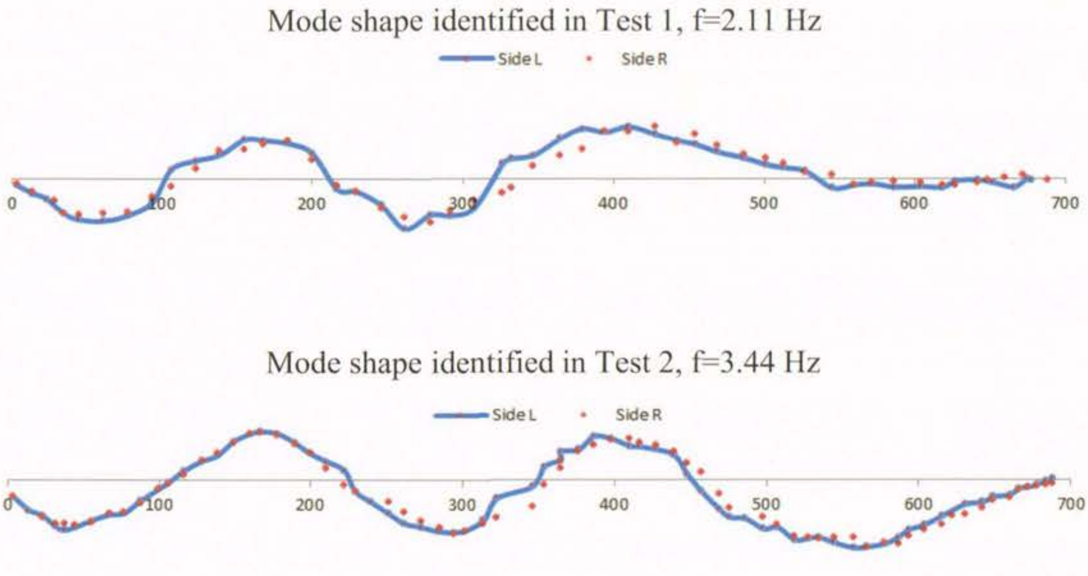

Figure 5.18. Comparison of mode shapes for the 2nd transverse mode in Test 1 and Test 2.

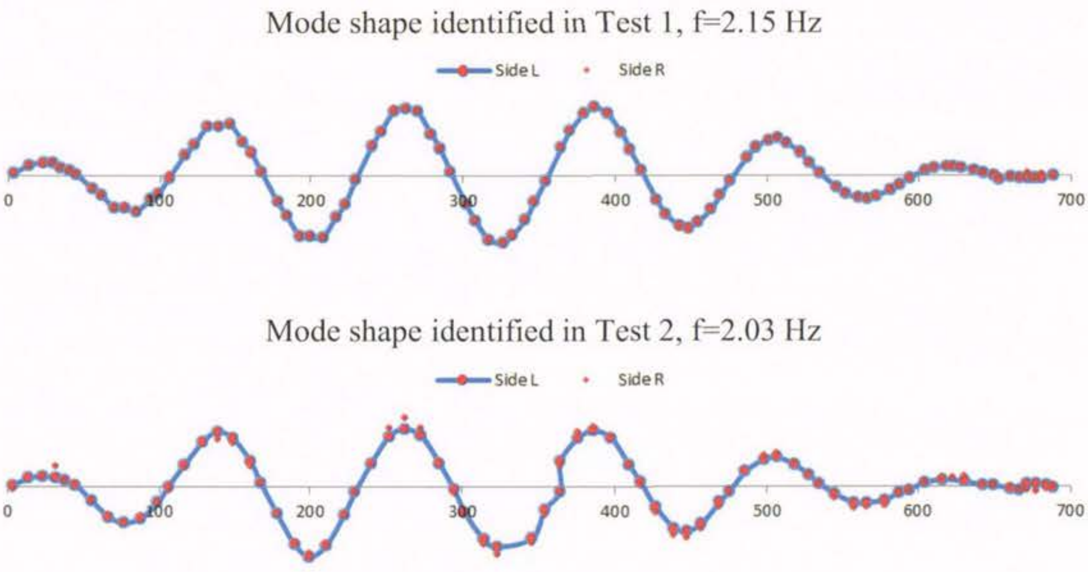

Figure 5.19. Comparison of mode shapes for the 1st vertical mode in Test 1 and Test 2.

Mode shape identified in Test 1, f=2.42 Hz

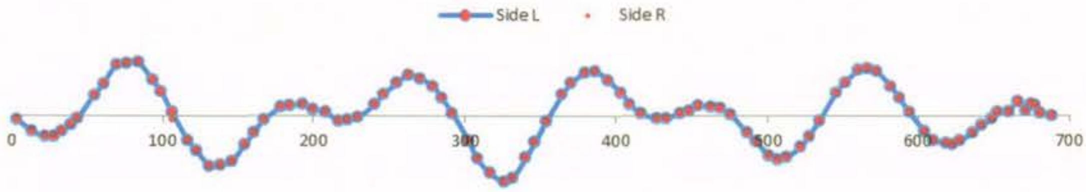

Mode shape identified in Test 2, f=2.34 Hz

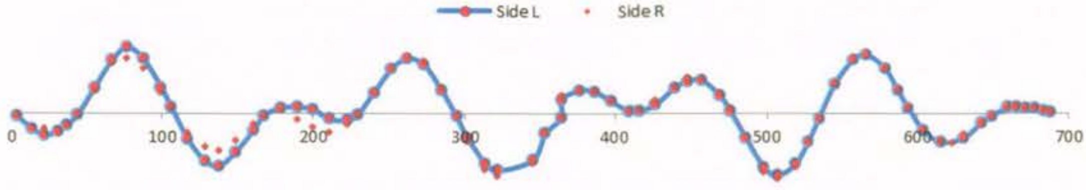

Figure 5.20. Comparison of mode shapes for the 2nd vertical mode in Test 1 and Test 2.

Figures 5.17-20 show a comparison of mode shapes identified before and after the in-situ casting of concrete 'stitch' for the first two transverse and the first two vertical modes. In those figures, side L means the side of the Southbound Bridge adjacent to the 'stitch', and side R means the side of the Southbound Bridge facing outwards. Considering the dynamic characteristics identified with the EFDD method applied to the data of the tests performed before and after casting of the in-situ concrete 'stitch' between two bridges, the following observations can be made. The frequencies of the first two transverse modes have increased markedly from 1.64 Hz to 2.14 Hz and from 2.11 Hz to 3.44 Hz, respectively. The frequencies of the first two vertical modes have decreased slightly, from 2.15 Hz to 2.03 Hz and from 2.42 Hz to 2.34 Hz, respectively. After the in-situ casting of concrete 'stitch', the two bridges work as one whole structure, where the increase in transverse stiffness is larger than the increase in inertia, leading to a significant increase in the transverse modal frequencies. For vertical vibrations, the increase in stiffness and mass are very similar and the corresponding frequencies do not change much. It can also be seen that the identified shapes agree well between the two tests. However, there is still a difference in the transverse deformability of the viaduct, which can be seen in the mode shapes identified for the second transverse vibration mode (Figures 5.18). The modal components identified for that mode are markedly different in the four spans at the right hand side end and also several nodal points appear in shifted locations. For Test 2, the amplitude at the end of the four spans is much larger than for Test 1.

5.6. Numerical modelling of the bridge

Throughout this study, specialised finite element software CSiBridge (Computers and Structures 2010) has been employed for modelling the structure. The superstructure was represented using solid elements, piers and pier caps were modelled using beam elements, and expansion joints and bearings using link elements. Fixed boundary conditions were specified at the base of the piers. The 3D FE models were developed referring to the two dynamic tests in the different construction stages. The model for the Southbound Bridge before casting of the 'stich' is show in Figure 5.21.

In order to model the bridge, it is necessary to know a number of material properties of the concrete used in construction. Twenty concrete 100 × 200 mm cylinder specimens were secured on site during construction. Six of these were used for measuring the compressive strength and elastic modulus, but authors' own results were amply supplemented by the analogous tests conducted by the contractor. Based on the concrete test results (Chen and Omenzetter 2012), in the finite element analysis the concrete in bridge girder was assumed to have compressive strength of 60 MPa, modulus of elasticity of 30 GPa and density of 2550 kg/m^3. The remaining cylinders were used for creep and shrinkage tests. For full details of the material testing programme please refer to Chen and Omenzetter (2012).

Eigenvalue analysis of the FE model was conducted and close agreement was obtained with the dynamic field test results. In Figures 5.22 and 23 and Table 5.3, the mode shapes and frequency values of vibration of the Southbound Bridge in Test 1 are presented. A very good agreement in frequencies can be seen with errors generally less than 4% and only one slightly over 8%. MACs are generally above 0.80 indicating a reasonably agreement.

Figure 5.21. 3D FE model of Southbound Bridges before casting of in-situ concrete 'stitch'.

f=2.11 Hz f= 2.67 Hz

Figure 5.22. Selected horizontal mode shapes of the Southbound Bridge obtained by numerical analysis.

f=2.15 Hz f=2.64 Hz

f=2.88 Hz f=6.88 Hz

Figure 5.23. Selected vertical mode shapes of the Southbound Bridge obtained by numerical analysis.

Table 5.3. Comparison of dynamic characteristics calculated from the measured accelerations and FE model in Test 1.

Mode no.	Type of mode	EFDD (Hz)	FE model (Hz)	Frequency error (%)	MAC
Mode 1	Transverse	1.64	1.65	0.6	0.90
Mode 2	Transverse	2.11	2.11	0	0.89
Mode 3	Vertical	2.15	2.15	0	0.96
Mode 4	Vertical	2.42	2.44	0.8	0.88
Mode 5	Vertical	2.62	2.64	0.8	0.87
Mode 6	Transverse	2.73	2.67	-2.2	0.84
Mode 7	Vertical	2.89	2.88	-0.4	0.94
Mode 8	Vertical	3.20	3.16	-1.3	0.94
Mode 9	Vertical	3.52	3.40	-3.6	0.88
Mode 10	Transverse	3.63	3.95	8.1	0.89
Mode 11	Vertical	3.75	3.70	-1.4	0.88
Mode 12	Vertical	4.20	4.22	0.5	0.90
Mode 13	Vertical	6.88	6.88	0	0.86

5.7. Conclusions

This Chapter presents the ambient dynamic tests performed on a 12-span viaduct in two different stages (before and after the two bridges making up the viaduct were joined together via a cast in-situ concrete 'stitch'). The performance of four different system identification methods based on vehicular excitation to determine modal dynamic parameters of the structure have been compared and discussed. The four methods were PP, EFDD, NExT-ERA and SSI. Within the frequency range 0-10 Hz, ten modal frequencies for vertical modes were successfully identified using the four methods. Although one frequency was not identified by the Next-ERA method, good agreements were found between the modal frequency estimates obtained from the four different methods. The comparison of mode shapes (MACs) showed that PP, SSI and EFDD agreed very well on the shape of the first vertical mode, however, NExT-ERA showed discrepancies. Similar discrepancies were noted for higher modes for all the identification methods used.

The dynamic characteristics identified at two construction stages were presented and compared in order to determine the actual bridge dynamics during construction and for the final state. The frequencies of the first two transverse modes have increased markedly, whereas the frequencies of the first two vertical modes decreased slightly. The experimental investigation was complemented by the development of a 3D FE models based on design drawings and material testing data. The FE results were compared with those obtained from experimental measurements and showed good correlation.

5.8. References

Altunisik, A., Bayraktar, A., & Sevim, B. (2011), Output-only system identification of post tensioned segmental concrete highway bridge, Journal of Bridge Engineering, ASCE, 16, 259-266.

Bendat, J., & Piersol, A. (1993), Engineering applications of correlation and spectral analysis, (2nd Ed.), New York, Wiley.

Beskhyroun, S. (2011), Graphical interface toolbox for modal analysis, Proceedings of the 9th Pacific Conference on Earthquake Engineering: Building an Earthquake-Resilient Society, paper no. 077.

Chen, X., & Omenzetter, P. (2012), A framework for reliability assessment of an in-service bridge using structural health monitoring data, Key Engineering Materials, 558, 39-51.

Computers and Structures (2010), CSiBridge: integrated 3D bridge design software, Computers and Structures, Berkeley, CA.

Farrar, C., & James III, G. (1997), System identification from ambient vibration measurements on a bridge, Journal of Sound and Vibration, 205, 1-18.

Farrar, C., Duffey, T., Cornwell, P., & Doebling, S. (1999), Excitation methods for bridge structures, Proceedings of IMAC XVII: 17th International Modal Analysis Conference, 1063-1068.

Gentile, C. (2006), Modal and structural identification of a RC arch bridge, Structural Engineering and Mechanics, 22, 53-70.

Gulf Coast Design Concepts (2013), http://www.gcdataconcepts.com/ products.html.

Jacobsen, N., Andersen, P., & Brincker, R. (2007), Using EFDD as a robust technique to deterministic excitation in operational modal analysis, Proceedings of the 2nd International Operational Modal Analysis Conference, 193-200.

James, G., Carne, T., & Lauffer, J. (1993), The natural excitation technique for modal parameter extraction from operating wind turbines, Report no. SAND92-1666, UC-261, Sandia National Laboratories, Albuquerque, NM.

Liu, T., Chiang, W., Chen, C., Hsu, W., Lu, L., & Chu, T. (2011), Identification and monitoring of bridge health from ambient vibration data, Journal of Vibration and Control, 17, 589-603.

Magalhães, F., Caetano, E. M., Cunha, A., Flamand, O., & Grillaud G. (2012), Ambient and free vibration tests of the Millau Viaduct: evaluation of alternative processing strategies, Engineering Structures, 45, 372-384.

Ren, W., & Zong Z. (2004), Output-only modal parameter identification of civil engineering structures, Structural Engineering and Mechanics, 17, 1-16.

Van Overschee, P., & De Moor, B. (1996), Subspace identification for linear systems: theory – implementation – applications, Kluwer, Dordrecht.

Whelan, M., Gangone, M., Janoyan, K, & Jha, R. (2009), Real-time wireless vibration monitoring for operational modal analysis of an integral abutment highway bridge, Engineering Structures, 31, 2224-2235.

CHAPTER 6

AMBIENT AND FORCED VIBRATION TESTING, SYSTEM IDENTIFICATION AND COMPUTER MODELLING OF A HIGHWAY OFF-RAMP BRIDGE

6.1. Introduction

Field dynamic testing of full-scale bridges is one of the most effective methods for investigating their real dynamic characteristics. It can provide valuable information of structures with correct boundary conditions and eliminates any need for scaling. This chapter describes the field testing programme conducted under ambient and forced conditions on the Nelson St off-ramp bridge, which is a part of the motorway system in central Auckland, New Zealand. In the ambient vibration tests, nearby traffic, wind, and possibly microtremors were used as excitation sources. The feasibility of obtaining dynamic properties of this type of bridges by ambient testing was checked. It was found that a few modes in the lateral direction could be identified with ambient data, while no modes were found in the vertical direction, most likely due to inadequate excitation energy and the relative high stiffness in the vertical direction. Several people also jumped on the deck in an attempt to obtain the vertical dynamic characteristics and the first two vertical mode shapes were successfully identified in this way. In the forced vibration tests, two ANCO MK-140-10-50 (ANCO Engineers 2013) eccentric mass shakers were utilized in a frequency sweep mode to excite the bridge in the vertical and lateral directions in the frequency range of up to 10.0 Hz. Two complementary system identification methods were implemented to extract the modal properties of the bridge: FDD and SSI. By varying the number of weights on the shakers, different levels of forcing were imparted to the structure and relationships of natural frequencies and damping ratios versus forcing and response magnitude obtained. A three-dimensional FE model was constructed, paying special attention to the various critical components and mechanisms such as hinges, bearings and boundary conditions. The FE model was manually adjusted until a good agreement with the experimentally measured natural frequencies and mode shapes was achieved. The calibration helped to understand the influence of the aforementioned critical components and mechanisms on the bridge dynamics.

6.2. Bridge description

The Nelson St off-ramp bridge is a part of the motorway network in central Auckland. The bridge has been permanently closed to traffic since 2005, because its role was taken over by a new structure as a part of the upgrade of the Central Motorway Junction in the early 2000s. The off-ramp remains standing as it is too expensive to demolish it and also provides redundancy in the junction. This created excellent opportunities for an extensive, undisturbed testing programme. The bridge was originally designed by Opus International Consultants (Opus) in 1976. Figures 6.1-3 show an aerial view, front view and side view of the bridge, respectively.

Figure 6.1. Aerial view of Nelson St off-ramp bridge.

Figure 6.2. Front view of Nelson St off-ramp bridge.

Figure 6.3. Side view of Nelson St off-ramp bridge.

The Nelson St off-ramp bridge is a curved, post-tensioned concrete, box girder, continuous bridge. It has a total length of 272 m and width of 7.5 m and consists of eleven spans with the longest span 40 m long. An elevation sketch with pier designations is shown in Figure 6.4. Information about span length is given in Table 6.1. The bridge was built using a moveable scaffolding system and contains a total of 137 precast box girder segments. Figures 6.5 and 6 show two representative cross sections of the girder.

The different sections are connected between Pier RD and RE with a hinge. The red arrow in Figure 6.7 shows the hinge connection as seen on the bridge deck. The hinge consists of a mild steel plate fixed to the box girder with a full strength weld and a TETRON SE125 bearing. The depth of the box section segments between Pier RD and hinge is gradually varying from 1.73 m to 1.09 m, which is shown in Figure 6.8 by a red arrow.

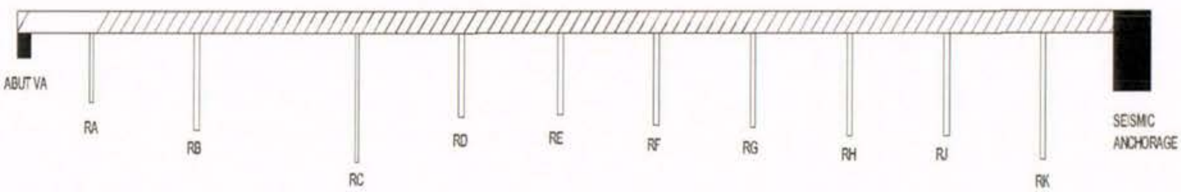

Figure 6.4. Elevation of Nelson St off-ramp bridge showing pier designations.

Table 6.1. Spans lengths of Nelson St off-ramp bridge.

Span	1	2	3	4	5	6	7	8	9	10	11
Piers	VA to RA	RA to RB	RB to RC	RC to RD	RD to RE	RE to RF	RF to RG	RG to RH	RH to RJ	RJ to RK	RK to Seismic Anchorage
Length (m)	18	26	40	26	24	24	24	24	24	24	18

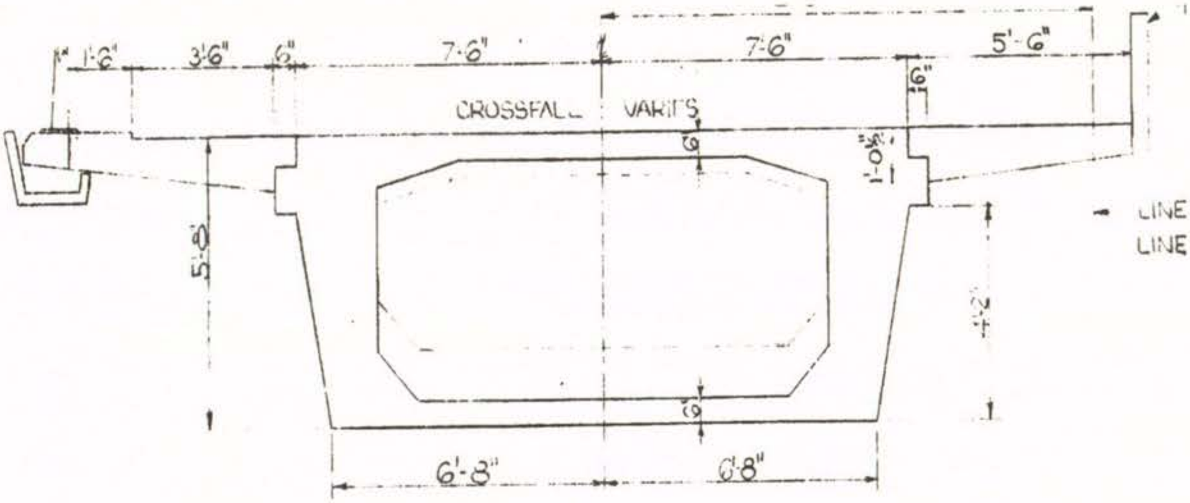

Figure 6.5. Typical girder section: Abutment VA to Pier RD (dimensions in feet and inches).

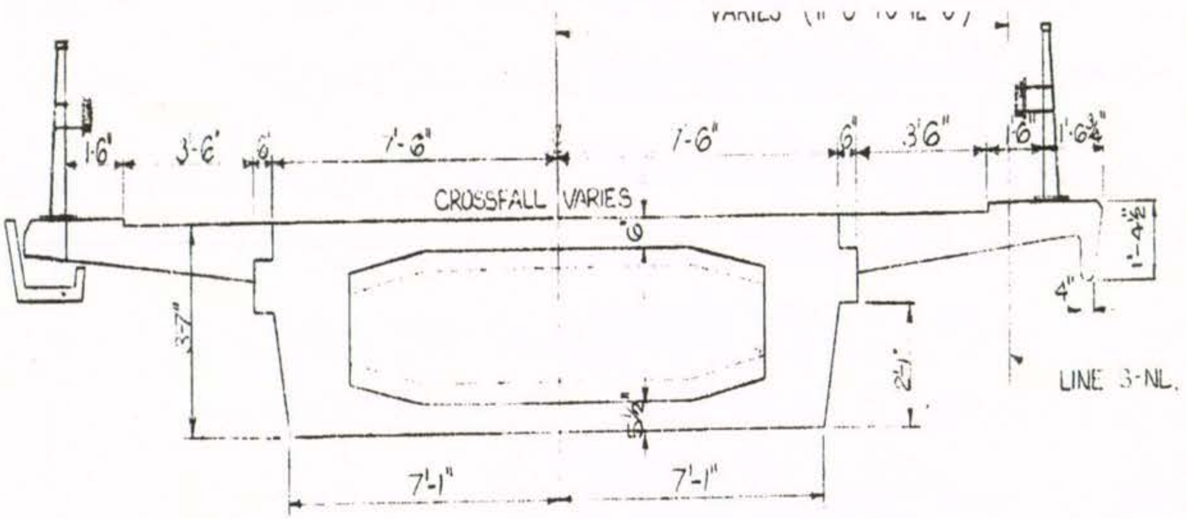

Figure 6.6. Typical girder section: Pier RD to Seismic Anchorage (dimensions in feet and inches).

A 40 mm thick layer of asphalt mixed with crushed stone gravel or sand was used for the bridge surface paving. The bridge roadway is slightly curved in plan and it has the longitudinal gradient of 3% rising towards the Seismic Anchorage and a transvers gradient of 4% rising towards East. Steel guardrails are bolted to the cantilevered part of deck slab on both sides along the whole length of the bridge (see e.g. Figure 6.2). A concrete water channel is also bolted to the cantilevered part of the deck slab as the drainage system for the bridge (Figure 6.9).

Figure 6.7. Hinge connection as seen on the bridge deck.

Figure 6.8. Varying depth of girder close to the hinge.

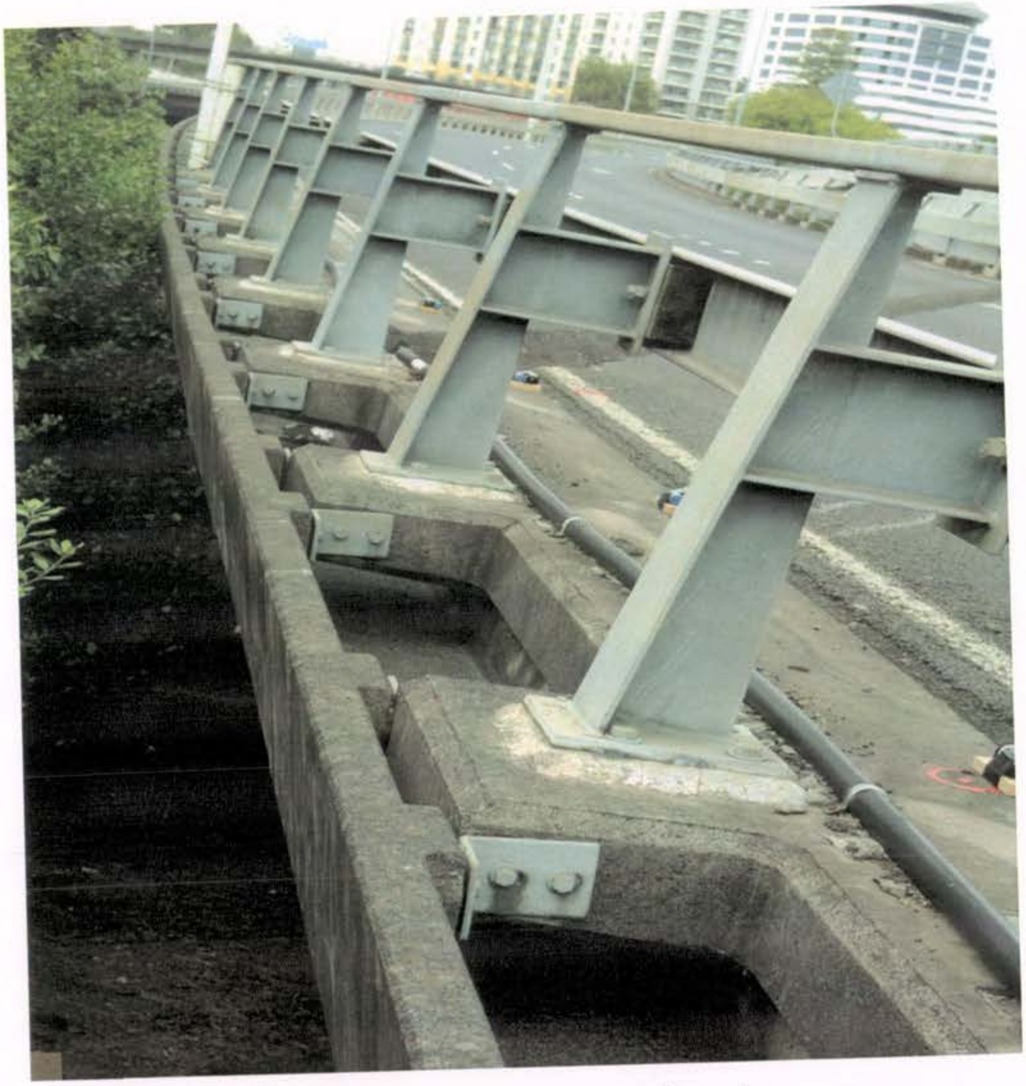

Figure 6.9. Concrete water channel.

The superstructure is supported by TETRON SE bearing at all the piers (Figure 6.10) and by ADYANX Q6 rubber bearing at both abutments. The TETRON SE bearing are accompanied on all the piers but Pier RA by a shear key (indicated by the black and red arrow, respectively, in Figure 6.11). It can be assumed that such as a combined support does not allow translation in any direction on the piers but permits rotation in two directions except torsion. The support on Pier RA additionally allows for lateral translation. Boundary conditions at the abutments turned out to be more complex in light of experimental results and are discussed later in Chapter 6.5 where FE modelling is undertaken.

The whole bridge is supported by ten solid single shaft piers with octagonal cross sections. The North and South end of the bridge are supported by a pile-bent type abutment and gravity abutment, respectively. Pile foundations are used under Pier RA, RB and RC. Footings of Piers RD to RK are placed directly on the prepared fill.

Figure 6.10. Bearing support on piers.

Figure 6.11. TETRON SE bearing (black arrow) and shear key (red arrow).

6.3. Ambient vibration testing

AVT only requires the measurement of the structural response under ambient excitation, usually due to wind, traffic or seismic excitations, and can lead to accurate estimates of the modal parameters quickly and inexpensively in the process known as operation modal analysis (OMA). Furthermore, it can avoid shutting-down traffic during the tests due to the installation of heavy shakers. The usual testing procedure for larger structures and limited number of sensors consists of performing measurements using several roving sensor setups with one or more reference points. Assuming that the excitation is uncorrelated white noise (a fair assumption for many sources of ambient excitations), OMA techniques can accurately identify natural frequencies and mode shapes, and give reasonable estimates of damping ratios.

AVT was performed on the Nelson street off-ramp bridge to obtain the information of modal properties of the bridge, i.e. natural frequencies, damping ratios and mode shapes. Due to the bridge having been permanently closed to traffic, excitation sources are mainly provided by nearby traffic, wind and possible micro-tremors. Two system identification methods are implemented to extract the modal properties of the bridge, namely FDD method in the frequency domain and SSI method in the time domain. The feasibility of obtaining accurate dynamic properties of this type of bridge by ambient testing was checked. It was found that a few mode shapes in the lateral direction could be identified from ambient data, while no mode shapes, only frequencies, were found in the vertical direction, possibly due to inadequate excitation energy and the relative high stiffness in the vertical direction. Several people then jumped on the deck in phase and at a particular frequency in an attempt to obtain the full vertical dynamic characteristics, and the first two vertical mode shapes have been successfully identified in this way.

For measuring accelerations in AVT, the same MEMS wireless USB accelerometers were used as for AVT of Newmarket Viaduct (see Chapter 5.3.2). Time stamped data in three perpendicular directions were recorded to the sensor microSD memory cards and the data downloaded via USB connection to a computer after test completion. The measuring units were attached to the selected measuring points on the bridge deck (Figure 6.12), piers (Figure 6.13), and an abutment (Figure 6.14), by using silicone adhesive to ensure good grip between the accelerometers and the bridge.

Figure 6.12. USB accelerometer installed on the bridge deck.

Figure 6.13. USB accelerometer installed on bridge pier.

Figure 6.14. USB accelerometer installed on bridge abutment.

6.3.1. Preliminary testing

The first on site visit to the bridge was on January 16th, 2013. The purpose of this visit was to gain information about the structural components, such as piers, abutments, bearings and girders, conduct preliminary testing and obtain estimates of natural frequencies of the bridge by installing 20 sensors on the bridge deck, and perform some preparations for the subsequent detailed AVT. Figure 6.15 shows a 20 min long vertical time history of accelerations measured at the midpoint of the longest Span 3. It can be observed the peak value of acceleration is 0.012 m/s^2. Figure 6.16 is the ASD of this signal. Two obvious peaks can be seen, at 3.164 Hz and 3.828 Hz, respectively. It can be assumed that they represent the first and second vertical natural frequencies, respectively, based on the span length and bridge structure type. The ASD graphs for the vertical response of other locations have also been checked, but the peaks were not as obvious and it was not possible to identify any mode shapes in the vertical direction due to weak excitation forces in this direction. Figure 6.17 shows a 20 min long time history of lateral accelerations obtained at the midpoint of Span 3. It can be observed that the peak value of acceleration is 0.00569 m/s^2, which is approximately half of the peak vertical acceleration value. Figure 6.18 shows the ASD of this signal. Two close peaks can be observed around 3.60 Hz and another small peak at 2.656 Hz.

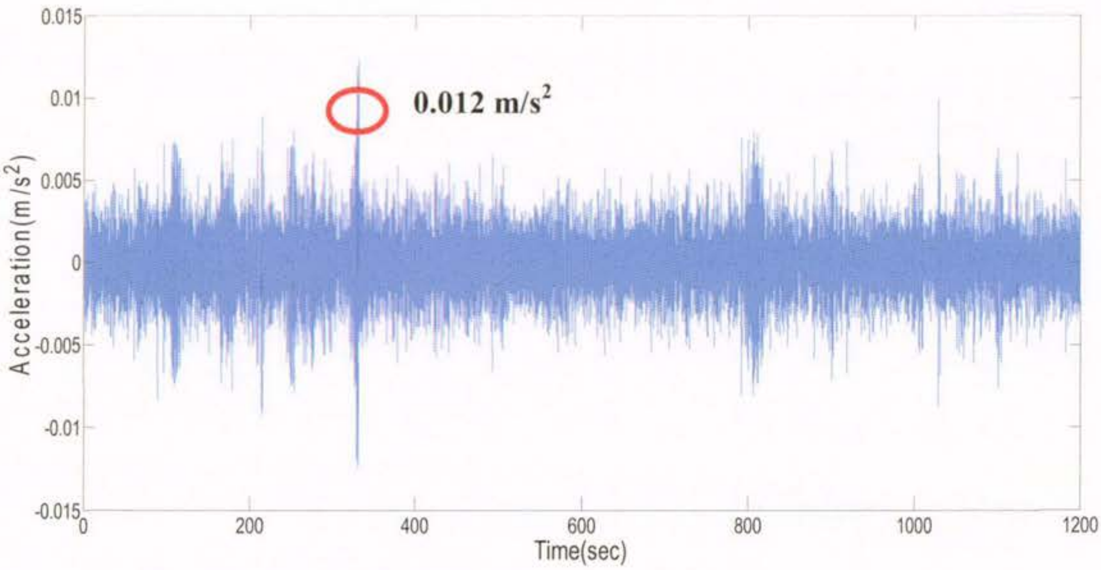

Figure 6.15. Typical recorded vertical acceleration response at the midpoint of Span 3.

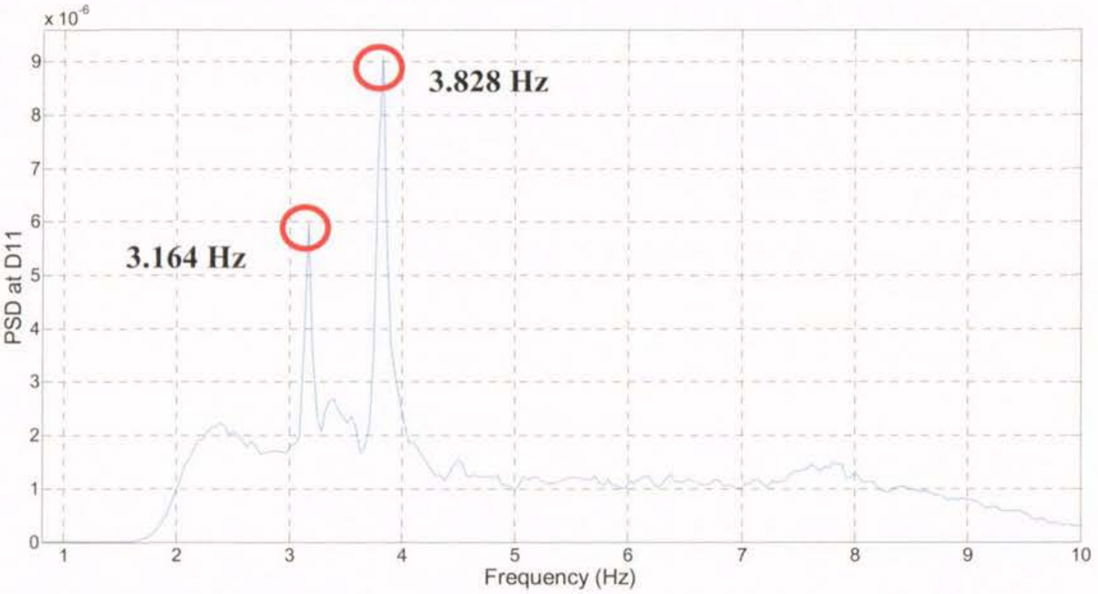

Figure 6.16. ASD of vertical acceleration at the midpoint of Span 3.

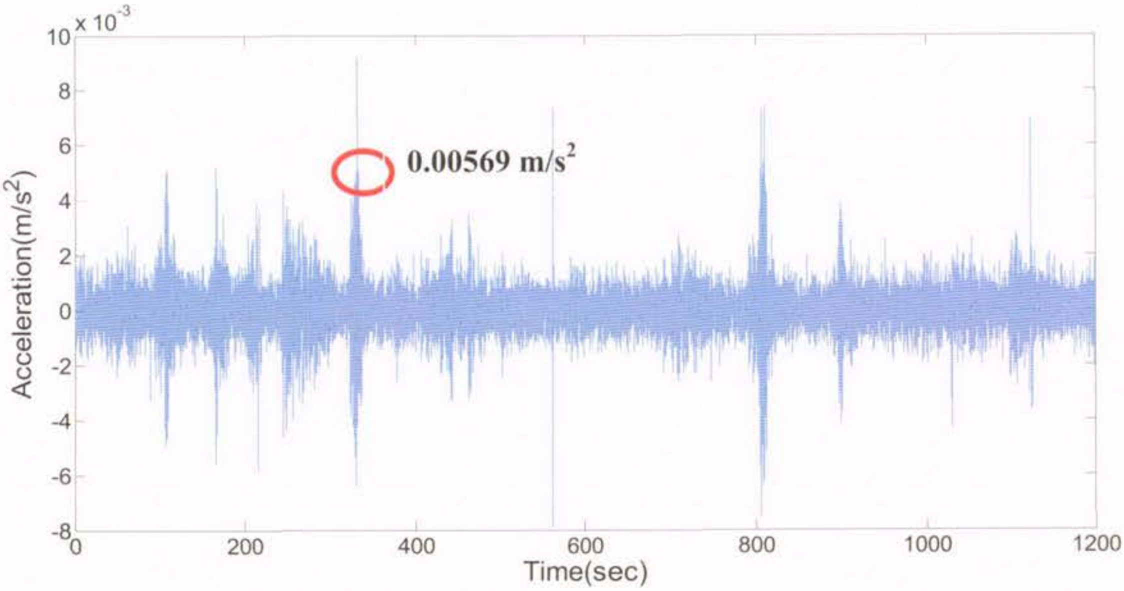

Figure 6.17. Typical recorded lateral acceleration response at the midpoint of Span 3.

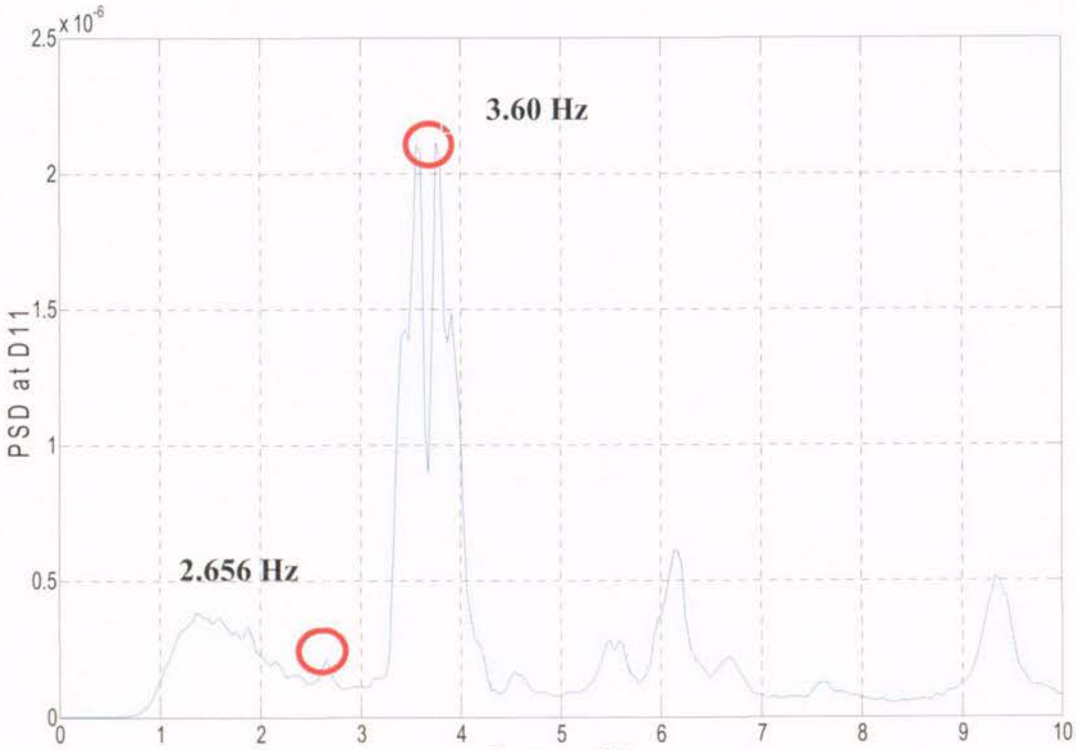

Figure 6.18. ASD of lateral acceleration at the midpoint of Span 3.

6.3.2. Detailed testing

A detailed AVT was conducted on March, 4th 2013. A dense measurement location plan on the bridge deck was proposed for this 272 m long bridge so that a good resolution for mode shapes could be achieved. The accelerometers were installed on both sides of bridge deck along the curbs (Figure 6.19). The distance between two measurement stations ranged from 2 m to 4 m. As a result, a total of 188 locations were measured. Four test setups were used to cover the whole length of the bridge. Four reference locations, hereinafter referred to as the base stations, were selected based on the mode shapes identified from the preliminary FE model of the structure. Each setup comprised four base triaxial accelerometer stations and 46 roving measurement stations. An example of typical measurement stations for Span 3 is shown is Figure 6.20.

Sampling frequency was chosen as 160 Hz since the frequency range of interest was below 25 Hz. The ambient vibration response of the bridge was then simultaneously recorded for 40 mins at all roving accelerometers and base stations for one setup, which yielded 384,000 data points per station per channel. Once the data was collected, the roving stations were moved to the locations of the next setup, while the base stations always remained in the same place. This sequence was repeated four times to cover the whole bridge from the North to the South end.

Figure 6.19. USB accelerometers arranged along the bridge curbs.

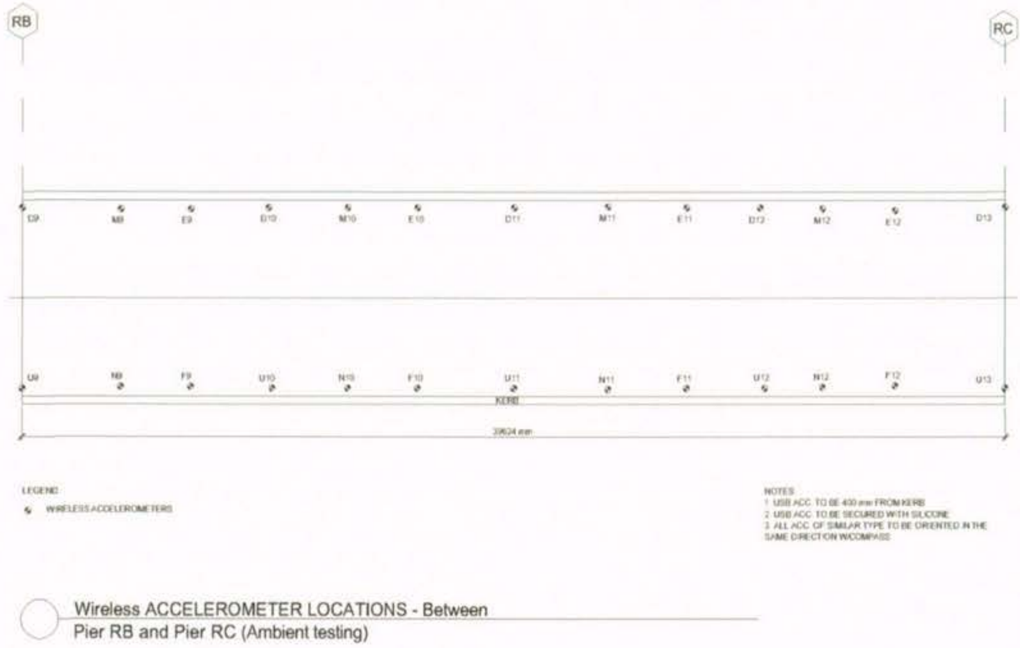

Figure 6.20. Example of typical measurement stations (Span 3).

6.3.3. System identification from ambient measurements

The extraction of modal parameters from ambient vibration data was carried out by using two different techniques: FDD in the frequency domain and SSI in the time domain. These techniques are described in Chapters 3.2.3 and 3.2.4, respectively, and are available in an in-house system identification toolbox written in MATLAB (Beskhyroun 2011). Table 6.2 lists the identification results for four lateral mode shapes. It can be observed that the results from the two different methods agree very well. Figures 6.21-24 show the identified normalised mode shapes based on FDD.

Table 6.2. Identified natural frequencies and damping ratios from AVT.

Mode no.	Experimental frequencies (Hz)		Difference (%)	Damping ratios (%)
	FDD	SSI		SSI
1	3.74	3.79	1.3	1.8
2	4.49	4.50	0.2	1.3
3	5.50	5.47	0.5	1.4
4	6.66	6.68	0.3	0.8

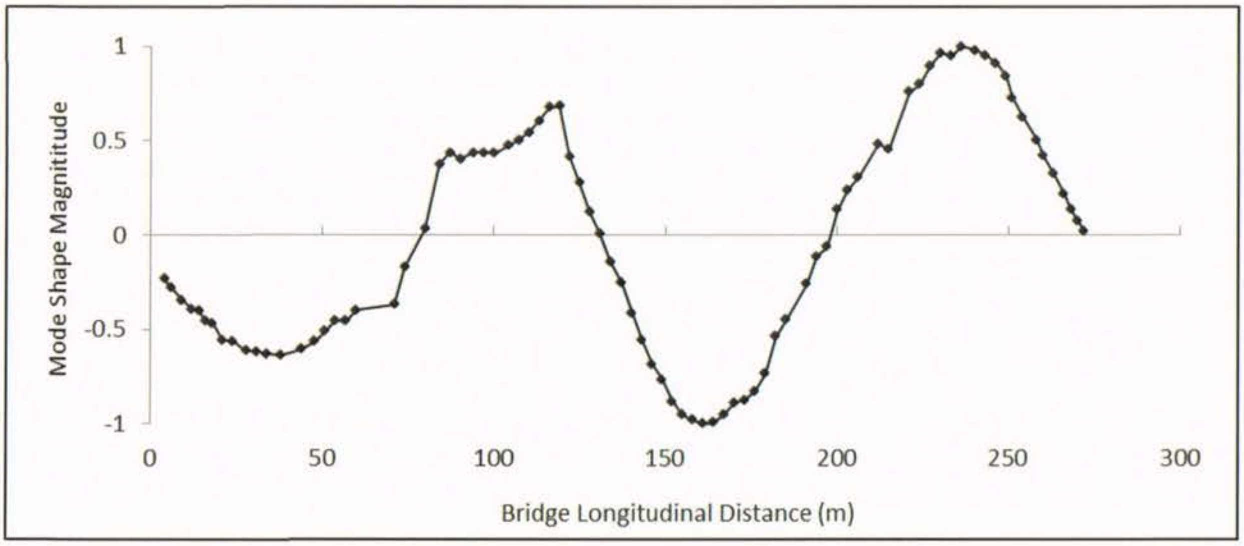

Figure 6.21. 1st lateral mode shape from AVT (3.74 Hz).

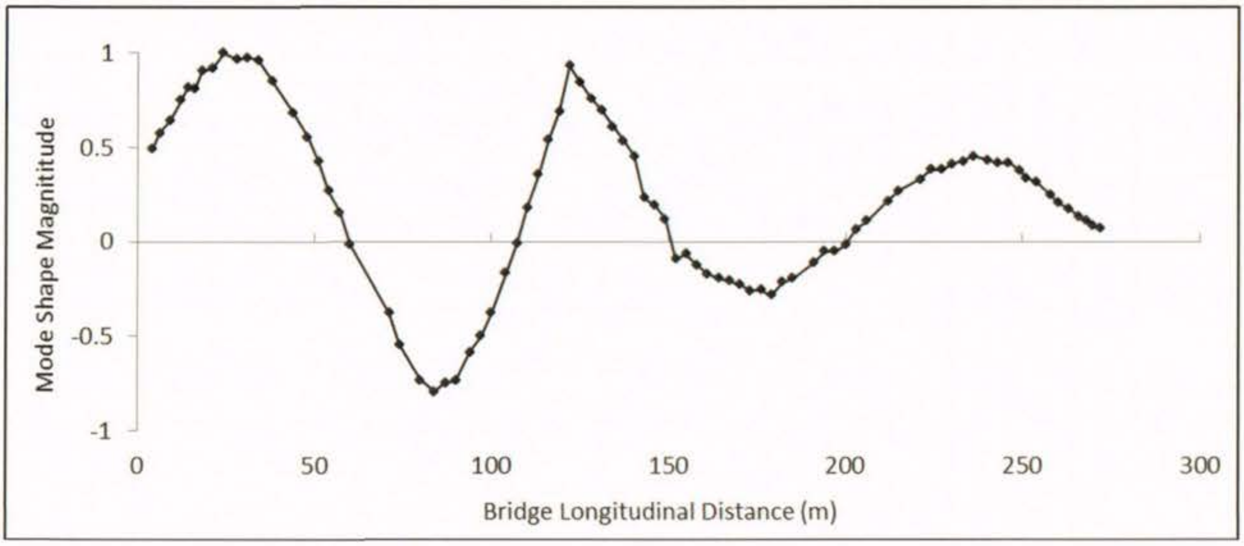

Figure 6.22. 2nd lateral mode shape from AVT (4.49 Hz).

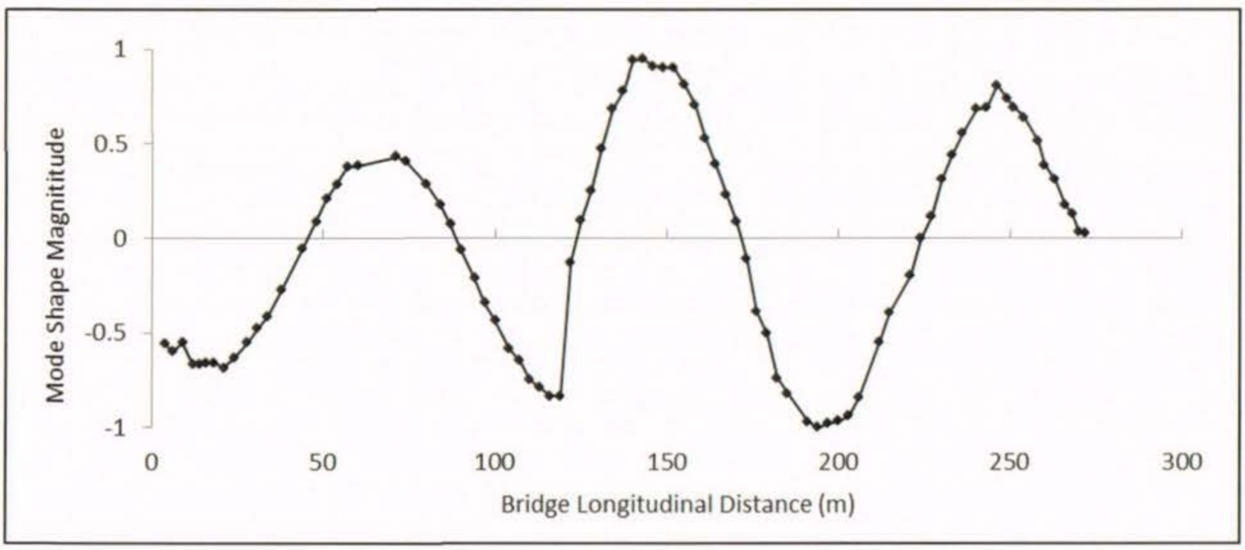

Figure 6.23. 3rd lateral mode shape from AVT (5.50 Hz).

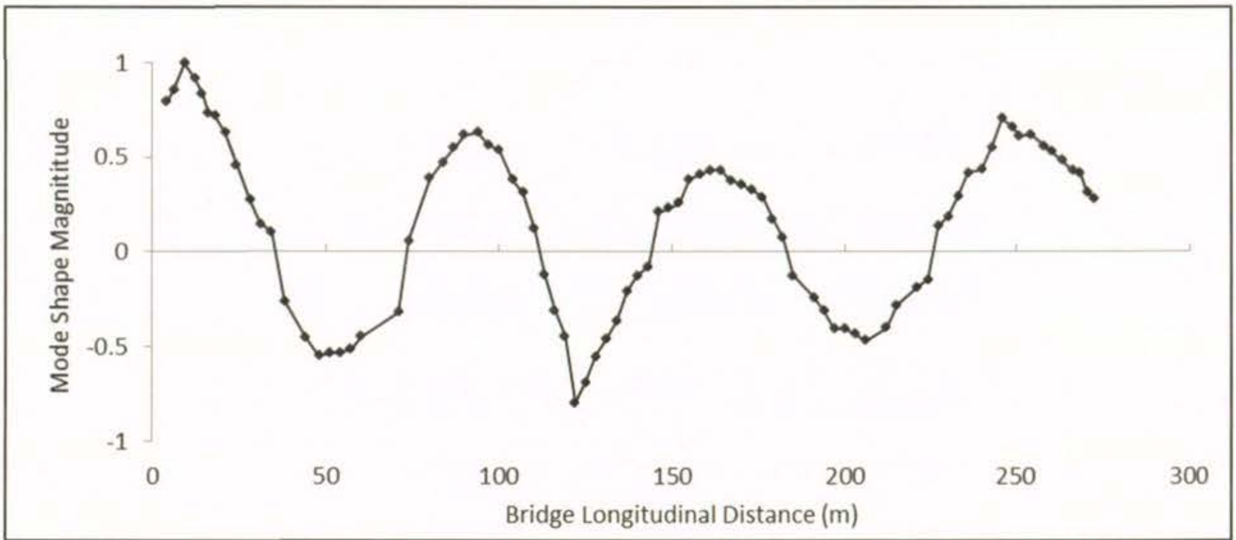

Figure 6.24. 4th lateral mode shape from AVT (6.66 Hz).

6.3.4. Jumping tests

For the jumping tests, the accelerometer arrangement was the same as in the ambient AVT described in Chapter 6.3.2. Four people (each weighing approximately 65 kg) jumped in unison at a nearly constant frequency following a mobile phone metronome for about 40 s to excite the bridge. Different jumping locations were selected for different accelerometer set-ups so that the jumping location was close to the accelerometer locations. The red arrow in Figure 6.25 shows the jumping location for setup 1 and setup 2 (the midpoint of Span 3) and the blue rectangle shows the length of the bridge covered with accelerometers. The black arrow in Figure 6.26 shows the jumping location for setup 3 and setup 4 (the midpoint of Span 7) and the purple rectangle shows the length of the bridge covered with accelerometers. Based on the ASD results from the preliminary testing (Chapter 6.3.1), 3.2 Hz and 3.8 Hz were selected as the jumping frequencies. Jumping was repeated three times for each testing setup. Experimental personnel could clearly feel vertical vibration of the bridge girder at 3.2 Hz when jumping at the location indicated by the red arrow in Figure 6.25, but only weak vertical vibration response at 3.8 Hz. On the contrary, notable vertical vibration of the bridge girder at 3.8 Hz could be felt when jumping occurred at the location indicated by the black arrow in Figure 6.26, but only week vertical vibration response at 3.2 Hz. These observations were in accordance with the mode shape results identified later, because the 3.2 Hz mode shape has significant magnitudes mainly in Span 3, whereas the 3.8 Hz mode shape has significant magnitudes mainly in the spans between Pier RD and RG. Figure 6.27 show the typical time history response when jumping at 3.2 Hz and 3.8 Hz. The corresponding ASDs are shown in Figure 6.28. Clear peaks at 3.19 Hz and 3.88 Hz can be seen. Figures 3.29 and 30 display the two identified mode shapes obtained using the jumping data.

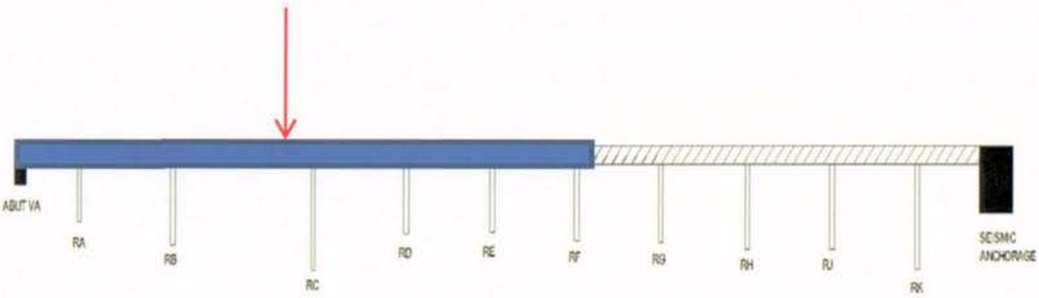

Figure 6.25. Jumping location for experimental setup 1 and setup 2.

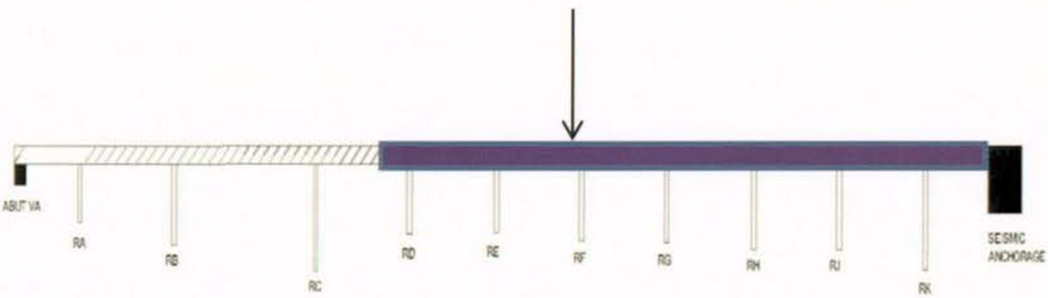

Figure 6.26. Jumping location for experimental setup 3 and setup 4.

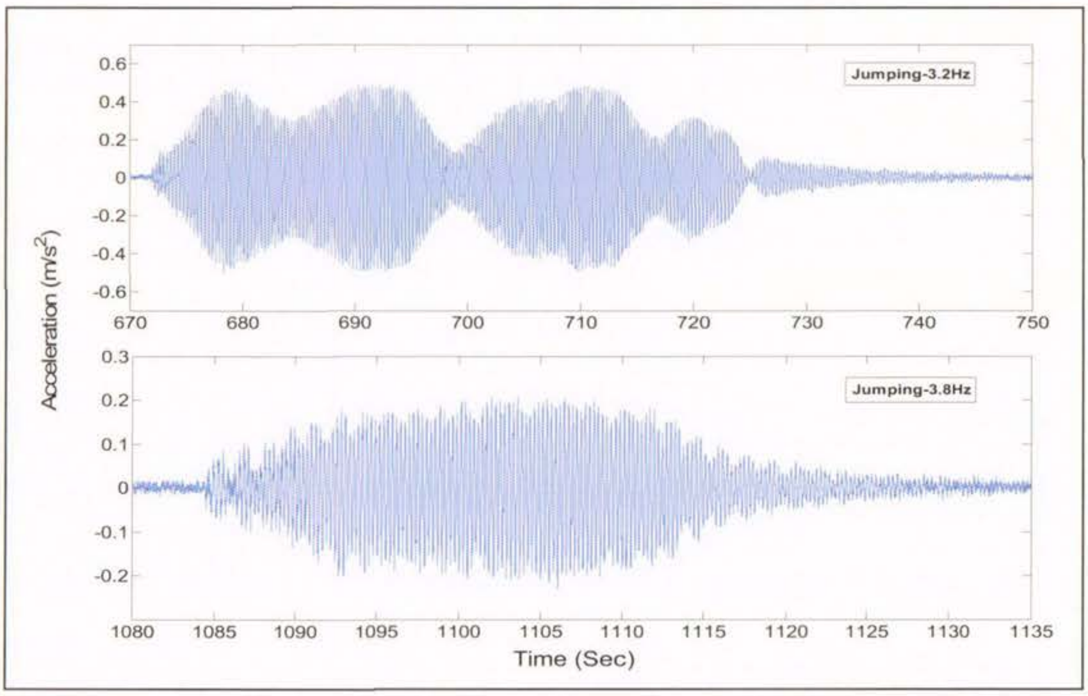

Figure 6.27. Typical vertical acceleration time histories during jumping tests.

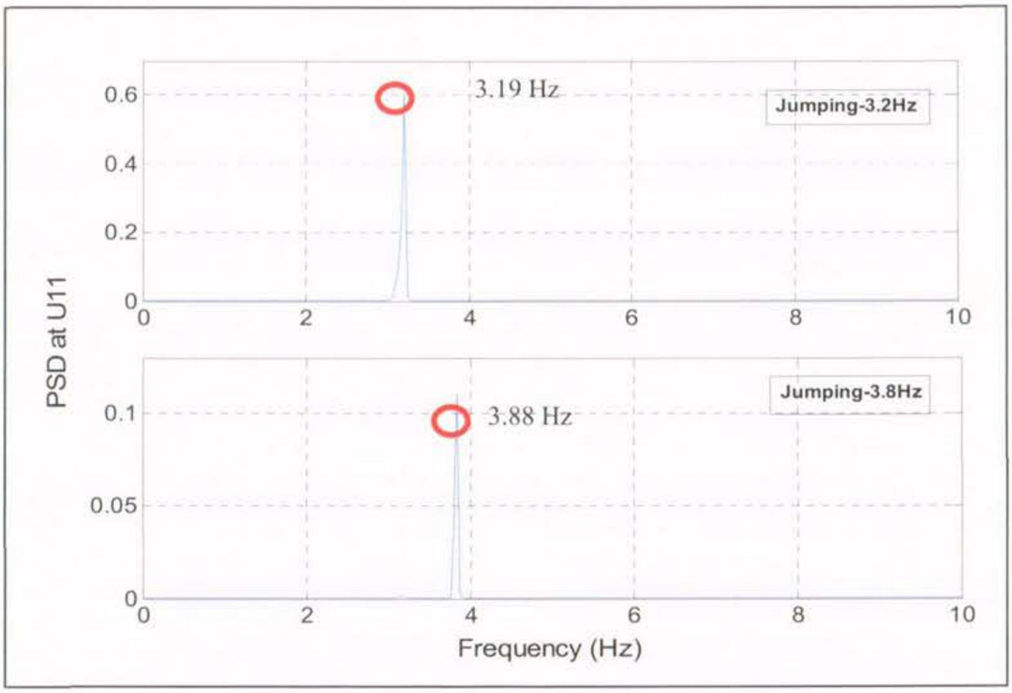

Figure 6.28. ASDs of vertical accelerations for jumping tests.

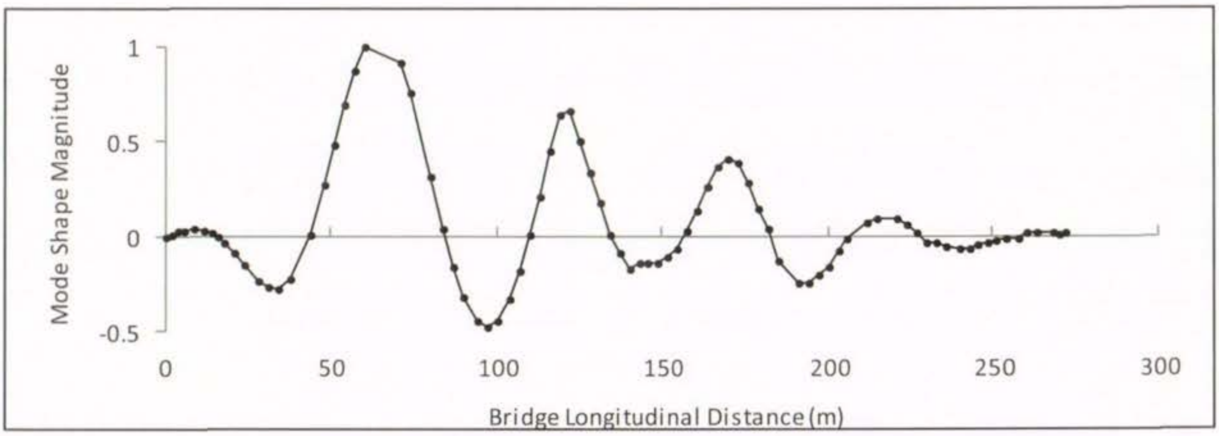

Figure 6.29. 1st vertical mode shape obtained via jumping test (3.19 Hz).

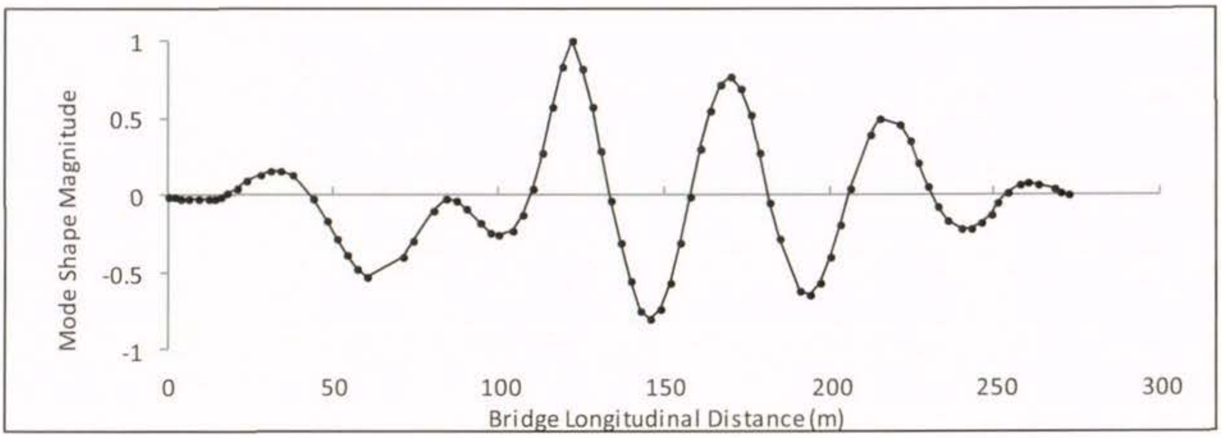

Figure 6.30. 2nd vertical mode shape obtained via jumping test (3.88 Hz).

6.4. Forced vibration testing using large eccentric mass shakers

6.4.1. Equipment and instrumentation

The two ANCO MK-140-10-50 large eccentric mass shakers (Figure 6.31) used in the testing use a dual-arm rotating eccentric mass mechanism, drive motor, timing belt speed reducer, Danfoss VLT-5011 variable frequency drive control system and are powered by three phase AC. The total mass of the each shaker is approximately 600 kg. They have unidirectional frequency and force capacities of 30 Hz and 98 kN in the horizontal direction. (For safety reasons, such as potential of loosening of anchors, the shakers operated during the field testing reported herein at levels not exceeding approximately 70 kN.) The force-frequency relationship for the shaker is controlled by the eccentricity provided by the configuration of the steel weights with a maximum of 8 big steel weights per shaft attached to the flywheel. The force-frequency relationship is shown in Figure 6.32 and is calculated as:

$$F = 4\pi^2 MRf^2 \tag{6.1}$$

where F is force output, MR is total eccentricity of the weight, and f is the shaker rotational frequency in Hz.

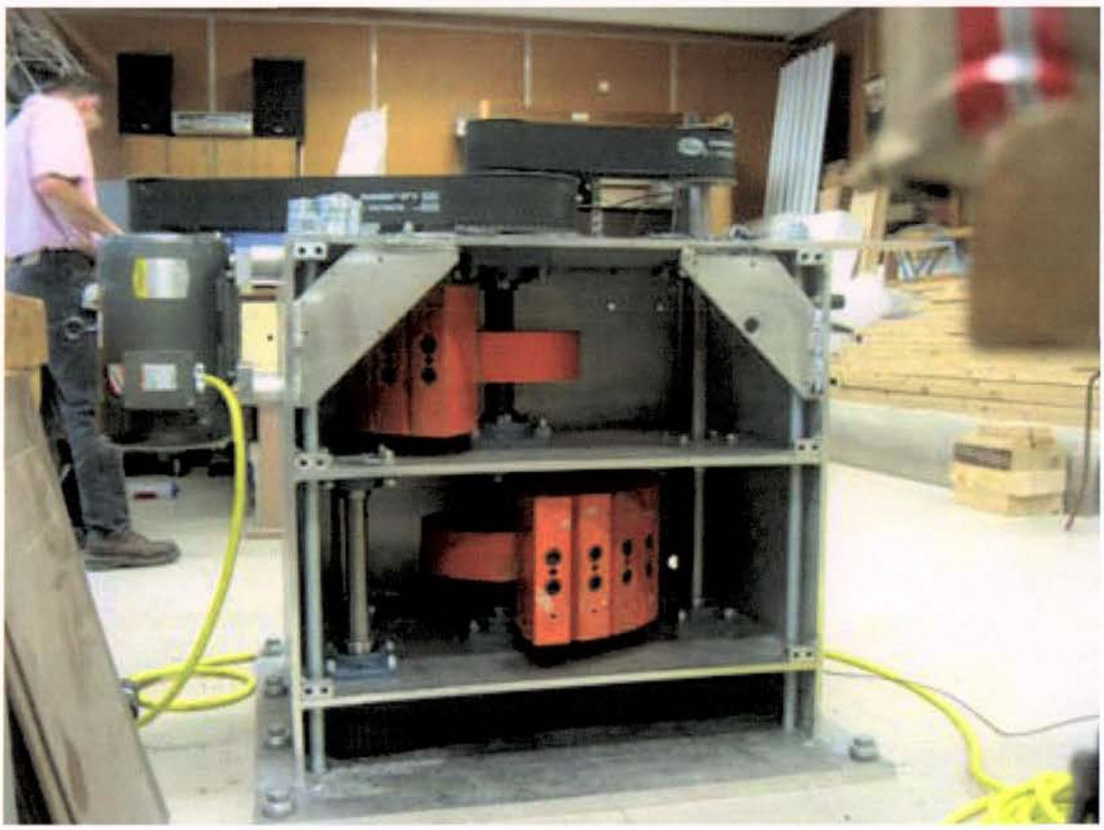

Figure 6.31. ANCO MK-140-10-50 eccentric mass shaker.

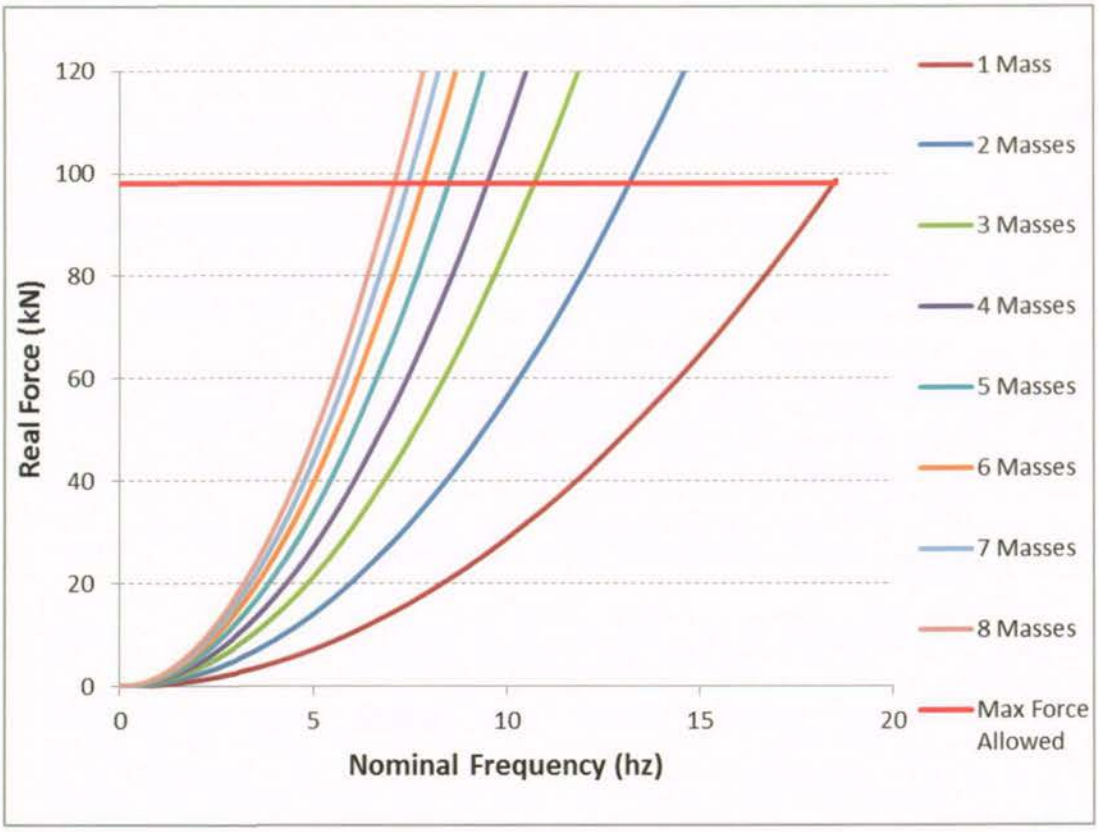

Figure 6.32. Force-frequency relationship for eccentric mass shaker.

A total of 8 holes were drilled for anchoring each of the two large shakers to the bridge deck. This was done after deck reinforcement was mapped using a cover meter in order to not damage the reinforcement. Figure 6.33 shows the hole drilling operation on site and marked reinforcement mesh locations. The two shakers and a box of steel weights were transported onsite (Figure 6.34) and placed on the bridge deck with the help of a hiab truck (Figure 6.35). Two shakers were bolted to the top of the bridge deck with Ø16 mm Hilti HSL-3 16M/50 anchors (Figure 6.36). Each anchor can provide 67.2 kN shear force and 33.6 kN tensile force capacity. Figure 6.37 shows the process of anchoring horizontal shaker and Figure 6.38 shows the anchored vertical shaker.

Figure 6.33. Drilling holes by using rotary hammer.

Figure 6.34. Transporting shakers with hiab truck.

Figure 6.35. Placing shakers with the help of hiab truck.

Figure 6.36. Hilti HSL-3 16M/50 anchors.

Figure 6.37. Anchoring horizontal shaker.

Figure 6.38. Anchored vertical shaker.

Based on preliminary finite element analysis, the longest span between Pier RB and Pier RC was selected to mount the shakers. The horizontal shaker was located at the mid-span along the midline of the bridge deck and the vertical shaker at 1/3 of the span length towards the west side lane so as to excite any existing torsional modes (though this was not eventually achieved). The detailed shaker locations are shown in Figures 6.39-42.

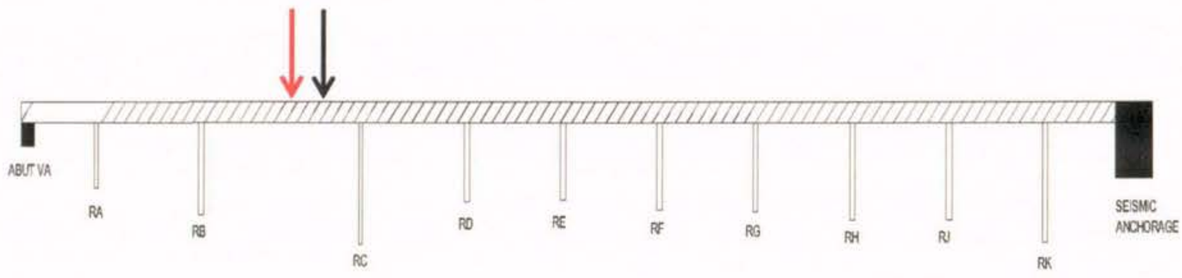

Figure 6.39. Side view of shaker locations between Piers RB and RC.

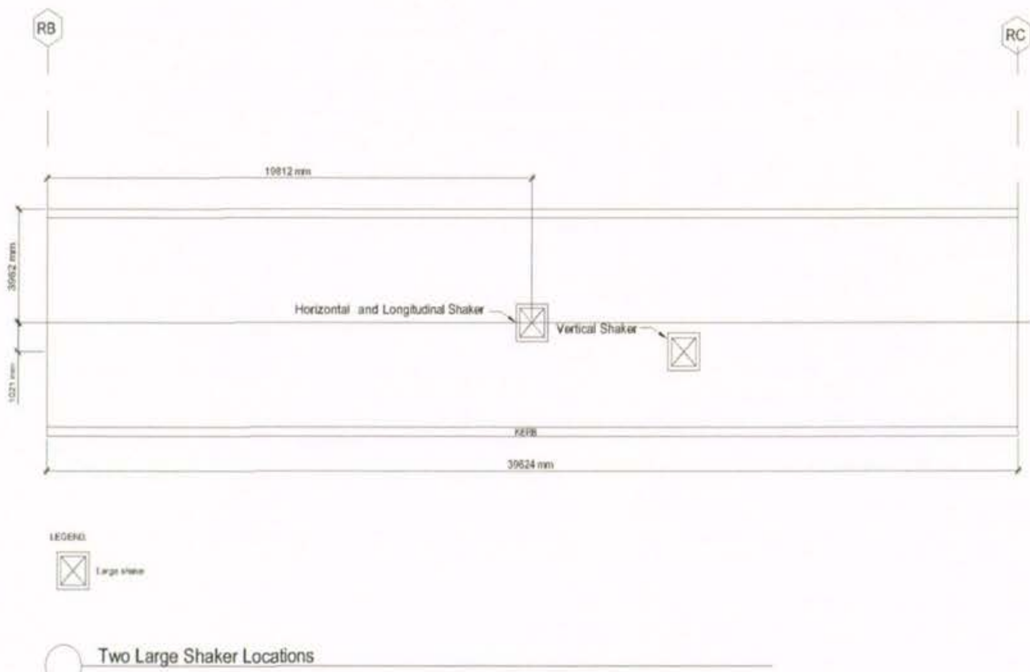

Figure 6.40. Bird's eye view of shaker locations between Piers RB and RC.

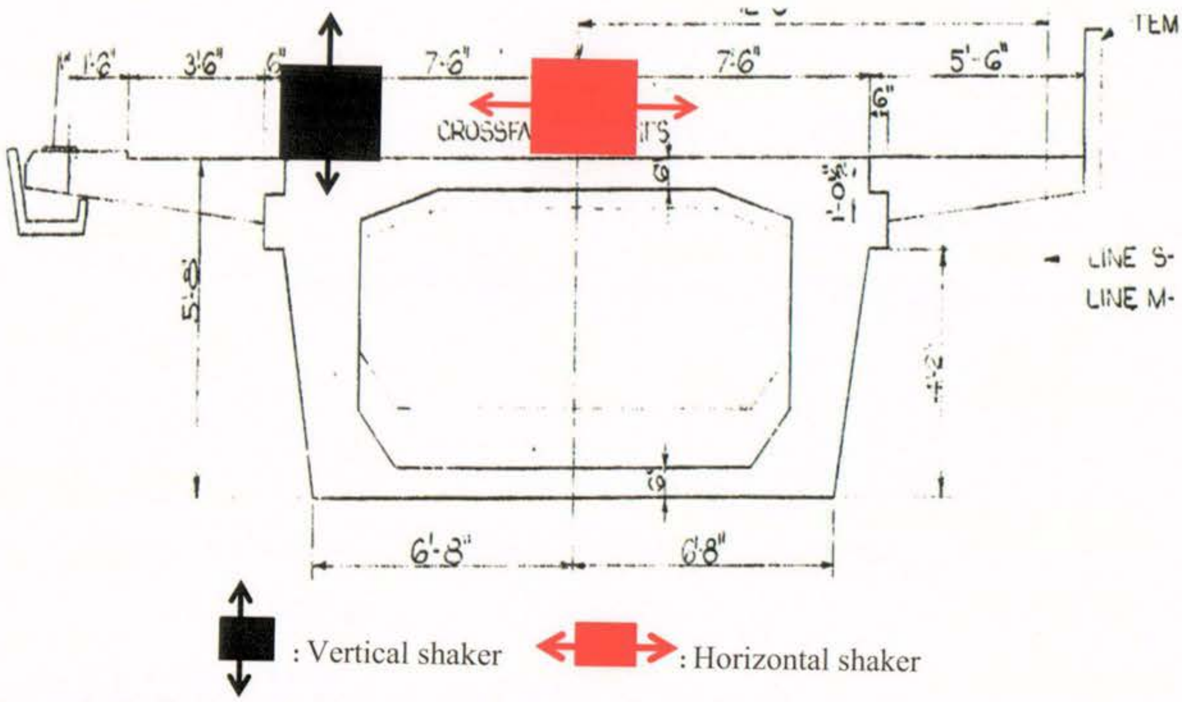

Figure 6.41. Cross-sectional view of shaker locations between Piers RB and RC.

Figure 6.42. Two shakers anchored to the bridge deck.

Eight uni-axial Honeywell Q-Flex QA-750 wired accelerometers and 61 three-axial USB MEMS accelerometers were utilized to collect data simultaneously during excitation testing. Figure 6.43 shows a Honeywell QA 750 accelerometer installed at a measuring location. The data from wired sensors were mainly used for performing quick data analysis on site, while the USB sensor data were used for detailed post-testing data analysis. A desktop computer fitted with an NI DAQ 9203 data acquisition card, data collecting channel cards installed in the grey box, Matlab based data acquisition tool-box (Compact DAQ V2) software were used to record the data on site, as shown in Figure 6.44. Electrical power on site was provided by a GENSET 60 kVA power generator (Figure 6.45).

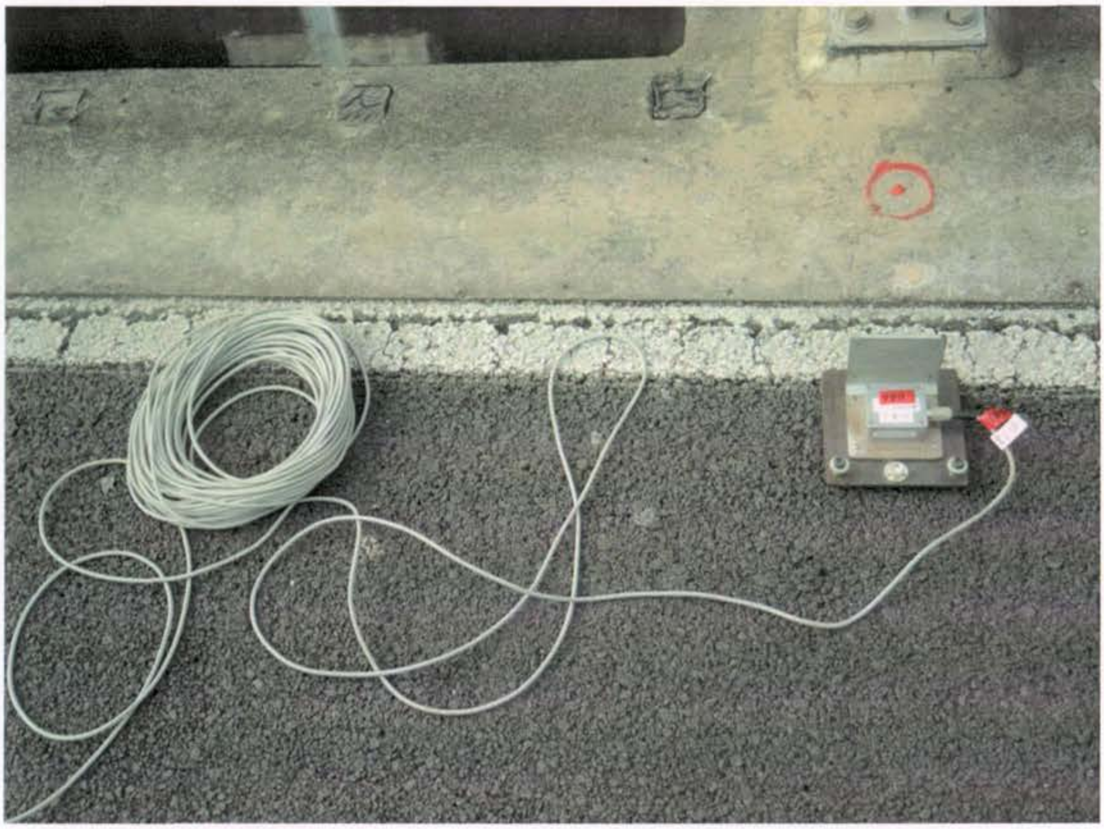

Figure 6.43. Honeywell Q-Flex QA-750 accelerometer.

Figure 6.44. Data acquisition system.

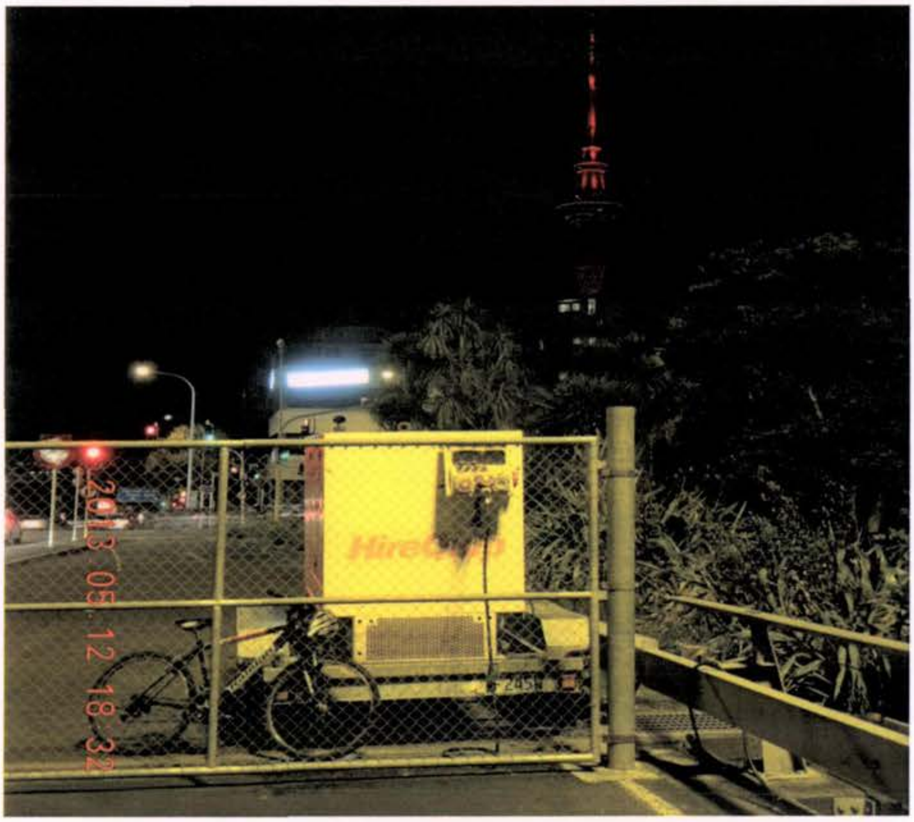

Figure 6.45. GENSET 60 kVA power generator.

During vertical forcing, the 61 USB accelerometers and eight wired accelerometers were installed along the both curb sides of the bridge deck so as to capture any torsional modes and distinguish them from vertical modes (although eventually no torsional modes were successfully identified). Figure 6.46 shows the USB accelerometers installed along both bridge curbs during vertical testing.

During horizontal forcing, to avoid any torsional component of bridge response, 61 USB accelerometers and eight wired accelerometers were arrayed along the centreline of the bridge deck. The locations on the bridge over the piers, abutments, and 1/2 and 1/4 span length points were selected as the measuring stations. Figures 6.47 and 48 show the wired and USB accelerometers installed along the centreline of the bridge deck, respectively.

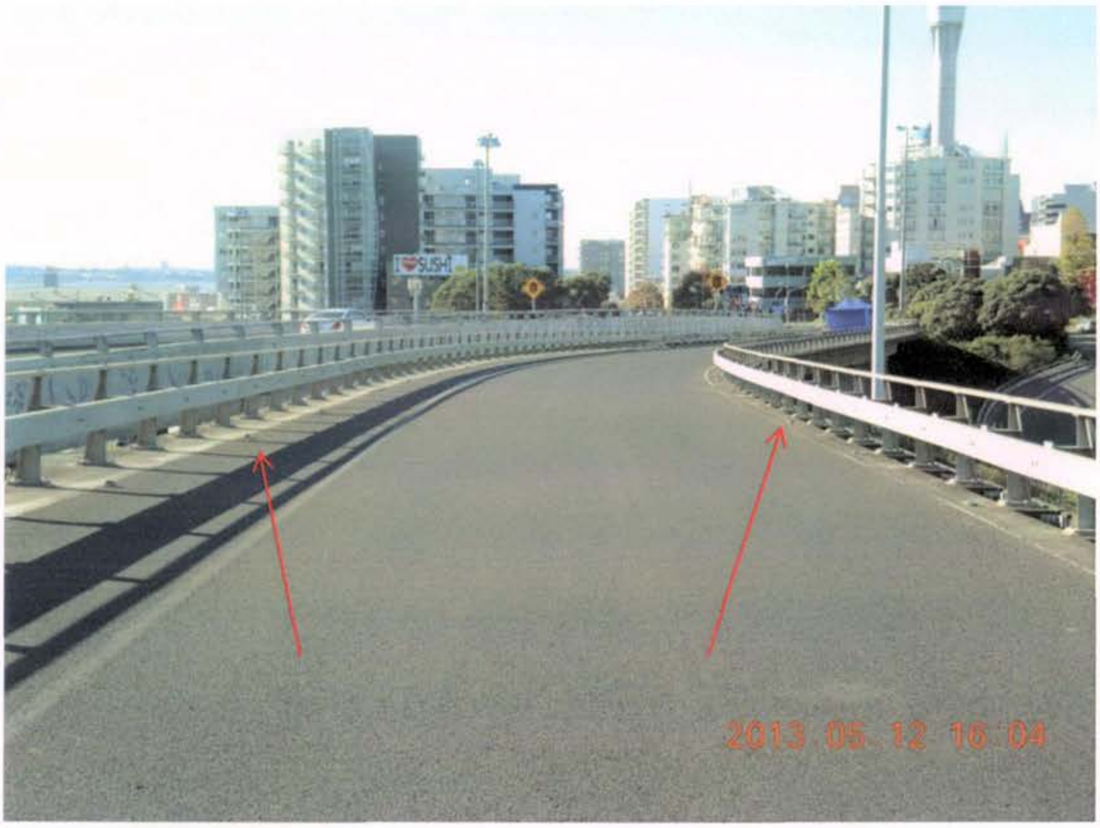

Figure 6.46. USB accelerometer arranged along both bridge curbs.

Figure 6.47. Wired accelerometers installed along centreline of the bridge deck.

Figure 6.48. USB accelerometers installed along centreline of the bridge deck.

6.4.2 Frequency sweep tests

A series of frequency sweeps were performed from May 8, 2013 to May 27, 2013. Low, moderate and high amplitude harmonic excitations were generated by changing the configuration and number of the steel weights attached to the flywheels of the shakers. The frequency sweep testing was used to determine dynamic characteristics of the bridge, i.e. natural frequencies, damping ratios and mode shapes in the frequency range up to 10.0 Hz. The change of shaker vibration frequency was controlled by manually operating the Danfoss VLT-5011 variable frequency drive control system (Figure 6.49). Several quick frequency sweeps between 0.0 and 10.0 Hz were conducted with 0.10 Hz increment and 15 s holding time at each frequency value. Rough natural frequencies estimates were quickly determined on site from these data. A series of slow frequency sweeps followed by operating in the vicinity of the identified natural frequencies with smaller increments down to 0.01 Hz. This time, at every increment the excitation frequency was held constantly for 60 seconds to allow the bridge response to achieve a steady state and record this response for a suitably long time. Timing of increments was controlled manually using an electronic wrist watch. Table 6.3 details the FVT testing programme.

Figure 6.49. Danfoss VLT-5011 variable frequency drive control system.

Table 6.3. FVT programme.

Excitation direction	Frequency range (Hz)	The number of masses per shaft	Frequency increment (Hz)	Holding time (s)
Vertical	0.0-10.0	1 small mass	0.1	15
Vertical	2.50-3.50	1 small mass	0.05	60
Vertical	3.30-4.30	1 small mass	0.05	60
Vertical	4.40-5.40	1 small mass	0.05	60
Vertical	5.50-6.50	1 small mass	0.05	60
Vertical	6.50-7.50	1 small mass	0.05	60
Vertical	7.40-8.40	1 small mass	0.05	60
Vertical	2.50-3.50	1 big mass	0.05	60
Vertical	3.30-4.30	1 big mass	0.05	60
Vertical	4.40-5.40	1 big mass	0.05	60
Vertical	5.50-6.40	1 big mass	0.05	60
Vertical	6.50-7.50	1 big mass	0.05	60
Vertical	7.40-8.40	1 big mass	0.05	60
Vertical	2.50-3.50	1 big & 1 small mass	0.05	60
Vertical	3.40-4.40	1 big & 1 small mass	0.05	60
Vertical	4.40-5.40	1 big & 1 small mass	0.05	60
Vertical	5.50-6.50	1 big & 1 small mass	0.05	60
Vertical	6.50-7.50	1 big & 1 small mass	0.05	60
Vertical	2.90-3.30	1 small mass	0.02	60
Vertical	3.56-3.96	1 small mass	0.02	60
Vertical	3.96-4.40	1 small mass	0.02	60
Vertical	4.50-5.00	1 small mass	0.02	60
Vertical	5.50-6.20	1 small mass	0.02	60
Vertical	6.84-7.32	1 small mass	0.02	60
Vertical	7.70-8.20	1 small mass	0.02	60
Vertical	2.80-3.40	1 big mass	0.02	60
Vertical	3.56-3.96	1 big mass	0.02	60

Vertical	3.96-4.40	1 big mass	0.02	60
Vertical	4.50-5.00	1 big mass	0.02	60
Vertical	5.50-6.40	1 big mass	0.02	60
Vertical	6.80-7.30	1 big mass	0.02	60
Vertical	7.60-8.20	1 big mass	0.02	60
Vertical	2.80-3.40	1 big & 1 small mass	0.02	60
Vertical	3.56-3.96	1 big & 1 small mass	0.02	60
Vertical	3.96-4.40	1 big & 1 small mass	0.02	60
Vertical	5.50-6.20	1 big & 1 small mass	0.02	60
Vertical	6.80-7.32	1 big & 1 small mass	0.02	60
Vertical	7.60-8.20	1 big & 1 small mass	0.02	60
Vertical	2.85-3.35	1 small mass	0.01	60
Vertical	3.60-4.00	1 small mass	0.01	60
Vertical	4.00-4.35	1 small mass	0.01	60
Vertical	4.55-4.90	1 small mass	0.01	60
Vertical	5.50-5.90	1 small mass	0.01	60
Vertical	6.90-7.25	1 small mass	0.01	60
Vertical	7.65-8.10	1 small mass	0.01	60
Vertical	2.90-3.30	1 big mass	0.01	60
Vertical	3.70-4.00	1 big mass	0.01	60
Vertical	4.00-4.30	1 big mass	0.01	60
Vertical	4.55-4.90	1 big mass	0.01	60
Vertical	5.55-5.85	1 big mass	0.01	60
Vertical	7.00-7.35	1 big mass	0.01	60
Vertical	7.65-8.10	1 big mass	0.01	60
Vertical	2.85-3.30	1 big & 1 small mass	0.01	60
Vertical	3.70-4.00	1 big & 1 small mass	0.01	60
Vertical	4.00-4.30	1 big & 1 small mass	0.01	60
Vertical	4.55-4.90	1 big & 1 small mass	0.01	60
Vertical	5.55-5.85	1 big & 1 small mass	0.01	60
Vertical	7.00-7.40	1 big & 1 small mass	0.01	60
Vertical	7.65-8.10	1 big & 1 small mass	0.01	60

Lateral	0.1-10.0	1 small mass	0.1	15
Lateral	0.0-10.0	1 big mass	0.1	15
Lateral	1.40-2.10	1 small mass	0.02	60
Lateral	2.20-2.90	1 small mass	0.02	60
Lateral	3.20-4.00	1 small mass	0.02	60
Lateral	6.00-6.80	1 small mass	0.02	60
Lateral	7.40-7.90	1 small mass	0.02	60
Lateral	8.30-8.80	1 small mass	0.02	60
Lateral	1.40-2.10	1 big mass	0.02	60
Lateral	2.20-2.90	1 big mass	0.02	60
Lateral	3.20-4.00	1 big mass	0.02	60
Lateral	6.00-6.80	1 big mass	0.02	60
Lateral	1.40-2.10	2 big masses	0.02	60
Lateral	2.20-2.80	2 big masses	0.02	60
Lateral	3.20-4.00	2 big masses	0.02	60
Lateral	6.00-6.80	2 big masses	0.02	60
Lateral	1.40-2.10	3 big masses	0.02	60
Lateral	2.20-2.80	3 big masses	0.02	60
Lateral	3.20-3.90	3 big masses	0.02	60
Lateral	6.20-6.80	3 big masses	0.02	60
Lateral	1.60-1.94	1small mass	0.01	60
Lateral	2.40-2.74	1small mass	0.01	60
Lateral	3.45-3.78	1small mass	0.01	60
Lateral	6.30-6.75	1small mass	0.01	60
Lateral	1.60-1.94	1 big mass	0.01	60
Lateral	2.40-2.74	1 big mass	0.01	60
Lateral	3.45-3.78	1 big mass	0.01	60
Lateral	6.30-6.75	1 big mass	0.01	60
Lateral	1.60-1.94	2 big masses	0.01	60
Lateral	2.40-2.74	2 big masses	0.01	60
Lateral	3.45-3.78	2 big masses	0.01	60
Lateral	6.30-6.75	2 big masses	0.01	60

Lateral	1.60-1.94	3 big masses	0.01	60
Lateral	2.40-2.74	3 big masses	0.01	60
Lateral	3.45-3.78	3 big masses	0.01	60
Lateral	6.30-6.75	3 big masses	0.01	60
Lateral	1.60-1.94	4 big masses	0.01	60
Lateral	2.25-2.74	4 big masses	0.01	60
Lateral	3.45-3.78	4 big masses	0.01	60
Lateral	6.30-6.75	4 big masses	0.01	60
Lateral	1.60-1.94	5 big masses	0.01	60
Lateral	2.25-2.74	5 big masses	0.01	60
Lateral	3.25-3.78	5 big masses	0.01	60
Lateral	6.30-6.75	5 big masses	0.01	60
Lateral	1.60-1.94	6 big masses	0.01	60
Lateral	2.25-2.74	6 big masses	0.01	60
Lateral	3.25-3.78	6 big masses	0.01	60
Lateral	6.30-6.75	6 big masses	0.01	60
Lateral	1.60-1.94	7 big masses	0.01	60
Lateral	2.25-2.74	7 big masses	0.01	60
Lateral	3.25-3.78	7 big masses	0.01	60
Lateral	1.60-1.94	8 big masses	0.01	60
Lateral	2.25-2.74	8 big masses	0.01	60
Lateral	3.25-3.78	8 big masses	0.01	60

6.4.3. System identification results for small response amplitude

The steady-state sine sweeping technique is commonly employed to excite bridges. It involves constructing a FRF through measurement of the magnitude and phase between the excitation and the response at varying frequencies. Because it is necessary to reach steady-state conditions for each frequency increment, this technique tends to involve long testing times. However, the method is valuable when it is necessary to examine in detail non-linear behaviour, or when it is necessary to maximise the level of excitation which can be applied by a particular shaker. Figure 6.50 shows a typical steady-state sine sweeping acceleration response. A series of ladder-shaped, steady-state response data can be observed when sweeping around the 1st vertical natural frequency.

During a particular steady-state sinusoidal sweeping test, a representative section from the steady state portion of the data is selected for each frequency (Figure 6.51). The acceleration amplitude is converted to displacement by dividing by $4\pi^2 f^2$, where f is the frequency in Hz. The displacement is in turn normalized by the applied shaker force to obtain the FRF at each frequency and fit to a sine wave to estimate the exact frequency, amplitude and phase. The estimates of natural frequency and damping ratio can be obtained by examining the peaks in the FRFs (Bendat and Piersol 1993, see also Chapter 3.2.2) and using the half-power method (Heylen et al. 1997, see also Chapter 3.2.3). Mode shapes can be extracted by observing the relative amplitudes and phase lags between responses from different locations when the structure is forced with the resonance frequency.

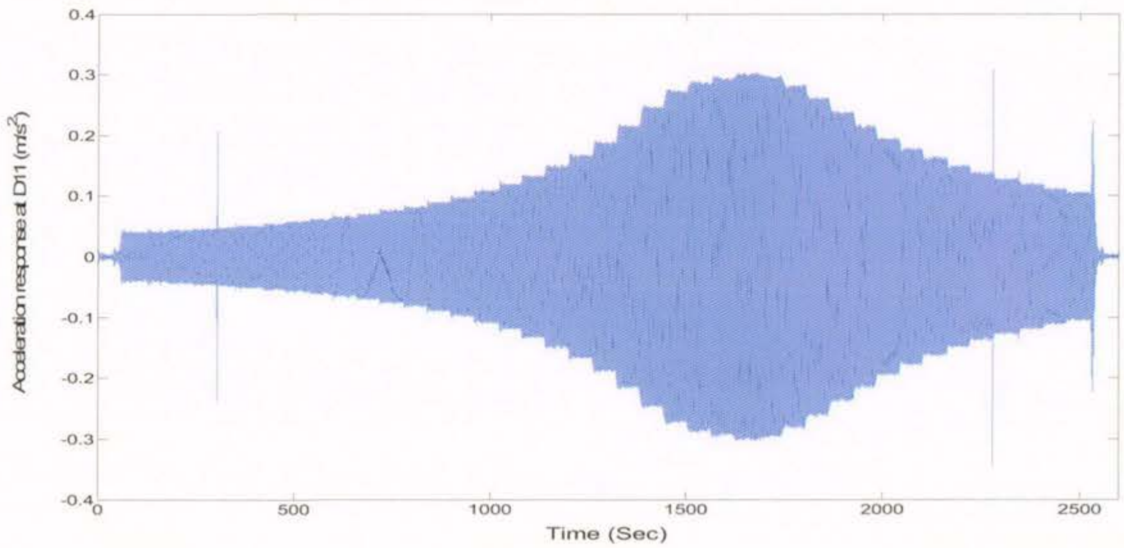

Figure 6.50. Typical steady-state sine sweeping acceleration response.

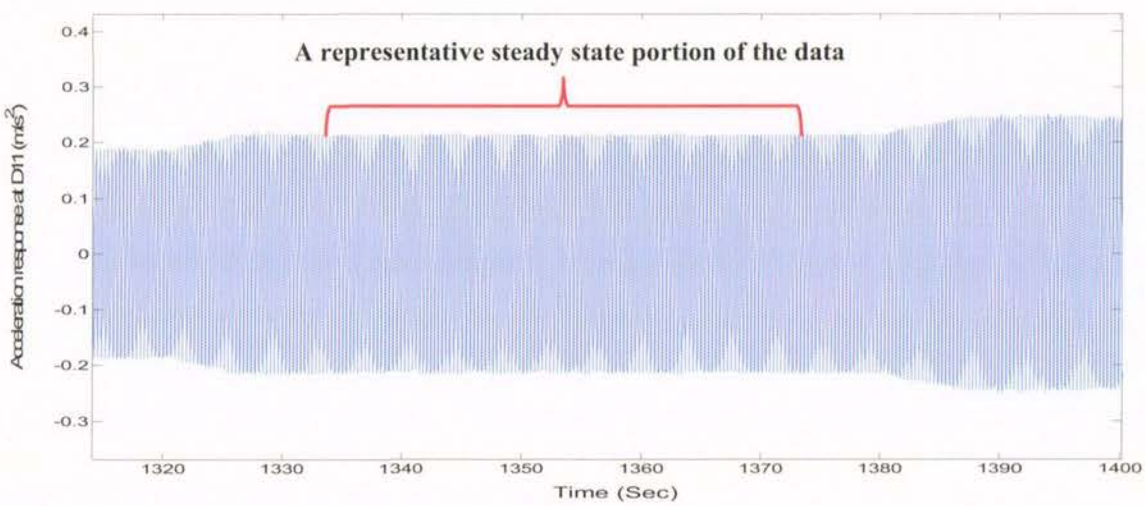

Figure 6.51. Representative sections from the steady state portion of the data.

This section presents baseline system identification results when the bridge was excited in either horizontal or vertical direction with one small weight per shaft on the flywheel (see Table 6-3). Like in the AVT described before, the same two modal parameter identification techniques were implemented to extract the modal properties of the bridge: FDD in the frequency domain and SSI in the time domain. The identified vertical and lateral natural frequencies and damping ratios are summarized in Table 6.4. Although excitation reached 10 Hz, quality results were only achieved up to 8 Hz. It can be observed that the good agreement of frequencies can be found between these two methods. Natural frequency differences of all modes are not more than 0.8%. This gives confidence that the identified frequencies are the true natural frequencies of the bridge rather than spurious results. All identified damping ratios are rather small between 0.6% and 1.8%. Normalized vertical and lateral mode shapes identified using FDD method are displayed is Figures 6.52-63.

Table 6.4. Identified natural frequencies and damping ratios from FVT.

Mode	Experimental frequencies (Hz)		Difference	Damping ratio (%)
	FDD	SSI	(%)	SSI
1st vertical	3.17	3.17	0.0	0.8
2nd vertical	3.87	3.88	0.3	1.5
3rd vertical	4.18	4.17	0.2	0.9
4th vertical	4.76	4.74	0.4	1.4
5th vertical	5.58	5.58	0.0	1.3
6th vertical	7.15	7.14	0.1	1.1
1st lateral	1.87	1.88	0.5	0.6
2nd lateral	2.54	2.54	0.0	0.8
3rd lateral	3.67	3.70	0.8	1.7
4th lateral	4.41	4.43	0.5	1.5
5th lateral	5.54	5.55	0.2	1.5
6th lateral	6.64	6.65	0.2	1.3

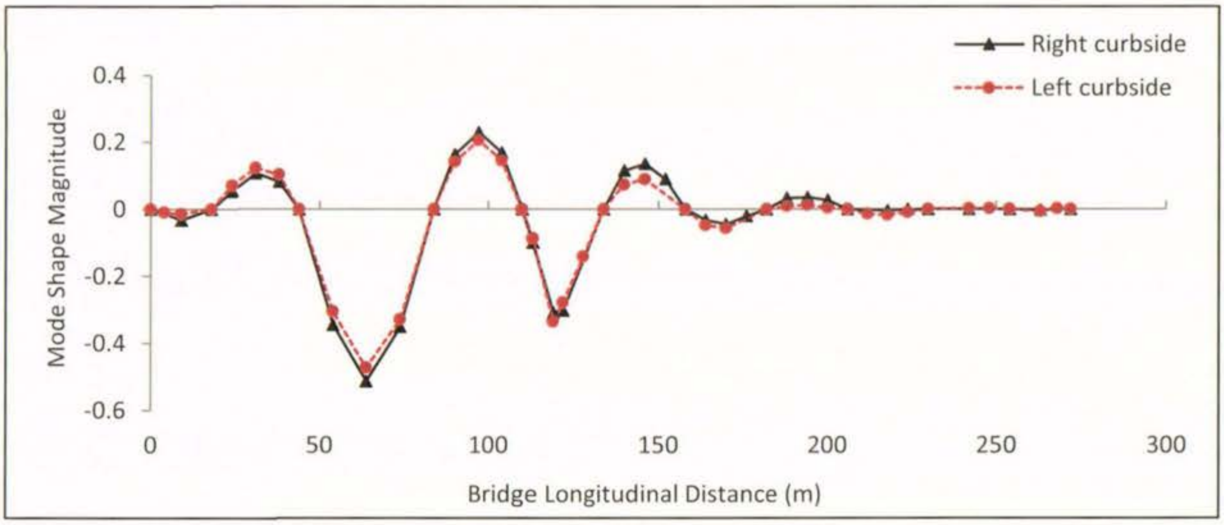

Figure 6.52. 1st vertical mode shape from FVT (3.17 Hz).

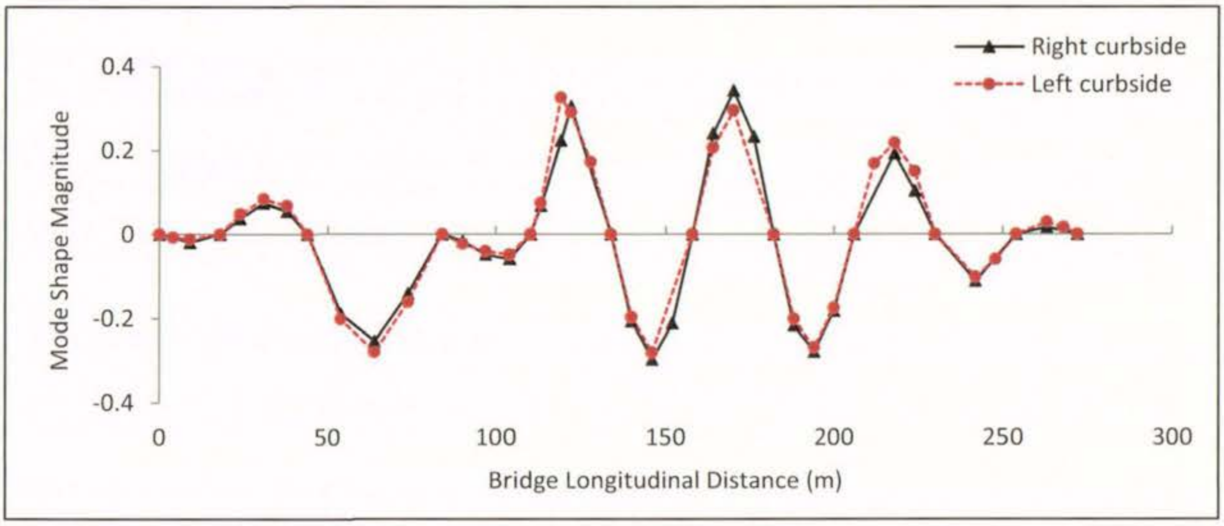

Figure 6.53. 2nd vertical mode shape from FVT (3.87 Hz).

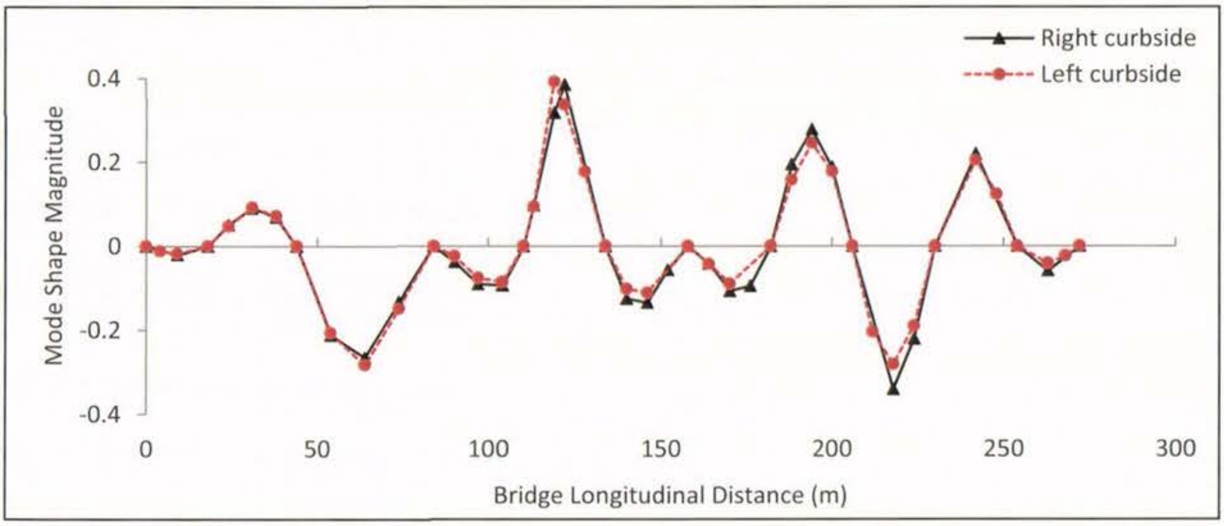

Figure 6.54. 3rd vertical mode shape from FVT (4.18 Hz).

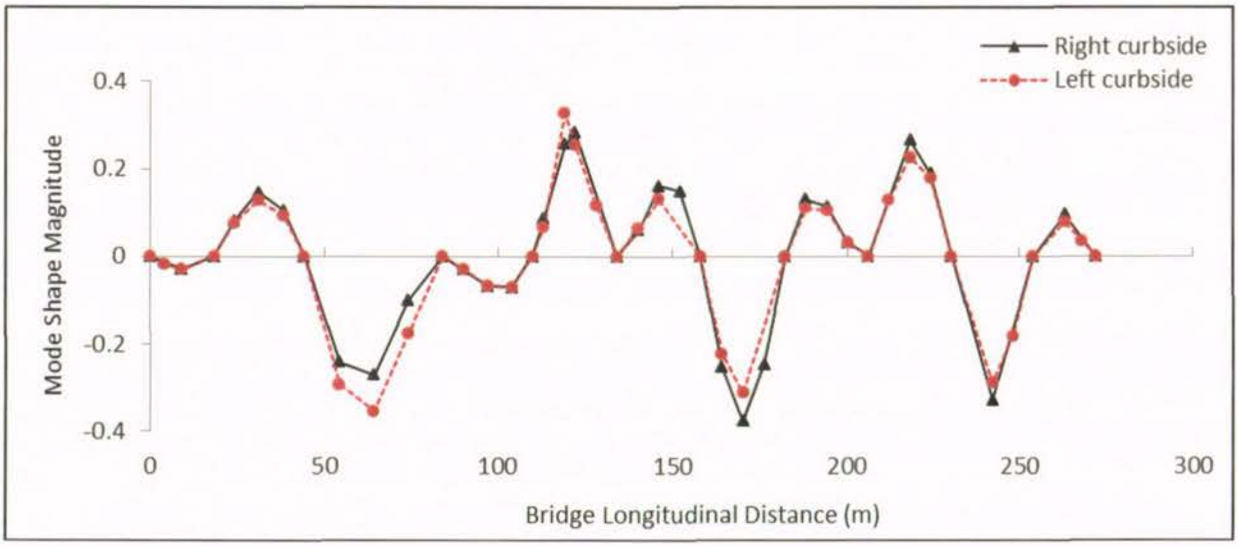

Figure 6.55. 4th vertical mode shape from FVT (4.76 Hz).

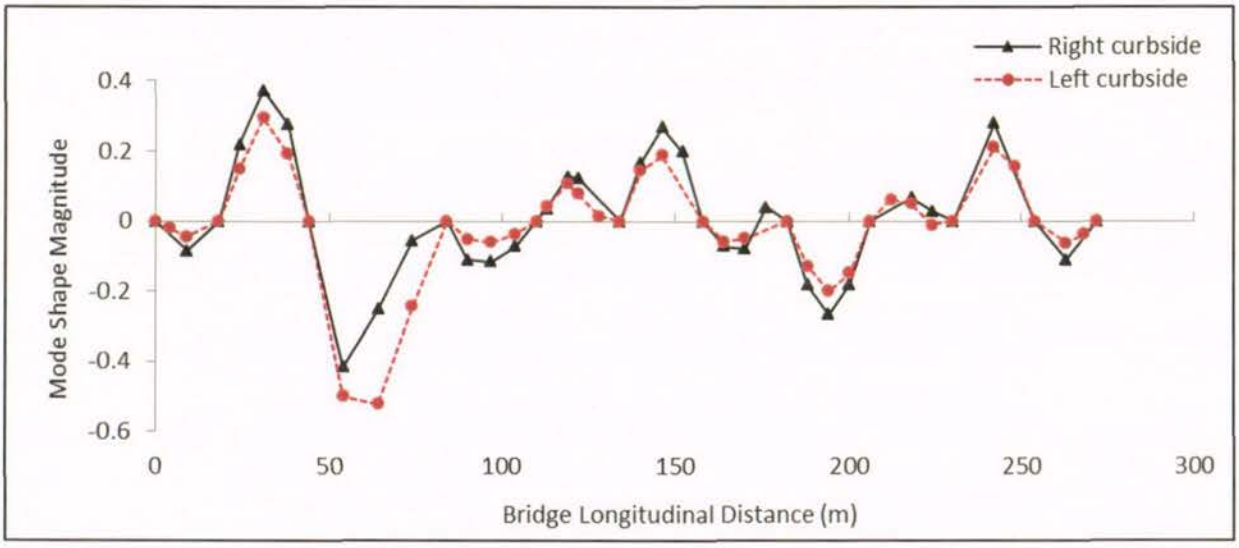

Figure 6.56. 5th vertical mode shape from FVT (5.58 Hz).

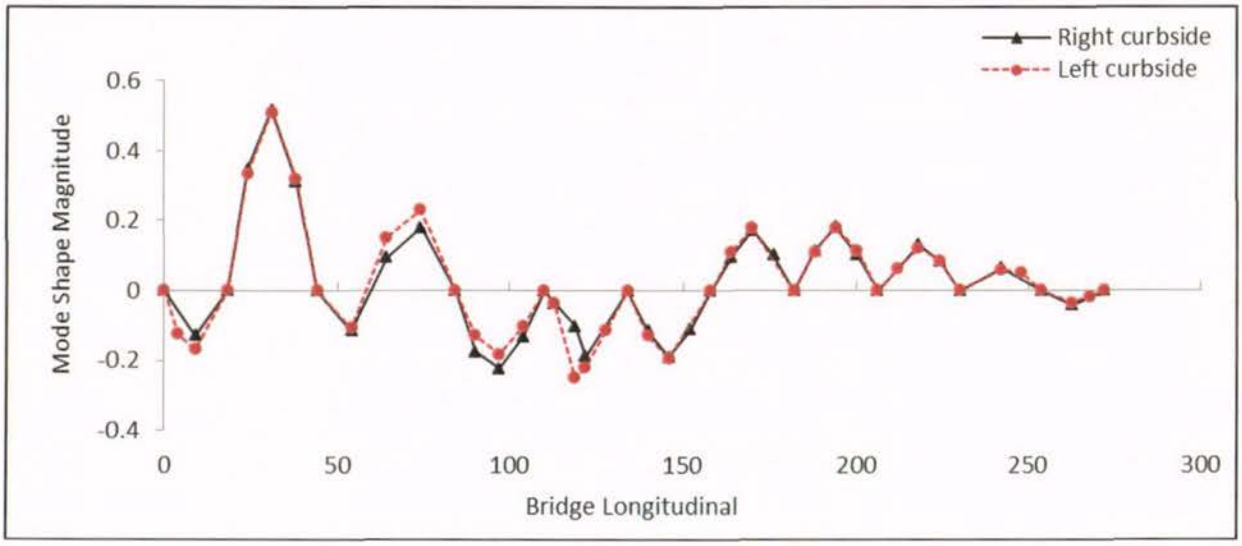

Figure 6.57. 6th vertical mode shape from FVT (7.15 Hz).

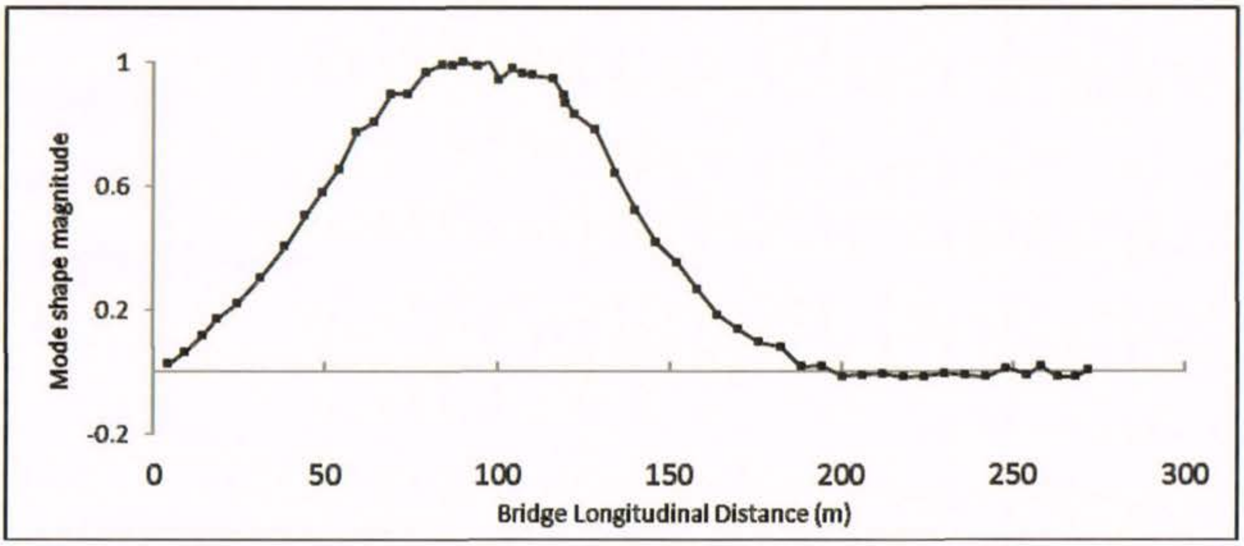

Figure 6.58. 1st lateral mode shape from FVT (1.87 Hz).

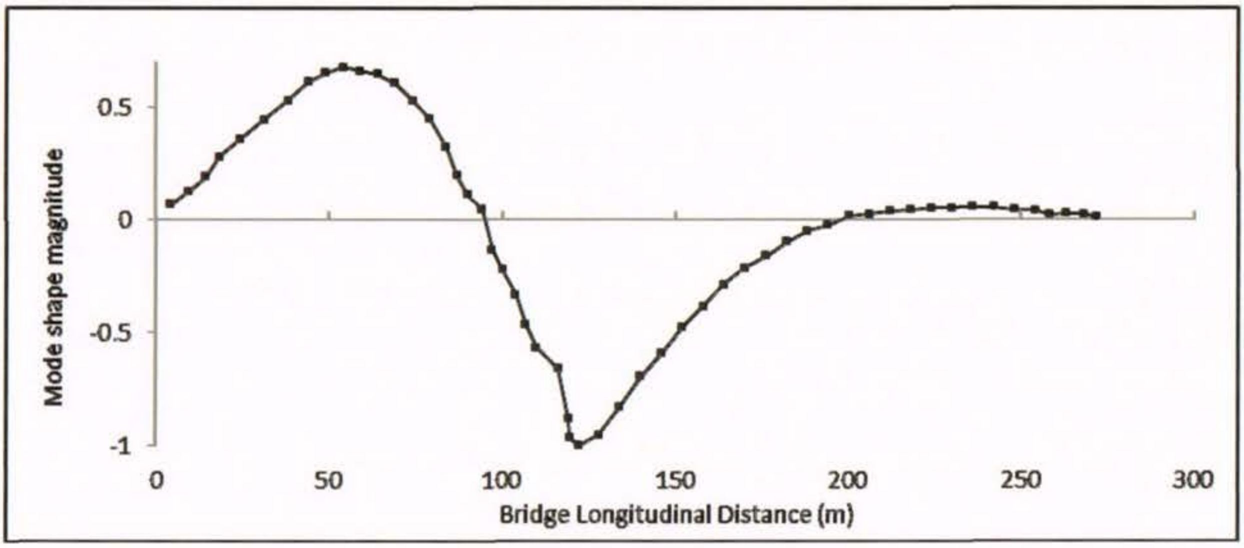

Figure 6.59. 2nd lateral mode shape from FVT (2.54 Hz).

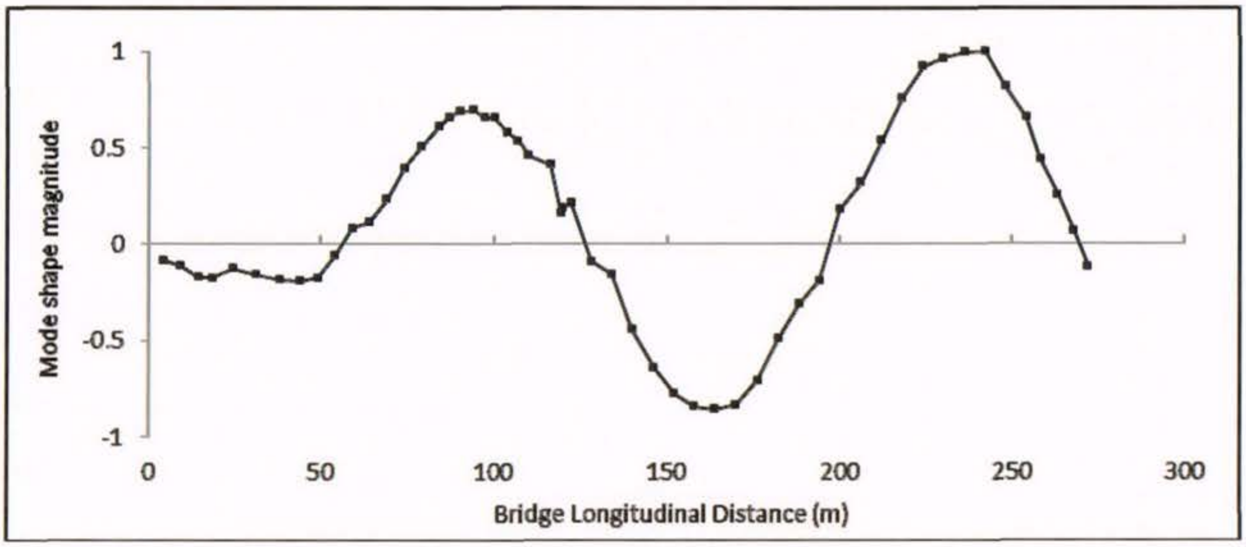

Figure 6.60. 3rd lateral mode shape from FVT (3.67 Hz).

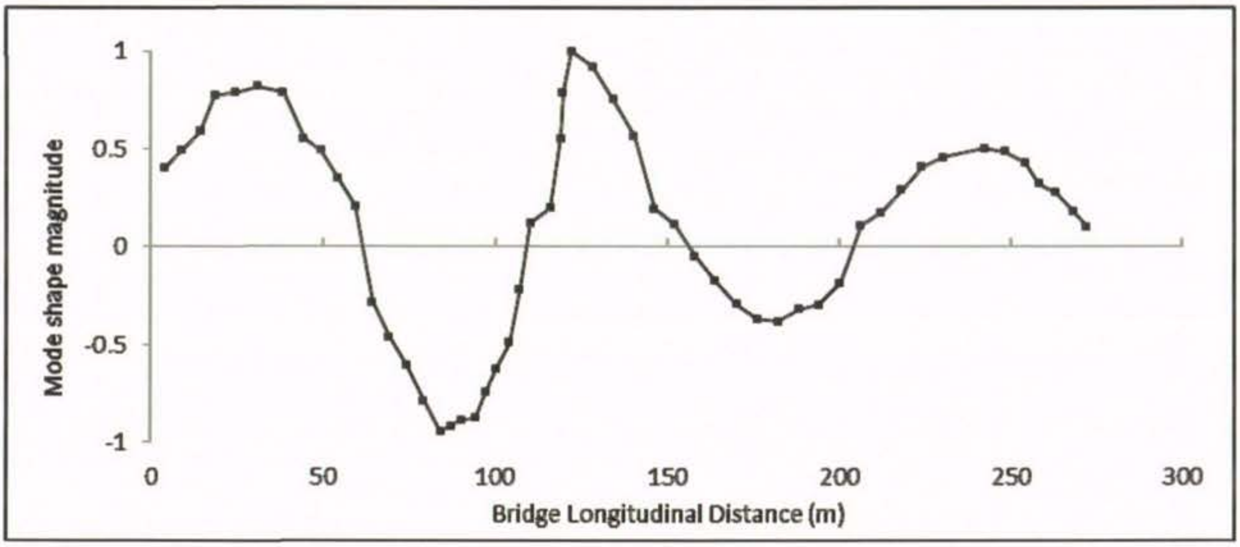

Figure 6.61. 4th lateral mode shape from FVT (4.41 Hz).

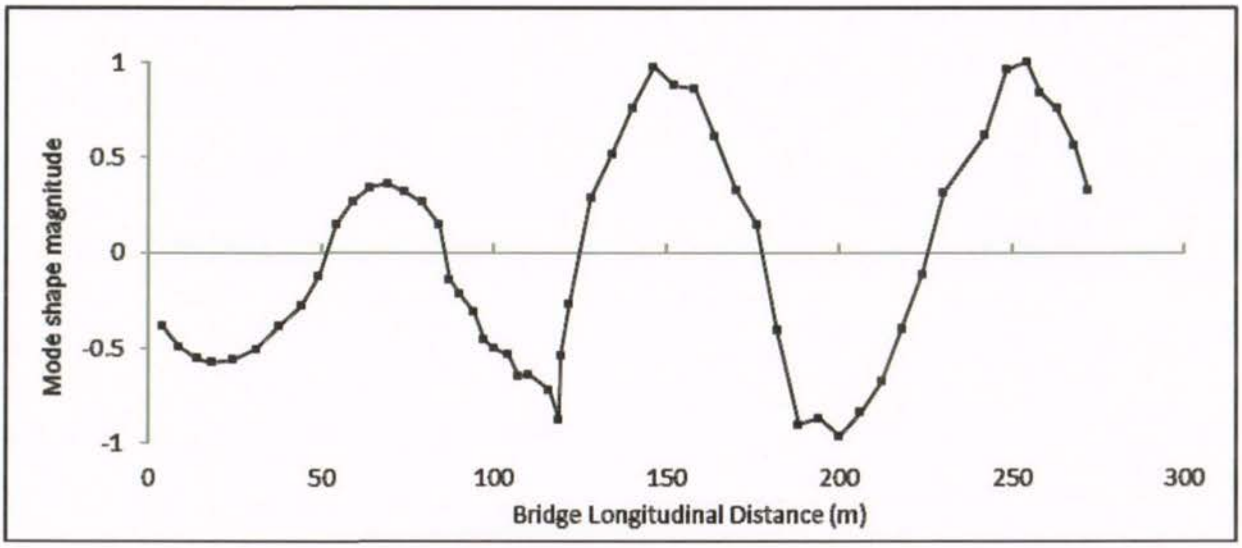

Figure 6.62. 5th lateral mode shape from FVT (5.54 Hz).

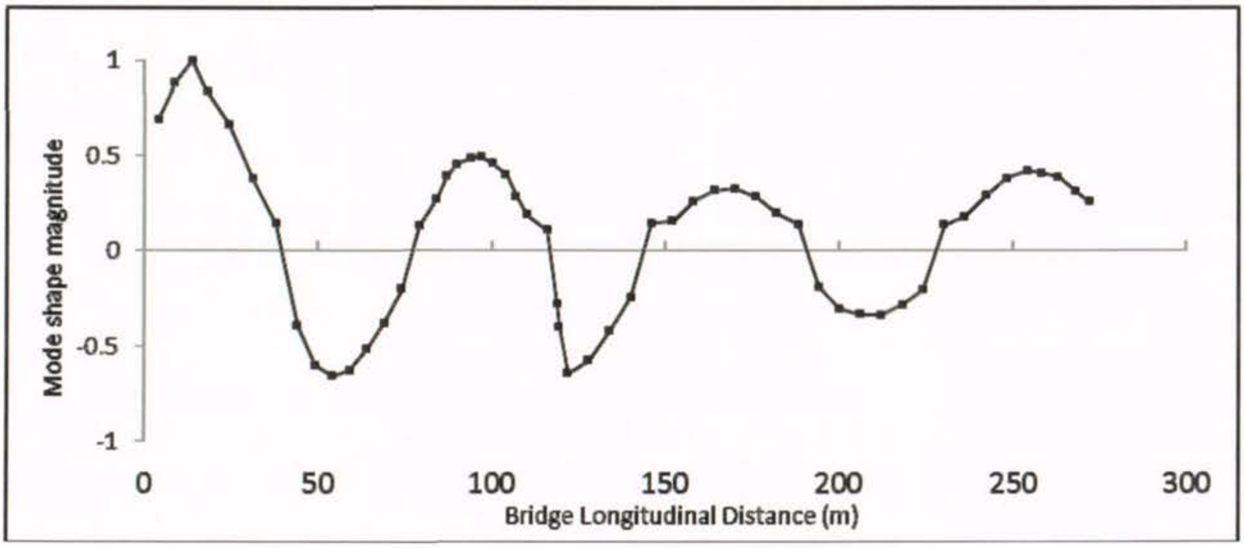

Figure 6.63. 6th lateral mode shape from FVT (6.64 Hz).

6.4.4. Amplitude-dependent modal properties

In the lateral sweeping tests, up to 8 big weights per shaft were gradually added to exert different levels of forcing as shown in Table 6.3. Figure 6.64 shows the normalised displacement curves of the measurement station on the deck located above Pier RC corresponding to different forcing levels when conducting lateral sweeping tests in the vicinity of 1^{st} lateral modal frequency. A clear peak shift towards lower frequencies can be observed as the magnitude of forcing increases. It means that the 1st lateral mode frequency decreases with the rise in shaking magnitude. Table 6.5 shows the identified natural frequencies and damping ratios for the 1st lateral mode for different levels of excitation.

Figures 6.65-67 display the trend lines between the steady state peak acceleration, displacement and force and 1st lateral natural frequency, respectively. The 1st lateral natural frequency decreases by 4.8% as the peak excitation force rises from 0.330 kN to 6.152 kN, peak acceleration from 0.011 m/s^2 to 0.208 m/s^2, and peak response grows from 7.6×10^{-5} m to 1.7×10^{-3} m. It can also be noticed that when the force increases by a factor of 18.6, the corresponding increase in acceleration is 18.9 and in displacement 22.4. The decrease in natural frequency and comparison of acceleration and displacement increase ratios to force increase ratio indicate a softening system.

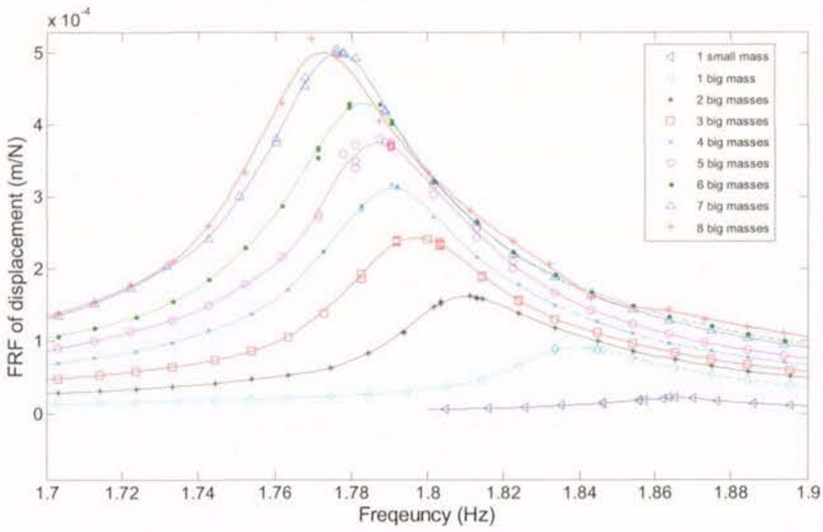

Figure 6.64. FRFs of displacement for 1st lateral mode with varying forcing magnitude.

Table 6.5. Summary of amplitude-dependent data analysis results for 1st lateral mode.

Number of masses per shaft	Peak force (kN)	Peak acceleration (m/s^2)	Peak displacement (m)	Natural frequency (Hz)	Damping ratio (%)
1 small mass	0.330	0.011	7.6×10^{-5}	1.87	0.8
1 big mass	0.975	0.041	3.1×10^{-4}	1.84	1.1
2 big masses	1.849	0.069	5.3×10^{-4}	1.81	1.2
3 big masses	2.767	0.100	7.8×10^{-4}	1.80	1.1
4 big masses	3.495	0.127	1×10^{-3}	1.79	1.1
5 big masses	4.352	0.151	1.2×10^{-3}	1.79	1.1
6 big masses	5.071	0.172	1.4×10^{-3}	1.78	1.2
7 big masses	5.595	0.196	1.6×10^{-3}	1.78	1.1
8 big masses	6.152	0.208	1.7×10^{-3}	1.78	1.2

A combination of two exponential trends was used to fit the frequency-acceleration data points in Figure 6.68. The fitting results are described by the following formula:

$$f = 0.1017\exp(-15.25a) + 1.781\exp(-0.02418a) \tag{6.2}$$

where f is 1st lateral natural frequency (Hz), and a is peak acceleration of steady state response (m/s^2). The coefficient of determination, R^2, indicates how well data points fit a given line or curve. An R^2 of 1 indicates that the regression line perfectly fits the data. The fitting for the exponential trend considered is very good because of the coefficient of determination in excess of 0.99.

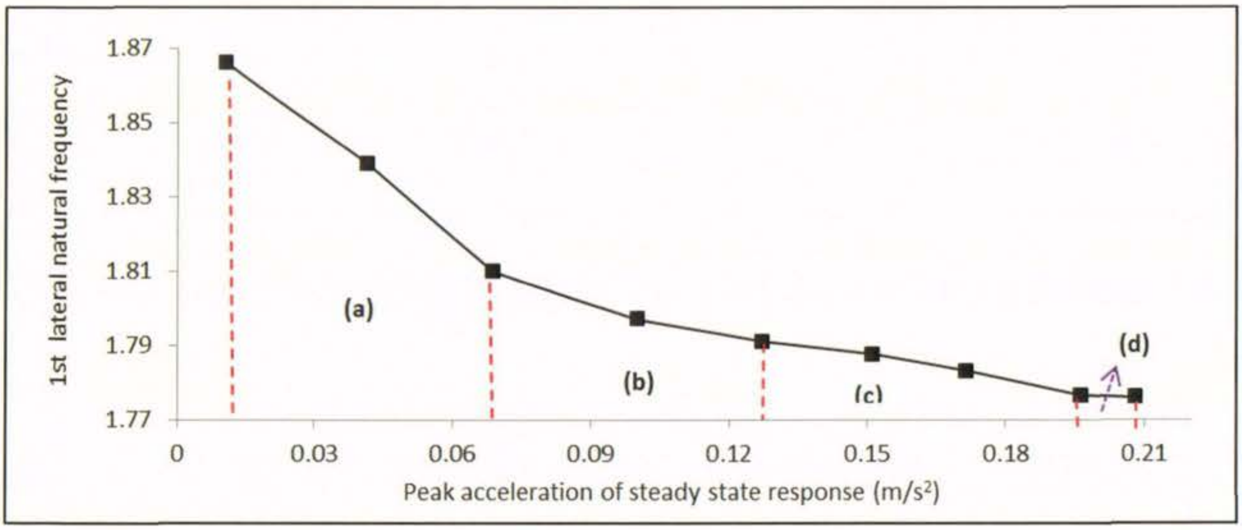

Figure 6.65. 1st lateral natural frequency vs. peak acceleration.

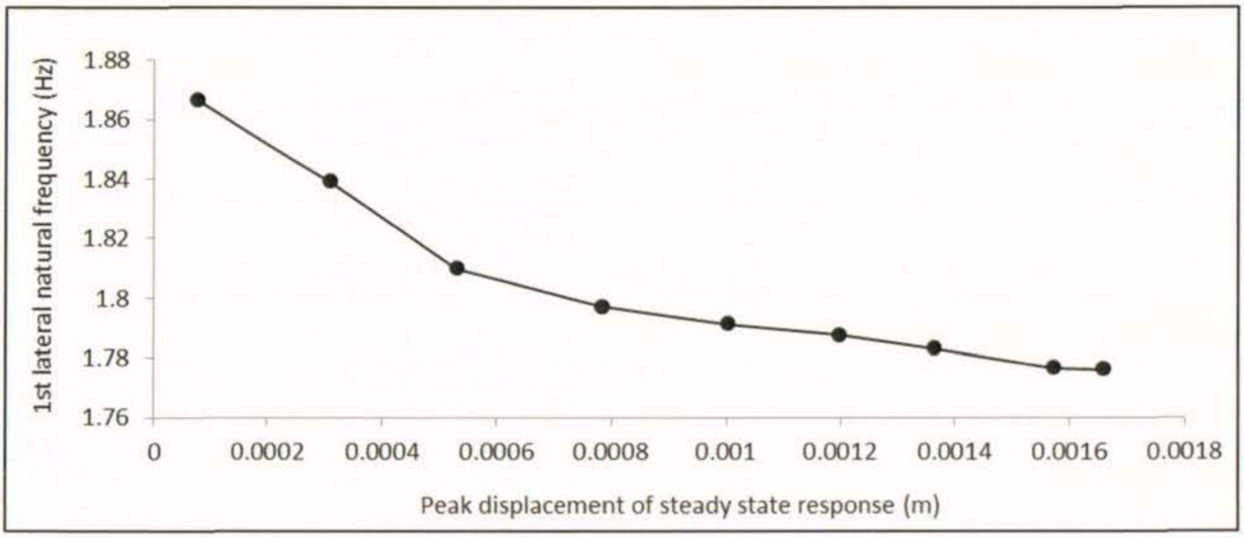

Figure 6.66. 1st lateral natural frequency vs. peak displacement.

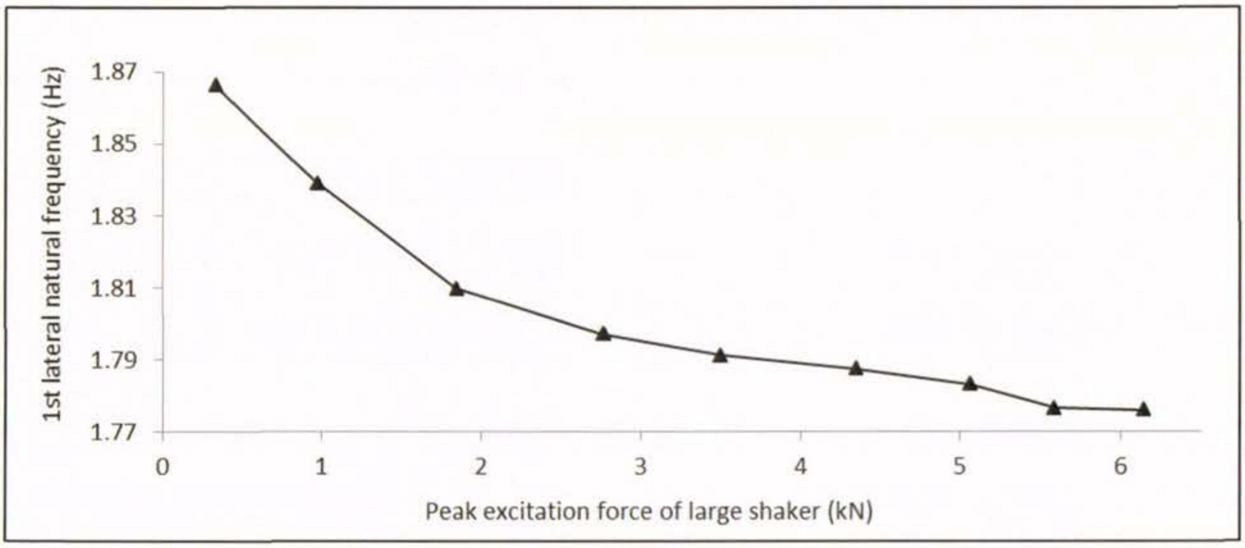

Figure 6.67. 1st lateral natural frequency vs. peak excitation force.

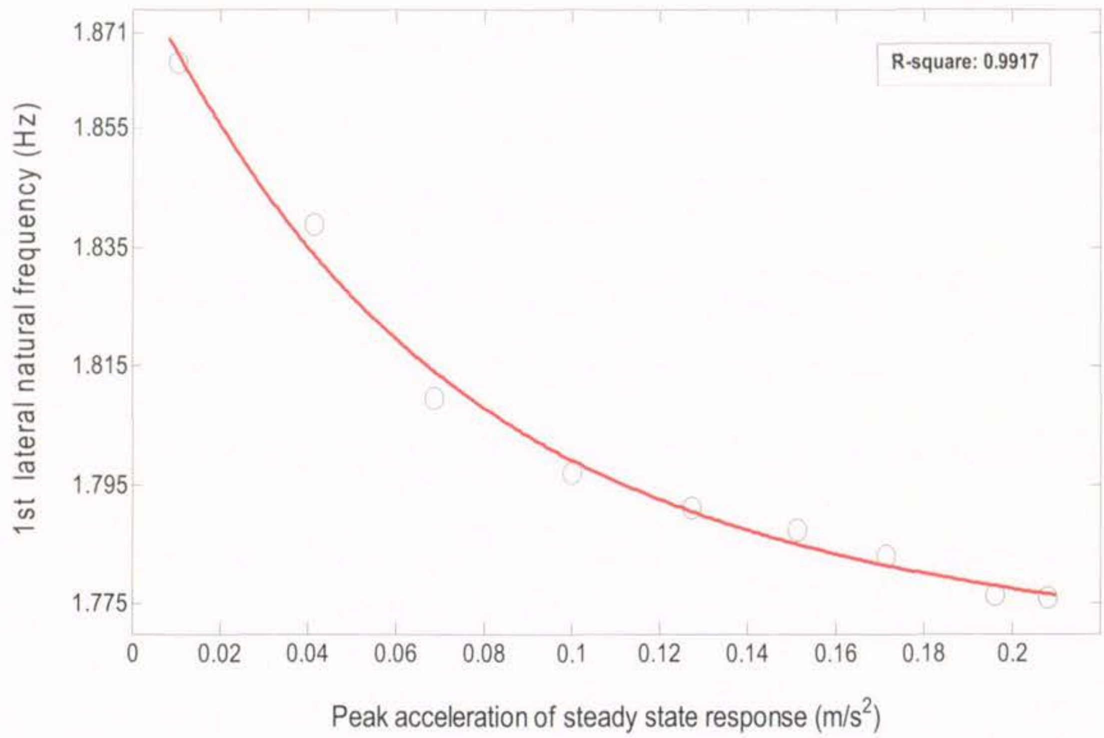

Figure 6.68. Exponential trend between 1st lateral natural frequency and peak acceleration.

Figure 6.69 shows the relationship between the peak acceleration of steady state response and the 1st lateral mode damping ratio. The 1st lateral mode damping ration increase by 44.5% as peak acceleration response rises from 0.011 m/s^2 to 0.041 m/s^2. However, in the range of peak accelerations from 0.041 m/s^2 to 0.0208 m/s^2, damping ratio remains almost constant. A possible physical explanation for this can be that all the structural joints that can slide are already mobilized and do so and all the cracks which are capable of acting as energy sinks have been fully opened at the elevated forcing level. A similar behaviour was also observed by Eyre and Tilley (1977) who conducted a series of measurements on 23 bridges having spans between 17 m to 213 m long. They found that damping initially increases with the amplitude of vibration and then stabilises at an elevated level which can be up to four times higher than the level at small amplitudes. The lower damping was hypothesised to be associated with the behaviour of the superstructure, the upper damping to include contributions from joints and substructure.

A bilinear formula was used to describe the observed damping change with the peak acceleration:

$$\xi = \begin{cases} 10.6a + 0.71 & 0 \le a \le 0.041\, m/s^2 \\ 1.14 & 0.041 < a \le 0.208\, m/s^2 \end{cases} \tag{6.3}$$

where ξ is 1st lateral mode damping ratio (%) and a is peak acceleration (m/s^2). This is graphically presented in Figure 6.70.

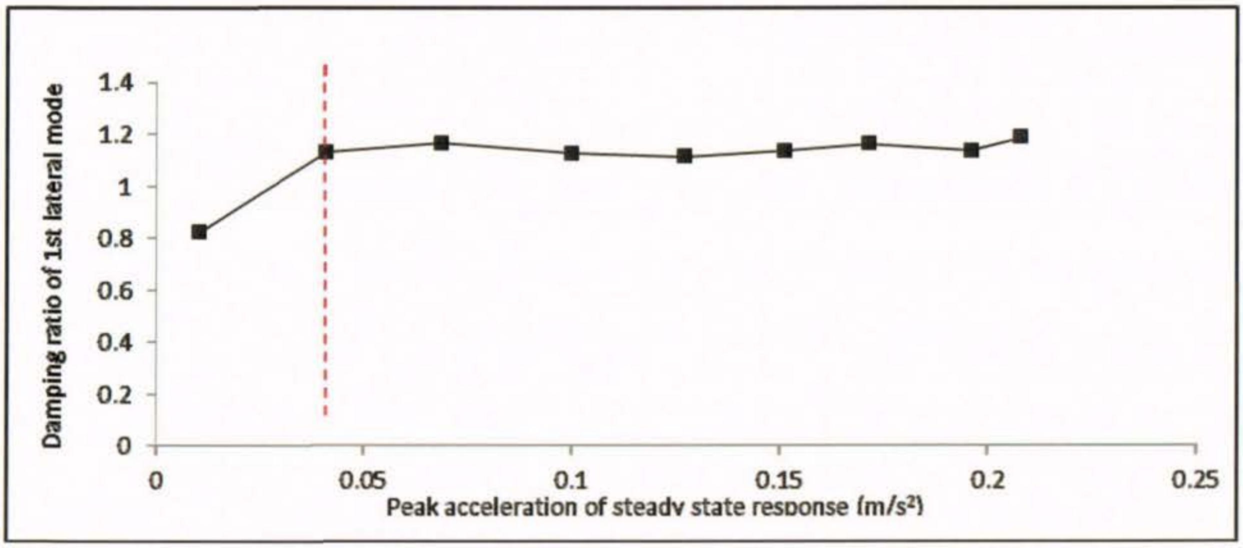

Figure 6.69. 1st lateral mode damping ratio vs. peak acceleration.

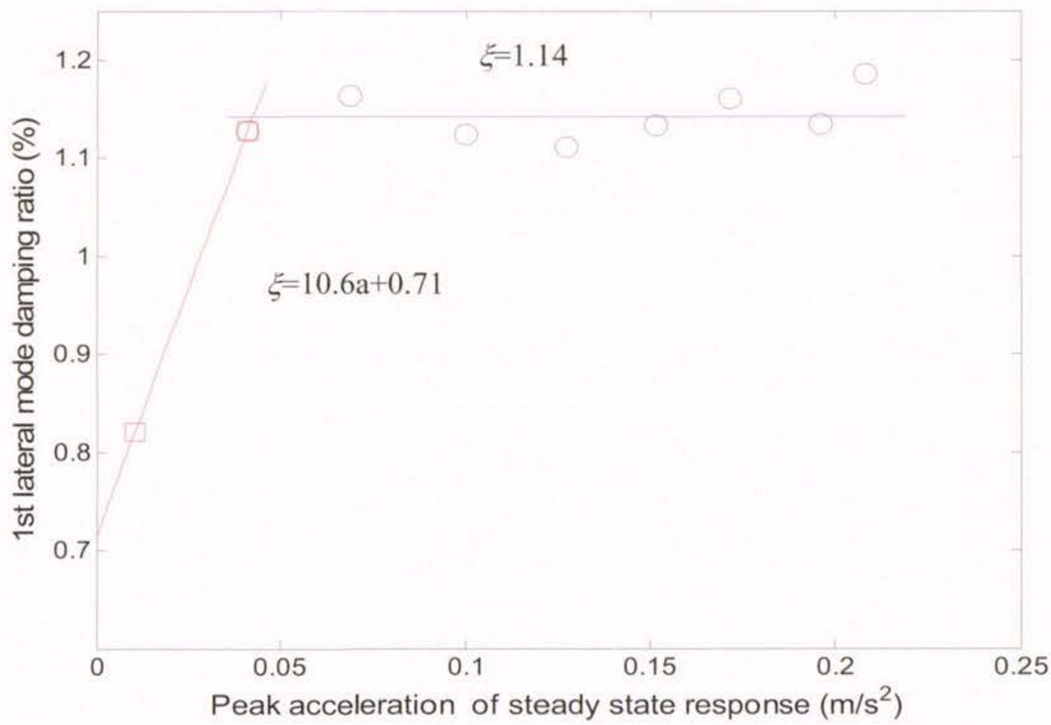

Figure 6.70. Bilinear trend between 1st lateral mode damping ratio and peak acceleration.

6.5. Finite element modelling

To perform theoretical modal analysis of the Nelson St off-ramp bridge, a 3D finite element model has been developed using ANSYS (ANSYS 1999). The model represents the bridge in its current as-built configuration with the geometry, structural properties and boundary conditions determined from the design drawings, during site visits, and also with knowledge acquired from the testing and system identification described above. Note that the inclusion of the latter type of information implies model tuning, although in this case only manual adjustments were made. Structural components, such as box section bridge girders and hexagonal piers, were modelled using 3D elastic beam elements (BEAM188). Material properties used in the model are listed in Table 6.6. The bridge girder was discretized into 0.3 m long beam elements, whereas piers into 0.5 m long beam elements. A total of 1454 nodes and 1200 elements were used.

The modelling of bridge boundary and connectivity conditions is an important aspect strongly influencing numerical results. Bearings on the piers, Abutment VA and Seismic Anchorage were simulated by coupling the corresponding translational DOFs of the piers and girder using link elements or introducing appropriate supports, except for the longitudinal translation at Abutment VA which was left unrestrained. Furthermore, during a site visual inspection it was found that only two bearings without a shear key were installed at the top of Pier RA while two bearings and shear keys could be seen at the top of the remaining piers. It was thus decided to remove the lateral translation restraint at the corresponding bearing location in the FE model. All bearings at the piers and Abutment VA were assumed to allow for unrestrained rotations in two directions except torsion which was restrained. At the Seismic Anchorage, the lowest experimental lateral modes appear to have zero slope (see Figures 6.58 and 59) and based on this in-plane rotation was additionally restrained there. Internal hinges were modelled by releasing all rotational DOFs in the corresponding connecting nodes. Pier footings were modelled as fixed at the base, and soil-structure interaction, Abutment VA and Seismic Anchorage were not included in the analysis. The constructed 3D FE model of the Nelson St off-ramp bridge is shown in Figure 6.71.

Table 6.6. Concrete material properties for FE model.

Component	Young's modulus (GPa)	Mass density (kg/m^3)	Poisson's ratio (-)
Concrete girder	35	2600	0.1667
Cantilever slab of girder	30	2400	0.1667
Piers	30	2400	0.1667

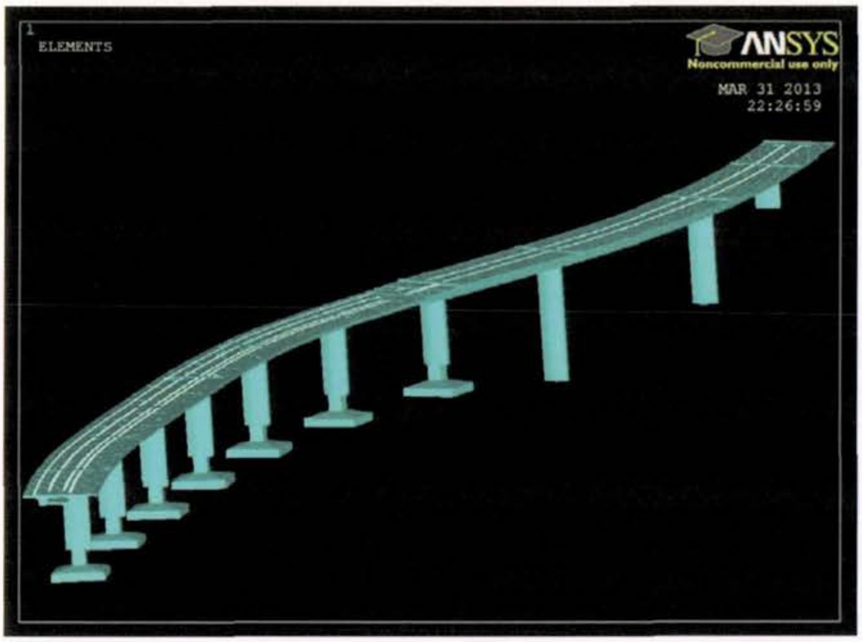

Figure 6.71. 3D FE model of the Nelson St off-ramp bridge.

6.5.1. Numerical modal analysis and comparison with experimental results

A shifted Block-Lanczos method (Grimes et al. 1994) employed in ANSYS (ANSYS 1999) was used to extract the eigenvalue-eigenvector pairs. MAC (Allemang and Brown 1982, see also Equation 3.47) was used for comparing the experimental and numerical mode shapes. Table 6.7 summarizes the natural frequency results from FVT and FE predictions, the frequency errors and MACs. Normalized vertical and lateral mode shapes calculated based on the tuned FE model are displayed in Figures 6.72-83.

It can be observed that the natural frequency results calculated based on FE model match well these obtained from field testing. The maximum vertical natural frequency error is only 1.3%, while for the lateral natural frequency it is 11.8%. Overall, the natural frequency errors of vertical modes are markedly smaller than for the lateral modes. As for the agreement of mode shapes between the FE model and field testing, MACs of four vertical modes are above 0.90, indicating a very good agreement. Two vertical modes have MACs of 0.76 and 0.58, which is still acceptable. It can be concluded that FE model simulates the boundary conditions, stiffness and mass distribution for the vertical direction well. The MACs of lateral modes are between 0.94 and 0.71 again pointing out to a generally successful modelling.

Although MACs are generally high, the examination of mode shapes in Figures 6.72-83 still reveals some discrepancies between the experiment and the numerical model. For example, several vertical modes show much larger experimental modal deformations in the right hand side spans than does the computer model. The higher experimental lateral modes, 3rd and above, also depart quite noticeably from their numerical counterparts. The reason for that could be the flexibility of soil not included in the current FE model. Also, the higher lateral mode shapes suggest that the full lateral displacement and in-plane rotational restraints assumed at Seismic Anchorage may need to be adjusted in future models. Full formal and systematic updating of FE model parameters should also be conducted to further improve the model.

Table 6.7. Comparison between identified and calculated frequencies and mode shapes.

Mode	FE model (Hz)	Experiment by FDD (Hz)	Frequency error (%)	MAC
1st vertical	3.17	3.13	-1.3	0.99
2nd vertical	3.87	3.87	0.0	0.94
3rd vertical	4.18	4.18	0.0	0.04
4th vertical	4.76	4.77	0.2	0.76
5th vertical	5.58	5.54	-0.7	0.58
6th vertical	7.15	7.14	-0.1	0.91
1st lateral	1.87	2.17	-16.0	0.94
2nd lateral	2.54	2.84	11.8	0.89
3rd lateral	3.67	3.52	-4.1	0.71
4th lateral	4.41	4.67	5.9	0.74
5th lateral	5.54	5.54	0.0	0.85
6th lateral	6.64	7.48	12.7	0.88

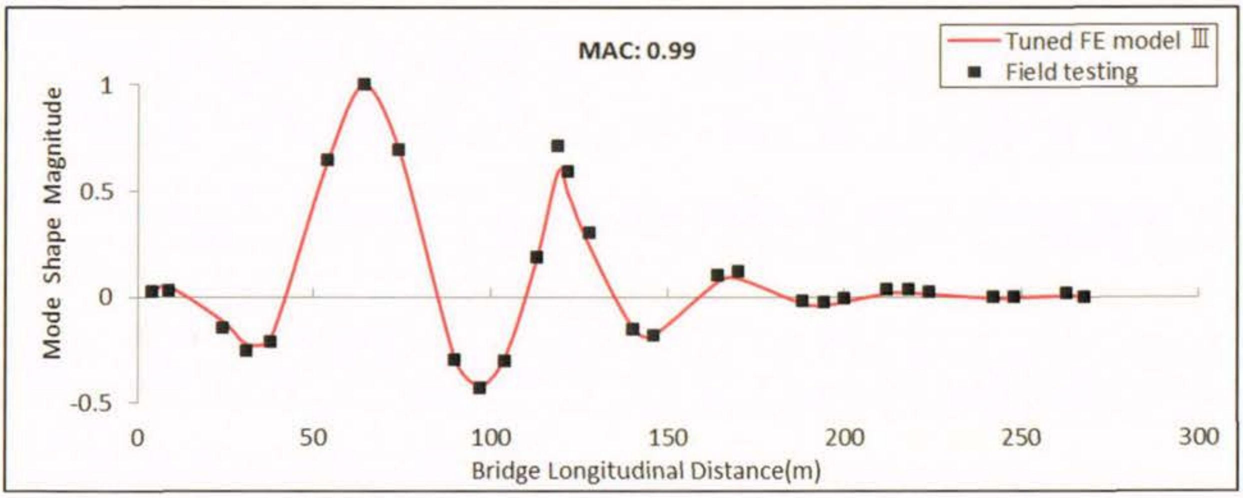

Figure 6.72. Comparison of 1st vertical mode shape from FVT and FE modelling.

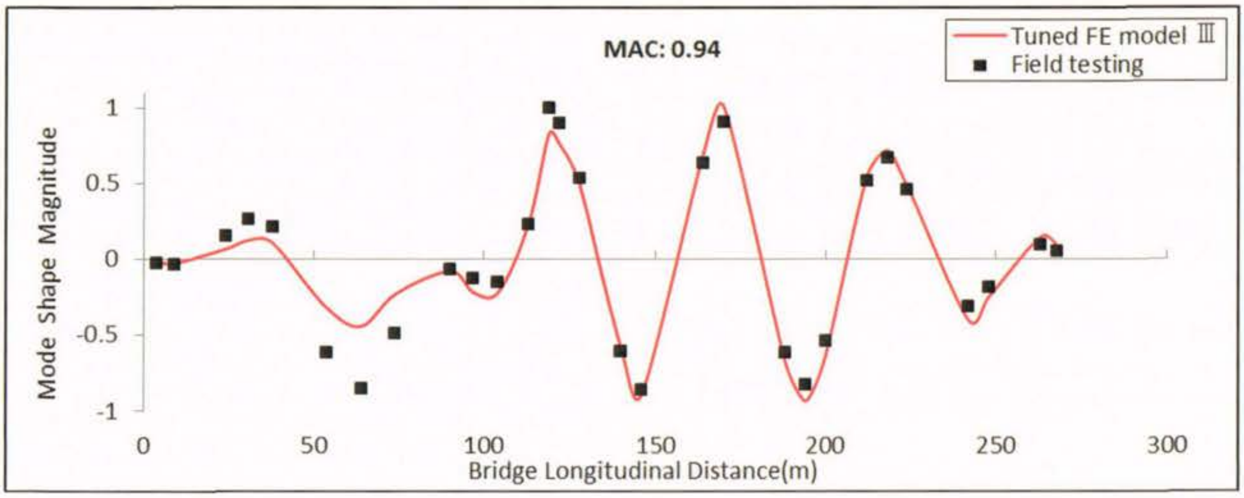

Figure 6.73. Comparison of 2nd vertical mode shape from FVT and FE modelling.

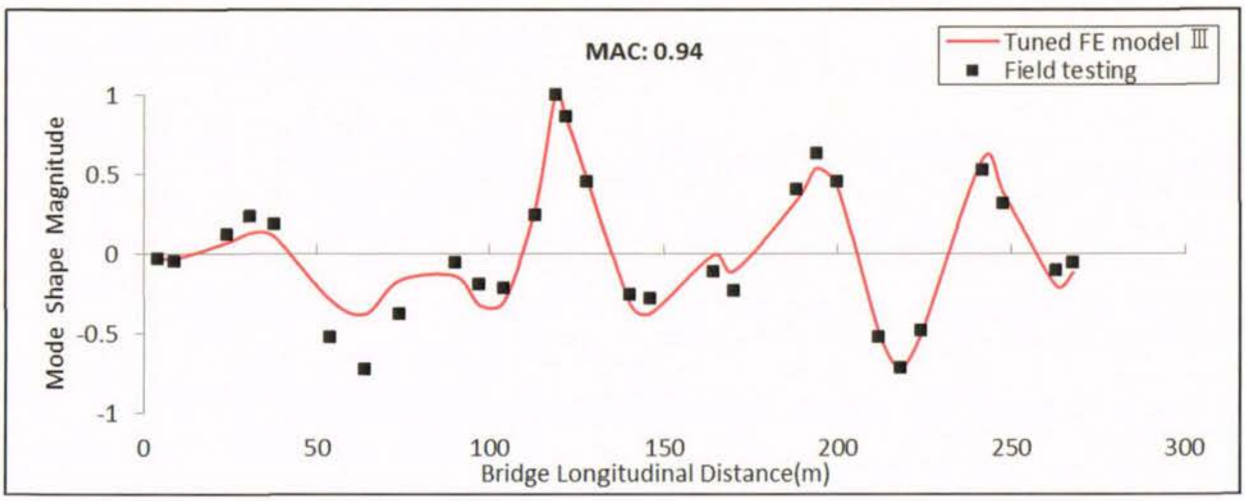

Figure 6.74. Comparison of 3rd vertical mode shape from FVT and FE modelling.

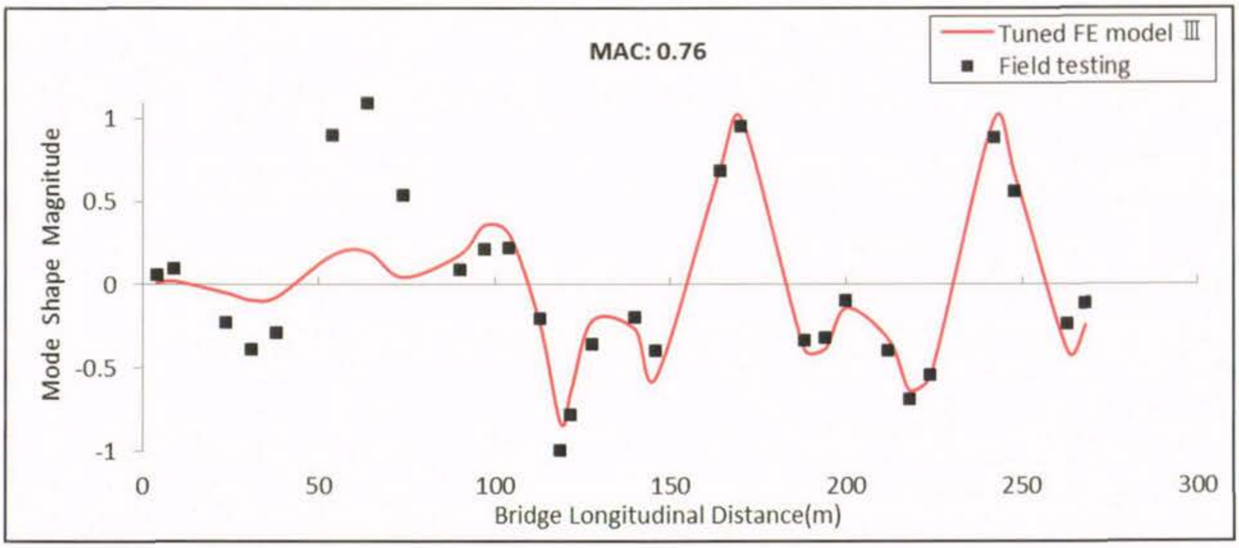

Figure 6.75. Comparison of 4th vertical mode shape from FVT and FE modelling.

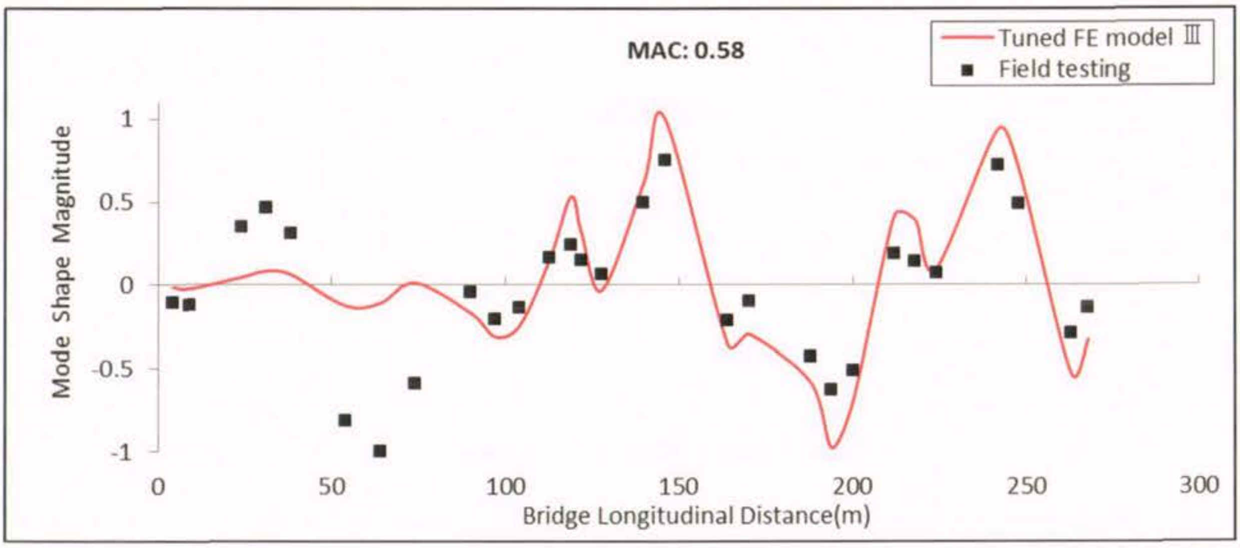

Figure 6.76. Comparison of 5th vertical mode shape from FVT and FE modelling.

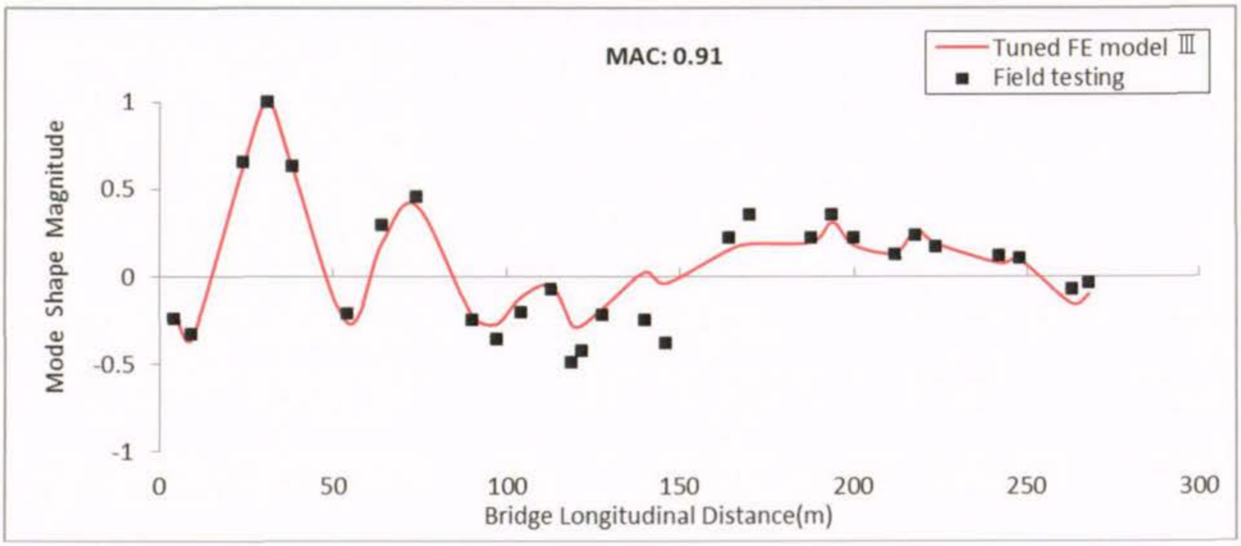

Figure 6.77. Comparison of 6th vertical mode shape from FVT and FE modelling.

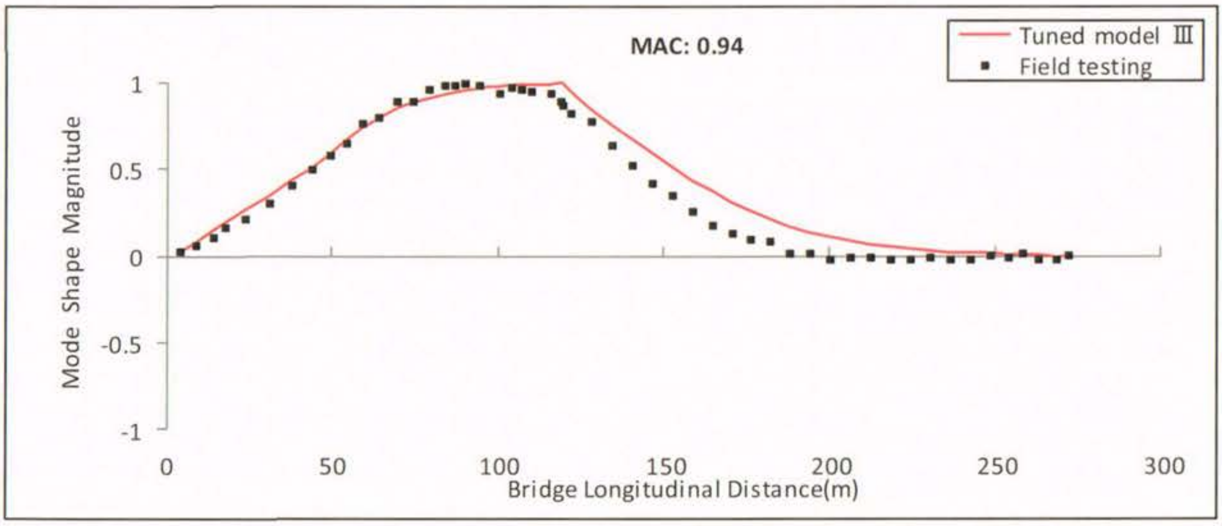

Figure 6.78. Comparison of 1st lateral mode shape from FVT and FE modelling.

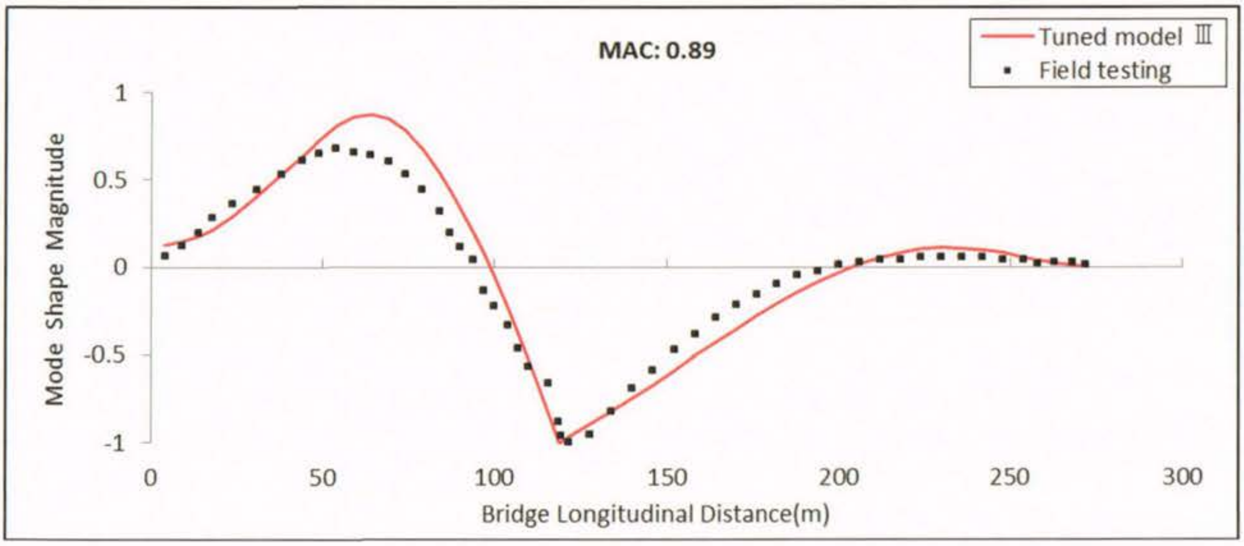

Figure 6.79. Comparison of 2nd lateral mode shape from FVT and FE modelling.

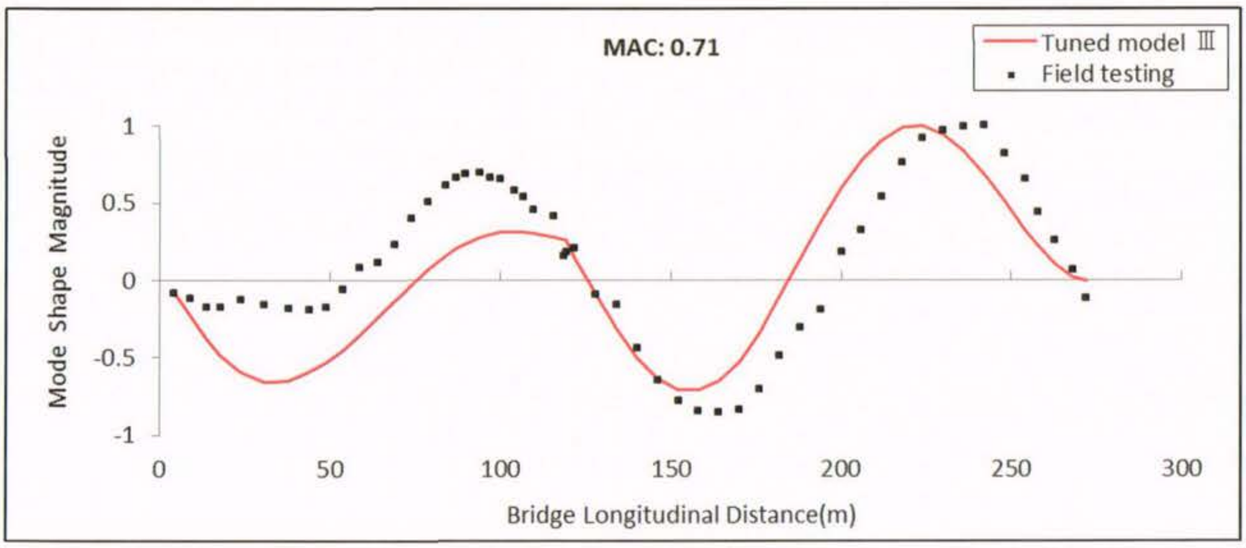

Figure 6.80. Comparison of 3rd lateral mode shape from FVT and FE modelling.

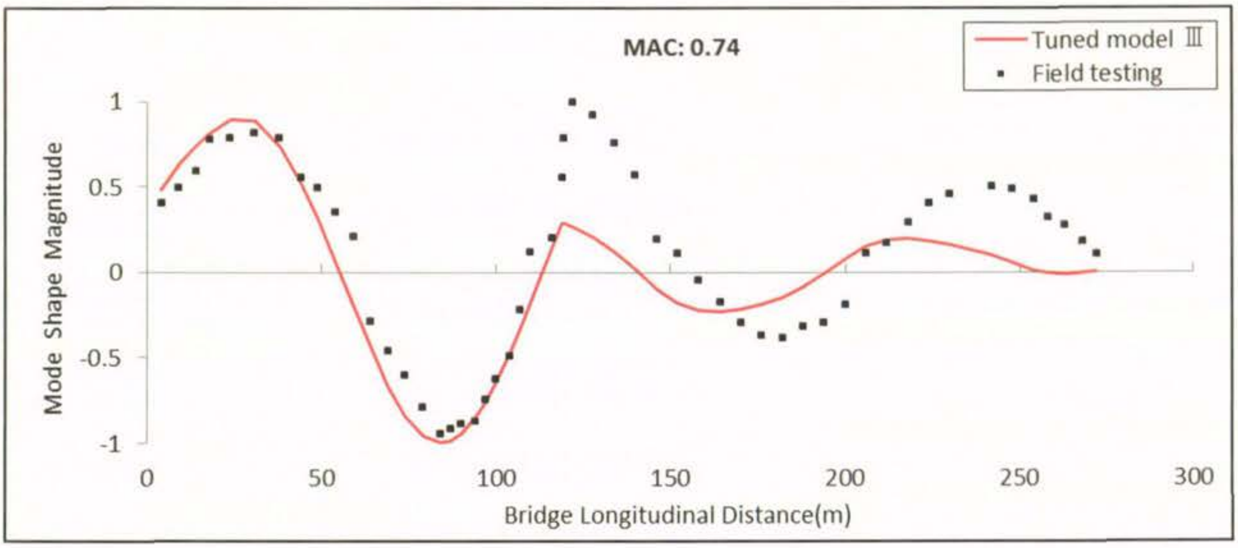

Figure 6.81. Comparison of 4th lateral mode shape from FVT and FE modelling.

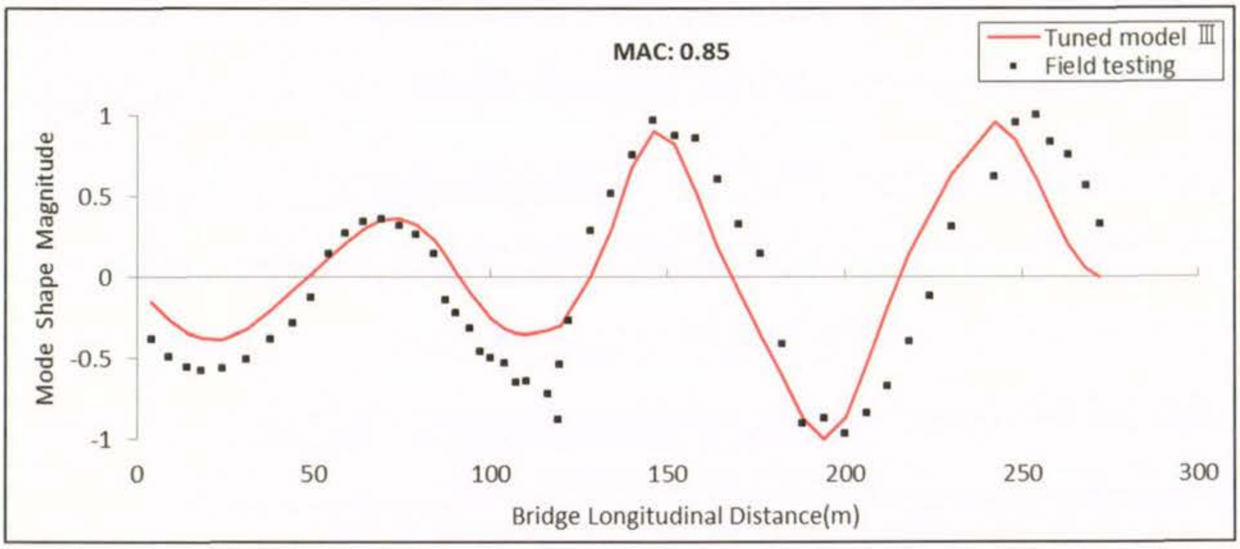

Figure 6.82. Comparison of 5th lateral mode shape from FVT and FE modelling.

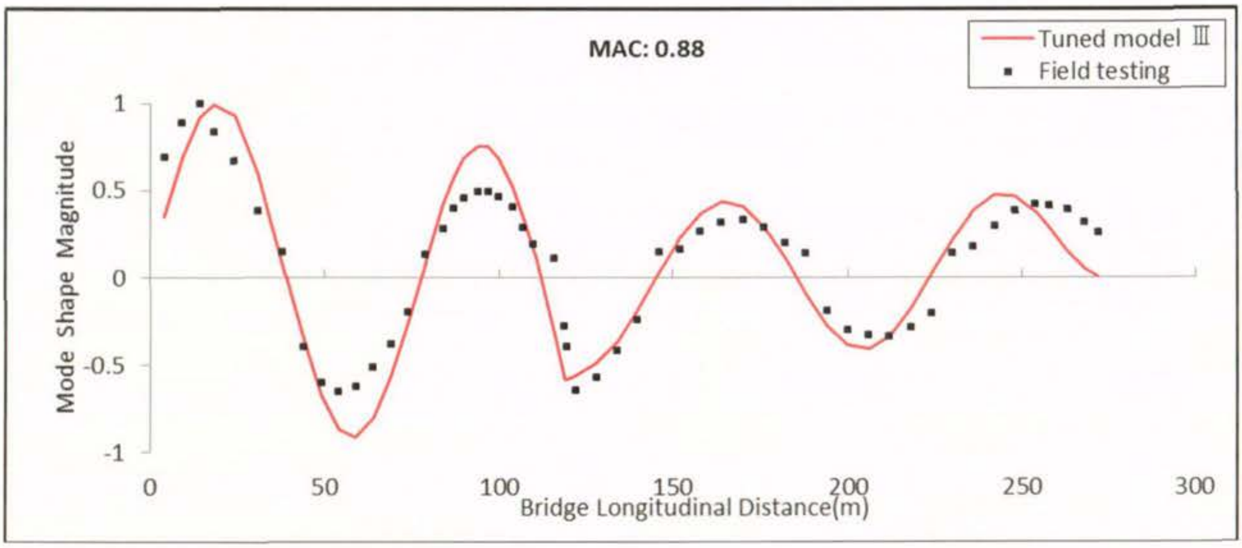

Figure 6.83. Comparison of 6th lateral mode shape from FVT and FE modelling.

6.6. Conclusions

This chapter presents field testing, system identification and numerical modelling of an 11-span motorway off-ramp closed to traffic. A series of ambient vibration tests were conducted first, where excitation was provided by traffic on nearby motorway and streets, wind, possible microtremors, and also people jumping on the deck. These tests helped to form an initial knowledge about the bridge dynamics, although some modes could not be excited or identified. The main testing programme consisted of forced vibration testing using two large eccentric mass shakers capable of imparting excitation in both lateral and vertical direction. In addition to performing frequency sweep tests for modal identification, the excitation force was varied in several increments in order to explore how modal frequencies and damping ratios depend on response magnitude. Finally, a detailed 3D computer model of the bridge was formulated and theoretical modal results compared to the experimental ones.

The forced vibration testing identified with confidence full modal properties (frequencies, damping ratios and mode shapes) for six vertical and six lateral modes in the frequency range up to 8 Hz. By gradually increasing the magnitude of forcing it was observed that the 1st lateral mode shows a consistent decrease in natural frequency that can be approximated by exponential functions. This indicates softening force-displacement characteristics of the structure. The damping ratio initially increased but later stayed constant at an elevated level, indicating that all energy dissipation mechanics have been engaged. This preliminary study should be extended by examining similar trends for other modes where appropriate data were collected and explaining the mechanisms responsible for the observed behaviour. FE modelling paid special attention to boundary and connectivity conditions, such as bearings and internal hinges. By carefully modelling these, it was possible to formulate a tuned structural model that replicates experimental modal results well. Future research should look at systematic updating of the FEM model to further improve the agreement with field testing results.

6.7. References

Allemang R.J., & Brown D.L. (1983), Correlation coefficient for modal vector analysis, Proceedings of IMAC I: 1st international modal analysis conference, 110-116.

ANCO Engineers (2013), http://www.ancoengineers.com.

ANSYS (1999), Theory reference, release 5.6, Canonsburg, PA.

Bendat, J.S., & Piersol, A.G. (1993), Engineering applications of correlation and spectral analysis, (2nd Ed.), Wiley, New York, NY.

Beskhyroun, S. (2011), Graphical interface toolbox for modal analysis, Proceedings of the 9th Pacific Conference on Earthquake Engineering: Building an Earthquake-Resilient Society, paper no. 077.

Eyre, R., & Tilly, G.P. (1977), Damping measurements on steel and composite bridges, Proceeding of Symposium on Dynamic Behaviour of Bridges, Transport and Road Research Laboratory, Crowthorne.

Grimes, R.G., Lewis, J.G., & Simon, H.D. (1994), A shift block Lanczos algorithm for solving sparse symmetric generalized eigenproblems, SIAM Journal of Matrix Analysis Applications, 15, 228–272.

Heylen, W., Lammens, S., & Sas, P. (1997), Modal analysis theory and testing, Katholieke Universiteit Leuven, Leuven.

CHAPTER 7

FORCED VIBRATION TESTING, SYSTEM IDENTIFICATION AND MODEL UPDATING OF A TWO-SPAN OVERBRIDGE

7.1. Introduction

The structure under investigation in this chapter is the Gillies Avenue overbridge which formed a section of the original Newmarket Viaduct passing over Gillies Avenue in Newmarket, Auckland, New Zealand. Nearing its design life, the bridge was tested prior to being demolished in April 2012 and replaced by a new bridge positioned parallel to the old bridge as part of the Newmarket Connection Project.

This testing exercise was the first time when the team of researchers behind this report performed full-scale testing using the large ANCO Engineers MK-140-10-50 eccentric mass shakers (ANCO Engineers 2013) and analysed collected data. Because of this, the exercise is described after the Nelson St off-ramp testing (Chapter 6), which it preceded, and the results presented are rather brief and preliminary. The exercise is included in this report nevertheless mainly for the sake of completeness and illustrating the learning process that later allowed conducting more complex bridge testing and data analyses, such as these for Nelson St off-ramp, more confidently.

The content of this chapter includes bridge characterisation, description of field testing programme, discussion of system identification results and subsequent FE model formulation and sensitivity based model updating.

7.2. Bridge description

Originally consisting of two parallel spans each supporting three lanes of traffic, only the Northbound section of Gillies Avenue overbridge remained prior to testing, albeit already subjected to heavy structural modifications necessitated by partial demolition and on-going construction of Newmarket Viaduct (whose ambient testing was the topic of Chapter 5).

The bridge, shown in side view in Figure 7.1, was approximately 50 m in length with a 12.9 m wide deck. There were two spans: a 20 m span starting from the abutment at the North end (on the left in Figure 7.1), and a 30 m span supported at the South end on a wall-type pier common with the old Newmarket Viaduct. Separating the two spans and providing intermediate supports were two round columns. The two columns had a measured above ground height of 5040 mm and 5300 mm for the East and West column, respectively. The RC girder had a box cross-section of total height of 1143 mm comprising four closed cells as shown in Figure 7.2. The West side of the bridge had a 1105 mm wide elevated kerb with a steel mesh and post fencing at approximately 1000 mm centres. The East side was adjacent, but separated, to the newly built highway bridge with a concrete barrier approximately 1200 mm in height. Furthermore, according to the supplied drawings the deck had a super-elevation and a slight tilt along the length of the bridge. Longitudinal and transverse tilting of the deck was at a nominal 0.42° and 3.15°, respectively.

Due to the deconstruction process additional stabilizing supports in the form of a braced steel frame (Figure 7.3) were provided at the South end. Four steel towers also penetrated through two rectangular 1250 × 3800 holes mm cut through the depth of the deck near the South end (Figure 7.4). The towers were for the provision of structural stability to the gantry used for the demolition of the old Newmarket Viaduct. Site investigations showed substantial amounts of soil were removed from the base of the two mid-span columns (Figure 7.5). In addition, the presence of bolts connecting the gantry towers to an endplate at their base made the boundary conditions of the system complex and uncertain.

Figure 7.1. Side view of Gillies Avenue overbridge.

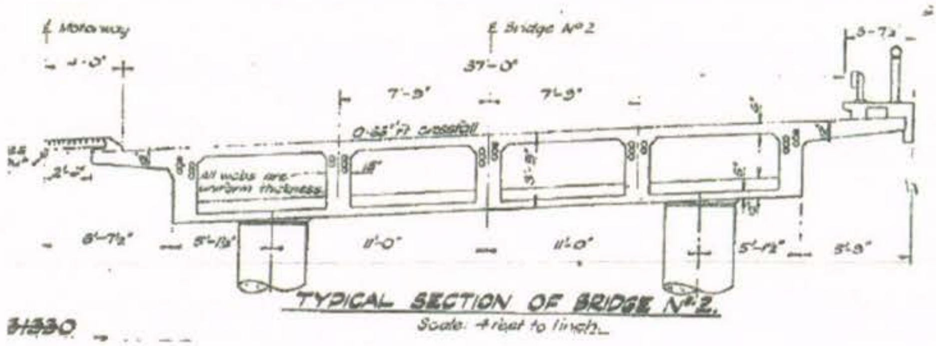

Figure 7.2. Typical cross-section of Gillies Avenue overbridge.

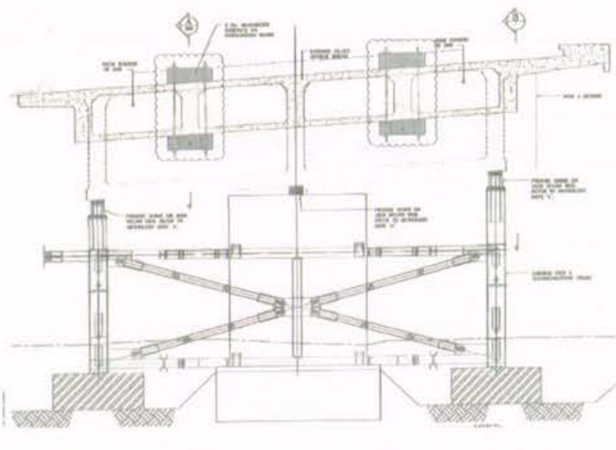

Figure 7.3. Braced steel frame providing additional supports at the South end.

Figure 7.4. Steel towers for demolition gantry penetrating through the deck.

Figure 7.5. Partially excavated column foundation.

7.3. Forced vibration testing and system identification

7.3.1. Forced vibration testing

The field testing consisted of subjecting the Gillies Avenue overbridge to forced vibrations and obtaining the response data as recorded by accelerometers. The vibrations were generated by two ANCO Engineers MK-140-10-50 eccentric mass shakers (see Chapter 6.4.1) with the data collected by 54 tri-axial wireless X6-1 and X6-1A MEMS accelerometers (see Chapter 5.3.2) and 18 uni-axial Honeywell QA 750 wired accelerometers (see Chapter 4.3) placed on the deck, piers and abutment of the bridge.

7.3.1.1. Instrumentation

Sketches showing accelerometer arrangement on the deck are shown in Figure 7.6. The wireless accelerometers (Figure 7.6a) were secured in two rows on the either edge of the bridge for each of the two spans with a resolution of ten accelerometers per edge per span. Two rows were required for torsional modes to be recovered, which would have been impossible if all sensors were placed in a single line. The wired accelerometers (Figure 7.6b) were only capable of logging acceleration in a single direction and were connected to a data acquisition box. Ten wired accelerometers were placed along the centreline of the deck at a spacing of 5 m. The deck accelerometers were always rotated and repositioned to measure accelerations in the direction of excitation (transverse, longitudinal or vertical). The wired accelerometers fed live data to a computer allowing immediate preliminary analysis of the acceleration records, enabling repetition or alteration of test procedures if the data was discovered to be incorrect.

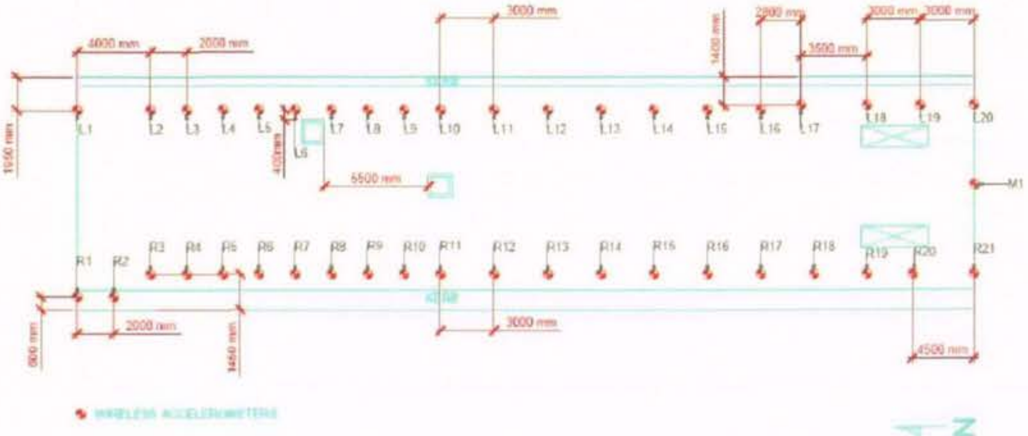

a)

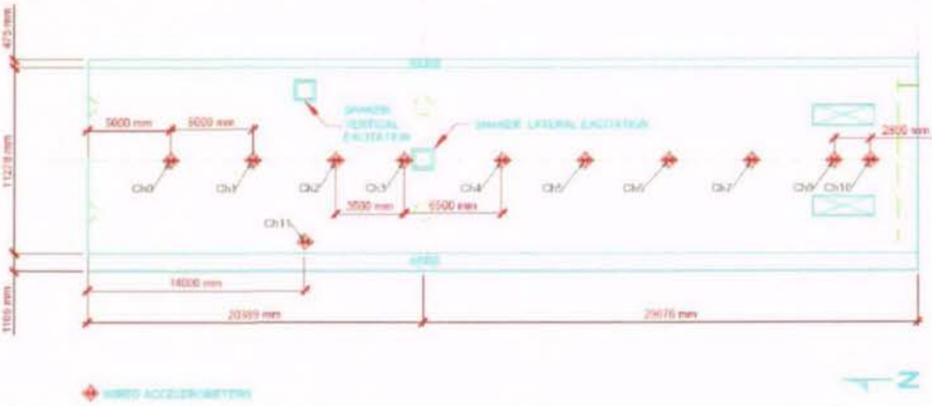

b)

Figure 7.6. Accelerometer and shaker placement on the deck: a) wireless accelerometers and shakers, and b) wired accelerometers and shakers on the deck.

The remaining accelerometers were placed on the abutment, columns and pier to detect their motion (see Figures 7.7 and 8). Prior to vibration testing, all the accelerometers were time synchronised to a common computer clock allowing for simultaneous data collection. The wireless accelerometers recorded continuously with the data extracted at the conclusion of testing.

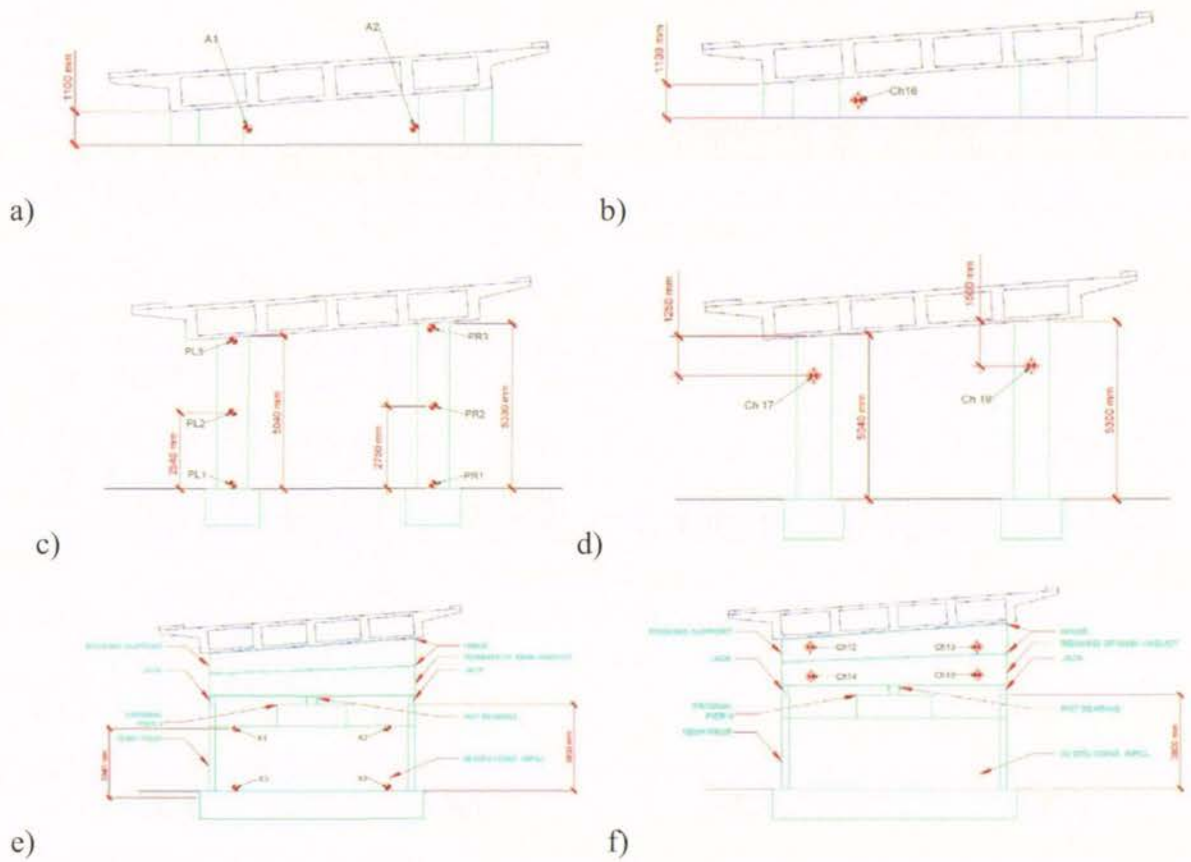

Figure 7.7. Accelerometer placement: a) wireless accelerometers on abutment, b) wired accelerometer on abutment, c) wireless accelerometers on columns, d) wireless accelerometers on columns, e) wireless accelerometers on pier, and f) wired accelerometers on pier.

a)  b) 

Figure 7.8. Accelerometers attached to column: a) wired accelerometer, and b) wireless accelerometer.

7.3.1.2. Excitation

The excitation was imparted onto the bridge in the three primary orientations: transverse, longitudinal and vertical. In order to facilitate vibration testing in three directions with only two shakers, one of the shakers was rotated after completion of the transverse test in preparation for longitudinal shaking, while the other always reminded positioned for vertical excitation. The exact locations of the shakers on the dec are shown in Figure 7.6, and a view onto the bridge deck with two shakers bolted is shown in Figure 7.9.

Figure 7.9. View of the deck with vertical shaker on the left and horizontal shaker in the centre, and blue demolition gantry in the foreground.

For the transverse and longitudinal tests, one large weight was used for each of the two fly wheels in the shaker. Testing consisted of an initial broad frequency sweep used to establish the key frequencies which generated significant responses as indicated by the real time values fed from the wired accelerometers. The remaining tests consisted of slower frequency sweeps around the significant frequencies. A maximum frequency of 11 Hz was reached for these tests.

Tests were conducted for the transverse direction with the initial sweep from 0 Hz to 11 Hz; the slow sweeps were concentrated around the frequencies of 6.7 Hz and 7.8 Hz as these were identified as potential modal frequencies. After the transverse direction tests were completed the shaker was rotated by a hiab to reposition it for testing in the longitudinal direction. All wired sensors were also rotated 90° in order to record the longitudinal accelerations expected from the new excitation direction. Three tests were conducted for the longitudinal direction with the initial sweep between 0 Hz and 10 Hz; slow sweeps were concentrated around frequencies of 7.1 Hz, 8.0 Hz and 9.8 Hz, although these were not able to be confirmed as modal frequencies later in the system identification stage.

However, only one test could be conducted in the vertical direction. As such, a slow frequency sweep commenced immediately (from 0 Hz) using two small weights on the flight wheel to cover a larger frequency band. The maximum frequency achieved for the single vertical excitation test was 15 Hz.

The frequency sweeps were controlled manually by adjusting the frequency of the excitation induced by the shaker by hand and watch. The slow sweeps used a step size of 0.2 Hz every 15 seconds. The shaker took approximately 5 seconds to reach the next frequency value, thus leaving 10 seconds of excitation for any given applied frequency. The duration of excitation for each test is shown in Table 7.1.

7.3.2. System identification

Since this testing exercise was run as an undergraduate research project with time limitation and the intention mostly to learn experimental and analytical arts rather than perform rigorous investigations, significant simplifications were used in the system identification phase. Because shaker excitation was controlled manually but no measurements of the actual forcing taken, only response signals were used. This is akin to OMA but obviously violets the white noise excitation assumption underlying OMA. However, quite accurate estimates of natural frequencies and mode shapes can still be obtained from peaks in the ASD, i.e. using the PP method (see Chapter 3.2.2). The frequencies identified in this way are shown in Table 7.2. Overall, two vertical, two torsional, one transverse and no longitudinal modes were identified up to around 10 Hz. Figure 7.10 shows the experimental mode shapes. It is interesting to mention that the identified modes were not necessarily recovered from the acceleration records corresponding to the direction of excitation. The majority of vertical and torsional modes were obtained by using vertical acceleration data from excitation in the transverse direction. This can be explained by the fact that shaker's horizontal force is acting above the deck and thus provides moment; on the other hand vertical excitation used only smaller forces which likely did not excite the bridge strongly enough.

Table 7.1. Duration and direction of excitation using eccentric mass shaker.

Test	Weights attached	Direction	Duration (mins)
T1	1 large*	Transverse	10
T2	1 large	Transverse	7
T3	1 large	Transverse	7
T4	1 large	Transverse	7
L1	1 large	Longitudinal	8
L2	1 large	Longitudinal	8
L3	1 large	Longitudinal	8
V1	2 small**	Vertical	24

* 1 large mass is 15.6 kg, ** 1 small mass is 3.6 kg

Table 7.2. Frequencies identified from forced vibration testing.

Mode no.	Type	Frequency (Hz)
1	Vertical	3.91
2	Torsional	5.78
3	Vertical	7.97
4	Transverse	8.59
5	Torsional	10.10

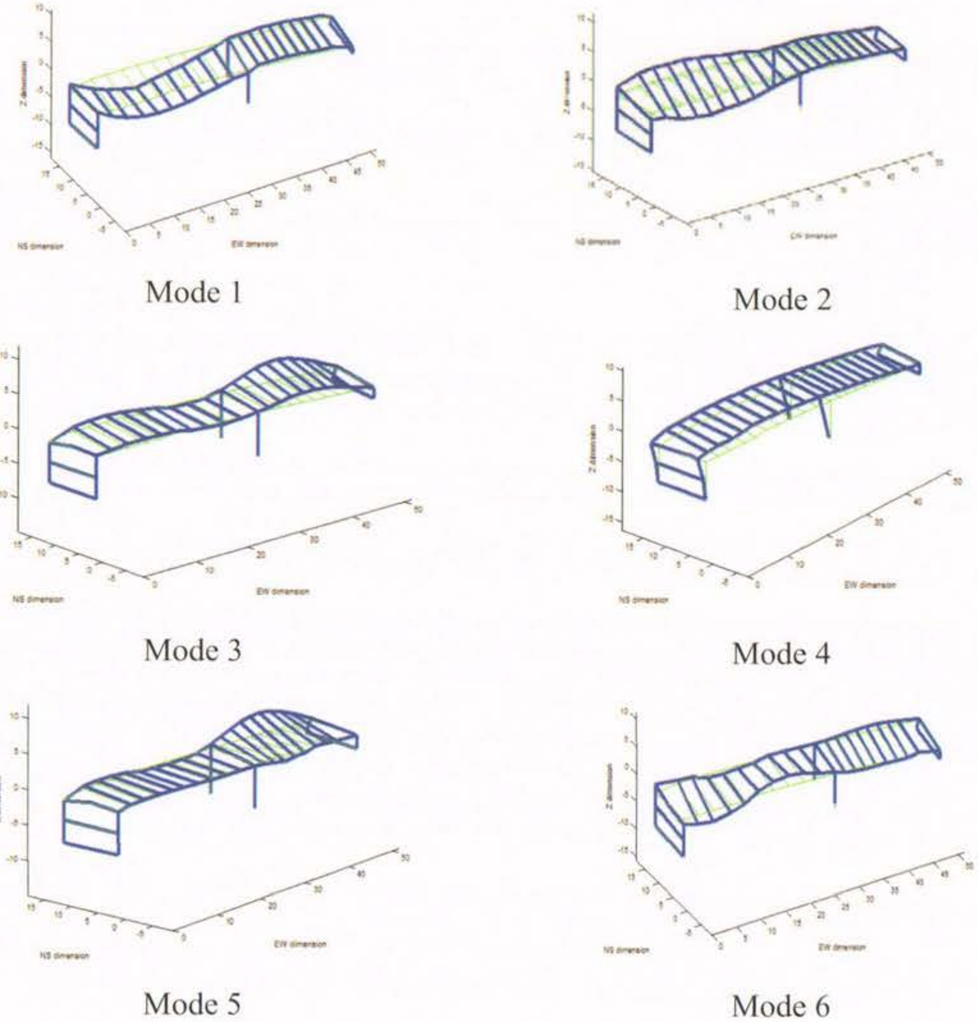

Mode 1

Mode 2

Mode 3

Mode 4

Mode 5

Mode 6

Figure 7.10. Experimental mode shapes.

7.4. Finite element modelling and model updating

7.4.1. Finite element modelling

A 3D numerical model (Figure 7.11) was created using the software package SAP2000 (Computers and Structures 2009). This allowed for the theoretical investigation of modal parameters consisting of natural frequencies and mode shapes in vertical, lateral and torsional directions. Although a geometrically simplified FE model can be adopted in the dynamic assessment of full scale bridges, this approach was deemed unfeasible within the current context. Due to the sheer complexity of the structure, creating a simplified model such that geometric relevance is compromised cannot reasonably simulate an accurate response. Subsequent updating of such a model will also likely result in meaningless results unless significant alterations are made to the inherent geometry (Brownjohn and Xia 2000). The created model therefore aims at realistically reflecting the structural composition of the bridge based on the supplied design drawings and measurements taken on site. Moreover, all additional features incorporated into the original structure prior to its demolition have also been taken into consideration.

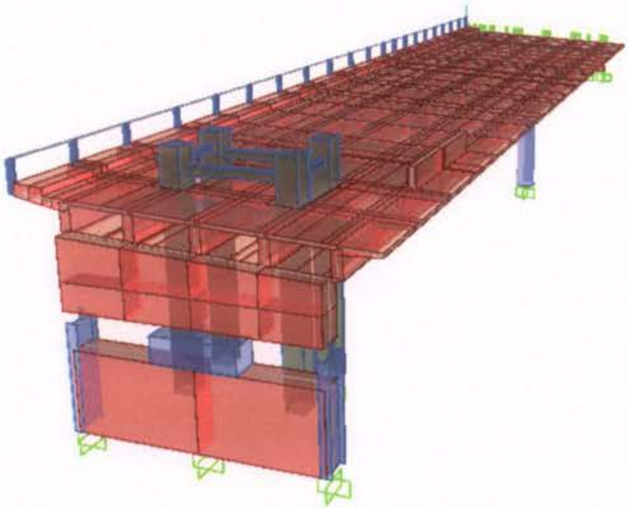

Figure 7.11. Finite element of Gillis Avenue looking from behind the South end.

Further discussions focus on characterising the makeup of the initial FE model and describing its various features and assumptions such as material properties and boundary conditions. Modelling of critical elements such as the deck, temporary tower struts and the pier supporting the South end of the bridge are also deliberated in detail.

The bridge in its entirety on the day of experimental testing was virtually solely composed of RC and structural steel. This is reflected by the materials defined in the numerical model. Normal concrete of unit weight of 2400 kN/m^3 and compressive strength 40 MPa was assumed throughout the structure. The corresponding modulus of elasticity was adopted after NZS3101:2006 (Standards New Zealand 2006) as 27.9 GPa. All structural steel elements were assumed to have Young's modulus of 200 GPa.

Boundary conditions consisting of restraints at the abutment and at the base of the pier, columns and gantry towers were initially assumed fixed. Although only approximate due to complex soil-structure interactions (Hogan et al. 2011), adopting full support fixity has been demonstrated in literature to give reasonable results for baseline models (Brownjohn and Xia 2000, Benedettini and Gentile 2011).

Thin shell elements were implemented to represent the flange, webs and soffit of the concrete box girder deck spanning the length of the structure. Although this task can theoretically be undertaken via equivalent beam members, the use of shell elements allows for a more realistic simulation of the dynamic response. The use of such elements has also been proven to deliver reliable results (Liu et al. 2007). The entire cross section of the deck was assumed effective in bending. Although some cracking was possible causing a reduction in stiffness, past analyses show models adopting such assumptions correlate well with experimental results. Furthermore, the deck was angled to the configuration specified in the drawings in order to maintain geometric accuracy.

Steel railings located along the eastern side of the bridge were modelled using frame elements. The additional stiffness contribution could potentially affect the overall modal response of the structure as shown by Pavic et al. (1998). It is also in the interest of uniformity between physical features and numerical constructs that such members are accounted for where possible within the FE model.

Modelling of the South pier adjacent to the temporary towers introduced difficulties regarding structural geometry. The sheer abundance of scaffolding on site surrounding this section prevented obtaining of adequate physical measurements. Thus, design drawings were largely relied upon, many of which lacking in detail. Furthermore, the dynamic response of the pier is most likely to be heavily influenced by two temporary steel jacks and a supporting concrete block with a pot bearing (indicated in Figure 7.11 in blue). This is on account of the connection lacking substantial stiffness relative to the pier on which the jacks and supporting block rests upon, likely rendering it the most flexible part of the pier.

The four temporary steel towers protruding through two rectangular holes cut into the deck are represented as hollow beam elements. Timber blocks were used to connect the towers to the deck and constraints were implemented to approximate the behaviour of the connections.

For the abutment, the bridge girder was modelled as being completely fixed to the abutment as it was observed in site investigations that the connection between the girder and the abutment was of sufficient rigidity to prevent any significant rotations or translations. The connection between the South pier and the bridge girder was modelled via a concrete solid element at the centre for the supporting block and two steel circular hollow sections at both ends to approximate what was observed on site and stated in the drawings. This connection is very flexible relative to the stiffness of the pier, and the response will be heavily dependent on the structural parameters adopted for this connection.

7.4.2. Model updating

A manual sequential approach as well as automatic updating process was adopted for the FE model comparisons with experimental data. Establishing natural frequencies as a basis of comparison, the FE model was calibrated accordingly in an attempt to draw it closer to the experimental results. In the manual updating phase, individual structural parameters were altered in several stages, while the effects of changes on the dynamic responses were noted. This process was repeated until all the considered theoretical natural frequencies differed not more than approximately 10% with respect to their experimental counterparts. Thus, at this stage adequate modal correlation can be assumed allowing for the automatic updating procedure to commence (Brownjohn and Xia 2000).

7.4.2.1. Manual model updating

The initial manual updating process comprised five stages. Further discussions summarise alterations introduced to the model during each stage.

Stage I: Material properties

As adjustments to material properties were observed by previous studies (e.g. Benedettini and Gentile 2011) to yield significant changes, altering concrete Young's modulus was elected as the preliminary modification to the FE model. This involved increasing the modulus of elasticity of the concrete deck from the initial 27.9 GPa to 40.0 GPa (or by 43%). This was accomplished in several steps until the adopted value gave, holistically judging, the best range of natural frequencies when compared with experimental results. Previous research (e.g. Pavic et al. 1998) indicates that this order of magnitude of Young's modulus change is realistic.

Stage II: Gantry tower connections

The second update involved adopting a more realistic mechanism to represent the connections between the temporary steel towers and bridge deck. The original use of constraints disallowed any deformation or rotations to occur at the connection points. Hence, the overall rigidity of the structure was likely to be exaggerated. In updating, links that permitted rotations at the joints were implemented to represent the timber blocks positioned between the tower and the deck. This also provided an insight into the stiffness contribution of the slender towers to the global structural stiffness.

Stage III: Transverse shear in deck elements

The third update changed the FE type adopted for the bridge deck. Elements used to model the flange, webs and soffit of the box girder were changed from thin shell to thick shell. This allowed for the consideration of shear deformations likely to be significant when shell thickness is greater than 1/10 of the plate-bending curvature span (De Soza 2012). Due to the concrete sections used in the model typically exhibiting large thicknesses, a more realistic representation of the structural behaviour was expected to be obtained via this update.

Stage IVa and IVb: Soil-structure interaction

This stage of updating involved experimenting with boundary conditions at the base of the mid-span columns, gantry towers and South pier. This aimed at testing the validity of initially assuming full base fixity at these locations. More realistic simulations of the modal response were attempted in Stage IV by including the effects of soil-structure interaction. To evaluate the significance of the removal of soil at the base of the columns and unknown stiffness contributions of the gantry and pier supports on the overall dynamic response, two independent alterations were conducted on the boundary conditions of the model:

- Stage IVa: Restraints at the base of the gantry towers and columns were switched from fixed to pinned connections, and
- Stage IVb: Springs (exhibiting both translational and rotational stiffness) were introduced to the foundations of the columns, gantry towers and South pier.

The use of pin connections is an inherently basic approximation to a lack of base fixity. This approach assumes that the gantry towers and columns are free to rotate about their foundations while completely restricting horizontal and vertical motion. Thus, it is implied that the impact of soil resistance on rotational stiffness is negligible. The use of springs in modelling boundary connections has been widely accepted throughout literature. Its ability to accurately simulate frictional resistance generated by the soil on structural foundations has been noted by Benedettini and Gentile (2011) as a distinct advantage.

Equations for calculating a preliminary value for the horizontal, vertical and rotational stiffness of the springs were adopted after Gazetas (1991). The depths of foundations were also taken into account when computing appropriate stiffness coefficients. Clayey soil existing in a homogeneous half-space was assumed for the purpose of generating the soil parameters required for the formulations. A value typical of clay (Zhu 2010) was selected for the shear modulus of soil as 300 MPa. Accounting for the unpredictable nature of soil, a large degree of uncertainty must be accommodated via the update. All stiffness values derived from formulas were permitted to vary by up to 30%. After sequential tweaking by trial and error, the final values adopted for the springs (Table 7.3) reflect coefficients that produced modal parameters in best agreement with system identification results.

Table 7.4 illustrates how frequencies changed due to modifications to the model introduced in Staged I-IV and comperes them with the experimental results. As can be seen, a general improvement in correlation between experimental and numerical results has been achieved for all modes except Mode 6. This is further evidenced in Figure 7.12, where manually updated frequencies are now much closer to the diagonal reference line indicating a better match with the experimental values. Additionally, MAC values (Equation 3.43) have been calculated for all the manual updating stages and are shown in Table 7.5. As can be seen all MAC values improved considerably, but still remain low for Modes 3, 5 and 6. FE model mode shapes are shown in Figure 7.13, where is can be seen that they compare well (at least qualitatively given the sometimes low MACs) with the experimental mode shapes in Figure 7.10.

Table 7.3. Final stiffness coefficients for foundations of mid-span columns, gantry towers and South pier.

Direction	Mid-span columns	Gantry towers	South pier
Longitudinal (X) (10^9 N/m)	6.08	0.76	6.46
Transverse (Y) (GN/m)	6.08	0.76	4.77
Vertical (Z) (GN/m)	4.59	1.02	5.26
X rotation (GNm/rad)	16.0	0.18	736
Y rotation (GNm/rad)	12.4	0.19	140
Z rotation (GNm/rad)	66.0	0.14	1.41

Table 7.4. Comparison between experimental and theoretical natural frequencies for manual updating Stages I-IV.

Mode no.	Mode type	Experimental frequency (Hz)	Initial model (Hz)	Stage I (Hz)	Stage II (Hz)	Stage III (Hz)	Stage IVa (Hz)	Stage IVb (Hz)
1	Vertical	3.91	4.06	4.84	3.44	3.81	3.79	3.77
2	Torsional	6.18	4.87	5.81	5.30	5.62	5.57	5.53
3	Vertical	7.97	6.45	7.72	7.38	7.91	7.91	7.80
4	Transverse	8.59	-	9.48	9.01	9.07	8.64	8.61
5	Torsional	10.10	8.61	10.13	9.74	10.10	10.10	10.00
6	Torsional	12.70	12.00	14.30	13.74	14.10	14.00	14.00

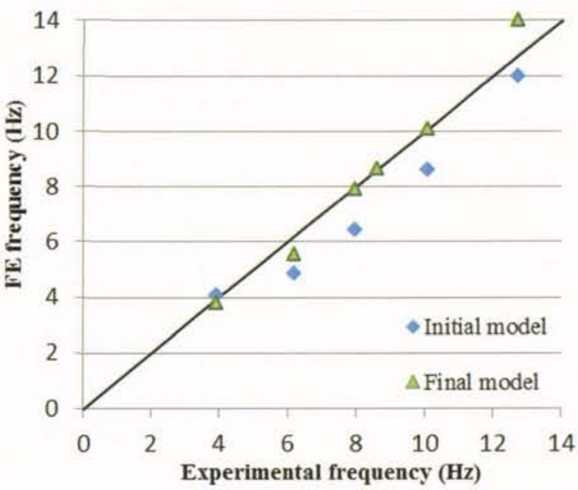

Figure 7.12. Comparison between frequencies of initial and manually updated FE model and their experimental counterparts.

Table 7.5. MAC values between experimental and theoretical modes for manual updating Stages I-IV.

Mode no.	Initial model (%)	I (%)	II (%)	III (%)	IVa (%)	IVb (%)
1	65	66	87	90	90	89
2	81	80	82	83	83	83
3	33	33	41	50	66	60
4	N/A	60	70	86	89	87
5	23	29	31	31	31	32
6	61	60	64	64	63	63

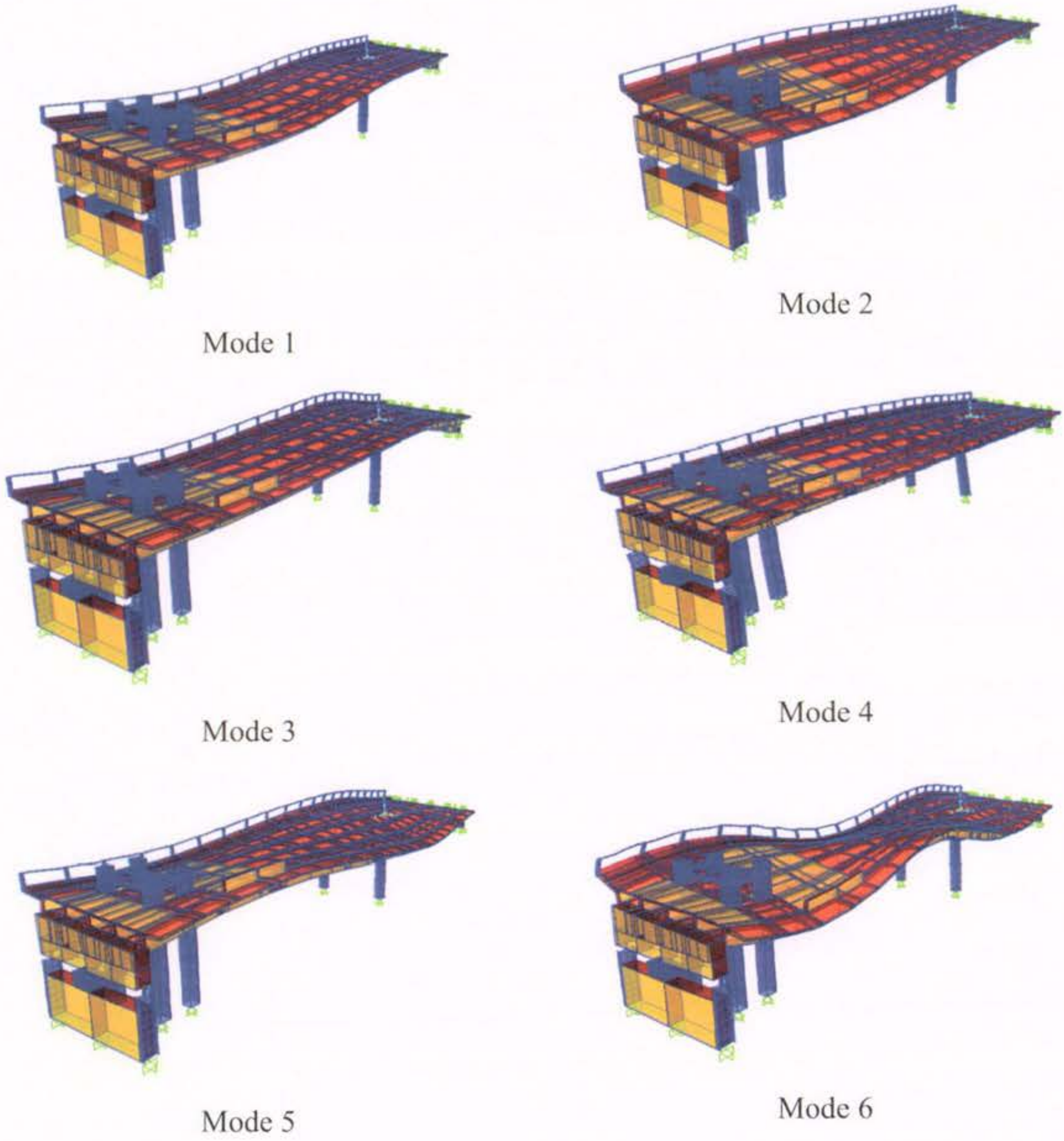

Figure 7.13. FE model mode shapes.

7.4.2.2. Sensitivity based model updating

Following the manual updating stage, automatic updating was attempted. The first five frequencies were considered for updating as the initial error of the sixth frequency (larger than 10%) suggested this mode would be difficult to improve. The model parameters considered as candidates for updating were concrete Young's modulus of the deck, South pier, additional supporting block at the South pier, columns, and Young's modulus of steel of gantry towers and railings.

The preliminary automatic updating exercise has to be interpreted while acknowledging several of its limitations. While deck concrete Young's modulus can be considered an actual physical parameter expected to vary, the other parameters were rather proxies for overall stiffness of these elements. For example, into the column stiffness uncertainty of soil flexibility and boundary conditions were lumped. This immediately suggests considering soil stiffness, omitted in the current simulations, as another candidate parameter for updating.

The relative sensitivities (i.e. ratios of the relative change in the response value caused by a relative change in the parameter value) of the first five frequencies to the six candidate updating parameters are shown in Figure 7.14. Three parameters were chosen based on significant sensitivities of natural frequencies to changes in their values, namely concrete Young's modulus of the deck, the columns and the additional supporting block at the South pier (indicated in Figure 7.11 in blue), while the influence of the remaining parameters can be seen as negligible. Note that both stiffness of the pier and supporting block influence strongly the frequency of Mode 4 (transvers) but not the other modal frequencies. This likely indicates an ill-posed updating problem where unique values of the two parameters cannot be determined. A remedy could be in using regularisation, as was done in Chapter 4, but this approach was not pursued in this preliminary exercise.

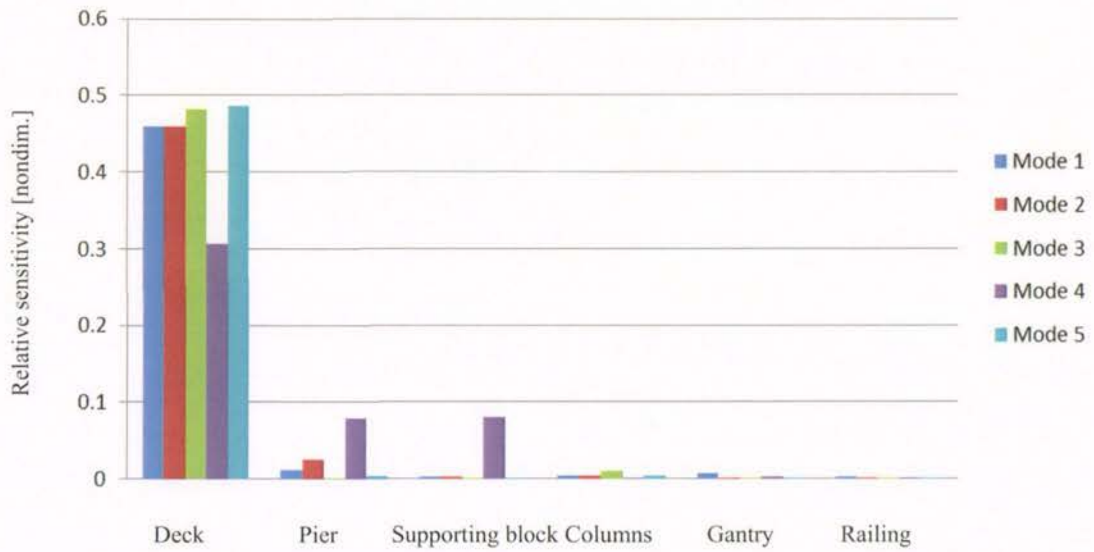

Figure 7.14. Relative sensitivities of frequencies to candidate updating parameters.

Table 7.6. Comparison of experimental and automatically updated frequencies.

Mode no.	Mode type	Experimental frequency (Hz)	Automatically updated FE model frequency (Hz)	Relative error (%)
1	Vertical	3.91	3.84	-1.8
2	Torsional	5.78	5.70	-1.4
3	Vertical	7.97	7.98	0.1
4	Transverse	8.59	8.59	0.00
5	Torsional	10.1	10.2	1.0

Table 7.7. Initial and automatically updated FE model parameters.

Parameter	Initial value (GPa)	Updated value (GPa)
Deck Young's modulus	40.0	40.7
Pier Young's modulus	40.0	39.1
Supporting block Young's modulus	27.9	21.25

With the aforementioned limitations, the results of updating are shown in Table 7.6. An improvement in the frequency match can clearly be seen with the individual errors not exceeding 1.8% after updating. The updated parameter values are shown in Table 7.7. As can be seen small adjustments to the deck and pier stiffness sufficed to bring the frequencies to a close agreement, but the supporting block stiffness had to be changed relatively more. Again it is likely that flexibility of the block-deck connection via the pot bearing, indeed even the possibility of sliding at their interface, was lumped into the updating parameter and contributed to its marked decrease.

7.5. Conclusions

This chapter presents forced vibration testing, system identification, and updating of a two-span highway overbridge. The bridge, the first tested by the team using the large ANCO MK-140-10-50 eccentric mass vibrators, served primarily as a learning ground. The bridge was tested within a few days from its demolition and at the time of testing was already heavily modified due to on-going demolition and construction activities. Testing used several frequency sweeps from which a total of six vertical, torsional and transverse modes were identified using the PP method. The computer model of the bridge was created, taking into account all modifications due to demolition and soil-structure interaction. This model was updated, first manually and then automatically using SM, to provide a close representation of the actual system.

7.6. References

ANCO Engineers (2013), http://www.ancoengineers.com.

Benedettini, F., & Gentile, C. (2011), Operational modal testing and FE model tuning of a cable-stayed bridge, Engineering Structures 33, 2063-2073.

Brownjohn, J.M.W., & Xia, P.Q. (2000), Dynamic assessment of curved cable-stayed bridge by model updating, Journal of Structural Engineering, ASCE, 126, 252-260.

Computers and Structures (2009), SAP2000 structural analysis program, Computers and Structures, Berkeley, CA.

De Soza, T. (2012). Note of use of the voluminal elements plates, shells SHB, grids and membranes, Code Aster.

Gazetas, G. (1991), Formulas and charts for impedances of surface and embedded foundations, Journal of Geotechnical Engineering, ASCE, 117, 1363-1381.

Hogan, L.S., Wotherspoon, L.M., Beskhyroun, S., & Ingham, J.M. (2011), Forced vibration testing of in situ bridge span, Proceedings of the 9th Pacific Conference on Earthquake Engineering, 1-8.

Liu, Z., Majumdar, P.K., Cousins, T.E., Lesko, J.J., Zhou A., & Sotelino, E.D. (2007), Finite element simulating and parametric studies of an FRP bridge deck supported on steel stringers, Proceedings of the International SAMPE Symposium and Exhibition, 1-19.

Pavic, A., Hartley, M.J., & Waldron, P. (1998), Updating of the analytical models of two footbridges based on modal testing of full-scale structures, Proceedings of ISMA23, 1111-1118.

Standards New Zealand (2006), Code of practice for the design of concrete structures, Standards New Zealand, Wellington.

Zhu, T. (2010), Some useful numbers on the engineering properties of materials (geologic and otherwise), Stanford University, Stanford, CA.

CHAPTER 8

CONCLUSIONS

Full-scale, in-situ dynamic testing on existing bridge structures can provide a wealth of information about their performance. Full-scale testing is free from many assumptions and simplifications inherently present in laboratory experiments and numerical simulations. For example, soil-structure interaction, non-structural components, and nonlinearities in stiffness and energy dissipation are always present in their true form in full-scale, in-situ testing. Thus, full-scale experimentation results present the ground truth about structural performance and provide the necessary calibration for analyses of actual constructed systems and laboratory and numerical investigations. The performance evaluated this way can be used for advanced assessment of structural condition, detection of damage, aging and deterioration, evaluation of the construction quality, validation of design assumptions, and also as lessons for future design and construction of similar structures.

In this research, four different bridges (a two-span cable-stayed pedestrian bridge, a two-span concrete motorway overbridge, an 11-span post-tensioned concrete motorway off-ramp, and a major 12-span post-tensioned concrete motorway viaduct) were tested using ambient excitation (e.g. vehicular traffic) and/or forcing provided by shakers. Experimental data were analysed using multiple system identification techniques to extract the resonant frequencies, damping ratios and mode shapes. Detailed computer modelling of the structures was also undertaken and enabled identification and understanding of the mechanisms responsible for their measured performance. Computer models of the bridges were calibrated against experimental data using several model updating approaches.

The experimental study on the two-span cable-stayed bridge used small shakers to impart dynamic excitation and a dense array of wired sensors to identify full set of modal properties, i.e. frequencies, damping ratios and mode shapes. A novel optimisation method for updating of structural models was proposed and investigated using the identified experimental modal data. The method, PSO with SNT, belongs to GOAs, mimics the behaviour of a swarm of bees or school of fish in search for the most fertile feeding location, systematically searches the updating parameter domain for multiple minima to discover the global one, and proved effective when applied to the experimental data from the pedestrian bridge. Its use increases the confidence in finding the global minimum in updating problems. The study also emphasised the need for assessing automatic updating results for their plausibility using critical engineering judgement.

For the 12-span viaduct, ambient dynamic tests were performed in two different construction stages (before and after the two bridges making up the viaduct were joined together via a cast in-situ concrete 'stitch') under regular vehicular traffic crossing the bridge. The use of a large number (nearly 60) of inexpensive, self-powered sensors with data storage capability enabled mapping of mode shapes for the sizeable structure in reasonable time of two to three days. The performance of four different system identification methods to determine modal dynamic parameters of the structure have been compared and discussed. The four methods were PP, EFDD, NExT-ERA and SSI. Within the considered frequency range 0-10 Hz, ten modal frequencies for vertical modes were successfully identified using the four methods. Although one frequency was not identified by the Next-ERA method, good agreements were found between the modal frequency estimates obtained from the four different methods. The comparison of mode shapes (MACs) showed that PP, SSI and EFDD agreed very well on the shape of the first vertical mode, however, NExT-ERA showed discrepancies. Similar discrepancies were noted for higher modes for all the identification methods used. The dynamic characteristics identified at two construction stages were presented and compared in order to determine the actual bridge dynamics during construction and for the final state. The frequencies of the first two transverse modes have increased markedly, whereas the frequencies of the first two vertical modes decreased slightly. These changes were traced back to the modification of stiffness introduced by connecting the two bridges. The experimental investigation was complemented by the development of a 3D FE models based on design drawings and material testing data. The FE results were compared with those obtained from experimental measurements and showed good correlation.

The analyses of experimental data included quantification of resonant frequency and damping ratio changes with the amplitude of forcing and response for the 11-span motorway off-ramp. The frequency of the 1st lateral mode was found to decrease monotonically with increasing response amplitude and an exponential trend approximated the change very accurately. The damping ratio showed an initial increase but later stabilized at an elevated level, which was modelled using a bilinear relationship. FE modelling paid special attention to boundary and connectivity conditions, such as bearings and internal hinges. By carefully modelling these, it was possible to formulate a tuned structural model that replicates experimental modal results well.

The last presented, but chronologically earlier than testing of the 11-span off-ramp bridge, testing exercise used large eccentric mass vibrators on a two-span highway overbridge within a few days from its demolition when the structure was already heavily modified due to on-going demolition and construction activities. A great deal of practical experience was gained via this project regarding logistics of using large shakers and their operation, and approaches to data collection, system identification and model updating. Testing used several frequency sweeps from which several vertical and lateral modes were identified using the PP method. Deficiencies in system identification were noted that resulted from the lack of appropriate measurement of forcing time histories. A computer model of the bridge was created and updated, first manually and then automatically using SM. The updating attempts highlighted the need to carefully model structural details, such as connections between structural elements and boundary conditions, and select updating parameters taking into account their influence on results and possible ill-posing of the updating problem.

A number of recommendations for future research and full-scale, in-situ experimental testing practice can be made based on learning that occurred over the duration of this project. Firstly, a more efficient and reliable methods for controlling and measuring the input force time history of the large shakers should be developed. The current approach based on controlling manually the excitation frequency and timing changes using a watch is of low accuracy, cumbersome and offers only limited certainty that the shaker is following closely the operator's instructions. Secondly, the inexpensive wireless sensors proved very convenient for testing of large structures, whereas with wired sensors these exercises would have been prohibitively time and labour intensive. However, these sensors are not without problems, including loss of data segments, spurious data, relatively frequent malfunctioning and inexact time keeping. It will be useful to look for alternatives balancing cost against performance.

The new model updating method based on PSO and SNT proved efficient but further gains could be made by optimising the various parameters controlling its performance. Furthermore, it should be compared to other GOAs, such as GA, SA or firefly algorithm. Also, the possibility of combining SM with GOAs should be considered, whereby the initial optimisation steps would be carried out by a GOA and, once possible locations of minima are identified, the quicker SM could finish the search.

It was often encountered in the updating attempts reported herein that ill-posed problems arose. They were detected by rather informal insights and in one case dealt with using regularisation. Future research should look into identifying and/or establishing rigorous, mathematically based methods of detecting whether an updating problem is ill-posed.

Finally, the preliminary study on the dependence of modal parameters of forcing and response magnitude should be extended by examining similar trends for other modes where data was collected. Furthermore, the mechanism for the observed trends should be identified and explained.